Design und Synthese von Metall-Porphyrinen für die funktionelle, medizinische Bildgebung sowie von metallfreien Bakteriochlorinen für die Photodynamische Therapie

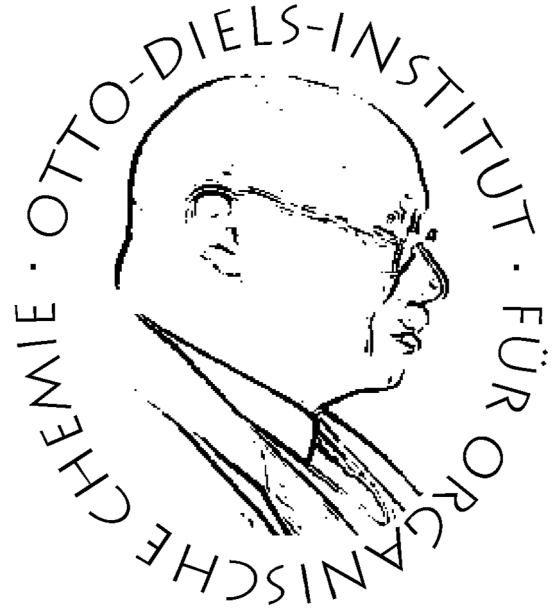

DISSERTATION

zur Erlangung des Doktorgrades
der Mathematisch-Naturwissenschaftlichen Fakultät
der Christian-Albrechts-Universität
zu Kiel

vorgelegt von
Morten Peters

Otto Diels-Institut für Organische Chemie
Kiel 2018

Referent: Prof. Dr. Rainer Herges
Korreferent: Prof. Dr. Felix Tuczek

Tag der mündlichen Prüfung: 29.01.2019
Zum Druck genehmigt: 29.01.2019

gez. Prof. Dr. W. J. Duschl, Dekan

Die vorliegende Arbeit wurde unter Anleitung von
Prof. Dr. Rainer Herges
am Otto Diels-Institut für Organische Chemie
der Christian-Albrechts-Universität
sowie im Rahmen des Sonderforschungsbereichs 677
"Funktion durch Schalten"
im Zeitraum von November 2014 bis Dezember 2018 angefertigt.

Eidesstattliche Erklärung

Hiermit erkläre ich, Morten Peters, an Eides statt, dass ich die vorliegende Doktorarbeit selbstständig und nur mit den angegebenen Quellen und Hilfsmitteln angefertigt habe. Die Arbeit ist nach Inhalt und Form, abgesehen von der Beratung durch meinen Betreuer, durch mich eigenständig erarbeitet worden. Die Arbeit wurde unter Einhaltung der Regeln guter wissenschaftlicher Praxis der Deutschen Forschungsgemeinschaft angefertigt. Die Dissertation wird ausschließlich an dieser Stelle zur Promotion vorgelegt. Es wurde noch kein früherer Promotionsversuch von mir unternommen und mir wurde auch kein akademischer Grad entzogen.

Kiel, den 12.12.2018

_____

Morten Peters

Kurzdarstellung

Die molekulare Spinschaltung ist für eine Vielzahl von Anwendungen interessant, wie beispielsweise für die Realisierung eines intelligenten schaltbaren Kontrastmittels für die Magnetresonanztomographie (MRT). Diesbezüglich ist der Light-Driven Coordination-Induced Spin State Switch (LD-CISSS) einer der erfolgreichsten Ansätze für die reversible Spinschaltung in homogener Lösung bei Raumtemperatur. Basierend auf diesem Konzept wird in dieser Dissertation die erste lichtgesteuerte molekulare Spinschaltung auf Fe(III)-Basis vorgestellt. Hierbei wird der Spin-Switching-Prozess durch einen photoschaltbaren Azopyridinliganden induziert, welcher zu einer reversiblen Schaltung zwischen High-Spin ($S = 5/2$) und Low-Spin ($S = 1/2$) führt. Um weitere Untersuchungen an diesem System vorzunehmen und es zu optimieren, erfolgten zahlreiche Synthesen zur Herstellung von überbrückten Porphyrinen und Azopyridinen.

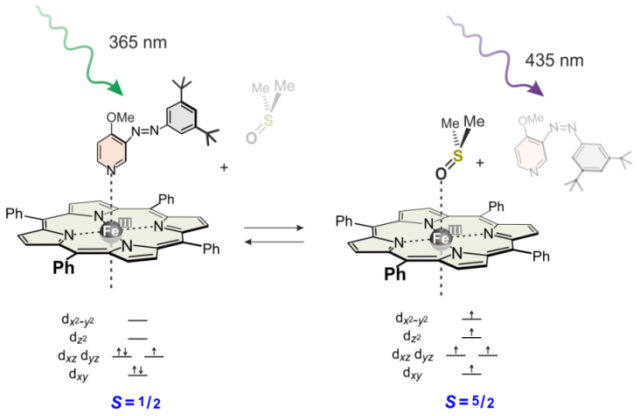

Zusätzlich stand die Funktionalisierung von Porphyrinen im Fokus, um das Schalten im bio-optischen Fenster zu ermöglichen. Hierbei wurden die Porphyrine mittels einer Diels-Alder-Reaktion in ihre reduzierten Derivate, Chlorine, Isobakteriochlorine und Bakteriochlorine überführt.

Durch die neu entwickelte, sehr milde sowie effiziente Methode, Nickel unter Verwendung von Bis(cycloocta-1,5-dien)nickel in Porphyrine einzulagern, konnte erstmals die gesamte Reihe von Hydroporphyrinen mit Ni(II) im Tetrapyrrolkern hergestellt und charakterisiert werden.

Desweiteren wurde das metallfreie Bakteriochlorin auf die Anwendbarkeit als Photosensibilisator untersucht und aufgrund der guten Eigenschaften weiterentwickelt. Das neu synthetisierte wasserlösliche Bakteriochlorin zeigt eine starke Absorption im Nahinfrarot-Bereich bei 733 nm und eine gute Quantenausbeute. Damit ist die Verbindung hervorragend für die Anwendung in der Photodynamischen Therapie geeignet.

Abstract

Molecular spin switching is of interest for a number of different applications, such as switchable contrast agents for magnetic resonance imaging (MRI). The Light-Driven Coordination-Induced Spin State Switch (LD-CISSS) concept is the most successful approach for reversible spin switching in homogeneous solution at room temperature. Based on this concept, this thesis presents the first light-controlled molecular spin switch based on Fe(III). This spin-switching process is induced by a photoswitchable azopyridine ligand. In this process the spin state can be reversibly switched between low-spin (S = 1/2) and high-spin (S = 5/2).

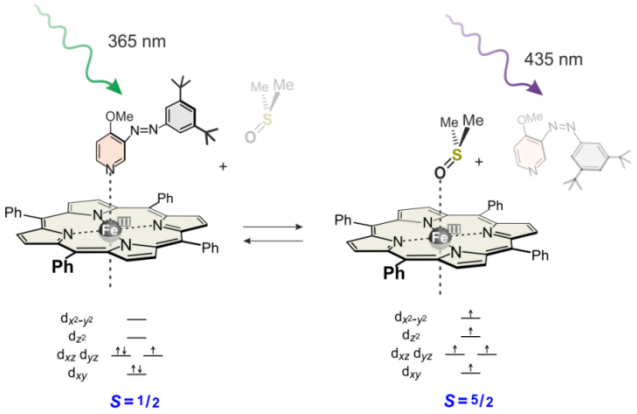

In order to investigate and optimize this system, a large number of bridged porphyrins and azopyridines were synthesized.

In addition, the functionalization of porphyrins has been studied to shift the switching frequencies into the bio-optical window. The porphyrins react as dienophiles with the highly reactive diene isobenzofuran in very high yields under mild conditions to the reduced derivatives, namely chlorins, isobacteriochlorins and bacteriochlorins.

The new, very mild and efficient method to insert nickel into porphyrins at room temperature using $Ni(COD)_2$ can be used to prepare the first whole series of hydroporphyrins with Ni(II) in the tetrapyrrolic core.

Furthermore, the metal-free bacteriochlorins were investigated as potential photosensitizers. Synthetic modification improved the properties of those compounds. The novel water-soluble bacteriochlorin shows strong near-infrared absorption at 733 nm and good quantum efficiency. This chromophore is a promising candidate for photodynamic therapy.

Danksagung

An dieser Stelle möchte ich die Gelegenheit nutzen, mich bei mehreren Personen zu bedanken, die zum Gelingen dieser Arbeit beigetragen haben. An erster Stelle möchte ich mich bei Prof. Dr. R. Herges für die interessante Aufgabenstellung sowie für die nette Aufnahme in seinem Arbeitskreis bedanken.
Ein großes Dankeschön geht an die Arbeitsgruppe HERGES, die mich freundlich aufgenommen und in jeder Lage unterstützt hat.
Für das zügige Anfertigen zahlreicher Spektren danke ich den Mitarbeitern der spektroskopischen Abteilung. Weiterhin danke ich den Mitarbeitern der Chemikalienausgabe für die Bereitstellung von Chemikalien und Herrn Prof. Dr. Christian Näther für die Einkristall-Röntgenstruturanalysen.

Ein ganz besonderer Dank geht an Dr. M. Dommaschk und Dr. D. Plaul, die mir zu Beginn meiner Promotion mit Rat und Tat helfend zur Seite standen und immer ein offenes Ohr für mich hatten. Des Weiteren danke ich allen, die diese Arbeit Korrektur gelesen haben.

Ein weiterer Dank gebührt meinem Kommilitonen Achim Fölster, ohne den ich sicherlich nicht so viel Spaß in meinem Studium gehabt hätte und es auch nicht so gemeistert hätte. Ein weiterer Dank geht an das Labor 218 und die ständigen Besucher, die für gute Stimmung gesorgt haben.

Meinen Eltern, meiner Schwester, meiner Freundin und meiner Oma gebührt ein ganz besonderer Dank. Euer kontinuierliches Interesse an meiner Arbeit, die aufmunternden Worte und nicht zuletzt die finanzielle Förderung haben mein Studium und diese Arbeit erst möglich gemacht. Vielen Dank für eure Unterstützung in allen Lebenslagen!

Inhaltsverzeichnis

1 Einleitung

In den letzten 150 Jahren ist es Wissenschaftlern gelungen, komplexe Molekülstrukturen eines natürlichen Ursprungs aufzuklären und mittels Totalsynthese herzustellen. Anschließende Untersuchungen konnten Einblicke in Biogenese und Metabolismus gegeben.[1] Durch die so gewonnen Informationen wurden in der Medizin große Fortschritte hinsichtlich der Heilung sowie Behandlung von zahlreichen Krankheiten gemacht.[2] Eines der bekanntesten Beispiele aus medizinischer Sicht ist das im Jahr 1928 von FLEMING entdeckte Penicillin.[3] Dieses konnte jedoch erst 29 Jahre später durch SHEEHAN in einer Totalsynthese hergestellt werden.[4] Hierdurch wurden das Verständnis von bakteriellen Krankheitserregern geprägt und der medizinische Nutzen als Antibiotika erkannt, was die Behandlung bakterieller Infektionen revolutionierte.[2] Aus diesem Grund ist das Teilgebiet der medizinischen Chemie, welche sich mit Design und Synthese neuer, therapeutisch verwendbarer Wirkstoffe beschäftigt, unerlässlich für die aktuelle Forschung.
In der Medizin spielt neben der Therapierbarkeit die Diagnostik von Krankheiten eine entscheidende Rolle. In den letzten Jahren rückte deshalb die Theranostik in den Vordergrund, welche beide Teilgebiete vereint. Generell kann hierbei zwischen zwei verschieden Herangehensweisen unterschieden werden.[5] Erstere stellt die therapiebegleitende Diagnostik dar. Hierbei werden die Auswirkungen der Behandlung schon während der Therapie selbst diagnostiziert, wodurch die Heilmethode anhand von gemessenen Werten immer weiter optimiert werden kann. In der *in situ* Diagnostik hingegen werden Therapie und Diagnostik in einem molekularen Target kombiniert. Dies sind zum Beispiel Nanopartikel, die einerseits mit verschiedenen Bildgebungsmethoden im Körper sichtbar gemacht werden können und andererseits ebenfalls in der Lage sind, einen Wirkstoff zu transportieren.[6] Eines der bekanntesten Beispiele stellt die Radiojodtherapie dar, die zur Diagnostik und Behandlung des differenzierten Schilddrüsenkarzinoms verwendet wird.[7]

1.1 Bildgebende Nachweismethoden von Erkrankungen

In der Medizin sind die bildgebenden Verfahren von enormer Bedeutung. Hierbei muss zwischen der anatomischen und funktionellen Bildgebung unterschieden werden. Mit letzterer Methode können Krankheiten, wie zum Beispiel Stoffwechselstörungen und Krebs, diagnostiziert werden, bevor sie soweit fortgeschritten sind, dass sie durch anatomische Veränderungen in der konventionellen Bildgebung sichtbar werden. Um auf dieser Basis Vorsorgeuntersuchungen zu ermöglichen, werden funktionelle Bildgebungsverfahren benötigt. Die hierzu gehörende Magnetresonanztomographie (MRT) ist neben der Computertomographie (CT) eines der aussagekräftigsten bildgebenden Verfahren in der modernen medizinischen Diagnostik.[8]

Die MRT kommt im Gegensatz zur CT ohne gesundheitsgefährdende ionisierende Röntgenstrahlung aus. In der klinischen MRT werden Frequenzen verwendet, welche im Radiowellenbereich zwischen 42 und 128 MHz liegen. Diese erweisen sich nach heutigem Wissensstand als unbedenklich für die Gesundheit. Zum Einsatz kommt eine solche Form der Therapie bei akuten Erkrankungen wie beispielsweise einem Schlaganfall. Des Weiteren bietet sie den besten Weichteilkontrast aller derzeit verfügbaren Bildgebungsmethoden, weshalb sie sich hervorragend für die Lokalisierung von Tumoren, Stoffwechselstörungen und Entzündungsherden eignet.[9]

1.1.1 Magnetresonanztomographie

Die Entwicklung der Magnetresonanztomographie begann im Jahre 1973 durch LAUTERBUR. In der dazugehörigen Veröffentlichung konnte der Unterschied zwischen zwei Körpern dargestellt werden, von denen einer mit Wasser und der andere mit Deuteriumoxid gefüllt war.[8] Anfang der 80er Jahre wurde diese Methode weiterentwickelt, sodass es durch die nukleare Magnetresonanztomographie möglich war, Einblicke in den menschlichen Körper zu erlangen.

Diese Schnittbilder ähneln denen einer CT, beruhen jedoch auf komplett anderen physikalischen Phänomenen. Die MRT basiert auf dem Prinzip der kernmagnetischen Resonanz (NMR) und ist somit eng mit der NMR-Spektroskopie verwandt.[10] Der Unterschied besteht jedoch in der räumlichen Zuordnung des MR-Signals, welches in der MRT mithilfe von Magnetfeldgradienten erreicht wird. Diese

Grundlagen wurden von LAUTERBUR und MANSFIELD entwickelt,[8,11] wofür die Forscher im Jahr 2003 mit dem Nobelpreis für Physiologie ausgezeichnet wurden.[12]
Die Bedeutung der MRT hat in den letzen Jahrzenten stetig zugenommen und ist zu einem wichtigen nicht-invasiven Bildgebungsverfahren geworden. Zusätzlich werden stetig Systeme für höhere räumliche Auflösungen der Öffentlichkeit präsentiert, so z.B. die FDA-Freigabe der ersten Ultrahochfeld-MRT-Systeme (7 Tesla, 300 MHz) für die klinische Diagnostik. Verfahren wie z.B. die molekulare Bildgebung,[13] die Durchführung interventioneller Eingriffe,[14] die bildgebungsgesteuerte Tumorablation mittels fokussiertem Ultraschall,[15] die sogenannten X-Kern-Bildgebung[16] oder die funktionelle MRT[17] tragen dazu bei, dass dieses interdisziplinäre Forschungsfeld noch sehr viel verborgenes Potenzial in sich trägt.
Die vermehrte Nutzung der MRT verdeutlicht zudem eine Statistik von Siemens aus dem Jahre 2012. Diese zeigt die Nutzung der MRTs pro 1 Million Einwohner in verschiedenen Ländern (Abbildung 1).[18]

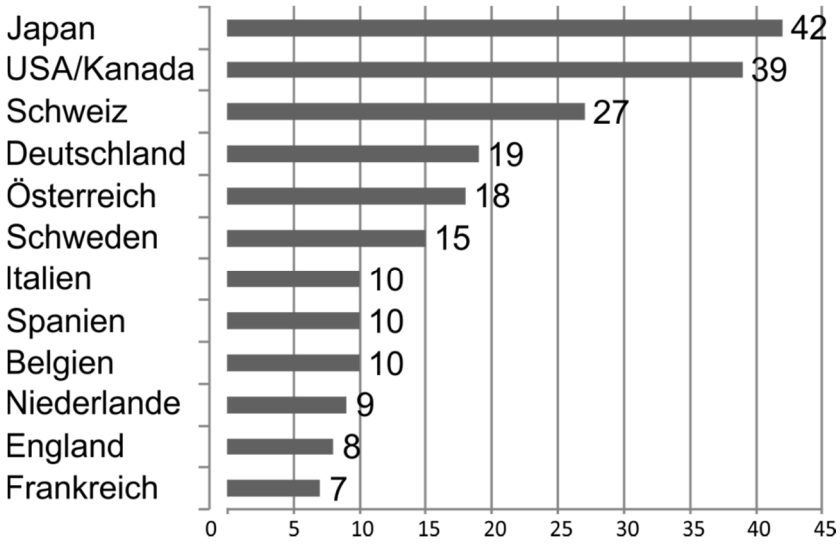

Abbildung 1: Anzahl der MRT-Scanner pro 1 Million Einwohner in verschiedenen Ländern im Jahr 2012.[18]

In der MRT werden die magnetischen Eigenschaften der Protonen genutzt. Die Relaxation des Kernspins ist stark von der Umgebung abhängig, in der sich ein Atomkern befindet, wodurch zwischen verschiedenen Gewebearten und Körperstrukturen unterschieden werden kann.[14]
Hierbei wird in der Regel das Augenmerk auf den ^{1}H-Kern gelegt, da dieser gute Eigenschaften für die Magnetresonanz mit sich bringt und zusätzlich in allen biologischen Systemen (Wasser, Aminosäuren, Kohlenhydraten und Fetten) ausreichend zu finden ist.

Die oben erwähnte Relaxationszeit des ^{1}H-Kerns ist von vielen Faktoren abhängig.[19] So spielen unter anderem die Viskosität wie auch das strukturelle Umfeld des Mediums, in dem sich die zu messenden Kernspins befinden, eine entscheidende Rolle. Ein elementares Beispiel hierfür ist das Tumorgewebe. Dieses weist aufgrund der unkontrollierten Teilung der betroffenen Zellen eine andere strukturelle Ordnung auf. Hierbei können sowohl tumorabhängige Bereiche verkürzter Relaxationszeit auftreten als auch Bereiche entstehen, in welchen Relaxationszeiten verlängert sind (z.B. in Nekrosen bei Glioblastomen).[20] In vielen Fällen lassen jedoch selbst die vielfältigen diagnostischen Möglichkeiten mittels MRT keine klare Identifikation des eigentlichen Tumors zu. Aus diesem Grund werden heutzutage bei etwa einem Drittel aller Untersuchungen Kontrastmittel eingesetzt (Abbildung 2, links), um auch solche Unterschiede darstellen zu können.[21,22]

1.1.2 Kontrastmittel

Der Kontrast in MR-Bildern kommt durch Signaldifferenzen, d.h. durch unterschiedliche T1- und T2-Relaxationszeiten der jeweiligen Gewebe, zustande. Relaxation ist ein dynamischer Prozess. Ein System kehrt aus einem Nichtgleichgewichtszustand in sein Gleichgewicht zurück. Bei der MRT spielen zwei Relaxationsprozesse eine Rolle: die so genannte Spin-Gitter-Relaxation (T1) und die Spin-Spin-Relaxation (T2). Oftmals ist der Unterschied zwischen den Gewebearten jedoch so gering, dass es in solchen Fällen inzwischen gängige Praxis ist, Kontrastmittel zur Steigerung des Informationsgehalts einer MRT-Aufnahme einzusetzen.[23] Aktuellen Schätzungen nach wurden bereits weltweit über 200 Millionen Kontrastmittel bei medizinischen Untersuchungen verabreicht, was auch die enorme Bedeutung in der Medizin widerspiegelt.[24]

MRT-Kontrastmittel sind paramagnetisch und haben somit ungepaarte Elektronen. Hierbei werden oft besonders hydrophile Gadolinium(III)-Komplexe verwendet. Diese sorgen dafür, dass zwischen den Elektronenspins der Kontrastmittel und den Kernspins der Wassermoleküle Dipol-Dipol-Wechselwirkungen auftreten, die zur Reduzierung der T_1- und T_2-Relaxationszeit führen.[21,25,26]

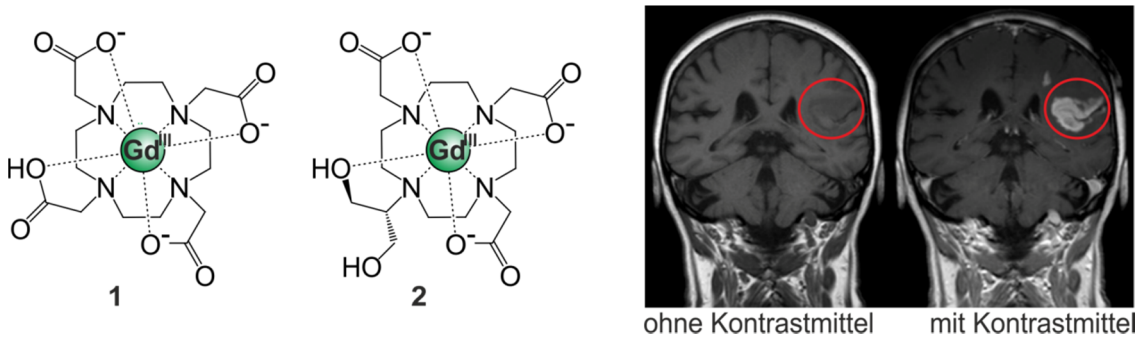

Abbildung 2: Links: Die Kontrastmittel Gadotersäure (**1**) und Gadobutrol (**2**). Rechts: Die MRT-Aufnahme eines Kopfes nach einem Hirninfarkt mit und ohne Kontrastmittel.[9] Das Eindringen des Kontrastmittels in das Hirngewebe ist auf eine Störung der Blut-Hirn-Schranke zurückzuführen.

Die Gadolinium(III)-Komplexe besitzen sieben ungepaarte Elektronen (S = 7/2) und haben damit ein großes magnetisches Moment. Dadurch wird eine sehr hohe Relaxivität erreicht. Letztere ist ein Maß für die Effektivität eines Kontrastmittels.[27] Durch diesen Aspekt sind die Gadolinium(III)-Komplexe anderen paramagnetischen Spezies überlegen und haben schon bei geringen Konzentrationen einen enormen Einfluss auf den Kontrast in MRT-Experimenten.[25] Aufgrund der Toxizität des freien Gadolinium(III)-Ions erfolgt die Anwendung als Kontrastmittel in stabilen Komplexverbindungen. Dies wird in der Praxis meistens durch koordinierende Chelatliganden bewerkstelligt.[22,28] Ein Beispiel hierfür ist die Gadotersäure (**1**) (Abbildung 2), bei welcher der Chelat-Ligand 1,4,7,10-Tetraazacyclododecan-1,4,7,10-tetraessigsäure (DOTA) verwendet wird. Dieser stellt die Basis der meisten Gd(III)-Kontrastmittel dar. Das ähnlich stabile Derivat Gadobutrol (**2**) weist verglichen mit **1** eine bessere Wasserlöslichkeit auf, wodurch es noch konzentrierter (1.00 mol/L) verabreicht und der Kontrast weiter verstärkt werden kann.
Kontrastmittel können mit Relaxivitätsänderung auf bestimmte Wechselwirkungen reagieren. Von solchen sogenannten intelligenten Kontrastmitteln erhofft man sich physiologische Parameter direkt im MRT messen zu können.

1.1.3 Intelligente Kontrastmittel

Die genannten Gd(III)-Kontrastmittel sind paramagnetisch und somit in MRT-Scans permanent sichtbar. Mit diesen Kontrastmitteln kann einerseits die Darstellung anatomischer Strukturen verbessert werden, andererseits kann die Injektion eines Kontrastmittel-Bolus für die Perfusionsbildgebung genutzt werden.[29] Um weitere neue Anwendungsfelder zu ermöglichen, wird an sogenannten intelligenten Kontrastmitteln geforscht, die durch ihre speziellen Eigenschaften auf metabolische Aktivitäten oder physiologische Parameter reagieren können.[30]

In den vergangen Jahren konnten einige Ansätze an intelligenten Kontrastmitteln veröffentlicht werden. So konnten Gd(III)-Chelate entwickelt werden, die auf bestimmte enzymatische Aktivitäten oder den pH-Wert reagieren.[31] Weitere neue Kontrastmittel zeigten eine Abhängigkeit von der Temperatur,[32] der Konzentration von Thiolen,[33] Kohlenhydraten[34] und bestimmten Ionen.[35]

Es gibt zwei unterschiedliche Mechanismen, die zu einer Relaxivitätsänderung führen können.[36] In der Abbildung 3 werden diese beiden Mechanismen schematisch dargestellt. Im ersten Fall (A) wird gezeigt, wie die Relaxivität durch eine Änderung des Abstandes zwischen dem paramagnetischen Zentrum und dem Kernspin (^{1}H-Kernspin der Wassermoleküle) verändert wird. Dies gelingt durch eine komplette Sättigung der Koordinationssphäre, wodurch ein direkter Kontakt zwischen Wassermolekülen und Metall unterbunden wird und somit keine bzw. nur eine geringere Relaxivität vorliegt. Durch die Unterbrechung der Abschirmung wird dem Wasser ein direkter Zugang zum paramagnetischen Zentrum ermöglicht. Hierdurch kommt es zu einer Aktivierung der *inner sphere*-Relaxation, welche verglichen mit der *second sphere*- und *outer sphere*-Relaxation den größten Parameter des Relaxationsprozesses ausmacht. Solch ein Modell wurde erstmals von MOATS vorgestellt.[37]

Hinsichtlich des Mechanismus (A) wir schnell deutlich, dass im vorliegendem Fall die Kontrastmittel durchgängig aktiviert sind, da der Einfluss der *second sphere* und *outer sphere* auf die Relaxation nicht verhindert werden kann. Somit ist die Stärke des Kontrastes änderbar, jedoch nicht komplett abschaltbar. Im zweiten Modell (B) hat dieser Nachteil keinen Bestand.

Mittels eines Spinübergangs kommt es zu einer Änderung des magnetischen Moments des Metallzentrums (Abbildung 3). Dies lässt sich dadurch erklären, dass bestimmte Metallionen sowohl im Low-Spin (LS)- als auch im High-Spin (HS)-Zustand vorliegen können. Die Metallionen im Zentrum des Kontrastmittels besitzen, verglichen mit dem HS im LS, keine oder weniger ungepaarte Elektronen, was das magnetische Moment verringert oder bei gerader Anzahl an Elektronen aufhebt. Dies kommt einem inaktiven Zustand des Kontrastmittels gleich. Aus diesem Grund ist die Änderung des Spins ein äußerst interessanter Prozess für Kontrastmittel, dessen Potential bisher völlig außer Acht gelassen wurde.

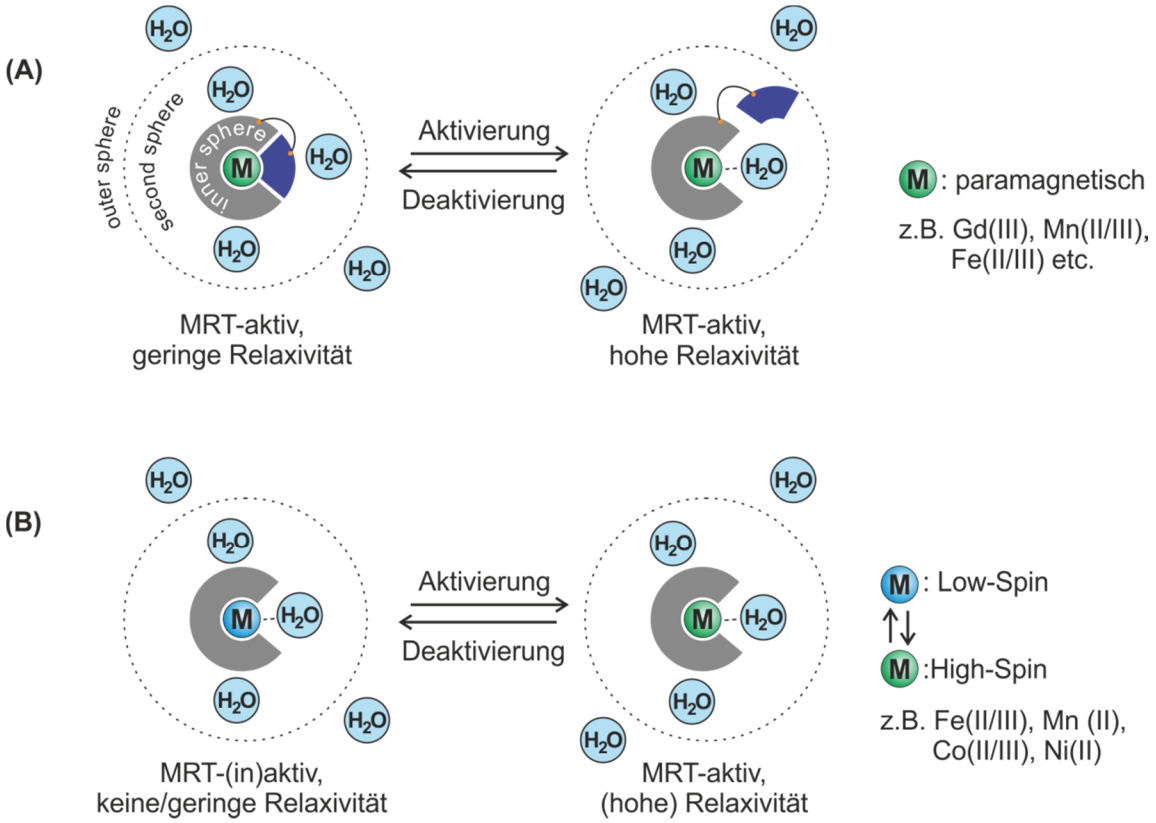

Abbildung 3: Darstellung zweier unterschiedlicher Mechanismen, welche die Relaxivität der MRT-Kontrastmittel beeinflussen. (A) Die Relaxivität des Kontrastmittels wird durch eine direkte Wechselwirkung zwischen paramagnetischem Zentrum und Kernspin verändert. (B) Eine Spin-Änderung des Metallions zwischen High-Spin und Low-Spin ändert das magnetische Moment des Komplexes und dadurch seine Relaxivität.[9]

1.1.4 Spin Crossover

Übergangsmetalle, welche in einer $3d^4$–$3d^7$ Elektronenkonfiguration vorliegen, können in verschiedenen elektronischen Zuständen vorliegen und in speziellen Fällen sogar ihren Zustand ändern. Hierbei ist das wohl bekannteste Beispiel der Spin Crossover (SCO), welcher erstmals im Jahr 1931 durch CAMBI *et al.* an einem Fe(III)-Komplex beschrieben wurde.[22,38] In den folgenden Jahren folgten weitere Veröffentlichungen.[39,40,41]

Als Spin Crossover selbst wird ein Übergang zwischen zwei metastabilen Zuständen beschrieben. Hierbei handelt es sich um einen energetisch niedrigen Zustand, dem Low-Spin (LS), und einen energetisch höheren Zustand, dem High-Spin (HS). Für oktaedrische Metallkomplexe der Elektronenkonfiguration $3d^4$–$3d^7$ gibt es für die Verteilung der Elektronen auf die Orbitale verschiedene Möglichkeiten: Bei der ersten Möglichkeit werden entsprechend der Hundschen Regel die d-Orbitale zunächst mit je einem Elektron desselben Spins aufgefüllt. Anschließend werden die restlichen Elektronen mit einem entgegengesetzten Spin auf die energetisch niedrigsten Orbitale gesetzt.[42] Hierbei wird von einem HS gesprochen. Der LS stellt die zweite

Möglichkeit der Verteilung dar. Bei dieser werden zuerst die energetisch niedrigeren d-Orbitale mit gepaarten Elektronen aufgefüllt, woraufhin die verbleibenden Elektronen auf die energetisch höheren d-Orbitale verteilt werden. Die meisten SCO sind für Fe(II)-Komplexe bekannt (Abbildung 4).[43]

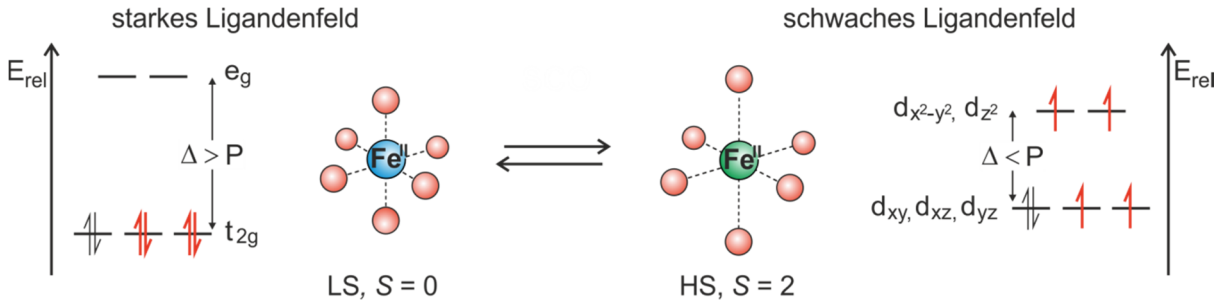

Abbildung 4: Darstellung des Spin Crossovers in oktaedrischen Fe(II)-Komplexen. Links: Ein starkes Ligandenfeld führt dazu, dass die Ligandfeldaufspaltung (Δ) größer ist als die Spinpaarungsenergie (P), wodurch ein Low-Spin vorliegt. Rechts: Ein schwaches Ligandenfeld führt dazu, dass die Ligandenfeldaufspaltung (Δ) kleiner als die Spinpaarungsenergie (P) ist, wodurch ein High-Spin vorliegt.[9]

Die reversible Änderung eines Spin-Zustandes kann durch das Zuführen von Energie erreicht werden, wie zum Beispiel durch Wärme oder Druck. Dabei kommt es zu einer Veränderung der Ligandenfeldaufspaltung (Δ), was zu einem Spin-Übergang führen kann (Abbildung 4). Die Änderung der elektronischen Struktur bringt meist eine Farbänderung des Materials mit sich.

Ein Spin-Übergang läuft auf unterschiedliche Arten ab. Dies hängt von dem Grad der kooperativen Wechselwirkungen ab, was als Betrag der durch den SCO verursachten Abstandsänderung durch das Gitter verstanden werden kann. In gelösten Komplexen läuft der Spin-Übergang immer graduell ab (Abbildung 5, Fall a)). Im Festkörper treten hingehen aufgrund der kooperativen Wechselwirkungen unterschiedliche Übergangsarten auf.

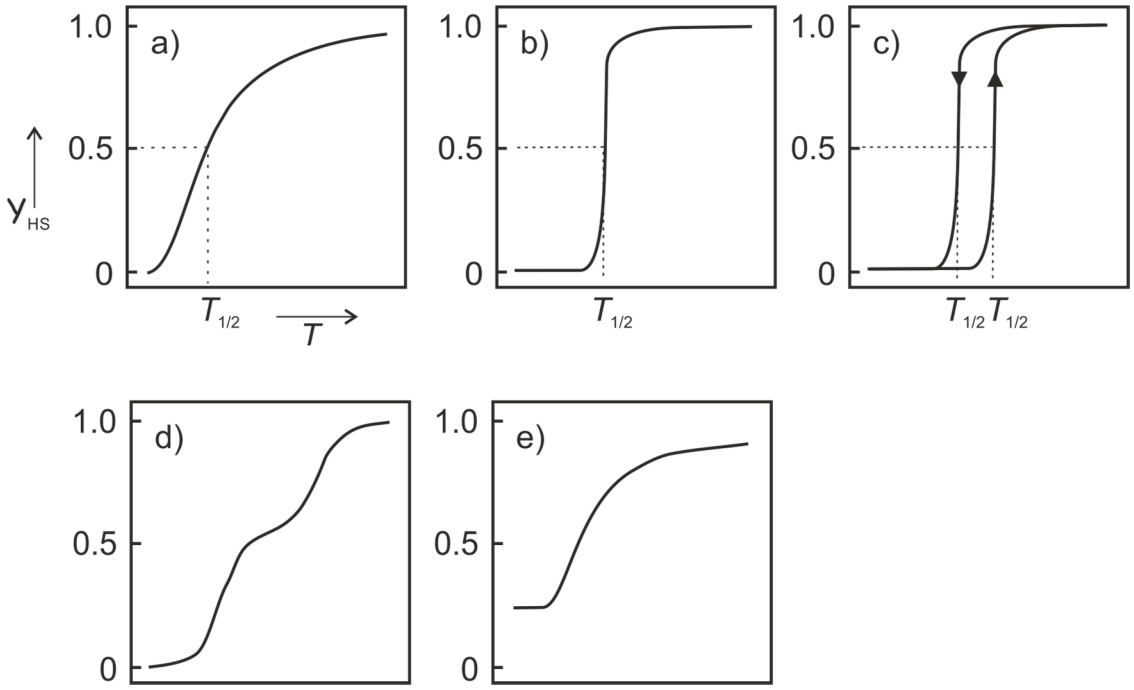

Abbildung 5: Darstellung der Spinübergangstypen a-e.[44]

Wenn zum Beispiel ein SCO innerhalb weniger Kelvin von der einen zur anderen Phase übergeht, wird dies als ein abrupter SCO bezeichnet. Hierbei wird zwischen Übergängen ohne Hysterese (Abbildung 5, Fall b)) und mit Hysterese (Abbildung 5, Fall c)) unterschieden. Des Weiteren kann der SCO ebenfalls über zwei Schritte graduell sowie abrupt verlaufen (Abbildung 5, Fall d)) oder ein Plateau enthalten (Abbildung 5, Fall e)).[44]

Neben dem Druck und der Temperatur spielt das Licht eine wichtige Rolle bei bestimmten Modellen der Spin-Änderung. So konnte in Jahr 1984 die Spin-Schaltung von oktaedrischen Fe(II)-Komplexen durch elektronische Anregung des Metallzentrums mittels Licht durchgeführt werden. Dieser Effekt ist sehr effizient sowie reversibel und wird als Light-Induced Excited Spin State Trapping (LIESST) bezeichnet. Zu erwähnen ist allerdings, dass sich der LIESST-Effekt auf Festkörperverbindungen bzw. sehr niedrige Temperaturen beschränkt.[41,45]

Eine Weiterentwicklung des LIESST ist der Ligand-Driven Light-Induced Spin Change Effekt (LD-LISC), welcher ebenfalls auf dem SCO beruht.[40,46,47] Hierbei wird der Spinübergang durch eine photoinduzierte Änderung der Ligandenfeldstärke bewerkstelligt und nicht wie bei LIESST mittels direkter elektronischer Anregung des Metallzentrums.

Basierend auf dem LD-LISC wurde für Nickel(II) der Light-Driven Coordination-Induced Spin State Switch (LD-CISSS) entwickelt.[48,49] Bei diesem Effekt wird durch

Licht keine Änderung der Ligandenfeldstärke hervorgerufen. Stattdessen kommt es zu einer lichtgetriebenen Assoziation bzw. Dissoziation der Liganden, wodurch die Koordinationszahl und demzufolge die Komplexgeometrie geändert werden. Angelehnt an den LD-CISSS wurden in der Arbeitsgruppe HERGES photoschaltbare MRT-Kontrastmittel entwickelt und als sogenannte Plattenspielermoleküle veröffentlicht.[49]

1.1.5 Prinzip des Plattenspielermoleküls und dessen Weiterentwicklung

Der Aufbau des Moleküls **3** kann mit einem Plattenspieler verglichen werden. Hierbei bildet ein Nickel(II)porphyrin die Schallplatte, während der Tonarm aus einer Azobiphenyleinheit besteht, die über eine der vier *meso*-Positionen mit dem Porphyrin verbunden ist. Als Nadel können verschiedene koordinierende Stickstoffbasen eingesetzt werden. In der Abbildung 6 ist der Prototyp mit Pyridin dargestellt.

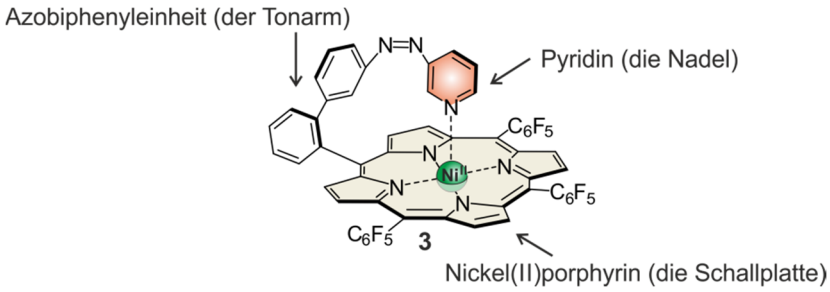

Abbildung 6: Strukturformel eines Plattenspielermoleküls **3**.

Bei dem Plattenspielerkonzept wird der LD-CISSS genutzt. Hierbei muss, um eine Anwendung als photoschaltbares MRT-Kontrastmittel zu ermöglichen, eine Unabhängigkeit der Spinschaltung von der Ligandenkonzentration gewährleistet sein. Dies lässt sich nur mittels eines intramolekularen Mechanismus realisieren. In dem gewählten Design ist nur die metastabile *cis*-Konfiguration zur intramolekularen Koordination in der Lage. Die *trans*-Konfiguration kann keine Konformation einnehmen, in der eine Koordination möglich ist.[50]

So konnte im Jahre 2011 durch VENKATARAMANI *et al*. der erste Plattenspieler publiziert werden, welcher in der Lage ist, durch einen intramolekularen LD-CISSS das Nickel(II)-Metallion zwischen LS und HS zu schalten. Folglich kommt es erst durch die Belichtung und das Schalten der Azoeinheit dazu, dass das Kontrastmittel eingeschaltet (paramagnetisch) wird und dieses somit einen Einfluss auf die Relaxationszeit nehmen kann.[49]

Um die Schalteffizienz des Plattenspielers zu verbessern, wurden die elektronischen Eigenschaften des Porphyrins sowie des photoschaltbaren Liganden genauer untersucht, da solch eine Änderung einen großen Einfluss auf die Koordination des Pyridins hat.

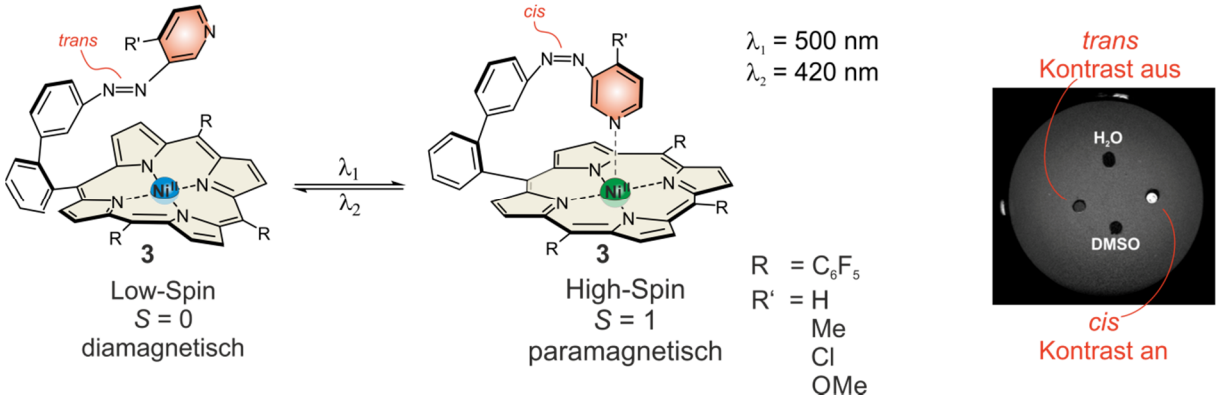

Abbildung 7: LD-CISSS durch intramolekulare Koordination.

Durch elektronenziehende *meso*-Substituenten am Porphyrin kann die Stärke der Assoziation des Pyridins erhöht werden (Abbildung 7).[51,52] Außerdem wird durch die Einführung elektronenschiebender Gruppen in *para*-Position, des koordinierenden Pyridin-Stickstoffes, die Donorstärke des Pyridins erhöht, was auch eine Erhöhung der Koordination zufolge hat.[53] Mit diesem Wissen konnten DOMMASCHK *et al.* die Schalteffizienz durch das Einführen verschiedener Substituenten in *para*-Pyridin-Position deutlich verbessern.[51,53]

Mit einer Methoxy-Gruppe in *para*-Position kann derzeit die höchste Schalteffizienz von über 80 % erreicht werden. Darüber hinaus weist dieser Plattenspieler eine hohe Photostabilität und die sehr lange thermische Halbwertszeit des metastabilen *cis*-Isomers auf.[53]

Wie im Kapitel über intelligente Kontrastmittel beschrieben, ist nicht nur die Schalteffizienz von großer Bedeutung, sondern auch die Temperatur- sowie die pH-Abhängigkeit. So gelang es HEITMANN *et. al.*, durch die Änderung des Tonarms zusätzlich auf diese Parameter einzugehen.[54]

Durch solche intelligenten Kontrastmittel ist nun der Grundstein für die funktionelle Tumordiagnostik gelegt, welche zusätzlich zur Lokalisierung auch physiologische Eigenschaften der Tumore darstellen kann. Dadurch wird eine Optimierung von Krankheitsbekämpfungen realisiert.

1.2. Konventionelle Krebstherapien

Jede Art von Krebs erfordert eine individuelle Behandlung, wofür eine Reihe von Therapien zur Verfügung stehen. Jedoch führen diese in fast allen Fällen zu starken Nebenwirkungen.[55] Am häufigsten richtet sich hierbei die Therapiewahl nach dem aktuellen Krankheitsstadium. Häufig angewandte Therapiearten sind:

1.2.1 Chirurgische Entfernung

Die älteste Behandlungsmethode ist die chirurgische Entfernung von Tumoren. Hierbei wird das betroffene Gewebe operativ entfernt, jedoch muss ebenfalls ein relativ großer Bereich vom umliegenden gesunden Gewebe entfernt werden, um sicherzustellen, dass keine Tumorzellen im Körper verbleiben. Da jedoch die Lokalisierung von Metastasen sehr schwer ist, werden diese oftmals nicht vollständig entfernt, wodurch das Risiko neuer Metastasen besteht.[56]

1.2.2 Strahlentherapie

Bei dieser Therapie wird der Tumor mit ionisierender Strahlung, z.B. hochenergetischer Röntgenbremsstrahlung, behandelt. Hierbei wird ausgenutzt, dass das Tumorgewebe strahlenempfindlicher ist als das gesunde Gewebe. Problematisch bei dieser Methode ist dennoch, dass die hohe Belastung durch Röntgenstrahlung schädlich für den Körper des Patienten ist.[56]

1.2.3 Chemotherapie

Eine weitere häufig verwendete Therapieform ist die Chemotherapie. Hierbei werden meistens Zytostatika verwendet, die aus natürlichen oder synthetischen Substanzen bestehen und Einfluss auf das Zellwachstum und die Zellteilung haben. Problematisch bei diesem Vorgehen ist jedoch, dass die Chemotherapie mehrfach durchgeführt werden muss, da immer nur ein gewisser Prozentsatz der malignen Zellen abgetötet wird und so einige der Tumorzellen Resistenzen gegen das Zytostatikum entwickeln können. Zusätzlich werden alle anderen gesunden Zellen im Körper gehemmt oder gar geschädigt. Dies führt beispielsweise zu dem bekannten Phänomen des Haarausfalls, da hier die Teilung der Haarwurzelzellen verhindert wird.[56]

1.2.4 Photodynamische Therapie

Unter dem Aspekt der Risiken und starken Nebenwirkungen der oben vorgestellten Krebstherapien ist es von großem Interesse, alternative Methoden zu entwickeln,

welche eine bessere Verträglichkeit und Selektivität haben, jedoch in der Effektivität vergleichbar sind. Solch eine Alternative stellt eine relativ neue Behandlungsform, die Photodynamische Therapie (PDT), dar.[57,58] Sie findet bereits Anwendung in vielen Bereichen, wie beispielsweise der Urologie, Dermatologie, Pulmonologie, Gastroenterologie und Ophthalmologie.[59]

1.2.4.1 Geschichtlicher Hintergrund

Geschichtlich blickt die Phototherapie auf eine lange Entwicklung zurück. Vor tausend Jahren war die therapeutische Wirkung von Licht schon bekannt und wurde in Ländern wie China, Indien und dem alten Ägypten zur Behandlung verschiedener Krankheiten eingesetzt.[60,61] Bei dieser Methode wurde Nutzen aus dem Licht und unterschiedlichen Bestandteilen von Pflanzenarten gezogen.[61,62] In der heutigen Zeit wird diese Art von Therapie als Photochemotherapie bezeichnet, welche auch der Grundstein der Entwicklung der PDT war.

Die eigentliche PDT weist hingegen eine deutlich jüngere Gesichte auf und wurde Anfang des letzten Jahrhunderts von dem damaligen Studenten RAAB eingeführt.[63] Dieser konnte den Zelltod von Wimperntierchen (*Paramecium caudatum*) durch eine Interaktion zwischen Licht und chemischen Substanzen nachweisen, was unmittelbar zur Entdeckung des photodynamischen Effekts führte.[64,65] Kurz darauf wurden die ersten Versuche am Menschen in Kooperation mit dem Hautarzt JODLBAUER durchgeführt, wobei unter anderem Hauttumore mit lokal aufgetragenem Eosin behandelt wurden.[66,67] Aufbauend auf diesen Ergebnissen konnte die PDT durch TAPPEINER, JESIONEK, JODLBAUER und HAUSMANN immer weiterentwickelt werden.[65,67,68]

Im Jahre 1975 wurde der nächste wichtige Meilenstein in der Entwicklung der PDT von DOUGHERTY gesetzt.[69] Hierbei konnte bei 48 % brustkrebserkrankter Mäuse ein Rückgang des Tumors beobachtet werden. 1984 wurde dann sogar der erste Photosensibilisator (Dihämatoporphyrin-ether) von der *American Food and Drug Administration* zugelassen.

Mittlerweile wird die PDT auf zahlreichen leicht zugänglichen Oberflächen wie bei Haut-, Blasen-, Lungen- und Speiseröhrenkrebs verwendet. Auch andere Krebsarten wie Hirntumore können durch die verbesserte Glasfasertechnik therapiert werden.[70]

1.2.4.2 Prinzip der Photodynamischen Therapie

Die Grundlagen der PDT lassen sich vereinfacht in zwei Schritte unterteilen, welche meist mehrere Stunden auseinander liegen. Schritt eins ist die Verabreichung des Photosensibilisators (PS). Daraufhin erfolgt in Schritt zwei die eigentliche Behandlung, die Bestrahlung des Tumorgewebes. Dies wird in Abbildung 8 verdeutlicht.

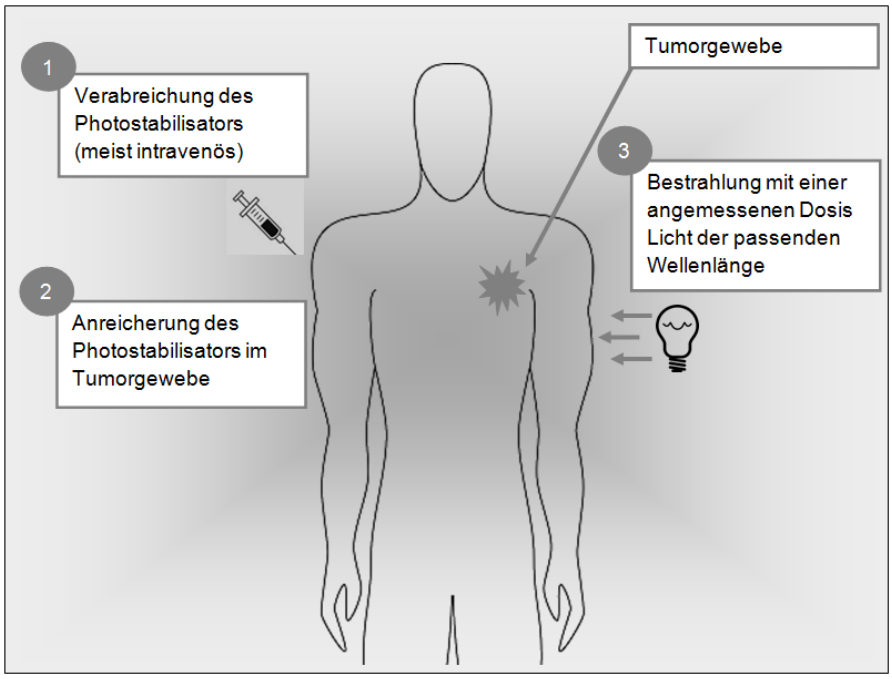

Abbildung 8: Schematische Darstellung des Prinzips der Photodynamischen Therapie.

Die meisten Photosensibilisatoren werden intravenös verabreicht. Im Falle von Oberflächentumoren können die PS auch als Creme auf die Haut aufgetragen werden. Ein besonders wichtiger Aspekt beim Verabreichen des PS ist, dass sich dieser nur im Tumorgewebe anreichert, damit keine gesunden Zellen bei der Behandlung beschädigt werden. Dies funktioniert in der Anwendung ausgezeichnet. Vermutet wird, dass es an dem viel höheren Stoffwechsel und anderen Eigenschaften der malignen Tumore liegt. Jedoch gibt es derzeit noch keine Beweise zu dieser These.[71]

Bei der darauffolgenden Behandlung wird der mit PS angereicherte Tumor mit einer Lichtquelle bestrahlt, wobei diese in dem Wellenlängenbereich des Absorptionsmaximums des PS liegt. Es kommt zur Anregung des PSs. Nun gibt es zwei mögliche Mechanismen: (1) Der aktivierte PS überträgt die Energie an weitere Moleküle, welche Sauerstoffgruppen beinhalten, wodurch dann wiederum Sauerstoffradikale generiert werden (Typ I-Reaktion). (2) Es findet ein direkter

Energietransfer auf molekularen Sauerstoff ($^3O_2$) statt, bei dem Singulett-Sauerstoff ($^1O_2$) gebildet wird (Typ II-Reaktion). Bei beiden Mechanismen sind die entstandenen Produkte in der Lage, zelluläre Strukturen zu schädigen. Vermutet wird jedoch, dass lediglich der Typ II-Mechanismus für die zytotoxische Wirkung der PS verantwortlich ist.[72]

PS sind allerdings nicht nur wegen ihrer toxischen Wirkung auf das Gewebe von hohem Stellenwert für die Medizin, sondern auch wegen zusätzlicher Eigenschaften. So sind die meisten PS in der Lage zu fluoreszieren und können folglich für die Diagnostik verwendet werden. Die PS werden hierbei nach Verabreichung durch Licht bestimmter Wellenlängen zur Fluoreszenz angeregt. So kann die genaue Lage des Tumors ermittelt werden, da der PS zum Großteil nur im malignen Gewebe angereichert wird und die Fluoreszenz dort am stärksten ist (Abbildung 9).

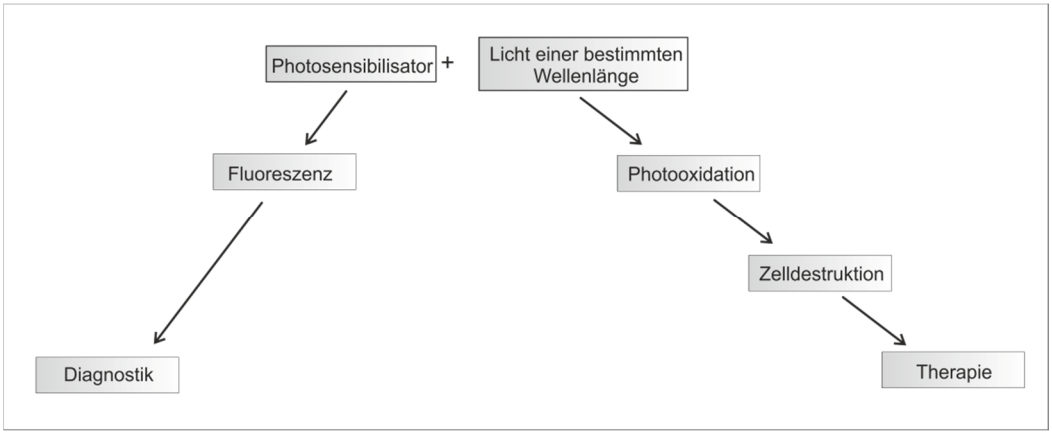

Abbildung 9: Einsatzmöglichkeiten von PS in der Medizin.

1.2.4.3 Die unterschiedlichen Photosensibilisatoren

Als Photosensibilisatoren werden Substanzen bezeichnet, welche in der Lage sind, absorbierte Lichtenergie durch Energie- bzw. Elektronentransfer auf andere Moleküle zu übertragen.[73] Zum Einsatz kommen beispielsweise Thiazin-Farbstoffe, welche ein dreifaches Ringsystem aufweisen und in der Zahnheilkunde verwendet werden. Darüber hinaus finden die wasserlöslichen Farbstoffe Methylen-Blau und Toluidin-Blau ihre Anwendung, da diese aufgrund ihrer chemischen Eigenschaften biologische Membranen schlecht passieren können.[73]

Die meisten derzeit verfügbaren PS gehören jedoch der Stoffklasse der Porphyrine und deren Derivaten an. Hierbei werden die Hämatoporphyrinderivate als Photosensibilisatoren der ersten Generation bezeichnet.[56] Als PS der zweiten Generation werden Porphyrine mit einer chemischen Struktur, welche eine

verbesserte Effektivität und Selektivität aufweisen, bezeichnet.[74] In Tabelle 1 wird eine Übersicht der derzeit klinisch am häufigsten verwendeten Photosensibilisatoren aufgezeigt.[75]

Tabelle 1: Übersicht häufig verwendeter Photosensibilisatoren.

Kurzname	Substanz	Handelsname	Anregungs-Wellenlänge
HPD	Hämatoporphyrinderivat	Photofrin	630 nm
BPD-MA	Benzoporphyrinderivat Monoacid Ring A	Verteporfin	690 nm
*m*THPC	*Meso*-tetrahydroxyphenylchlorin	Foscan	652 nm
ALA	5-Aminolävulinsäure	Levulan	630 nm
Lu-Tex	Lutetiumtexaphyrin	Lutrin	732 nm

Zusätzlich sollten die Photosensibilisatoren für aktuelle klinische Anwendungen möglichst viele der folgenden Forderungen erfüllen:[76]

- großtechnische und kostengünstige realisierbare Synthesen,
- hohe Stabilität gegenüber chemischen/enzymatischen Reaktionen im Organismus,
- geringe Toxizität des Photosensibilisators und aller durch Bestrahlung entstehenden Produkte,
- gute Wasserlöslichkeit,
- gute Dosierbarkeit,
- einfaches Verabreichen (z. B. Injektion, Salbe, Spray),
- selektive Anreicherung im umliegenden Tumorgewebe,
- hohe Absorption im NIR-Bereich,
- hohe Triplett-Quantenausbeute und lange Triplett-Lebenszeit,
- vollständige Ausscheidung aus dem Organismus,
- geringe Ausbleichung während der Belichtung.

Bei der Entwicklung neuer PS wird ein großes Augenmerk auf eine bathochrome Verschiebung gelegt. Hierdurch wird erreicht, dass der Farbstoff eine starke Absorptionsbande innerhalb der Grenzen des therapeutischen Fensters aufweist, welches als bio-optisches Fenster bezeichnet wird.

1.2.4.4 Das bio-optische Fenster

Das bio-optische Fenster liegt im Wellenlängenbereich von 600 - 900 nm und somit im nahinfraroten Spektralbereich (NIR).[77] Im NIR-Wellenlängenbereich weist Licht im Gewebe eine gute Transmission auf und ist in der Lage, mehrere Zentimeter tief in den menschlichen Körper einzudringen.[78] Hierbei nimmt die Eindringtiefe von Licht zwischen 600 nm und 900 nm kontinuierlich zu.[79]

Das bio-optische Fenster wird im kurzwelligen Wellenlängenbereich vom Hämoglobin und Cytochromoxidase abgegrenzt,[79] die im Bereich unterhalb der 600 nm die wichtigsten Absorber des Gewebes sind. Im höherliegenden Wellenlängenbereich wird das bio-optische Fenster durch die starke Absorption des Wassers oberhalb von 900 nm geschlossen und lässt somit keine starke Transmission mehr zu.[78,80]

Aus diesem Grund ist es besonders wichtig, PS sowie auch Kontrastmittel zu entwickeln, welche eine starke Absorption im bio-optischen Fenster aufweisen. Diese Thematik ist ein Hauptbestandteil der vorliegenden Arbeit.

2 Aufgabenstellung

Diese Arbeit ist dem Design und der Weiterentwicklung von neuen intelligenten Kontrastmitteln sowie der Synthese von effizienten wasserlöslichen NIR-Photosensibilisatoren gewidmet.

Basierend auf dem Konzept des Plattenspielers, welches von HERGES publiziert wurde, wird der Light-Driven Coordination-Induced Spin State Switch (LD-CISSS) von Fe(III) erforscht.

Fe(III)-Porphyrine existieren wie Ni(II)-Porphyrine in unterschiedlichen Spinzuständen, sodass sie ideal als schaltbare Kontrastmittel verwendet werden können. Hierbei liegen die fünffach koordinierten Komplexe überwiegend im High-Spin von S = 5/2 vor, wohingegen sechsfach koordinierte Komplexe zu einem Low-Spin von S = 1/2 tendieren.

Aufgrund des höheren Spinunterschieds zwischen dem High-Spin- und dem Low-Spin-Zustand in Eisen(III)-Porphyrinen ist, verglichen mit Ni(II)-Porphyrinen, ein besserer Kontrast im MRT-Experiment zu erwarten. Da das Eisen(III)-Zentralatom im Vergleich zu Nickel(II) einen zusätzlichen anionischen Liganden in der Koordinationssphäre bevorzugt, muss das Porphyrindesign angepasst werden. Um die Koordinationsumgebung abzuschirmen, soll die Koordinationsstelle durch eine Brücke über das Porphyrin, die zusätzlich über eine koordinierende Triazoleinheit verfügt, belegt werden. Das Design von LD-CISSS Fe(III)-Porphyrinen ist in der Abbildung 10 schematisch dargestellt.

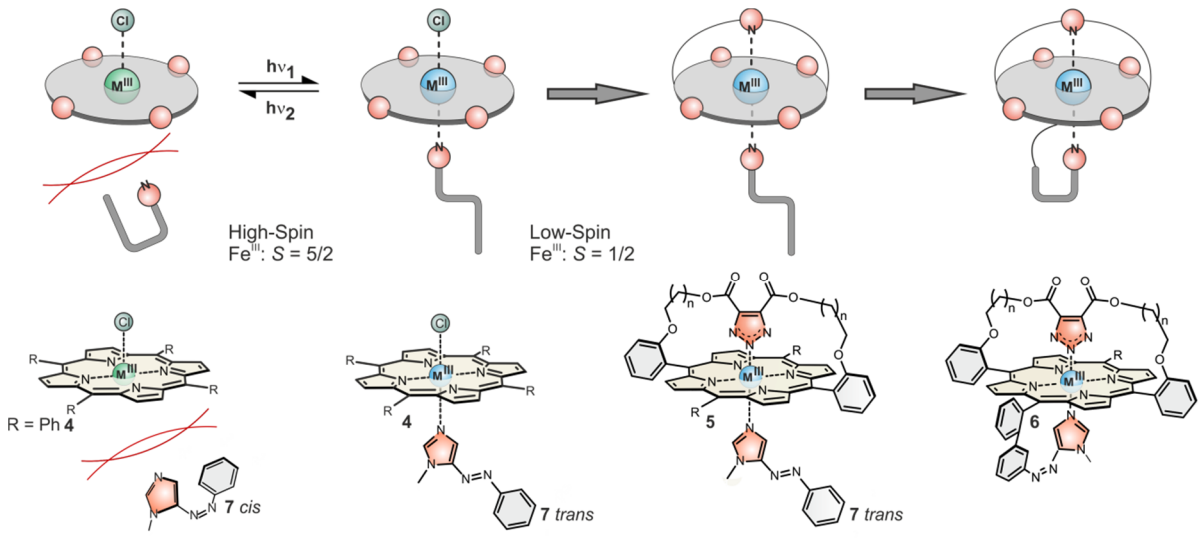

Abbildung 10: Schematische Darstellung eines verbrückten Eisen(III)-Plattenspielers.

Für die Weiterentwicklung intelligenter MRT-Kontrastmittel ist jedoch nicht nur der Paramagnetismus (Spindifferenz ΔS) von großer Bedeutung, sondern auch die Anwendbarkeit im menschlichen Körper. Aus diesem Grund wurde sich in einem Teilbereich dieser Arbeit mit der Funktionalisierung von Porphyrinen beschäftigt.
Hierbei sollen die Porphyrine mittels einer Diels-Alder-Reaktion in ihre reduzierten Derivate, Chlorine, Isobakteriochlorine und Bakteriochlorine überführt werden (Abbildung 11).

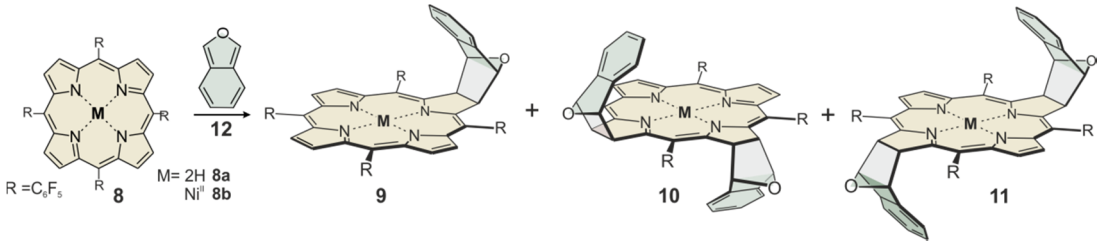

Abbildung 11: Darstellung einer möglichen Funktionalisierung von Porphyrinen.

Der Zugang zu diesen neuen Molekülen würde ein weiteres Spektrum an Anwendungen ermöglichen. Bezogen auf die Nickel- und Eisen-Plattenspieler könnten so MRT-Kontrastmittel synthetisiert werden, welche eine Absorption im NIR-Bereich besitzen. Dies würde erstmals ein LD-CISSS im bio-optischen Fenster ermöglichen, wodurch eine reversible Schaltung im menschlichen Körper durch Belichtung mit externen Lichtquellen anstelle von Sonden gelingen könnte.
Darüber hinaus spielen die reduzierten Porphyrinderivate in der Photodynamischen Therapie als Photosensibilisatoren eine entscheidende Rolle. Aus diesem Grund sollte zudem auch die Erzeugung von Singulett-Sauerstoff und somit ihr Nutzen für die photodynamische Therapie untersucht werden.

3 Publikationen und deren Zusammenfassungen

3.1 Lichtinduzierte Änderung des Spinzustandes von Eisen(III)

Das kontrollierte Schalten des Spinzustandes von Übergangsmetallionen, insbesondere von Fe(II) und Fe(III), ist eine wichtige Voraussetzung für selektives, effizientes und katalysiertes Schalten in einer Vielzahl von Metalloenzymen.[81,82] Derzeitigem Stand zufolge kann die Änderung des Spins von oktaedrischen Fe(II)-Komplexen mittels elektronischer Anregung durchgeführt werden. Dieser Effekt ist seit 1984 unter dem LIESST (Light-Induced Excited Spin State Trapping)-Effekt bekannt (Abbildung 12).[41,45] Der Spinübergang von Fe(II) mittels LIESST ist reversibel und effizient, jedoch funktioniert dieser Effekt nur bei niedrigen Temperaturen und ist auf Festkörper beschränkt. Eine weitere Möglichkeit, den Spin zu ändern, kann über den LD-LISC (Ligand-Driven Light-Induced Spin Change)-Effekt realisiert werden (Abbildung 12), welcher ebenfalls auf dem Spin Crossover beruht.[40,46,47] Hierbei wird jedoch nicht das Metallzentrum elektronisch angeregt, stattdessen kommt es zu einer photoinduzierten Änderung der Ligandenfeldstärke.

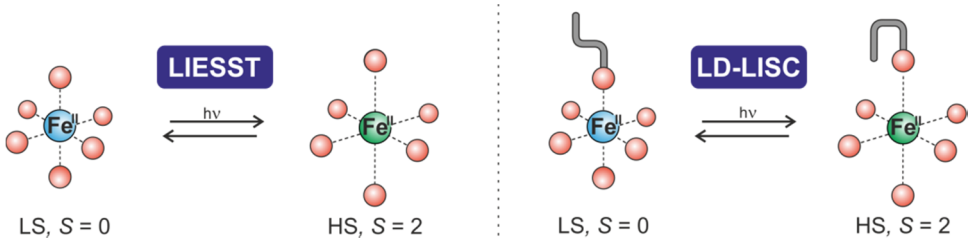

Abbildung 12: Schematische Darstellung des LIESST-Effektes (links) und des LD-LISC-Effektes (rechts).

Als Liganden eignen sich Moleküle, die in unterschiedlichen Photoisomeren vorliegen können und dabei ihre Koordinationsstärken ändern, um so eine Änderung des Spinzustands hervorzurufen.[83] Problematisch ist dennoch die unzureichende Stabilität der Moleküle, die eine Anwendung ausschließlich unter inerten Bedingungen zulässt. Des Weiteren sind die Photostabilität und die Schalteffizienz gering. Aus diesem Grund sind bis jetzt weder der LIESST noch der LD-LISC für das breite Spektrum an Anwendungen geeignet, welches der SCO von Eisen ermöglicht. Hierzu zählen unter anderem die Entwicklung von neuen Speichermedien sowie die Erforschung intelligenter photoschaltbarer MRT-Kontrastmittel.

Light Controlled Switching of the Spin State of Iron(III)

Sreejith Shankar, Morten Peters, Kim Steinborn, Bahne Krahwinkel, Frank Sönnichsen, Dirk Grote, Wolfram Sander, Thomas Lohmiller and Rainer Herges

Nature Communications **2018**, *9*, 1-12.
doi:10.1038/s41467-018-07023-1

Eigenanteil: Die Synthesen des überbrückten Porphyrins und die dazugehörigen Messungen (EVANS, ^{1}H-NMR, HR-MS, UV) wurden von Morten Peters durchgeführt. Das Manuskript wurde von Dr. Sreejith Shankar und Prof. Dr. Rainer Herges verfasst.

Zusammenfassung

In dieser Publikation wird die erste lichtgesteuerte molekulare Spinschaltung auf Fe(III)-Basis vorgestellt. Hierbei wird als Ausgangskomplex das leicht zugängliche Fe(III)tetraphenylporphyrinperchlorat verwendet, welches in einer Aceton/ Dimethylsulfoxid-Lösung einen High-Spin-Komplex ($S = 5/2$) mit zwei axialen DMSO-Liganden bildet (Abbildung 13).

Der Spin-Switching-Prozess wird durch einen photoschaltbaren Azopyridinliganden induziert, welcher so entworfen ist, dass er in seiner *trans*-Konfiguration mit einer 180-fach stärkeren Bindungskonstante als Dimethylsulfoxid (DMSO) zum Eisenporphyrin koordiniert und somit einen Low-Spin-Komplex ($S = 1/2$) mit zwei axialen *trans*-Azopyridin-Liganden bildet (Abbildung 13). Wird das *trans*-Azopyridin mit Licht der Wellenlänge 365 nm bestrahlt, erfolgt die Isomerisierung zum *cis*-Isomer. Dieses *cis*-Isomer ist durch *tert*-Butylgruppen sterisch gehindert und ist in diesem System nicht mehr in der Lage, an das Eisenporphyrin zu binden. Dadurch kordiert das DMSO wieder, wodurch der High-Spin-Zustand regeneriert wird. Dieser Ligandenaustausch bzw. Spin-Switching-Prozess ist reversibel. Mit einer Wellenlänge von 435 nm kann das *cis*-Azopyridin wieder in die *trans*-Form überführt werden, welche wiederum die DMSO-Liganden verdrängt. Dieses Experiment zeigt nach mehr als 1000 Schaltzyklen unter Luft, Feuchtigkeit und Raumtemperatur keine Veränderungen, Nebenreaktionen oder Zersetzungen.

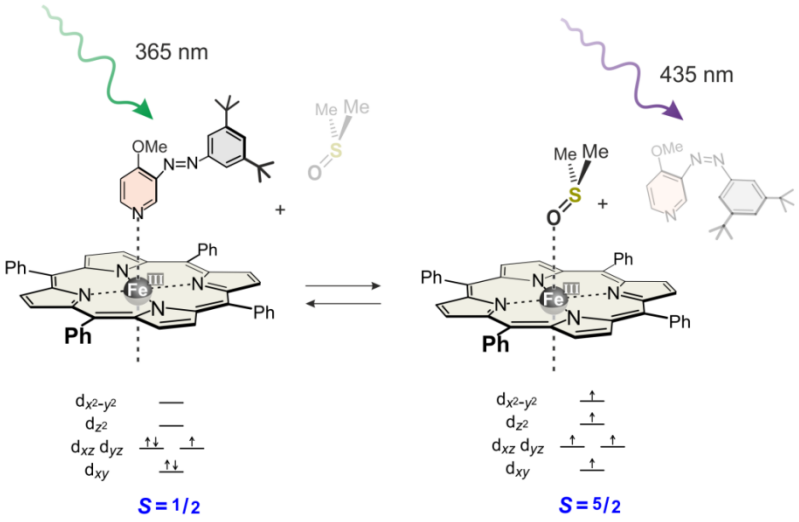

Abbildung 13: Darstellung der lichtgesteuerten molekularen Spinschaltung auf Fe(III)-Basis.

Neben der Spin-Schaltung ändern sich in diesem Modell auch noch einige andere Parameter reversibel. Zum Beispiel verschiebt sich das Redoxpotential analog zu enzymatischen Hämproteinen um 58 mV, beim Wechsel von $S = 1/2$ zu $S = 5/2$.[81,82] Eine weitere besonders interessante Fähigkeit dieses Systems ist, dass die NMR-Protonenrelaxationszeit (Relaxivität) reversibel um den Faktor zehn geschaltet werden kann. Somit ist der Grundstein gelegt, Eisen(III)-Porphyrine als intelligente Kontrastmittel in der MRT zu verwenden und einen Eisen-Plattenspieler auf der Basis dieser Arbeit zu synthetisieren.[49,53]

nature COMMUNICATIONS

ARTICLE

DOI: 10.1038/s41467-018-07023-1 OPEN

Light-controlled switching of the spin state of iron(III)

Sreejith Shankar[1,2], Morten Peters[1], Kim Steinborn[1], Bahne Krahwinkel[1], Frank D. Sönnichsen[1], Dirk Grote[3], Wolfram Sander[3], Thomas Lohmiller[4,5], Olaf Rüdiger[4] & Rainer Herges[1]

Controlled switching of the spin state of transition metal ions, particularly of Fe^{II} and Fe^{III}, is a prerequisite to achieve selectivity, efficiency, and catalysis in a number of metalloenzymes. Here we report on an iron(III) porphyrin with a photochromic axial ligand which, upon irradiation with two different wavelengths reversibly switches its spin state between low-spin ($S = {}^1/_2$) and high-spin ($S = {}^5/_2$) in solution (DMSO-acetone, 2:598). The switching efficiency is 76% at room temperature. The system is neither oxygen nor water sensitive, and no fatigue was observed after more than 1000 switching cycles. Concomitant with the spin-flip is a change in redox potential by ~60 mV. Besides serving as a simple model for the first step of the cytochrome P450 catalytic cycle, the spin switch can be used to switch the spin-lattice relaxation time T_1 of the water protons by a factor of 15.

[1] Otto Diels-Institute for Organic Chemistry, University of Kiel, 24118 Kiel, Germany. [2] Photosciences and Photonics Section, Chemical Sciences and Technology Division, CSIR – National Institute for Interdisciplinary Sciences and Technology (CSIR – NIIST), Industrial Estate P.O., Pappanamcode, Thiruvananthapuram 695019, India. [3] Ruhr-Universität Bochum, Organic Chemistry II, 44801 Bochum, Germany. [4] Max-Planck-Institute for Chemical Energy Conversion, 45470 Mülheim a. d. Ruhr, Germany. [5] Present address: Berlin Joint EPR Lab, Institute for Nanospectroscopy, Helmholtz Zentrum Berlin für Materialien und Energie, Kekuléstraße 5, 12489 Berlin, Germany. Correspondence and requests for materials should be addressed to R.H.(email: rherges@oc.uni-kiel.de)

Spin-state switching is the key step in a number of enzymatic reactions, particularly in C-H activation processes. Controlled spin flips guide reactants and intermediates into reaction pathways with low barriers, and induce catalytic cycles leading to products that otherwise would be formed only under drastic reaction conditions. Cytochrome P450 is a particularly well-investigated example[1,2]. Substrate binding to cytochrome P450 triggers a change in the spin state of the heme-bound Fe(III) from the resting state, low spin ($S = {}^1/_2$), to high spin ($S = {}^5/_2$). Concomitantly, the reduction potential changes, and a cascade of reactions follows, leading to the selective oxidation of alkyl and aromatic C-H bonds. Methane monooxygenases (MMOs) even convert methane to methanol under ambient conditions[3], a process without precedence in artificial systems. Besides the importance in spin-catalysis, molecular spin-state switching in solution and on surfaces is gaining importance in other fields as well. Molecular spin switches have been proposed as components in molecular electronics, photonics, and spintronics[4]. Particularly interesting, as well, is their potential use as responsive contrast agents in magnetic resonance imaging (MRI), providing spatial information of metabolic parameters in vivo[5].

Whereas spin-state switching in the solid state (spin-crossover mainly in Fe(II) complexes) is a well-investigated phenomenon, the first magnetically bistable compound in solution was published only recently (2011)[6]. Since then, research in the field considerably gained momentum[7–10]. The original molecular spin switches were based on Ni(II) porphyrins[11–13]. The square planar complexes are diamagnetic ($S = 0$), but turn paramagnetic ($S = 1$) upon coordination of axial ligands. Coordination/decoordination from the Ni ion was achieved by the use of photoswitchable axial ligands that were either covalently bound to the porphyrin or substituted in such a way that the *cis* configuration would not bind because of steric hindrance. A number of further transition metal ions change their spin state upon changing their coordination number, such as Fe^{2+}, Fe^{3+}, Co^{2+}, Mn^{2+}, and Mn^{3+}, providing larger variations ($\Delta\mu$) in their magnetic moments than Ni^{2+}.

Herein, we report the first photoswitchable, magnetically bistable Fe(III) porphyrin in solution that is stable at ambient conditions in solution, including moisture and air. Upon irradiation with light of 365 and 435 nm, the spin-state switches reversibly between low spin ($S = {}^1/_2$) and high spin ($S = {}^5/_2$), accompanied by a change in redox potential. The species involved and their spin states are characterized using several independent methods, and the mechanism is elucidated in detail.

Results

Spectroscopic investigations. In terms of redox behavior and spin states, iron is probably the most complicated and adaptable element in the periodic table. A number of different spin states are possible in every oxidation state, many of which are close in energy. More than 3000 papers have been published solely on iron porphyrins, particularly in view of their biological relevance. Several reviews summarize the field[14,15]. Iron(III) porphyrins exhibit four different spin states: low spin, $S = {}^1/_2$, $(d_{xz}d_{yz})^4(d_{xy})^1$, low spin, $S = {}^1/_2$, $(d_{xy})^2(d_{xz}d_{yz})^3$, intermediate spin, $S = {}^3/_2$, $(d_{xy})^2(d_{xz},d_{yz})^2(d_z2)^1$, and high spin, $S = {}^5/_2$, $(d_{xy},d_{xz},d_{yz},d_z2,d_x2_{-y}2)$. Moreover, if the energy difference of intermediate spin ($S = {}^3/_2$) and high spin ($S = {}^5/_2$) is close to the spin-orbit coupling constant (which is mostly the case), linear combinations of high-spin and intermediate-spin states are formed, which have been coined admixed-spin states, $S = a\ {}^3/_2 + (1 - a)\ {}^5/_2$ ($a = 0$–1)[16]. The axial ligands and the nature of the porphyrin are the primary determinants of the spin state. Pure 4-coordinate Fe(III) porphyrins without axial coordination are intermediate spin ($S = {}^3/_2$)[17]. Axial coordination of two oxygen ligands gives rise to an admixed-spin state ($S = {}^3/_2, {}^5/_2$) if they are weak, or a high-spin species ($S = {}^5/_2$) if they are strong. Fe(III) porphyrins with two strong nitrogen ligands are low spin ($S = {}^1/_2$). Besides their electronic properties, the steric bulk of axial ligands is decisive in controlling the spin state. Bulky substituents neighboring the coordinating nitrogen atom not only reduce the binding constant, but also favor the high-spin state[18]. If the counter-ion is weakly binding (e.g., ClO_4^-) and the axial ligands are weak, more basic porphyrins (i.e., electron-donating substituents) favor admixed-spin states, and less basic porphyrins (electron-withdrawing substituents) favor low-spin states. Strongly binding anions, such as chloride in the absence of axial ligands, favor the formation of high-spin complexes. Hydrogen bonding to the chloride weakens coordination and the spin-state changes to intermediate spin[19]. Upon judicious choice of the electronic and steric properties of the porphyrin and axial ligands, the complexes can be tuned in such a way that they are close to the $S = {}^1/_2 \rightleftharpoons S = {}^5/_2$ spin-crossover point[20,21]. In this region, small changes in ligand field strength or steric hindrance would switch the spin state of Fe(III). Since spin-state chemistry and axial ligand exchange processes of Fe(III) porphyrin complexes are very intricate, we used several independent methods to characterize our compounds in solution: (a) proton nuclear magnetic resonance (^{1}H NMR) pyrrole and phenyl shifts, (b) ultraviolet–visible (UV–vis) absorption, (c) magnetic moments, and (d) electron paramagnetic resonance (EPR) spectroscopy. The largest change in spin state ($\Delta S = 2$) in Fe(III) porphyrins is achieved upon switching between high spin ($S = {}^5/_2$) and low spin ($S = {}^1/_2$). In designing our molecular spin switch, we avoided admixed-spin ($S = {}^5/_2, {}^3/_2$) and intermediate-spin states ($S = {}^3/_2$), not only because they reduce the change in magnetic moment ($\Delta\mu$) but also because these species are sensitive to water and oxygen, and they are difficult to characterize (e.g., the ^{1}H NMR pyrrole shift varies between +80 and −63 ppm)[14]. To achieve a reliable, robust, and large spin switch, we designed a system which would change the axial coordination between two strong oxygen ligands (high spin, $S = {}^5/_2$) and two strong nitrogen ligands (low spin, $S = {}^1/_2$) upon irradiation with two different wavelengths.

For our experiments, we chose the readily available Fe(III) tetraphenylporphyrin perchlorate ($FeTPPClO_4$) as the base porphyrin, and photoswitchable azopyridines as axial ligands (photodissociable ligands, PDLs). $FeTPPClO_4$ is admixed-spin ($S = {}^3/_2, {}^5/_2$) in non-coordinating and weakly coordinating solvents[11,22–24], and very sensitive towards water and oxygen[25]. In acetone, a 6-coordinate complex (Fig. 1) is formed with two weakly binding acetone molecules as axial ligands. The formation constants $K_1'' = 0.82$ and $K_2'' = 1.08$ L mol^{-1} have been determined by following the ^{1}H NMR shifts of the phenyl protons upon titration of a solution of $FeTPPClO_4$ in CD_2Cl_2 with acetone-d_6 (see Supplementary Figures 21, 24, 25, Supplementary Table 4, and Methods, Calculation of apparent equilibrium constants). Pyrrole shift (40.2 ppm), magnetic moment (4.5 B.M., see Methods, Magnetic susceptibility—Evans measurements) and EPR signals (medium-intensity, high-spin signals at $g = 5.94$ and 2.0, and a very small signal at $g = 4.7$–4.8[16] (see Supplementary Figures 36-37 and Methods, EPR spectroscopy) are indicative that the species is admixed spin with a substantial contribution of high spin. To generate a pure high-spin ($S = {}^5/_2$) complex, and to increase ΔS upon switching, we added dimethyl sulfoxide (DMSO)-d_6 to the solution which is known to form a 2:1 high-spin ($S = {}^5/_2$) complex with $FeTPPClO_4$ (Fig. 1 and Supplementary Figure 1)[26]. High-spin iron(III) porphyrins exhibit a typical Q band at ~690 nm (Supplementary Figure 19a). Upon titration with DMSO and monitoring the increase of the absorption at 686 nm, we

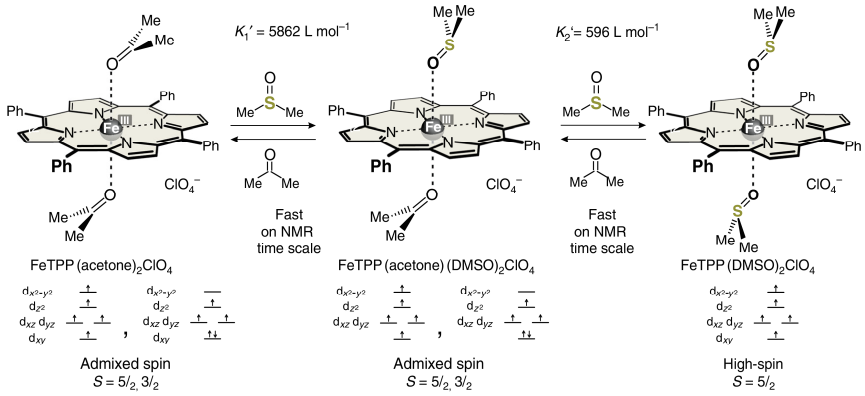

Fig. 1 Determination of formation constants. Formation constants of high-spin FeTPP(DMSO)$_2$ClO$_4$ determined by following the absorption at 686 nm upon titration of the FeTPP(acetone)2ClO$_4$ complex in acetone with DMSO-d_6 at 25 °C. These values were confirmed by NMR titration

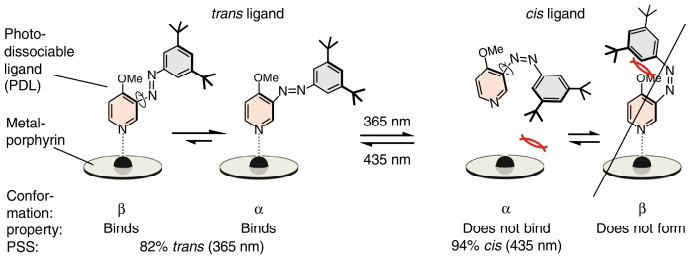

Fig. 2 Design of the photodissociable ligand (PDL) based on photoswitchable phenyl azopyridine. Irradiation with UV light (365 nm) switches the *trans* isomer to the *cis* form. Visible light triggers reisomerization back to the *trans* form. The photostationary states (PSS) of the two processes are *trans*/*cis* 75:25 (435 nm), and 6:94 (365 nm). The methoxy group in 4-position of the pyridine was introduced to increase the coordination strength, and to prevent the formation of the *β* conformation of the *cis* isomer. The two *t*-Bu groups at the phenyl ring increase steric repulsion with the porphyrin in the *cis* form, however, have no effect on the coordination of the *trans* configuration

determined the complex formation constants $K_1' = 5862\ \mathrm{L\ mol^{-1}}$ and $K_2' = 596\ \mathrm{L\ mol^{-1}}$ (see Supplementary Figures 19b, 26-28). These formation constants were confirmed by NMR titration ($K_1' = 5372\ \mathrm{L\ mol^{-1}}$ and $K_2' = 580\ \mathrm{L\ mol^{-1}}$) following the phenyl and pyrrole shifts (see Supplementary Figures 22, 29, 30, Supplementary Table 7, and Methods, Calculation of Apparent equilibrium constants)[27,28].

The magnetic moment of 5.8 B.M. (Evans, see Methods, Magnetic susceptibility—Evans measurements) and the EPR data (large-intensity, high-spin signals at $g = 5.92$ and 2.0, see Supplementary Figure 36 and Methods, Electron paramagnetic resonance (EPR) spectroscopy) confirm a high-spin $S = {}^5/_2$ state for a solution of 0.2 mM FeTPP$^+$ and 47.12 mM DMSO-d_6 in acetone-d_6. The precise composition of the solution derived from K_1' and K_2' is 0.01% FeTPP(acetone)$_2^+$, 3.5% FeTPP(acetone)(DMSO)$^+$, and 96.5% FeTPP(DMSO)$_2^+$. This stable solution, mainly consisting of high-spin FeTPP(DMSO)$_2$ClO$_4$, was used for further switching experiments with PDLs based on azopyridine.

Azopyridine-based PDL. The azopyridine was designed in such a way that it strongly coordinates to Fe(III) in its *trans* configuration (Fig. 2), forming a low-spin $S = {}^1/_2$ complex. However, upon switching to the *cis* isomer under UV light, steric hindrance between the *t*-Bu groups and the porphyrin ring prevents binding (for the synthesis of the azopyridine see Supplementary Figure 41 and Methods, Synthesis)[29,30].

Irradiation with visible light (435 nm) regenerates the *trans* isomer which returns to the coordination site. Conversion of the thermodynamically more stable *trans* to the metastable *cis* isomer with UV light is very efficient. The photostationary state (PSS) at 365 nm is 94% *cis*, and 6% *trans*, and the PSS of the back-reaction at 435 nm is 75% *trans*, and 25% *cis* (see Supplementary Figure 5, Supplementary Table 1, and Methods, PSS of the phenyl azopyridine **2** and PSS of azopyridine). This incomplete conversion to the binding *trans* isomer does not compromise the overall switching efficiency, because an excess of the ligand is used[21]. Hence, the azopyridine is ideally suited as a PDL. The PSS are virtually the same in the presence of the porphyrin (Supplementary Figure 6, Supplementary Tables 1, 11, 12). Obviously, no quenching of the excited state of the azopyridine by the porphyrin occurs. Substitution of the pyridine ring in 4-position with a methoxy group was necessary to increase the binding constant, and to prevent the formation of the *β* conformation of the *cis* isomer (see Fig. 2 and Supplementary Figure 4). Thermal half-life of the metastable *cis* isomer with 164 days at 27 °C is very long (Supplementary Figure 7). In the presence of the Fe(III) porphyrin the half-life is reduced to 18 days which is still more than sufficient to serve as a

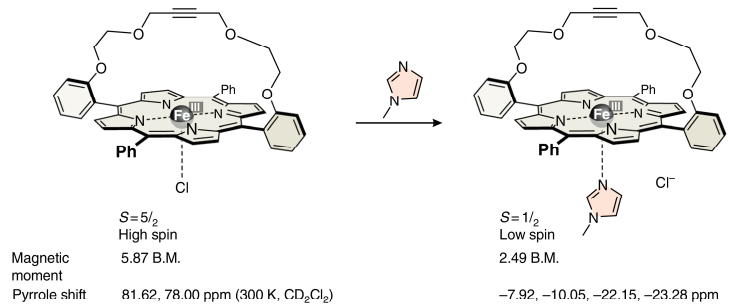

Fig. 3 A strapped porphyrin as a model compound. A strapped porphyrin was used to model the properties of a 5-coordinate Fe(III) porphyrin with one strong axial nitrogen ligand. The ^{1}H NMR pyrrole shifts and the effective magnetic moment indicate that the chloride complex is high spin and the 1:1 imidazole complex is low spin

photochemical switch (see Supplementary Figure 8 and Methods, Half-life ($t_{½}$) of *cis* azopyridine (*cis*-**2**)). With a strong Soret band of the Fe(III) porphyrin around 400 nm (Supplementary Figure 17), the photoexcitation may not be restricted to the PDL ; the event of the Fe(III) porphyrin getting excited, at least partially, cannot be rigorously excluded while irradiating at 365 or 435 nm. The porphyrin in its excited state does not seem to have a noticeable impact on the photoisomerization mechanism of the PDL, since the PSS of the ligand remains largely unaffected by the presence or absence of the porphyrin. However, a slightly longer irradiation time is required for the PDL to arrive at its PSS in the presence of the strongly absorbing porphyrin.

Discussion

The light-driven spin-state switching experiments with our electronically fine-tuned Fe(III) porphyrin system and the sterically and electronically designed axial ligand were monitored by several methods: NMR, UV–vis, EPR, Evans, and potentiometry, to unanimously determine the structure and magnetic properties of the species involved in the spin-state switching process.

In contrast to acetone/DMSO, axial ligand exchange of DMSO/azoypyridine is slow on the NMR time scale. Upon titration of the high-spin acetone/DMSO solution of $FeTPPClO_4$ (0.2 mM $FeTPP^+$, 47.12 mM DMSO-d_6 in acetone-d_6) with the PDL, the signal of the pyrrole protons at 68.6 ppm decreases and a new signal at −14.7 ppm appears (Supplementary Figure 2). Unfortunately, the high-spin signal at 68.6 ppm is very broad, and integration of the NMR signals is not sufficiently accurate to derive a binding model, and to accurately determine coordination constants. We therefore monitored the titration by UV–vis spectroscopy (Supplementary Figure 20). High-spin ($S = {}^5/_2$) $FeTPP^+$ complexes exhibit characteristic bands (Q bands) at 690 nm (Supplementary Figure 19a)[31,32], whereas low-spin ($S = {}^1/_2$) $FeTPP^+$ does not absorb above 650 nm (Supplementary Figure 20a). The decreasing absorption at 686 nm as a function of added azopyridine yields a binding isotherm (Supplementary Figure 20b), which was analyzed by non-linear optimization[33] (see Methods, Calculation of apparent equilibrium constants). A binding model that includes all conceivable species should consider the starting complex $FeTPP(DMSO)_2^+$, the mixed complex $FeTPP(DMSO)(azopy)^+$, and the 1:2 complex $FeTPP(azopy)_2^+$. The solution of the initial DMSO complex $FeTPP(DMSO)_2^+$ has been thoroughly characterized (see above), the properties of the pure low-spin 1:2 complex $FeTPP(azopy)_2^+$ can be determined by dissolving $FeTPPClO_4$ in pure 4-methoxypyridine. However, the properties of the mixed complex cannot be directly determined, since it is not a stable species. It is not known whether coordination of a single strong nitrogen ligand to $FeTPP^+$ is sufficient to induce a spin switch to the low-spin state. We therefore synthesized a strapped porphyrin in which one of the two axial binding sites is sterically shielded (Fig. 3, see Methods, Syntheses). The chloride complex (similar to FeTPPCl) is high spin as indicated by the pyrrole proton shifts (81.6, 78.0 ppm), and by the magnetic moment (5.87B.M., see Methods, Magnetic susceptibility—Evans measurements). Note that in contrast to $FeTPP^+$, the structure of the strapped porphyrin does not exhibit a fourfold symmetry axis and the eight pyrrole protons are not symmetry equivalent. Upon addition of *N*-methyl-imidazole, the chloride is replaced by the strong nitrogen ligand. The coordination of a second ligand is prevented by the bridge. Magnetic moment (2.49 B.M.) and the pyrrole proton shifts (−7.92, −10.05, −22.15, and −23.28 ppm) clearly indicate that the complex is low spin ($S = {}^1/_2$) with a slow exchange of the ligand on the NMR time scale (see Supplementary Figures 42-43 and Methods, Synthesis). Hence, coordination of one nitrogen ligand is sufficient to induce the spin switch.

Based on the properties of the strapped porphyrin, we assume that the mixed complex $FeTPP(DMSO)(azopy)^+$ is low spin as well. Further evidence for the low-spin state of the mixed complex is provided by the fact that the fitting of the binding isotherm is considerably superior with the assumption that the spin change is induced by the coordination of the first azopyridine ligand (see Supplementary Figures 31–33 and Methods, Calculation of apparent equilibrium constants). Based on this model, both binding constants K_1 and K_2 can be accurately determined by UV–vis titration of the DMSO complex with the azopyridine (see above). According to the analysis of the binding isotherm, the first DMSO ligand is replaced by azopyridine with $K_1 = 314\ \mathrm{L\ mol^{-1}}$ and the second with $K_2 = 868\ \mathrm{L\ mol^{-1}}$ (Fig. 4 and Supplementary Table 10). Thus, azopyridine is a much stronger ligand than DMSO and displacement of the second DMSO is much more favorable than expulsion of the first DMSO ligand. Therefore, the concentration of the mixed (DMSO/azopyridine) complex is always small. This is favorable for our spin switching efficiency, because the isomerization of one azopyridine ligand should facilitate the replacement of the second by DMSO leading to an efficient conversion to the high-spin $FeTPP(DMSO)_2^+$ complex.

Spectroscopic parameters as well as magnetic properties consistently prove that the addition of azopyridine converts the high-spin ($S = {}^5/_2$) $FeTPP(DMSO)_2^+$ to a low-spin ($S = {}^1/_2$) complex. Upon addition of 75 equivalents of *trans* azopyridine to a solution of 0.1 mM $FeTPP^+$, and 25.87 mM DMSO-d_6 in acetone$_6$, the EPR high-spin signals at $g = 5.92$ and 2.0 are reduced to approximately 3% of their initial intensity (see Supplementary

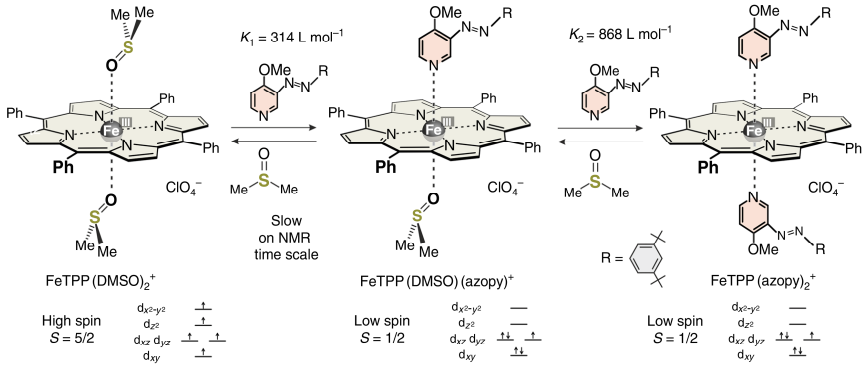

Fig. 4 Titration of high-spin FeTPP(DMSO)$_2^+$ with the photodissociable ligand (PDL) azopyridine. The binding isotherm was derived from the decrease of the UV-vis absorption band at 686 nm upon addition of the *trans* azopyridine to a solution of 0.1 mM FeTPP$^+$, and 25.87 mM DMSO-d_6 in acetone-d_6 at 25 °C (see Methods, Far-vis spectroscopy of the spin-state changes and Calculation of apparent equilibrium constants). The binding constants K_1 and K_2 were determined under the assumption that the mixed complex FeTPP(DMSO)(azopy)$^+$ is low spin

Figure 36 and Methods, EPR spectroscopy), and the UV–vis absorption at 686 nm almost completely vanished (Supplementary Figure 20a). According to Evans measurements (see Methods, Magnetic susceptibility—Evans measurements), the effective magnetic moment of the solution is 2.1 B.M. The high-spin pyrrole proton signal at 68.8 ppm disappeared, and a new signal at −14.7 ppm (typical for low-spin FeTPP$^+$ complexes) appeared (Supplementary Figure 2). Unfortunately, only a very low intensity large g_{max} signal for the low-spin complex at $g = 3.4$ was visible in the EPR spectrum in frozen acetone (Supplementary Figure 36), most probably because of solubility problems, and aggregation. In frozen CH_2Cl_2, however, the low-spin signal is visible more clearly (Supplementary Figures 37-38). More detailed information about the exact composition of the solution can be derived from the binding constants: K_1', K_2' and K_1, K_2. In a solution of 0.2 mM FeTPP$^+$, 47.12 mM DMSO-d_6, and 15 mM *trans* azopyridine in acetone-d_6, the following species are in equilibrium: 0.0006% FeTPP(acetone)$_2^+$, 0.17% FeTPP(acetone)(DMSO)$^+$, 4.7% FeTPP(DMSO)$_2^+$, 11.9% FeTPP(DMSO)(azopy)$^+$, and 83.2% FeTPP(azopy)$_2^+$. The species with at least one strong nitrogen ligand (azopyridine), and that with two strong oxygen ligands (DMSO), add up to 95.1% low-spin and 4.7% high-spin porphyrin, respectively, which is consistent with the EPR observations.

This solution that is predominantly low spin was subjected to irradiation with light of 365 nm. The *trans* azopyridine isomerizes to the *cis* configuration with a conversion rate of 94.4% *cis* (determined by ^{1}H NMR, Supplementary Figure 5) in the PSS. Isomerization, in turn, leads to increasing steric demand, and dissociation of the *cis* azopyridine ligand. The binding constant of *cis* azopyridine to FeTPP$^+$ was too low to be determined. Addition of a solution of 94% *cis* and 6% *trans* azopyridine to an acetone-d_6 or acetone-d_6/DMSO-d_6 solution of FeTPP$^+$ does not change the ^{1}H NMR spectrum beyond what would be expected from the coordination of the residual *trans* isomer (6%) (see Supplementary Figure 3b and Methods, Switching experiments in NMR,). Hence, *cis* azopyridine is a much weaker ligand than DMSO (in contrast to the *trans* isomer); therefore, DMSO rebinds to the axial coordination sites replacing the azopyridine. The situation is rather complicated since both azopyridine ligands must be replaced by DMSO to switch the spin state. Mixed complexes, such as FeTPP(DMSO)(azopyridine)$^+$ in the equilibrium, have to be considered as well. The exact composition of the solution in the PSS can be calculated from the binding constants of DMSO (K_1', K_2'), and *trans* azopyridine (K_1, K_2) to FeTPP$^+$ determined by NMR and UV–vis titration (see above), and the *cis*/*trans* ratio of azopyridine at the PSS, determined by ^{1}H NMR (Supplementary Figure 6). At the PSS (365 nm) the solution contains 81.4% high-spin FeTPP(DMSO)$_2^+$, 11.3% low-spin FeTPP(azopy)(DMSO)$^+$, and 4.3% low-spin FeTPP(azopy)$_2^+$ (and very small amounts of the acetone complexes, for a detailed list see Table 1). Upon irradiation with light of 435 nm, the *cis* azopyridine returns to its strongly binding *trans* configuration (24.5% *cis*, 75.5% *trans*), and replaces the DMSO ligands. At the PSS (435 nm), 77.2% low-spin FeTPP(azopy)$_2^+$, 14.7% low-spin FeTPP(DMSO)(azopy)$^+$, and 7.8% high-spin FeTPP(DMSO)$_2^+$ are in equilibrium. In essence, upon irradiation with 365 and 435 nm, we are able to switch between 92:8 and 16:81 low-spin/high-spin equilibria. This corresponds to a switching efficiency of 76%, considering the low-spin ratios (Fig. 5, Table 1, see also Methods, Calculation of apparent equilibrium constants).

To investigate the fatigue resistance of the spin switch, we irradiated the above solution with 365 and 435 nm in an alternating sequence and monitored the ^{1}H NMR spectrum as a function of the number of switching cycles (Fig. 6a and Supplementary Figure 35b). After 5 min irradiation of the NMR tube with 365 nm (light-emitting diode (LED), 12 × 400 mW), the low-spin signal at −14.7 ppm disappeared, and the broad high-spin signal at 66.8 ppm appeared. Upon irradiation of the NMR tube with 435 nm (LED, 12 × 380 mW), the high-spin signal disappeared and the low-spin signal reappeared. There was no observable change in the ^{1}H NMR spectrum after 1000 switching cycles under ambient conditions (air, moisture, 300 K, Supplementary Figure 3a).

Paramagnetic metal ions such as Mn^{2+} ($S = {}^5/_2$) or Gd^{3+} ($S = {}^7/_2$) are known to reduce the longitudinal (or spin–lattice) (T_1), and the transverse (spin spin) relaxation times (T_2) of the solvent nuclei[34]. The relaxation mechanism is mainly due to magnetic dipole interactions during coordination of the solvent molecule to the paramagnetic ion (inner sphere relaxation)[35,36]. Upon rapid coordination/decoordination, a single paramagnetic metal ion can relax more than 10^6 solvent protons within an NMR or MRI experiment, which finally leads to a reduction of T_1 and T_2 of the bulk solvent. Switching of the spin state of FeTPP$^+$ between $S = {}^5/_2$ and $S = {}^1/_2$ leads to a switching of the capability to induce nuclear spin relaxation R_1 (relaxivity $R_1 = \Delta T_1^{-1} \cdot c^{-1}$,

Table 1 Photostationary states of the PDL and different possible complexes of FeTPP$^+$

	PSS 435 nm (%)		PSS 365 nm (%)		
trans azopy	75.5		5.6		
cis azopy	24.5		94.4		
FeTPP(azopy)$_2^+$	77.2	91.9	4.4	15.7	low-spin
FeTPP(azopy)(DMSO)$^+$	14.7		11.3		low-spin
FeTPP(DMSO)$_2^+$	7.8		81.4		high-spin
FeTPP(acetone)(DMSO)$^+$	0.3		2.9		admixed-spin
FeTPP(acetone)$_2^+$	0.001		0.01		admixed-spin

At the photostationary state generated upon irradiation with light of 435 nm (PSS 435 nm), the combined concentration of low-spin species is 91.9%, and at PSS 365 nm this concentration decreases to 15.7%. Hence, the switching efficiency is 76.2%

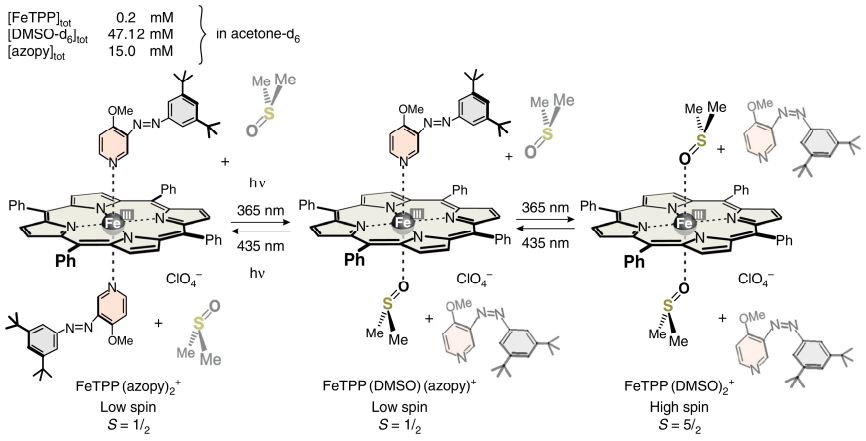

Fig. 5 Light-induced spin switching of iron(III) porphyrin (FeTPP$^+$) using azopy as a PDL. The composition of the solution is calculated from the binding constants K_1',K_2' and K_1, K_2, and is listed for the photostationary states (PSS) at 435 and 365 nm in Table 1. The calculations are based on the assumption that *cis* azopyridine does not coordinate to FeTPP$^+$, and that FeTPP(DMSO)(azopy)$^+$ is a low-spin complex

where ΔT_1 is the difference of T_1 with and without relaxation agent and c the concentration of the relaxation agent). High-spin FeTPP$^+$ has a larger magnetic moment than low-spin FeTPP$^+$ and therefore exhibits a larger relaxivity. Low-spin FeTPP$^+$ ($S = {}^1/_2$) is not completely diamagnetic; however, both axial coordination sites are occupied by strong nitrogen ligands which prevent a fast exchange with the solvent on the NMR time scale (inner sphere relaxation). The low magnetic moment as well as the blockage of axial coordination sites lead to a considerably smaller relaxivity R_1 of the low-spin complex. The relaxivity values R_1, and relaxation times T_1 of a 2.0 mM solution of the high-spin FeTPP$^+$ complex in an acetone-d_6/DMSO-d_6 solution containing 1% acetone and 1% water are given in Table 2. The relaxivity R_1 of acetone, and water with FeTPP$^+$ in the high-spin state is 12.9, and 17.7 times higher than in the low-spin state. The relaxation time T_1 changes from 5.05 to 1.68 s (acetone), and from 0.56 to 0.04 s (water) upon low-spin to high-spin conversion (Table 2, Supplementary Figures 9–11, 13–16, and Supplementary Table 2). Thus, the efficiency in relaxivity switching is considerably higher than in a previous Ni^{2+} porphyrin-based system[5].

In nature, upon binding of a substrate to cytochrome P450 in its low-spin, 6-coordinate resting state, the axial water ligand is released and a 5-coordinate high-spin Fe(III) porphyrin is formed[2]. Concomitant with the spin flip is a change in redox potential[37]. A similar trend has been observed by Walker et al.[38] who investigated a number of iron porphyrins (as models of cytochromes) including FeTPP$^+$ in *N*,*N*-dimethylformamide in the presence and absence of pyridine ligands. Switching of the azopyridine ligand from the *trans* to the *cis* configuration should lead to a shift of the reduction potential. Typical cyclic voltammograms (CVs) obtained for the Fe(III)/Fe(II) redox couple for the low-spin FeTPP$^+$ complex before and after irradiation at 365 nm for 20 min are shown in Fig. 6b. The low-spin complex was found to exhibit a well-defined $1e^-$ oxidation–reduction curve with a half-wave potential of 82±4 mV (vs. standard hydrogen

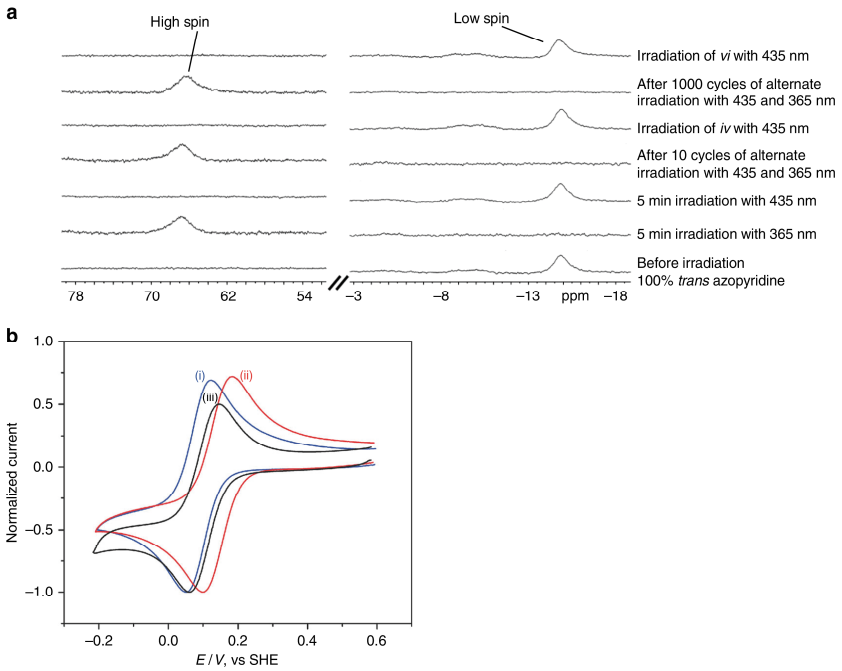

Fig. 6 Switching of the properties of iron porphyrin $FeTPP^+$. **a** Long-term stability (1000 switching cycles) of a solution of 0.2 mM $FeTPPClO_4$, 47.12 mM DMSO-d_6, and 15 mM azopyridine in acetone-d_6 at 300 K upon irradiation with 365 and 435 nm in an alternating sequence (left) sections of ^{1}H NMR spectra between 54 and 78 ppm (high-spin region) and (right) between −18 and −3 ppm (low-spin region). **b** Light-induced switching of the redox potential of a solution containing 0.2 mM $FeTPPClO_4$, 40 mM tetrabutylammonium perchlorate as the supporting electrolyte and 47.2 mM DMSO in acetone (see Methods, Electrochemical measurements). Blue: cyclic voltammogram before irradiation; red: after irradiating with 365 nm for 20 min; black: after irradiation of the above with 435 nm light for 30 min. The experiment was performed using a platinum disk working electrode, platinum counter electrode, and $Ag/AgNO_3$ 0.01M reference electrode at a scan rate of 50 V/s (see Methods, Electrochemical measurements)

Table 2 Relaxivities and relaxation times of the solvent protons

		Relaxivity R_1 ($mM^{-1}s^{-1}$)		Relaxation time T_1 (s)	
		Acetone	Water	Acetone	Water
i	High spin	0.219	10.6	1.68	0.037
ii	Low spin	0.017	0.6	5.05	0.564

Relaxivities R_1 and relaxation times T_1 of a solution of 2.0 mM $FeTPP^+$ and 47.12 mM DMSO-d_6 (i) without and (ii) with 15 mM *trans* azopyridine in acetone-d_6, containing 1% acetone and 1% water

potential (SHE)). After 30 min under 435 nm illumination, the Fe (III)/Fe(II) reduction potential almost returns to its value before the 365 nm illumination (Fig. 6b). If the electrochemical experiments are performed strictly under nitrogen, the switching is reversible (see Supplementary Figure 39 and Methods, Electrochemical measurements). Under air obviously the reduced Fe(II) species reacts with oxygen and the reaction becomes irreversible.

This work presents the first light-controlled molecular spin switch based on Fe(III). Starting complex is the readily accessible, admixed-spin ($S = {}^3/_2$, ${}^5/_2$) Fe(III) tetraphenylporphyrin perchlorate. In an acetone/DMSO solution it forms a well-defined high-spin ($S = {}^5/_2$) complex with two axial DMSO ligands. The spin switching process is induced by a photoswitchable azopyridine ligand. This ligand is designed in such a way that it coordinates to the iron porphyrin in its *trans* configuration with a binding constant 180 times stronger than DMSO, forming a low-spin ($S = {}^1/_2$) complex with two axial *trans* azopyridine ligands. Upon irradiation with 365 nm, the *trans* isomer of the azopyridine ligand photoisomerizes to the *cis* configuration with a conversion ratio of 94.4%. The *cis* isomer is sterically hindered and does not bind to the iron porphyrin, and thus is replaced by DMSO, regenerating the high-spin state. This ligand exchange/spin switching process is reversible. Light (435 nm) converts the *cis* azopyridine back to the *trans* form, which again replaces the DMSO ligands. No fatigue or side reactions have been observed after more than 1000 switching cycles under air and moisture at room temperature.

Alongside the spin-state flipping, several properties change reversibly. The capability of reducing the NMR proton relaxation time (relaxivity) changes by a factor of more than 10. Properly designed iron(III) porphyrins could therefore be used as functional contrast agents in MRI[5,6]. Upon switching the spin state from $S = {}^1/_2$ to $S = {}^5/_2$, the redox potential shifts to more positive values. The active center of cytochrome P450 contains a low spin Fe(III) porphyrin in its resting state. The iron(III) center undergoes a spin flip upon substrate binding, leading to a change in redox potential, which in turn triggers a cascade of reactions,

which finally leads to selective C-H oxidation[1,2]. Spin state switching is also a crucial step in the conversion of methane to methanol by methanotrophic bacteria, using Fe^{3+}-containing enzymes (MMOs)[39]. Nature obviously uses spin flipping to solve difficult catalytic problems that are not susceptible to simple transition state lowering on a given spin-state energy hypersurface.

Control of the spin state might as well be used as a key step in a number of particularly obstinate cases of catalysis in artificial systems, or even industrial processes. We believe that our results could provide a contribution towards this end.

Methods

General experimental procedure. All reactions were carried out in hot air-dried glassware with magnetic stirring under nitrogen atmosphere (when required) using commercially available reagent-grade solvents (dried when necessary, but without purification), and all evaporations were carried out under reduced pressure on Büchi rotary evaporator or Heidolph rotary evaporator below 50 °C, unless otherwise noted. Yields refer to chromatographically and spectroscopically homogeneous materials, unless otherwise stated. Most reagents were purchased from Sigma-Aldrich, ABCR, Alfa Aesar, or Merck and were used as received. Solvents (reagent grade) were purchased from Sigma -Aldrich, ABCR, and Merck. Specific experimental conditions are provided under each section below.

The high-resolution (HR) mass spectra were measured with an APEX 3 FT-ICR with a 7.05 T magnet by co. Bruker Daltonics. Electron impact and matrix-assisted laser desorption/ionization (MALDI) mass spectra were measured with a Biflex III by co. Bruker.

For column chromatography purifications silica gel (Merck, particle size 0.040–0.063 mm) was used. R_f values were determined by thin layer chromatography on Polygram® Sil G/UV$_{254}$ (Macherey–Nagel, 0.2 mm particle size).

Infrared spectra were measured on a Perkin-Elmer 1600 Series FT-IR spectrometer with an A531-G Golden-Gate-Diamond-ATR-unit. Signals were abbreviated with *w*, *m*, and *s* for weak, medium, and strong intensities. Broad signals were additionally labeled with br.

^{1}H and ^{13}C{^{1}H} NMR spectra were recorded on Bruker DRX 500 (^{1}H NMR: 500 MHz, carbon-13 nuclear magnetic resonance (^{13}C NMR): 125 MHz) and Bruker AV 600 (^{1}H NMR: 600 MHz, ^{13}C NMR: 150 MHz) instruments. Chemical shifts are expressed in ppm (δ), using tetramethylsilane (TMS) as internal standard for ^{1}H and ^{13}C nuclei (δH = 0; δC = 0). Multiplicities of NMR signals are designated as s (singlet), d (doublet), t (triplet), q (quartet), quin (quintet), b (broad), and m (multiplet, for unresolved lines). ^{13}C NMR spectra were recorded with complete proton decoupling, on above-mentioned spectrometers.

NMR spectra were measured in deuterated solvents (Deutero). The degree of deuteration is given within parentheses. ^{1}H NMR spectra in reference to the following signals:

$$\text{Chloroform}{-}d_1(99.8\%) : \delta = 7.26\,\text{ppm(s)}.$$

$$\text{Dichloromethane}{-}d_2(99.6\%) : \delta = 5.32\,\text{ppm(t)}.$$

$$\text{Acetone}{-}d_6(>99.5\%) : \delta = 2.05\,\text{ppm(quin)}.$$

NMR investigations. Long term ^{1}H NMR switching experiments were performed on a Bruker 500 MHz NMR spectrometer in acetone-d_6 (>99.5% d). To a 0.2 mM solution of FeTPPClO$_4$ (**1**) in acetone-d_6 (523 µL) in an NMR tube, DMSO-d_6 was added (2 µL), followed by a 120 mM acetone-d_6 solution of *trans* azopyridine (75 µL, final concentration of 15 mM). The NMR tube was sealed and shaken well before measurement. The ^{1}H NMR spectrum showed a characteristic low-spin signal at −14.72 ppm. The tube was then irradiated for 5 min with light of wavelength 365 nm using a custom-made LED machine (12 × 400 mW). During irradiation, constant mixing was ensured via rotating the tube by a mechanical rotator with air cooling using an electric ventilator (fan). The NMR tube was then transferred to the spectrometer and the corresponding spectrum showed the characteristic high-spin signal at +66.8 ppm. The first cycle of irradiation was completed by irradiating the sealed tube with light of wavelength 435 nm (LED 12 × 380 mW) for another 5 min using the exact same set up as described above. The partial switching experiments were repeated for 1000 cycles. Each cycle consisted of the photoconversion of *cis* azopyridine to *trans* azopyridine via alternate irradiation using lights of two different wavelengths (365, 435 nm) and measurement after regular intervals. The LEDs were connected to an automated timer device and the on and off times were fixed at a constant values of 5 min each for each wavelength. The solution was stable even after 1000 continuous cycles of partial switching.

PSS of the phenyl azopyridine **2**: A 15 mM solution of the azopyridine in acetone-d_6 (598 µL) containing DMSO-d_6 (2 µL) in a sealed NMR tube was kept at 60 °C for 24 h. The ^{1}H NMR spectra of this sample confirmed 100% *trans* azopyridine. The sample was then irradiated for 2, 7, and 120 min with a light of wavelength 365 nm using the exact same set up as described above. ^{1}H NMR spectra of the sample irradiated for 2, 5, and 10 min showed negligible changes in the concentration of *cis* azopyridine, suggesting that the photostationary equilibrium (94.4 ± 0.3% *cis*, 5.6 ± 0.3% *trans*) was reached within 2 min. Similar irradiation of the sample with light of wavelength 435 nm again resulted in a photostationary equilibrium (24.6 ± 0.3% *cis*, 75.4 ± 0.3% *trans*) as shown in Supplementary Table 1. The PSS was not greatly affected by the presence of the porphyrin in the system.

Half-life ($t_{½}$) of *cis* Azopyridine (*cis*-**2**): *Cis* azopyridines, in general, usually exhibit a similar half-life as the corresponding azobenzenes. The half-life ($t_{½}$) of *cis* azopyridine (*cis*-**2**) was measured using ^{1}H NMR. *Cis*-**2** at its photostationary equilibrium (94.4 ± 0.3% *cis*, 5.6 ± 0.3% *trans*) in a sealed NMR tube was measured for several days in a 500 MHz NMR spectrometer. The half-life ($t_{½}$) of *cis*-**2** was found to be extremely high (>164 days, Supplementary Figure 7) at room temperature in acetone-d_6 or acetone-d_6/DMSO-d_6, whereas the same in presence of the paramagnetic Fe(III) porphyrin was significantly lower (~18 days, Supplementary Figure 8).

Magnetic susceptibility—Evans measurements: The paramagnetic susceptibility of admixed-spin complex FeTPP(acetone)$_2^+$, high-spin and low-spin complexes FeTPP(DMSO)$_2^+$ and FeTPP(azopy)$_2^+$ were determined via the standard Evans measurements using ^{1}H NMR spectroscopy. An NMR tube with a coaxial insert, both sealable, was used. For the admixed-spin complex FeTPP(acetone)$_2^+$, the outer tube was filled with a 0.2 mM solution of porphyrin FeTPPClO$_4$ (**1**) in acetone-d_6 (530 µL) and the inner tube was filled with a 0.2 mM solution of diamagnetic ZnTPP (zinc tetraphenylporphyrin) in acetone-d_6 (60 µL). ZnTPP that is completely diamagnetic compensates the diamagnetic contribution of the porphyrin macrocycle to the observed magnetic susceptibility. For the high-spin complex FeTPP(DMSO)$_2^+$, the outer tube was filled with a 0.2 mM solution of porphyrin FeTPPClO$_4$ in acetone-d_6–DMSO-d_6 (530 µL, 598:2 v v^{-1}) and the inner tube was filled with a 0.2 mM solution of diamagnetic ZnTPP in acetone-d_6–DMSO-d_6 (60 µL, 598:2 v v^{-1}). For the low-spin complex FeTPP(azopy)$_2^+$, the outer tube was filled with a 0.2 mM solution of porphyrin FeTPPClO$_4$ containing 15 mM azopyridine in acetone-d_6–DMSO-d_6 (530 µL, 598:2 v v^{-1}) and the inner tube was filled with a 0.2 mM solution of diamagnetic ZnTPP containing 15 mM azopyridine in acetone-d_6–DMSO-d_6 (60 µL, 598:2 v v^{-1}). For the strapped high-spin complex **17**, the outer tube was filled with a 0.721 mM solution of strapped porhyrin **17** in dichloromethane d_2 (530 µL) and the inner tube was filled with a 0.721 mM solution of diamagnetic ZnTPP in dichloromethane-d_2 (60 µL). For the strapped low-spin complex **18**, the outer tube was filled with a 1.63 mM solution of strapped porphyrin **18** containing 66.8 mM 1-methylimidazole in dichloromethane-d_2 (530 µL) and the inner tube was filled with a 1.63 mM solution of diamagnetic ZnTPP containing 1-methylimidazole (66.8 mM) in dichloromethane-d_2 (60 µL). The concentration of the internal standard, TMS, was maintained constant in the inner and outer tubes. ^{1}H NMR spectra were recorded in a 500 MHz spectrometer at a constant temperature of 300 K. The sample (inner and outer tubes) was allowed to equilibrate at this temperature for at least 15 min before measurement. The following Eq. (1) was used to calculate the paramagnetic susceptibility from the experimentally measured shift in TMS signals between the inner and outer tubes:

$$\chi_M = \frac{3\delta f M}{4\pi f m} + \chi_M^0 + \frac{\chi_M^0(d_0 - d_x)}{m}\chi_{dia}^M, \quad (1)$$

where χ_M is the molar paramagnetic susceptibility in (cm^3 mol^{-1}), δf is the frequency difference between the TMS peaks of the inner and outer tube (Hz), M the molecular weight of the substance (g mol^{-1}), f the frequency of the NMR instrument (Hz), m the mass of the substance in 1 mL of solution (g), χ^0_M the mass susceptibility of the solvent (cm^3 mol^{-1}), d_0 the density of the solvent (g cm^{-3}), d_x the density of the solution (g m^{-3}), and $\chi^M_{dia}$the diamagnetic correction to the magnetic susceptibility (cm^3 mol^{-1}).

Since all the solutions used in this experiment are dilute, the density of the solvent and the solutions may be considered equal, thereby nullifying the factor $(d_0 - d_x)$. The diamagnetic correction (χ^M_{dia}) has been taken care of by using equivalent diamagnetic components in the inner tube. Since the same solvents are used in the inner and outer tubes, the solvent correction factor χ^0 could also be neglected. Thus, the equation for calculating the molar paramagnetic susceptibility effectively reduces to Eq. (2):

$$\chi_M = \frac{3\delta f M}{4\pi f m}. \quad (2)$$

From the known values of molar paramagnetic susceptibility, the corresponding magnetic moment (μ_{eff}) may be obtained via Eq. (3):

$$\mu\text{eff} = 2.828\sqrt{\chi_M T}, \quad (3)$$

where T is the temperature (K).

For a 0.2 mM solution of the high-spin complex $FeTPP(DMSO)_2^+$, $\delta f = 5.78$ Hz, $\chi_M = 0.0138\ cm^3\ mol^{-1}$, and $\mu_{eff} = 5.76$ B.M.

For a 0.2 mM solution of low-spin complex $FeTPP(azopy)_2^+$, $\delta f = 0.78$ Hz, $\chi_M = 0.00186\ cm^3\ mol^{-1}$, $\mu_{eff} = 2.11$ B.M.

For a 0.2 mM solution of admixed-spin complex $FeTPP(acetone)_2^+$, $\delta f = 3.53$ Hz, $\chi_M = 0.00843\ cm^3\ mol^{-1}$, and $\mu_{eff} = 4.50$ B.M.

For a 0.721 mM solution of 5,15-strapped iron(III) porphyrin chloride **17**, $\delta f = 24.8$ Hz, $\chi_M = 0.01434\ cm^3\ mol^{-1}$, and $\mu_{eff} = 5.87$ B.M.

For a 1.63 mM solution of 5, 15-strapped iron(III) porphyrin methylimidazole **18**, $\delta f = 8.79$ Hz, $\chi_M = 0.00258\ cm^3\ mol^{-1}$, and $\mu_{eff} = 2.49$ B.M.

Relaxivity measurements: The relaxation time of acetone and water were determined via NMR spectroscopy (Bruker AC 200) in acetone-d_6 + DMSO-d_6 + 1% acetone. The longitudinal (or spin-lattice) relaxation time (T_1) of acetone and water were obtained by an inversion recovery pulse sequence. The integral of the acetone and water signals were observed as a function of the delay time (Supplementary Figure 8). See Supplementary Table 3 for the calculated values of T_1.

The transverse (or spin–spin) relaxation time T_2 was determined by a spin echo pulse sequence. The integral of the DMSO signal was observed as a function of the spin echo (n) with an echo time (τ) of 10 ms (Supplementary Figure 12). The efficiency of paramagnetic ions in shortening the relaxation time of solvent protons may be determined based on relaxivity (R_1 and R_2). The plot of the relaxation rate ($1/T_1$ or $1/T_2$) vs. the concentration of the paramagnetic species shows a linear relation and the slope is defined as relaxivity, R_1 and R_2.

UV–vis and far–vis spectroscopy investigations. UV–vis and far–vis absorption spectra were recorded on a Perkin-Elmer Lambda-14 spectrophotometer using quartz cells of 1 cm path length. Spectrophotometric grade solvents (2.0 mL) were employed in optical spectroscopic measurements. Irradiation experiments were performed in acetone containing small amounts of DMSO-d_6 (25.87 mM). The temperature during every measurement was fixed at 25 °C using a water-flow system connected to a thermostat.

PSS of azopyridine **2**: Fifty micromolar and 1.0 mM solution of the azopyridine in acetone/DMSO (2 mL, 25.87 mM) in sealed quartz cells were irradiated for 2 min with a light of wavelength 365 nm, with stirring. The UV–vis spectrum was recorded. Extended irradiation (up to 10 min) showed negligible changes in the spectrum of *cis* azopyridine (predominant species), suggesting that the photostationary equilibrium was reached within 2 min. Similar irradiation of the sample with a light of wavelength 435 nm again resulted in a photostationary equilibrium as shown in Supplementary Figure 18. See Supplementary Table 1 for the *cis*/*trans* ratio in the PSS determined by ^{1}H NMR.

Far–vis spectroscopy of the spin-state changes: To a solution of $FeTPP(acetone)_2^+$ at room temperature, increasing amounts of DMSO-d_6 was added and shaken well. The final concentration of the porphyrin was fixed at 0.1 mM and the final volume at 2.0 mL. The optical spectra were recorded for each addition of DMSO-d_6, 3 min after placing the quartz cells in the measurement chamber for temperature equilibration. Near isosbestic point was observed around 626 nm, suggesting transformation from $FeTPP(acetone)_2^+$ to $FeTPP(DMSO)_2^+$, with intermediates having the similar optical characteristics as either of the species in solution. The process was followed by plotting the corresponding change in absorption at 686 nm at each concentration of DMSO added—the intensity increased with successive addition of DMSO at least until a final DMSO concentration of 10 mM and levelled off thereafter.

To a solution of porphyrin $FeTPP(acetone)_2^+$ at room temperature containing DMSO-d_6 (25.87 mM), increasing amounts of *trans* azopyridine were added and shaken well. The final concentration of the porphyrin was fixed at 0.1 mM and the final volume at 2.0 mL. The optical spectra were recorded for each addition of *trans* azopyridine, 3 min after placing the quartz cells in the measurement chamber for temperature equilibration. An isosbestic point was observed around 621 nm, suggesting a transformation from $FeTPP(DMSO)_2ClO_4$ to $FeTPP(azopy)_2ClO_4$, without any intermediates or with intermediates having the same optical characteristics as either of the species in solution. The process was followed by plotting the corresponding change in absorption at 686 nm at each concentration of *trans* azopyridine added—the intensity was found to decrease with successive addition of azopyridine at least until a final concentration of 7 mM and levelled off thereafter.

Switching experiments in optical spectroscopy: To a 0.1 mM solution of $FeTPPClO_4$ in acetone, containing DMSO-d_6 (25.87 mM) in a sealed quartz cell, *trans* azopyridine (trans-**2**) (75 eq., 7.5 mM) was added. The quartz cell was sealed and shaken well before acquiring the optical spectrum in the visible region (500–800 nm). The cell was then irradiated for 2 min with a light of wavelength 365 nm, under magnetic stirring and the optical spectrum was obtained. The first cycle of irradiation was completed by irradiating the sealed cell with a light of wavelength 435 nm for another 3 min. The partial switching experiments were repeated for 10 cycles. Each cycle consisted of the photoconversion of *cis* azopyridine to *trans* azopyridine via alternate irradiation using lights of two different wavelengths (365, 435 nm) and measurement after regular intervals. Supplementary Figure 35 right shows reversible changes in absorption at 686 nm as a function of number of irradiation cycles.

Calculation of apparent equilibrium constants. The optical changes accompanying the spin-state changes were used to derive the corresponding apparent equilibrium constants. The model reactions as shown in Supplementary Figure 23 were assumed and validated using the excel tool for equilibrium speciation (Equilibrium Speciation Tool)[33] based on Newton–Raphson method and the reported hybrid generic algorithm, in combination with Excel's Solver.

To determine the relevant species in acetone, the change in the phenyl shifts of the porphyrin, upon addition of increasing amounts of acetone-d_6 to a solution of 0.2 mM $FeTPPClO_4$ in CD_2Cl_2, was analyzed, using binding models for both 1:1 and 2:1 complexation. The pyrrole protons were not visible over the complete range of the titration, and thus could not be used for analysis (see Supplementary Figure 21 and Supplementary Table 4).

Formation of $FeTPP(acetone)_2^+$ via $FeTPP(acetone)ClO_4$ with $K_1'' = 0.865\ L\ mol^{-1}$ and $K_2'' = 1.077\ L\ mol^{-1}$ is the most likely model. The observed and calculated shifts are given in Supplementary Table 4 and are depicted in Supplementary Figure 24. The composition of the corresponding solutions is given in Supplementary Table 5 and shown in Supplementary Figure 25. Based on these results the main component in pure acetone-d_6 (13600 mM) is complex $FeTPP(acetone)_2^+$ (~93%, see supplementary Table 5)[31].

Absorption changes for the titration of a 0.1 mM solution of $FeTPPClO_4$ in acetone with DMSO-d_6 (see Supplementary Figure 19) were analyzed using both 1:1 and 2:1 binding models as well as different assumptions for the absorption of the intermediate species $FeTPP(acetone)(DMSO)^+$ in the 2:1 binding model.

Several binding models have been tested and their fitting has been compared: (a) No intermediate (mixed) complex is formed during ligand exchange (very strong cooperativity of ligand exchange). (b) Formation of only the mixed complex (no double ligand exchange, which is very unlikely because DMSO is known to form 2:1 complexes with $FeTPPClO_4$), (c) absorption of the mixed complex $FeTPP(acetone)(DMSO)^+$ is identical to the absorption of $FeTPP(acetone)_2^+$, (d) absorption of the mixed complex $FeTPP(acetone)(DMSO)^+$ is identical to the absorption of $FeTPP(DMSO)_2^+$, (e) the absorption of the mixed complex is in between $FeTPP(acetone)_2^+$ and $FeTPP(DMSO)_2^+$. The SSR (sum of squared residuals) values are (a) and (b) 1.5×10^{-3}, (c) 6.2×10^{-4}, (d) 8.1×10^{-5}, and (e) 2.9×10^{-5}. This suggests formation of an intermediate species $FeTPP(acetone)(DMSO)^+$ according to model (d) or (e). Model (e) is in accordance with the course of the absorption shown in Supplementary Figure 19, which shows a nearly isosbestic point at 621 nm but a different behavior above 750 nm.

In Supplementary Table 6, the composition of the species in solution, and the observed and calculated absorption at 686 nm are given. The speciation is shown in Supplementary Figure 27. Supplementary Figure 26 shows the comparison of observed and calculated absorption. Apparent binding constants are given in Supplementary Table 10.

With the binding constants obtained from the UV–vis experiments (K'_1=5862 L mol^{-1}, K'_2=596 L mol^{-1}), we were able to fit the shifts of the phenyl and pyrrole protons of $FeTPPClO_4$. These shifts were followed upon subsequent addition of DMSO-d_6 to a solution of $FeTPPClO_4$ in acetone-d_6 with a fixed concentration of 0.2 mM porphyrin and a fixed total volume of 600 µL (see Supplementary Tables 7-8 and Supplementary Figure 22). Fitting the NMR data with different initial assumptions for the association constants gave similar results. The best fit was obtained for K'_1=5372 L mol^{-1} and K'_2=580 L mol^{-1} ($\Delta_{SSR} = 4 \times 10^{-5}$ (sum of squared residuals)), which results in a difference of 8.4% and 2.8%, respectively. This close agreement can be interpreted as an additional confirmation of the validity of our model.

For the titration of a solution of $FeTPPClO_4$ (0.1 mM) in acetone containing DMSO-d_6 (25.87 mM) with *trans* azopyridine, the binding isotherm was analyzed considering both single or double coordination of azopyridine (see Supplementary Table 9. Occurrence of an isosbestic point at 621 nm suggested either clean transformation to a single product or formation of an intermediate $FeTPP(DMSO)(azopy)^+$ with the same optical characteristics as either species in solution (see Supplementary Figure 20). The most likely model was stepwise coordination of two azopyridines, assuming that $FeTPP(DMSO)(azopy)^+$ has the same absorption as the final complex ($FeTPP(azopy)_2$). This implicates that the first coordination of azopyridine induces spin change from high spin to low spin.

Titration with *trans* azopyridine was also followed by ^{1}H NMR spectroscopy, but neither the pyrrole shift (slow exchange, broad signals) nor the phenyl shifts (not observable because of excess of azopyridine) could be analyzed.

A refined binding model could be obtained by fitting the data of the titration with *trans* azopyridine by taking into account the apparent binding constants for DMSO-d_6 (see Supplementary Table 10). This provided the basis to calculate the concentration of all relevant species in solution for the single titration points and for the switching experiments (see above).

Using the combined model, we were able to determine the composition of the species in the solution of the NMR switching experiments. Assuming that the binding constants of *cis* azopyridine are much lower than those of DMSO-d_6 and, consequently, that *cis* azopyridine does not bind, we determined the composition of the solutions in the PSSs after irradiation with 365 and 435 nm, respectively (see Supplementary Tables 11 and 12). Further evidence that *cis* azopyridine is a very weak ligand, or does not bind at all, is provided in Supplementary Figure 3b. With these values, the switching efficiency could be calculated as 76.3% (see Supplementary Figure 34).

EPR spectroscopy. Sample solutions of Fe(III) porphyrin complexes were vacuum-sealed in EPR quartz-glass tubes. X-band (≈9.5 GHz) continuous wave (CW) EPR experiments on samples in acetone at 8 K were performed with a Bruker ESP 380E spectrometer equipped with an Oxford Instruments Ltd. ITC liquid He flow system and temperature controller. X-band CW EPR spectra on samples in CH_2Cl_2 were recorded at 4.8 K using a Bruker ELEXSYS E500 spectrometer equipped with an Oxford Instruments Ltd. ESR 900 liquid He flow cryostat and an ITC503 temperature controller. All spectra presented were baseline corrected by subtraction of a background spectrum of the resonator with an empty sample tube.

X-band EPR experiments at liquid He temperatures were performed on the various Fe(III) porphyrin complexes dissolved in acetone or CH_2Cl_2 to verify their spin states. Supplementary Figure 36 contains spectra of the following complexes of $FeTPP^+$ at a concentration of 0.2 mM with acetone as the solvent: $FeTPP(acetone)_2^+$ (**1a**), $FeTPP(DMSO)_2^+$ (**2**), $FeTPP(azopy)_2^+$ (**3**), $FeTPP(MeOPy)_2^+$ (**4**). **1a**, **2**, and **3** each exhibit a peak around $g = 6$ of different intensity together with a smaller, sharper peak at $g \approx 2$, indicative of either high-spin $S = 5/2$ states ($g_\perp \approx 6$, $g_\parallel \approx 2$) or admixed-spin $S = 3/2$, 5/2 states[40]. As expected, **2** shows the most intense high-spin signal, while in **3**, its intensity is much smaller (~3% of **2**). **1a** exhibits a $g \approx 6$ signal broader than the one from **2**, of intermediate intensity, and there possibly is another, small feature around $g = 4.7$–4.8. This appearance indicates a contribution from an intermediate $S = 3/2$ spin state and thus an admixed $S = 3/2$, 5/2 state for **1a**. **4** does not contain any $S = 5/2$ component, as expected, but also no other strong signals. In the spectra of **3** and **4**, there could however be weak signals around $g = 3.3$ and $g = 3.1$, respectively, of very small intensity. These g values are characteristic for the so-called "large g_{max}" signals[41,42], originating from low-spin $S = 1/2$ states, as expected for these complexes, of $(d_{xy})^2(d_{xz},d_{yz})^3$ electronic ground state configuration.

In pulse mode, in contrast, no signals from the $FeTPPClO_4$ complexes in acetone could be observed. The reason for this is thought to be the bad glassing properties of acetone, possibly promoting agglomeration of the complexes. Magnetic interactions between the iron centers and concomitant enhanced relaxation rates prevent that electron spin echoes can be detected, while their CW signals can still be measured.

Hence, dichloromethane (CH_2Cl_2), which possesses more favorable glassing properties, was chosen as solvent for further experiments. Supplementary Figure 37 shows X-band CW EPR spectra of complexes **3** and **4** (0.2 mM in CH_2Cl_2). As in the samples containing acetone, **3** exhibits a high-spin signal at $g = 5.99$, while **4** does not. Both samples show large g_{max} signals of a low-spin $S = 1/2$ state around $g = 3.4$. In Supplementary Figure 38, the EPR spectra of **3** and **4** in samples with acetone or CH_2Cl_2 as the solvent are compared. Samples with CH_2Cl_2 as the solvent did show also EPR signals in pulse mode (not shown).

Illumination of **3** with UV light of 365 nm wavelength at room temperature results in a ~20-fold increase of the component at $g = 5.99$ (Supplementary Figure 38), consistent with an increase of the fraction of $S = 5/2$ complexes by low-spin to high-spin conversion. However, there is no concomitant decrease of the large g_{max} low-spin signal, which would be expected as a result of such a process. Hence, there is a significant overall increase of EPR signal intensity. Further illumination at room temperature with blue light of 435 nm wavelength of this sample exposed to UV light before did not lead to a decrease of the $g = 5.99$ signal; thus, not indicating a back-conversion process from high spin to low spin that has been observed before for this type of sample. These results from the photoswitching experiments are not quite consistent with the light-induced behavior observed in the corresponding NMR, Evans, and UV–vis experiments at room temperature. Especially, the increase of overall signal intensity upon UV irradiation suggests that not all the Fe(III) ions present in the sample contribute to the measured EPR spectra. The reason is thought to be non-ideal complex solvation in the frozen samples, possibly resulting in cluster formation, even when using CH_2Cl_2 as the solvent.

Electrochemical measurements. The electrochemical measurements were performed on an Autolab PGSTAT204 potentiostat equipped with a 3-electrode setup. A platinum disk (5 mm diameter) was used as the working electrode, a platinum wire was used as the counter electrode and a $Ag/AgNO_3$ 0.01 M in acetonitrile was used as the reference electrode. The reference electrode was separated from the main cell chamber with a frit on a side-arm filled with supporting electrolyte in acetone. The CVs were obtained in acetone at a porphyrin concentration of 0.2 mM. Tetrabutylammonium perchlorate (TBAP, 40 mM) was used as the supporting electrolyte. The experiments were conducted inside a glovebox at room temperature at a scan rate of 50 mV s^{-1}. All measurements were repeated at least three times to obtain reliable potential values. All the potentials are referred to the SHE. The potentials were corrected using hydroxymethyl ferrocene (Fc-MeOH) as an internal reference. At the end of each measurement, 0.2 mg of Fc-MeOH was added to the solution and the midpotential was determined. The reported value of 420 mV vs. SHE was used for the conversion. Upon irradiation of the solution of Fe(III)porphyrin, DMSO, *trans* azopyridine, and TBAP (concentrations see Supplementary Figure 39a), the reduction peak shifts towards a more positive potential, whereas a shift to a more negative potential would be expected if the *cis* azopyridine would not interfere with the electrochemical process. We attribute this behavior to complexation of the reduced Fe(II) species with *cis* azopyridine. Further implications arise from the presence of high concentrations of the supporting electrolyte (TBAP), which is required for the electrochemical experiment. The electrolyte may perturb the equilibrium between the different spin states since it has been shown to favor the admixed state of porphyrins[5]. Independent experiments towards the elucidation of the chemistry of the Fe(II) species applying NMR, magnetic measurements, EPR and UV are currently underway and shall be reported in due course.

Syntheses. Synthesis of porphyrin **1**: Tetraphenylporphyrin and FeTPPCl were synthesized as reported[43,44]. $FeTPPClO_4$ (**1**) was prepared via a modified literature method[45]. The toluene complex obtained after crystallization from toluene was dissolved in dichoromethane (purified over basic alumina) and the solvent was removed in vacuo. This procedure was repeated several times until no toluene signals were visible in ^1H NMR.

HR masses of $FeTPPClO_4$ (**1**) with different ligands (see Supplementary Figure 40):

(a) acetone: 784.24952 (calc.), 784.24891 (found) for $C_{50}H_{40}N_4O_2Fe$,
(b) 4-methoxypyridine: 886.27132 (calc.), 886.27059 (found) for $C_{56}H_{42}N_6O_2Fe$,
(c) DMSO: 822.17801 (calc.), 822.17609 (found) for $C_{46}H_{38}N_4O_2FeS_2$.

Synthesis of azopyridine **2**, general strategy: The azopyridine **2** was synthesized in three steps from commercially available 3,5-di-*tert*-butylaniline **5** and 3-amino-4-chloropyridine **8** as shown in Supplementary Figure 41. Oxidation of the aniline **5** to the corresponding nitrosobenzene **6** was achieved using oxone® in a mixture of water and CH_2Cl_2. Base-mediated coupling of the nitrosobenzene **6** with the aminopyridine **8** afforded the azo-product **9**, which on dechlorination–methoxylation resulted in the azopyridine **2**.

Synthesis of nitrosobenzene **6**[46]: To a solution of Oxone® (12.0 g, 39.0 mmol) in water (100 mL) was added a solution of 3,5-di-*tert*-butylaniline **5** (2.00 g, 9.74 mmol) in CH_2Cl_2 (40 mL) and the resulting mixture was stirred at room temperature for 5 h. The formation of the nitroso compound was evident by a change in color of the solution to light green. After 5 h, the phases were separated and the aqueous phase was extracted with CH_2Cl_2 (2 × 25 mL). The organic phases were combined, dried over anhydrous $MgSO_4$, and evaporated under reduced pressure. The temperature during evaporation was maintained at 30 °C. The crude solid thus obtained was purified by column chromatography (silica gel, 2:5 CH_2Cl_2/pentane as eluent) to afford the nitroso compound **6** as a light green solid. Fourteen percent of the corresponding nitro compound **7** was also isolated as a yellow powder (1.84 g, 8.34 mmol, 84%). ^1H NMR (600 MHz, 300 K, $CDCl_3$, TMS) $\delta =$ 7.82 (t, $^4J_{4,2} = 1.8$ Hz, 1H, *H*-4), 7.78 (d, $^4J_{2,4} = 1.8$ Hz, 2H, *H*-2), 1.40 (s, 18H, C(CH_3)$_3$) ppm; ^{13}C NMR (150 MHz, 300 K, $CDCl_3$, TMS): $\delta = 167.2$ (*C*-1), 152.4 (*C*-3), 129.7 (*C*-4), 115.9 (*C*-2), 35.1 (C(CH_3)$_3$), 31.3 (C(CH_3)$_3$) ppm; HRMS (ESI) 219.16231 (calc.), 219.16191 (found) for $C_{14}H_{21}N_1O_1$.

Synthesis of azo-compound **9**: To a solution of the aminopyridine **8** (1.00 g, 7.78 mmol) in pyridine (25 mL), 60% KOH in water (75 mL) was added and the resulting mixture was heated to 80 °C. A solution of the nitrosobenzene **6** (1.80 g, 8.19 mmol) in pyridine (50 mL) was added dropwise over 15 min. The reaction mixture was then heated and kept at 80 °C for 8 h with vigorous stirring. After cooling to room temperature, the phases were separated. The aqueous phase was washed with ethyl acetate (2 × 50 mL). The organic phases were combined, dried over anhydrous $MgSO_4$, and evaporated in vacuo. The crude product was purified by column chromatography (1:4 ethyl acetate/cyclohexane as eluent) to obtain the azo-compound **9** as an orange solid (1.38 g, 4.18 mmol, 54%); m.p.: 93 °C; ^1H NMR (500 MHz, 300 K, $CDCl_3$, TMS): *trans* isomer: $\delta = 8.77$ (s, 1H, *H*-2), 8.54 (d, $^3J_{6,5} = 5.3$ Hz, 1H, *H*-6), 7.84 (d, $^4J_{8,10} = 1.8$ Hz, 2H, *H*-8), 7.64 (t, $^4J_{10,8} = 1.8$ Hz, 1H, *H*-10), 7.52 (d, $^3J_{5,6} = 5.3$ Hz, 1H, *H*-5), 1.41 (s, 18H, C(CH_3)$_3$) ppm; *cis* isomer: $\delta = 8.24$ (d, $^3J_{6,5} = 5.3$ Hz, 1H, *H*-6), 7.57 (s, 1H, *H*-2), 7.36 (d, $^3J_{5,6} = 5.3$ Hz, 1H, *H*-5), 7.23 (t, $^4J_{10,8} = 1.8$ Hz, 1H, *H*-10), 6.75 (d, $^4J_{8,10} = 1.8$ Hz, 2H, *H*-8), 1.17 (s, 18H, C(CH_3)$_3$) ppm; ^{13}C NMR (125 MHz, $CDCl_3$, 300 K, TMS): *trans* isomer: $\delta =$ 152.7 (*C*-7), 152.1 (*C*-9), 150.7 (*C*-6), 144.8 (*C*-3), 143.3 (*C*-4), 139.4 (*C*-2), 126.7 (*C* 10), 125.4 (*C* 5), 118.0 (*C* 8), 35.1 (*C*(CH_3)$_3$), 31.2 (C(*CH*$_3$)$_3$) ppm; *cis* isomer: $\delta = 153.2$ (*C*-7), 151.9 (*C*-9), 147.8 (*C*-6), 148.8 (*C*-3), 135.8 (*C*-4), 139.4 (*C*-2), 122.7 (*C*-10), 124.5 (*C*-5), 115.0 (*C*-8), 34.9 (*C*(CH_3)$_3$), 31.1 (C(*CH*$_3$)$_3$) ppm; HRMS (ESI): 329.16587 (calc.), 329.16492 (found) for ($C_{19}H_{24}N_3Cl$); FT-IR (film): $\tilde{\nu} =$ 2963 (s), 2903 (w), 2866 (w), 1602 (m), 1562 (s), 1460 (m), 1361 (m), 1247 (m), 1187 (m), 1162 (m), 1087 (m), 882 (m), 840 (s), 746 (s), 697 (s), 680 (s) cm^{-1}; UV–vis (toluene): $\lambda_{max} = 344$ nm, $\log \varepsilon = 4.233$ L mol^{-1} cm^{-1}.

Synthesis of azopyridine **2**: Metallic sodium (3.60 g) was dissolved in MeOH (100 mL) under cooling by an ice bath. The resulting solution was added slowly to a MeOH solution (20 mL) of the azo-compound **9** (1.63 g, 4.94 mmol, the azo-compound **9** was not completely soluble in MeOH). The resulting mixture was heated to 50 °C for 2 h with vigorous stirring and was then allowed to cool to room temperature. Stirring was then continued for another 8 h and the solvent was removed under reduced pressure. Crushed ice was added to the residue and was extracted with CH_2Cl_2 (3 × 50 mL). The combined organic extracts were dried over anhydrous $MgSO_4$ and the solvent was removed under reduced pressure. The crude product thus obtained was purified by column chromatography (silica gel, 2:1 ethyl acetate/cyclohexane as eluent) to give the azopyridine **2** as a dark orange solid (1.46 g, 4.49 mmol, 91%); m.p.: 100 °C; ^1H NMR (500 MHz, 300 K, $CDCl_3$, TMS): *trans* isomer: $\delta = 8.62$ (s, 1H, *H*-2), 8.54 (d ≈ s, 1H, *H*-6), 7.75 (d, $^4J_{8,10} = 1.8$ Hz, 2H, *H*-8), 7.58 (t, $^4J_{10,8} = 1.8$ Hz, 1H, *H*-10), 7.02 (d, $^3J_{5,6} = 5.7$ Hz, 1 H, *H*-5), 4.06

(s, 3H, OCH_3), 1.39 (s, 18 H, C(CH_3)$_3$) ppm; *cis* isomer: $\delta = 8.23$ (d, $^3J_{6,5} = 5.7$ Hz, 1H, *H*-6), 7.78 (s, 1H, *H*-2), 7.20 (t, $^4J_{10,8} = 1.8$ Hz, 1H, *H*-10), 6.74 (s, 1H, *H*-5), 6.73 (d, $^4J_{8,10} = 1.8$ Hz, 2H, *H*-8), 3.73 (s, 3H, OCH_3), 1.17 (s, 18H, C(CH_3)$_3$) ppm; ^{13}C NMR (125 MHz, $CDCl_3$, 300 K, TMS): *trans* isomer: $\delta = 161.7$ (*C*-4), 153.2 (*C*-7), 152.4 (*C*-6), 152.2 (*C*-9), 139.2 (*C*-2), 138.9 (*C*-3), 126.0 (*C*-10), 117.7 (*C*-8), 108.0 (*C*-5), 56.3 (OCH$_3$), 35.2 (C(CH$_3$)$_3$), 31.6 (C(CH$_3$)$_3$) ppm; *cis* isomer: $\delta =$ 154.9 (*C*-4), 153.9 (*C*-7), 151.4 (*C*-9), 149.6 (*C*-6), 140.7 (*C*-3), 140.5 (*C*-2), 121.9 (*C*-10), 114.4 (*C*-8), 106.7 (*C*-5), 55.4 (OCH$_3$), 34.8 (C(CH$_3$)$_3$), 31.2 (C(CH$_3$)$_3$) ppm; MS (MALDI-TOF): $m/z = 326.06$ $[M\text{-}H]^+$; HRMS (ESI): 325.21541 (calc.), 325.21520 (found) for ($C_{20}H_{27}N_3O$); FT-IR (film): $\tilde{\nu} = 2953$ (s), 2869 (w), 1602 (m), 1581 (s), 1480 (m), 1361 (m), 1272 (s), 1193 (s), 1022 (s), 883 (s), 805 (s), 700 (s) cm^{-1}; UV–vis (toluene): $\lambda_{max} = 344$ nm, $\log \varepsilon = 4.288$ L mol^{-1} cm^{-1}.

Synthesis of strapped porphyrin **17**, general strategy: The ether bridge **15** was synthesized in two steps from commercially available chemicals with a yield of 24%. The *meso*-phenyl dipyrromethane **14** was synthesized with a yield of 81%. The strapped iron porphyrin **17** was prepared from **14** and **15** in two steps (see Supplementary Figures 42-43).

Synthesis of meso-phenyl dipyrromethane **14**[47]: Pyrrole **13** (24.0 mL, 347 mmol) and benzaldehyde **12** (850 mg, 8.00 mmol) were dissolved under nitrogen atmosphere and stirred for 15 min. TFA (150 µL) was added and the mixture was stirred at room temperature for 25 min. Subsequently, 200 mL of DCM were added and the mixture was washed with a 0.1 M potassium hydroxide solution (120 mL) and twice with water (120 mL). The combined organic layers were dried over anhydrous magnesium sulfate and the solvent was removed under reduced pressure. The crude product was purified by column chromatography (dichloromethane/cyclohexane: triethylamine (1%), 1:1, $R_f = 0.61$). A colorless solid was obtained (1.44 g, 6.48 mmol, 81%). ^{1}H NMR (500 MHz, $CDCl_3$): $\delta = 7.90$ (br s, 2H, N*H*), 7.37–7.18 (m, 5H, *H*-7, *H*-8, *H*-9), 6.70–6.68 (m, 2H, *H*-4), 6.17–6.15 (m. 2H, *H*-3), 5.93–5.91 (m. 2H. *H*-2), 5.48 (s, 1H. *H*-5) ppm; ^{13}C NMR (150 MHz, 300 K, $CDCl_3$): $\delta = 142.2$ (*C*-6), 132.4 (*C*-1), 128.6 (*C*-7) 128.5 (*C*-8), 126.9 (*C*-9), 117.2 (*C*-4), 108.4 (*C*-3), 107.2 (*C*-2), 44.1 (*C*-5) ppm.

Synthesis of 1,4-bis(2-bromoethoxy)-2-butyne **11**[48]: 1,4-Bis(2-hydroxyethoxy)-2-butyne **10** (1.00 g, 5.75 mmol) was dissolved in dry dichloromethane (10 mL) under nitrogen atmosphere. Subsequently, tetrabromomethane (4.20 g, 12.7 mmol) was added, then triphenylphosphine (3.30 g. 12.7 mmol) was dissolved in dry dichloromethane (20 mL) and slowly added dropwise. The reaction mixture was stirred at 0 °C for 90 min and 15 h at room temperature and afterwards poured onto mixture of dichloromethane (50 mL) and distilled water (50 mL). The combined organic layers were separated, dried over anhydrous magnesium sulfate, and the solvent was removed under reduced pressure. The crude product was purified by column chromatography (cyclohexane/ethylacetate, 1:1, $R_f = 0.60$) to yield **12** as a yellow oil (1.70 g, 5.70 mmol, 99%). ^{1}H NMR (500 MHz, 300 K, $CDCl_3$): $\delta = 4.27$ (s, 4H, *H*-2), 3.85 (t, $^3J = 5.5$ Hz, 4H, *H*-3), 3.49 (t, $^3J = 5.5$ Hz, 4 H, *H*-4) ppm; ^{13}C NMR (150 MHz, 300 K, $CDCl_3$): $\delta = 82.3$ (*C*-1), 69.7 (*C*-3), 58.5 (*C*-2), 30.0 (*C*-4) ppm.

Synthesis of the bridge **15**: Salicylaldehyde (223 mg, 1.92 mmol) was dissolved in acetonitrile (20 mL) under nitrogen atmosphere. Potassium carbonate (264 mg, 1.92 mmol) and 1,4-bis(2-bromoethoxy)-2-butyne **11** (375 mg, 1.25 µmol) were added and the reaction mixture was stirred for 16 h at 80 °C. The reaction solution was concentrated and was poured onto distilled water (150 mL). The aqueous phase was extracted three times with dichloromethane (50 mL). The combined organic layers were dried over anhydrous magnesium sulfate and the solvent was removed under reduced pressure. The crude product was purified by column chromatography (cyclohexane/ethylacetate, 1:1, $R_f = 0.49$). A colorless oil was obtained (87.0 mg, 229 µmol, 24%). ^{1}H NMR (500 MHz, 300 K, $CDCl_3$): $\delta = 10.53$ (s, 2H, *H*-1), 7.83 (dd, $^3J = 7.6$ Hz, $^4J = 1.8$ Hz, 2H, *H*-7), 7.53 (td, $^3J = 8.0$ Hz, $^4J =$ 1.8 Hz, 2H, *H*-5), 7.03 (t, $^3J = 7.6$ Hz, 2H, *H*-6) 6.99 (d, $^3J = 8.4$ Hz, 2H, *H*-4), 4.31 (s, 4H, *H*-10), 4.27 (t, $^3J = 4.7$ Hz, 4H, *H*-8), 3.95 (t, $^3J = 4.7$ Hz, 4H, *H*-9) ppm; ^{13}C NMR (150 MHz, 300 K, $CDCl_3$): $\delta = 189.8$ (*C*-1), 161.1 (*C*-3), 135.9 (*C*-5), 128.3 (*C*-7), 125.2 (*C*-2), 121.1 (*C*-6), 112.8 (*C*-4), 82.43 (*C*-11), 68.0 (*C*-8, *C*-9), 58.9 (*C*-10) ppm; HRMS (EI): 382.14275 (calc.). 382.14164 (found) for $C_{22}H_{22}O_6$; FT-IR (film): $\tilde{u} = 2865$ (w), 1682 (s), 1597 (s), 1482 (s), 1452 (s), 1395 (m), 1350 (m), 1285 (m), 1241 (m), 1189 (s), 1161 (s), 1100 (s), 1025 (s), 925 (m), 831 (m), 755 (s), 655 (m), 606 (w), 530 (w) cm^{-1}.

Synthesis of 5,15-strapped porphyrin **16**: The bridge **15** (375 mg, 983 µmol) and trifluoro boro etherate (13.9 mg, 98.3 µmol) were dissolved in dichloromethane (350 mL) under nitrogen atmosphere. To this solution *meso*-phenyl dipyrromethane **14** (436 mg, 1.96 mmol), dissolved in dichloromethane (50 mL), was added under stirring over a period of 1 h. After stirring for 15 h, *p*-chloranil (504 mg, 2.05 mmol) was added and stirred for 5 h at 40 °C. Then, the solvent was removed under reduced pressure and the crude product was purified by column chromatography (dichloromethane, $R_f = 0.54$). A purple solid was obtained (80.0 mg. 102 µmol. 10%): m.p.: 372 °C; ^{1}H NMR (600 MHz. $CDCl_3$, 300 K): $\delta = 8.81$ (s. 8H, *H*-13, *H*-14), 8.54 (dd, $^3J = 7.2$ Hz, $^4J = 1.6$ Hz, 2H, *H*-9), 8.36 (s, br, 2H, *H*-*o*-Ph), 8.03 (s, br, 2H, *H*-*o*-Ph′), 7.82–7.68 (m, 8H, *H*-7, *H*-*m*-Ph, *H*-*m*-Ph′, *H*-*p*-Ph), 7.50 (t, $^3J = 7.5$ Hz, 2H, *H*-8), 7.07 (d, $^3J = 8.2$ Hz, 2H, *H*-6), 3.72–3.69 (m, 4H, *H*-4), 2.53–2.48 (m, 4H, *H*-3), 1.06 (s, 4H, *H*-2), −2.59 (s, br, 2H, N*H*) ppm; ^{13}C NMR (150 MHz, 300 K, $CDCl_3$): $\delta = 159.3$ (*C*-5), 142.1 (*C*-17), 134.6 (*C*-*o*-Ph′), 134.4 (*C*-*o*-Ph), 133.4 (*C*-9), 131.8 (*C*-10), 130.6 (*C*-13, *C*-14), 130.0 (*C*-7), 127.6 (*C*-*p*-PH), 126.7 (*C*-*m*-Ph, *C*-*m*-Ph′), 120.1 (*C*-8), 119.9 (*C*-15), 119.7 (*C*-16), 116.4 (*C*-12), 115.5 (*C*-11), 112.0 (*C*-6), 78.7 (*C*-1), 69.8 (*C*-4), 66.9 (*C*-3), 56.5 (*C*-9) ppm; MS (MALDI, TOF): $m/z = 785$ $[M]^+$; HRMS (EI): 784.30495 (calc.). 784.30323 (found) for $C_{52}H_{40}N_4O_4$; FT-IR (film): $\tilde{u} = 2924$ (w), 1596 (w), 1471 (m), 1441 (m), 1348 (m), 1284 (m), 1247 (m), 1184 (m), 1112 (m), 965 (s), 796 (s), 728 (s), 698 (s), 658 (m), 579 (m), 519 (m), 408 (s) cm^{-1}.

Synthesis of 5,15-strapped iron(III) porphyrin chloride **17**: The 5,15-strapped porphyrin **16** (27.0 mg, 37.2 µmol) and iron(II) chloride tetrahydrate (180 mg, 669 µmol) were dissolved in degassed acetonitrile (30 mL) under nitrogen atmosphere and refluxed for 4 h. Then, the solvent was removed under reduced pressure and the crude product was dissolved in dichloromethane (40 mL), and then washed twice with brine (50 mL) and water (100 mL). The combined organic layers were dried over anhydrous magnesium sulfate and the solvent was removed under reduced pressure. A brown solid was obtained (30.0 mg, 34.3 µmol, 92%); m.p.: 131 °C; ^{1}H NMR (500 MHz, CD_2Cl_2, 300 K): $\delta = 81.62$ (s, br, 4H, *H*-pyrrole), 78.00 (s, br, 4H, *H*-pyrrole) ppm; MS (MALDI, TOF): $m/z = 839$ $[M\text{-}Cl]^+$, 874 $[M]^+$; HRMS (EI): 838.22299 (calc.), 838.22174 (found) for $C_{52}H_{38}FeN_4O_4$; FT-IR (film): $\tilde{u} = 2921$ (w), 1597 (m), 1442 (m), 1336 (m), 1243 (m), 1000 (m), 801 (m), 719 (m), 659 (m), 541 (m), 463 (s), 436 (w), 418 (w), 408 (s) cm^{-1}. Due to the highly diluted NMR samples, the large number of quaternary C-atoms and the paramagnetism, ^{13}C NMR spectroscopy of **17** did not provide sufficient signal intensities. Therefore, the ^{13}C NMR spectrum was not analyzable.

Synthesis of 5,15-strapped iron(III)porphyrin 1-methylimidazole complex **18**: The 5,15-strapped iron(III) porphyrin chloride **17** (1.42 mg, 1.63 µmol) was dissolved in 400 µL dichloromethane-d_2. To this solution 1-methylimidazole (5.48 mg, 66.8 µmol) dissolved in 80 µL of dichloromethane-d_2, was added. ^{1}H NMR (500 MHz, CD_2Cl_2, 300 K): $\delta = -7.92$ (s, 2H, *H*-pyrrole), −10.05 (s, 2H, *H*-pyrrole), −22.15 (s, 2H, *H*-pyrrole), −23.28 (s, 2H, *H*-pyrrole) ppm; HRMS (ESI): 920.27680 (calc.), 920.27580 (found) for $C_{56}H_{44}N_6O_4Fe$. Due to the highly diluted NMR samples, the large number of quaternary C-atoms and the paramagnetism, ^{13}C NMR spectroscopy of **18** did not provide sufficient signal intensities. Therefore, the ^{13}C NMR spectrum was not analyzable.

Data availability

All the data that support the findings of this study are available within the paper and its Supplementary Information files, or from the corresponding author on reasonable request.

Received: 2 July 2018 Accepted: 8 October 2018
Published online: 12 November 2018

References

1. Meunier, B., de Visser, S. P. & Shaik, S. Mechanism of oxidation reactions catalyzed by cytochrome P450 enzymes. *Chem. Rev.* **104**, 3947–3980 (2004).
2. Denisov, I. G., Makris, T. M., Sligar, S. G. & Schlichting, I. Structure and chemistry of cytochrome P450. *Chem. Rev.* **105**, 2253–2277 (2005).
3. Baik, M.-H., Newcomb, M., Friesner, R. A. & Lippard, S. J. Mechanistic studies on the hydroxylation of methane by methane monooxygenase. *Chem. Rev.* **103**, 2385–2419 (2003).
4. Ferrando-Soria, J. et al. Molecular magnetism, quo vadis? A historical perspective from a coordination chemist viewpoint. *Coord. Chem. Rev.* **339**, 17–103 (2017).
5. Dommaschk, M. et al. Photoswitchable magnetic resonance imaging contrast by improved light-driven coordination-induced spin state switch. *J. Am. Chem. Soc.* **137**, 7552–7555 (2015).
6. Venkataramani, S. et al. Magnetic bistability of molecules in homogeneous solution at room temperature. *Science* **331**, 445–447 (2011).
7. Shores, M. P., Klug, C. M. & Fiedler, S. R. in *Spin-Crossover Materials: Spin-state Switching in Solution* (ed Halcrow, M. A.) Ch. 10 (Wiley, Oxford, 2013).
8. Senthil, K. K. & Ruben, M. Emerging trends in spin crossover (SCO) based functional materials and devices. *Coord. Chem. Rev.* **346**, 176–205 (2017).
9. Nihei, M., Suzuki, Y., Kimura, N., Kera, Y. & Oshio, H. Bidirectional photomagnetic conversions in a spin-crossover complex with a diarylethene moiety. *Chem. Eur. J.* **19**, 6946–6949 (2013).
10. Milek, M., Heinemann, F. W. & Khusniyarov, M. M. Spin-crossover meets diarylethenes: efficient photoswitching of magnetic properties in solution at room temperature. *Inorg. Chem.* **52**, 11585–11592 (2013).
11. Heitmann, G., Schuett, C. & Herges, R. Spin state switching in solution with an azoimidazole-functionalized nickel(II) porphyrin. *Eur. J. Org. Chem.* www.eurjoc.org, 3817–3823 (2016).
12. Heitmann, G., Schuett, C., Grocbner, J. & Huber, L. Azoimidazole functionalized Ni-porphyrins for molecular spin switching and light responsive MRI contrast agents. *Dalton Trans.* **45**, 11407–11412 (2016).
13. Dommaschk, M. et al. Coordination-induced spin-state switching with nickel chlorin and nickel isobacteriochlorin. *Inorg. Chem.* **54**, 9390–9392 (2015).
14. Scheidt, W. R. & Reed, C. A. Spin-state/stereochemical relationships in iron porphyrins: implications for the hemoproteins. *Chem. Rev.* **81**, 543–555 (1981).

15. Walker, F. A. & Simonis, U. in *Encyclopedia Inorganic Chemistry: Iron Porphyrin Chemistry* (ed King, R. B.) 2390–2521 (Wiley, Chichester, 2006).
16. Reed, A. C. & Guiset, F. A "magnetochemical" series. Ligand field strengths of weakly binding anions deduced from $S = 3/2$, 5/2 spin state mixing in iron(III) porphyrins. *J. Am. Chem. Soc.* **118**, 3281–3282 (1996).
17. Toney, G. E. et al. Characterization of a true intermediate-spin (porphinato) iron(III) complex. *Inorg. Chem.* **23**, 2561 (1984).
18. Walker, F. A., Lo, M.-W. & Ree, M. T. Electronic effects in transition metal porphyrins. The reactions of imidazoles and pyridines with a series of *para*-substituted tetraphenylporphyrin complexes of chloroiron(III). *J. Am. Chem. Soc.* **98**, 5552–5560 (1976).
19. Sahoo, D., Quesne, M. G., de Visser, S. P. & Rath, S. P. Hydrogen-bonding interactions trigger a spin-flip in iron(III) porphyrin complexes. *Angew. Int. Ed.* **54**, 4796–4800 (2005).
20. Geiger, D. K. & Scheidt, W. R. Control of spin state in (porphinato)iron(III) complexes. Effect of the porphyrin ligand. *Inorg. Chem.* **23**, 1970–1972 (1984).
21. Geiger, D. K., Chunplang, V. & Scheidt, W. R. Control of spin state in (porphinato)iron(III) complexes. A new crystalline phase of (isothiocyanato) (pyridine) (meso-tetraphenylporphinato)iron(III) with two magnetically distinct sites. *Inorg. Chem.* **24**, 4736–4741 (1985).
22. Bertrand, I., Theodule, F. X., Gayda, J. P., Mispelter, J. & Momenteau, M. Determination of the zero-field splitting in a spin-admixed ($S = 5/2$, $S = 3/2$) iron III porphyrin. *Chem. Phys. Lett.* **102**, 442–445 (1983).
23. Boersma, A. D. & Goff, H. M. Multinuclear magnetic resonance spectroscopy of spin-admixed $S = 5/2$, 3/2 iron(III) porphyrins. *Inorg. Chem.* **21**, 581–586 (1982).
24. Toney, G. E. et al. ^{1}H and ^{13}C NMR study of the effects of meso substituents on the $S = 3/2$, 5/2 spin state admixture of (perchlorato)(tetraarylporphinato) iron(III) complexes. *Inorg. Chem.* **23**, 4350–4352 (1984).
25. Kastner, M. E., Scheidt, W. R., Mashiko, T. & Rees, C. A. Molecular structure of diaquo.alpha.,.beta.,.gamma.,.delta.-tetraphenylporphinatoiron(III) perchlorate and perchlorato-.alpha.,.beta.,.gamma.,.delta.-tetraphenylporphinatoiron(III). Two new structural types for iron(III) porphyrins. *J. Am. Chem. Soc.* **100**, 666–667 (1978).
26. Mashiko, T., Kastner, M. E., Spartalian, K., Scheidt, W. R. & Reed, C. A. Six coordination in high-spin ferric porphyrins. A new structural type and models for aquomethemoglobin. *J. Am. Chem. Soc.* **100**, 6354–6362 (1978).
27. Hoshino, A. & Nakamura, M. Determination of the field strengths of weak neutral ligands having oxygen as coordination atom. *Chem. Lett.* **33**, 1234–1235 (2004).
28. Hoshino, A., Ohgo, Y. & Nakamura, M. Electronic structures of six-coordinate ferric porphyrin complexes with weak axial ligands: usefulness of ^{13}C NMR chemical shifts. *Inorg. Chem.* **44**, 7333–7344 (2005).
29. Thies, S. et al. Light-driven coordination-induced spin-state switching: rational design of photodissociable ligands. *Chem. Eur. J.* **18**, 16358–16368 (2012).
30. Thies, S. et al. Light-induced spin change by photodissociable external ligands: a new principle for magnetic switching of molecules. *J. Am. Chem. Soc.* **133**, 16243–16250 (2011).
31. Bottomley, L. A. & Kadish, K. M. Counterion and solvent effects on the electrode reactions of iron porphyrins. *Inorg. Chem.* **20**, 1348 1357 (1981).
32. Otsuka, T., Ohya, T. & Sato, M. EPR studies of hydrogen bonding in ferric porphyrin complexes. Low-spin dimethoxo(tetraphenylporphinato)ferrate (111) in dimethyl sulfoxide-methanol. *Inorg. Chem.* **24**, 776–782 (1985).
33. Del Piero, S. et al. Excel tool for equilibrium speciation based on newton–raphson method and on a hybrid genetic algorithm. *Ann. Chim.* **96**, 29–49 (2006).
34. Lauffer, R. B. Paramagnetic metal complexes as water proton relaxation agents for NMR imaging: theory and design. *Chem. Rev.* **87**, 901–927 (1987).
35. Bloembergen, N. J. Proton relaxation times in paramagnetic solutions. *Chem. Phys.* **27**, 572 (1957).
36. Solomon, I. Relaxation processes in a system of two spins. *Phys. Rev.* **99**, 559 (1955).
37. Sligar, S. G., Cinti, D. L., Gibson, G. G. & Schenkman, J. B. Spin state control of the hepatic cytochrome P450 redox potential. *Biochem. Biophys. Res. Commun.* **90**, 925–932 (1979).
38. Nesset, M. J. M., Shokhirev, N. V., Enemark, P. D., Jacobson, S. E. & Walker, F. A. Models of the Cytochromes. redox properties and thermodynamic stabilities of complexes of "hindered" iron(III) and iron(II) tetraphenylporphyrinates with substituted pyridines and imidazoles. *Inorg. Chem.* **35**, 5188–5200 (1996).
39. Huang, S.-P., Shiota, Y. & Yoshizawa, K. DFT study of the mechanism for methane hydroxylation by soluble methane monooxygenase (sMMO): effects of oxidation state, spin state, and coordination number. *Dalton Trans.* **42**, 1011–1023 (2013).
40. Nakamura, M., Ohgo, Y. & Ikezaki, A. in *Handbook of Porphyrin Science* Vol. 7 (eds Kadish, K. M., Smith, K. M. & Guilard, R.) 1–146 (World Scientific, Singapore, 2010).
41. Walker, F. A., Huynh, B. H., Scheidt, W. R. & Osvath, S. R. *J. Am. Chem. Soc.* **108**, 5288–5297 (1986).
42. Watson, C. T., Cai, S., Shokhirev, N. V. & Walker, F. A. *Inorg. Chem.* **44**, 7468–7484 (2005).
43. Adler, A. D. et al. A simplified synthesis for meso-tetraphenylporphine. *J. Org. Chem.* **32**, 476–476 (1967).
44. Adler, A. D., Longo, F. R., Kampas, F. & Kim, J. On the preparation of metalloporphyrins. *J. Inorg. Nucl. Chem.* **32**, 2443 (1970).
45. Reed, C. A. et al. The missing heme spin state and a model for cytochrome *c*′. The mixed $S = 3/2$, 5/2 intermediate spin ferric porphyrin: perchlorato(meso-tetraphenylporphinato)iron(III). *J. Am. Chem. Soc.* **101**, 2948–2958 (1979).
46. Thies, S. et al. Light-driven coordination-induced spin-state switching: rational design of photodissociable ligands. *Chem. Eur. J.* **18**, 16358–16368 (2012).
47. Littler, B. J. et al. Refined synthesis of 5-substituted dipyrromethanes. *J. Org. Chem.* **64**, 1391–1396 (1999).
48. Cagnoni, A. J., Varela, O., Uhrig, M. L. & Kovensky, J. Efficient synthesis of thiolactoside glycoclusters by ruthenium-catalyzed cycloaddition reaction of disubstituted alkynes on carbohydrate scaffolds. *Eur. J. Org. Chem.* **5**, 972–983 (2013).

Acknowledgements

We gratefully acknowledge support by the DFG via Sonderforschungsbereich 677. S.S. thanks the Alexander von Humboldt Foundation, Germany and DST-SERB, India, respectively, for Humboldt and Ramanujan research fellowships and O.R. for funding by the Max-Planck Society. This work was supported by the Cluster of Excellence RESOLV (EXC 1069) funded by the Deutsche Forschungsgemeinschaft (DFG).

Author contributions

R.H. and S.S. designed the experiments; S.S. performed the photoswitching, electrochemistry, and relaxivity experiments; S.S. and B.K. performed titration experiments; K.S. analyzed the binding isotherms; F.D.S. assisted in the NMR data acquisition and interpretation; M.P. synthesized and investigated the strapped porphyrin and performed electrochemistry experiments together with S.S. and O.R.; T.I., D.G., and WS measured the EPR spectra; Evans measurements have been performed by B.K., S.S., and M.P.; R.H. supervised the project; and S.S. and R.H. wrote the manuscript.

Additional information

Supplementary Information accompanies this paper at https://doi.org/10.1038/s41467-018-07023-1.

Competing interests: The authors declare no competing interests.

Reprints and permission information is available online at http://npg.nature.com/reprintsandpermissions/

Publisher's note: Springer Nature remains neutral with regard to jurisdictional claims in published maps and institutional affiliations.

3.2 Synthese von überbrückten Porphyrinen

Im letzten Jahrhundert wurden vermehrt Veröffentlichungen von überbrückten Porphyrinen publiziert. Grund hierfür sind die unterschiedlichen Strukturmerkmale und elektronischen Eigenschaften, welche eine Vielzahl von Anwendungen ermöglichen.[84] So werden überbrückte Porphyrine als chirale Epoxidierungs-Katalysatoren[85] und als Modelle für Enzyme wie Cytochrom P450 verwendet.[86] Darüber hinaus dienen sie als Bausteine für die Synthese von Catenanen,[87] für selbstorganisierte photonische Drähte[88] und als Modelle für eine Reihe von biomimetischen Porphyrinen.[89]

Zusätzlich eignet sich diese Art von Verbindungen hervorragend, um ein pentavalentes Porphyrin zu designen, welches das Gegenion des Fe(III)-Porphyrins kovalent bindet und somit einen Austausch verhindert.

Im Prinzip können drei Strategien zur Synthese von überbrückten Porphyrinen verfolgt werden. (a) Als erstes kann ein vorgefertigtes Porphyrin mit einem kettenförmigen Baustein verknüpft werden. (b) Alternativ kann ein Baustein, der zwei Aldehyde und die bereits fertige Brücke enthält, verwendet werden, um hiermit das Porphyrin nach LINDSEY aufzubauen.[90] (c) In der letzten Strategie werden ein verbrücktes Bisdipyrromethan und zwei Äquivalente eines Aldehyds verwendet (Abbildung 14).[84]

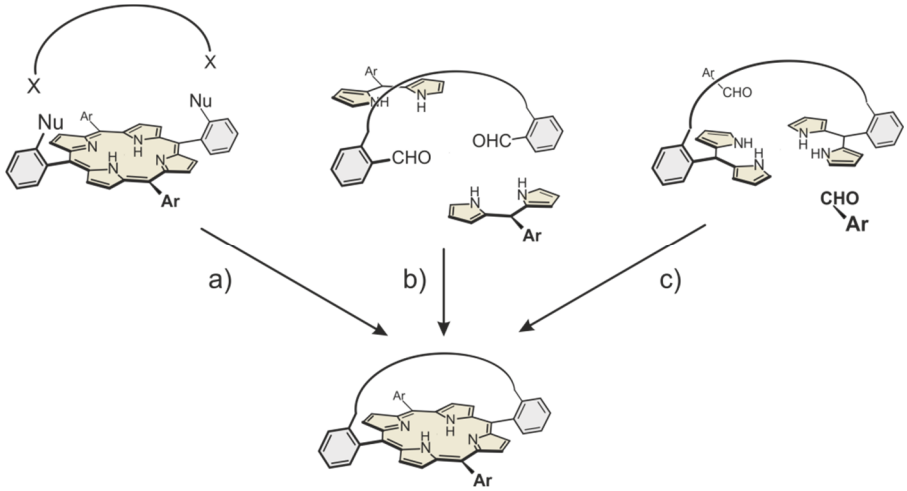

Abbildung 14: Drei Strategien zur Synthese von überbrückten Porphyrinen.

Spin switching of ferrous porphyrins strapped with triazolate

Morten K. Peters, Sebastian Hamer, Torben Jäkel, Fynn Röhrich, Carolina von Essen, Manu Lahtinen, Christian Näther, Frank Sönnichsen, Kari Rissanen and Rainer Herges

Manuskript für
Inorganic Chemistry

Eigenanteil: Die Synthesen und Messungen wurden von Morten Peters durchgeführt. Die Eiskristallstrukturanalyse wurde von Prof. Dr. Christian Näther und Kari Rissanen gelöst. Das Manuskript wurde von Morten Peters und Prof. Dr. Rainer Herges verfasst.

Zusammenfassung

In dieser Publikation wird die effiziente Synthese von mehreren acetylenüberbrückten Porphyrinen vorgestellt, welche durch eine 1,3-dipolare Cycloaddition mit Azid in 1,2,3-Triazole umgewandelt werden kann. Zudem wurde erfolgreich Eisen(III) in diese Porphyrine eingelagert (Abbildung 15).

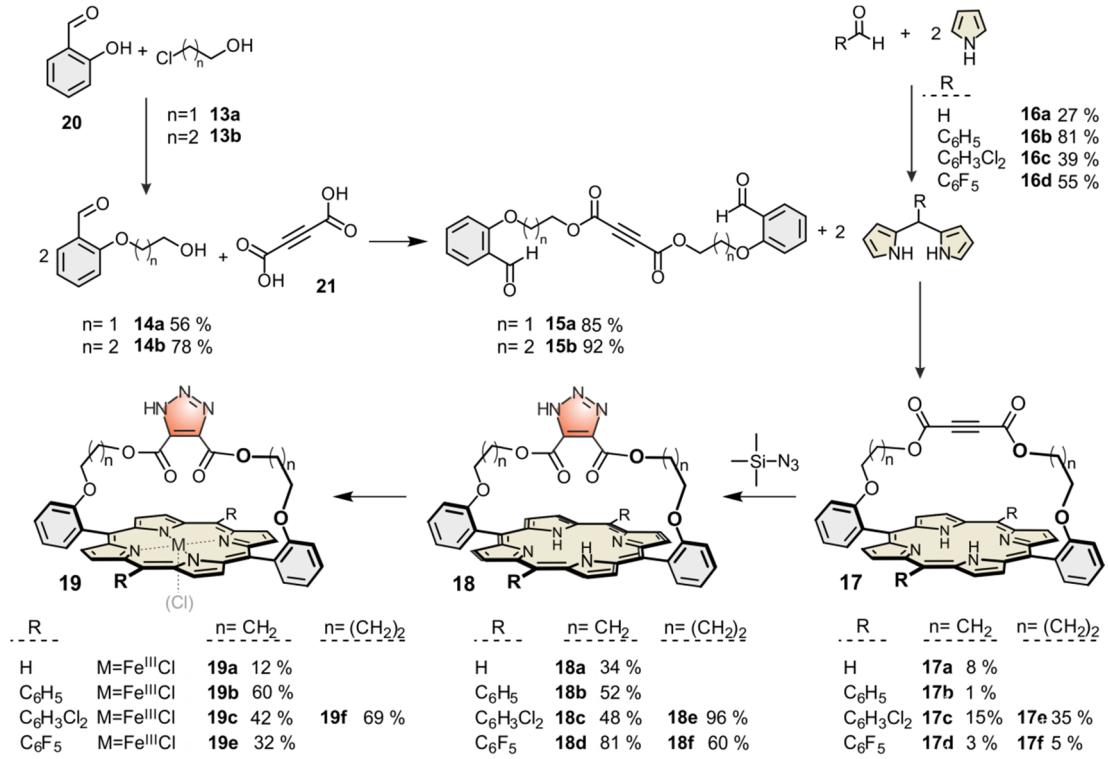

Abbildung 15: Darstellung der Synthese überbrückter Porphyrine durch den Syntheseweg b.

Die UV/Vis- sowie NMR-Untersuchungen von **19c** zeigen, dass die Triazoleinheit nicht in der Lage ist, an das Fe(III)-Zentrum zu koordinieren, da das Triazol ein zu schwacher Ligand ist. Durch die Zugabe einer Base und der damit verbundenen Deprotonierung wird das stärker bindende Triazolat gebildet. Dieses verdrängt das Chlorid und liefert in Folge dessen den gewünschten fünffach koordinierten neutralen High-Spin-Komplex **20**, der durch einen weiteren axialer Ligand wie zum Beispiel das *p*-Methoxypyridin zum LS übergeht (Abbildung 16).

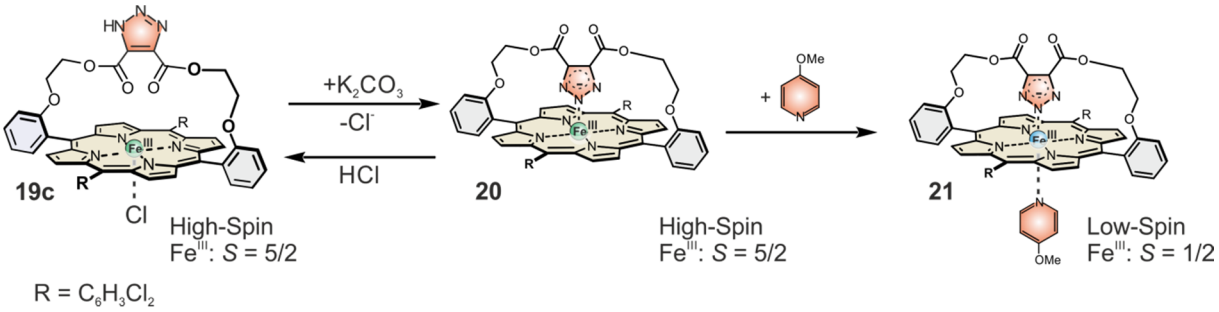

Abbildung 16: Die Deprotonierung des Triazols führt zur Koordination des Triazolats, wobei der HS-Zustand ($S = 5/2$) erhalten bleibt. Eine zusätzliche Koordination eines externen Liganden führt zu dem Molekül **21**, welches im LS-Zustand ($S = 5/2$) vorliegt.

Dieser fünffach koordinierte High-Spin-Komplex **20** kann nun als Modellverbindung für eine Reihe wichtiger Eisen(III)-Porphyrine in der Natur eingesetzt werden, wie zum Beispiel für das Cytochrom P450.

Spin switching of ferrous porphyrins strapped with triazolate

Morten K. Peters[1], Sebastian Hamer[1], Torben Jäkel[1], Fynn Röhrich[1], Carolina von Essen[3], Manu Lahtinen[3], Christian Näther[2], Frank Sönnichsen[1], Kari Rissanen[3] and Rainer Herges[1]

[1]Address: Otto-Diels-Institut für Organische Chemie, Christian Albrechts-Universität, Otto-Hahn-Platz 4, 24098 Kiel, Germany

[2]Address: Anorganische Chemie, Christian-Albrechts-Universität,

Kiel Max-Eyth-Str. 2 24118 Kiel, Germany

[3]Address: PL 35, 40014, Universität Jyväskylä, Finnland

KEYWORDS

strapped porphyrins; spin switch; magnetic moment; iron porphyrins; bridged porphyrins; triazole ligand

ABSTRACT

Fe(III) porphyrins bridged with 1,2,3-triazole ligands were synthesized. Upon deprotonation, the triazolate ion coordinates to the Fe(III) ion. An overall neutral high-spin Fe(III)porphyrin is formed with triazolate serving as an axial ligand as well as the counterion. The second axial

coordination site is now activated for coordination and binds methoxypyridine forming a 6-coordinate low-spin complex. Upon addition of a phenylazopyridine as a photodissociable ligand, the spin of the complex can be reversibly switched with UV and visible light.

Introduction

Ferrous porphyrins with anionic ligands serving both as axial ligand and as counterions are abundant in Nature. They perform as catalysts in selective CH activation (cytochrome P450),[1,2,3,4] hydrogen peroxide decomposition (catalyses) and a number of other biologically important processes.[5,6,7] Controlled spin switching is essential for the function of these enzymes. During its catalytic cycle, cytochrome P450 switches between 6-coordinate low-spin resting state, and 5-coordinate high-spin state.[8] Spin state control, particularly of iron complexes is also a prerequisite in a number of further bio-catalytic processes such as C-H activation by methane monooxygenases.[9] The design of artificial systems whose spin states are responsive to external stimuli is the first step towards machine-type catalysts performing particular difficult catalytic processes such as the conversion of hydrocarbons to alcohols under ambient conditions.[10] Single molecule spin state switching is also the prerequisite to molecular spintronics,[11] responsive contrast agents[12,13] and a number of further applications.[14] Recently, we presented the first artificial ferrous porphyrin system that changes its spin state between high-spin ($S=^5/_2$) and low-spin ($S=^1/_2$) upon irradiation with light.[15] However, the complex consists of 6 components (Fe(III)porphyrin, the counter ion, two oxygen and two nitrogen ligands) that are in equilibrium in solution. Notwithstanding the high switching efficiency (76%), being a multi-component system, the system is quite sensitive to changes in composition and environment. We here report

on a two-component system, which includes a covalently attached triazole unit and only one separate ligand.

Fe(III)tetraphenylporphyrin chloride (FeTPPCl) is commercially available and in principle meets the structural requirements for spin switching. FeTPPCl is 5-coordinate and high-spin with a chloride ion serving as the counterion and axial ligand (Figure 1a).[15] However, the chloride ligand is strongly bound and the second axial coordination site only binds very strong nitrogen ligands, such as 1-methylimidazole. Moreover, the mixed chloride/imidazole complex is still high-spin.[16,17] Upon replacing the chloride ligand in FeTPPCl by azide ($FeTPPN_3$) the iron(III) ion is closer to the spin crossover point. $FeTPPN_3$ is 5-coordinate and high-spin but in contrast to FeTPPCl it is considerably more prone to bind a second axial ligand leading to a low-spin complex.[9,18,19]

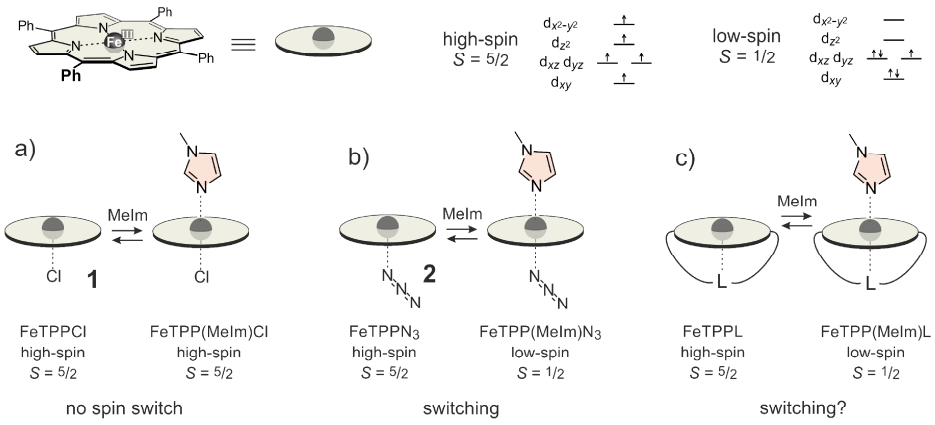

Figure 1: Spin states of Fe(III)porphyrins with one anionic axial ligand with and without 1-methylimidazole as the second axial ligand. a) with a chloride ligand (**1**), b) with azide (**2**), and

c) schematic representation of a ferrous porphyrin strapped with an anionic ligand (**3**) (target structure for spin switching).

However, $FeTPPN_3$ **2** has several disadvantages. The azide ligand is easily replaced by Cl^- forming FeTPPCl **1** and by OH^- leading to the μ-oxo compound $(FeTPP)_2O$. To avoid these problems we designed a strapped porphyrin including an anionic ligand L^- in the bridge complying with the following preconditions: 1. L^- should be strongly binding, 2. The 5-coordinate complex should be high-spin, 3. The free axial coordination site should bind ligands with low or medium ligand field strength (see Figure 1). 4. Binding of the second axial ligand should induce a spin switch to the low-spin state.

Results and Discussion

Several Fe(III)porphyrins with covalently linked anionic ligands are known.[20,21,22,23,24] However, strapped anionic nitrogen ligands have not been realized so far. Among the non-covalently coordinated nitrogen ligands, imidazolate, isocyanate [25] and azide are the most common.[26] Unfortunately, azide and isocyanate cannot be tethered to the porphyrin because there is no free valence available to form a covalent bond. Imidazolate suffers from the fact that only one position is available to attach a tether (the C atom distant from the coordinating N atom) and imidazolates are easily protonated (pKa: 14.3)[27] and the corresponding complexes would not be water stable. We therefore considered triazoles as anionic ligands for strapping in 4,5 position. The parent triazole has a pK_a of 8.8.[28] The 4,5-diester substituted triazole unit should be considerably more acidic (pK_a~5) and coordinated to Fe(III) it should be inert to protonation (water stable) at neutral pH.

To check if triazolates would be suitable anionic ligands for an integration into the bridge of a strapped porphyrin, we performed preliminary experiments with 4,5-dimethyl-1,2,3-triazole-4,5-dicarboxylate (DMTDH). In a preliminary experiment a solution of iron(III) tetraphenyl-porphyrin chloride (FeTPPCl **1**, 100 µM) in acetonitrile was treated with an 1000-fold excess of 4,5-dimethyl-1,2,3-triazole-4,5-dicarboxylate (DMTDH). No changes in NMR or UV were observed, indicating that there is no coordination of the free ligand DMTDH to the Fe(III) ions. Obviously, the coordination power of neutral DMTDH is not sufficient for coordination. However, upon deprotonation of the triazole (DMTDH) with solid K_2CO_3 the color of the FeTPPCl/DMTDH solution changes from brown to yellow and the UV-vis spectrum exhibits the characteristic absorption bands of low-spin $FeTPPL_2$ (550 nm, 575 nm shoulder, 640 nm) (Figure 2, see supporting information (SI) (V.1)).[29] The low-spin signals NMR spectrum at -14 ppm further confirm the $[FeTPP(DMTD)_2]^-$ low-spin state. Density functional theory (DFT) calculations confirm that the triazolate coordinates with its nitrogen in 2 position to the Fe(III) ion forming a symmetrical complex (see SI (III)). A FeTPP(DMTD) (1:1 complex) is very unlikely, because it is known that $FeTPP^+$ with one anionic nitrogen ligand is high-spin (see Figure 2a).[10,11,30,31,32] (Triazolate ($DMTD^-$), however, does not coordinate to a strapped Fe(III)porphyrin **6** whose second axial coordination side is sterically shielded.[8] This lack of reactivity proves that the triazolate has to attack from the opposite axial side to replace the chloride ligand (see Figure 2b). We conclude that a strapped triazolate should bind to the metal ion.

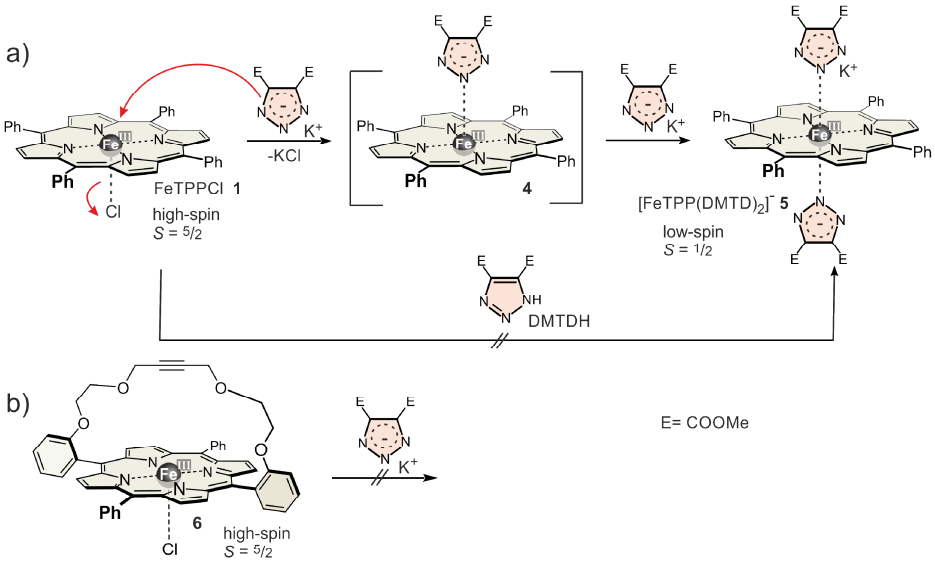

Figure 2: Coordination of Fe(III)porphyrin chlorides with triazole (DMTDH) and triazolate ($DMDT^-$). a) FeTPPCl **1** reacts with triazolate but not with triazole to form a 2:1 complex. b) Strapped porphyrin **3** does not react with triazolate.

DFT model reactions predict that a -O-CH_2-CH_2- or a -O-CH_2-CH_2-CH_2- chain connecting the ester function of the DMTDH with the *ortho* position of the *meso* phenyl rings should provide a suitable preorientation of the central nitrogen atom of $DMTD^-$ for coordination with Fe(III) (**7** and **8** (Figure 3b) and c)). As compared to a structurally similar reference compound (Figure 3a)) with an unconstrained triazolate ligand and optimal coordination geometry, structure **7** with the short tether exhibits a somewhat shorter Fe-N coordination bond, and compound **8** with the longer tether has a larger Fe-N distance. Obviously, the tether in structure **7** is somewhat to small drawing the triazolate ligand towards the Fe(III) ion, and the tether in **8** is a bit too long. A conformational analysis of **7** revealed that the tethers are still flexible. The O-CH_2-CH_2-O units

adopt gauche and anti conformations, which are similar in energy (see Supporting Information (III)). Nevertheless, the accuracy of fit is quite good and **7** and **8** were selected as target structures for synthesis.

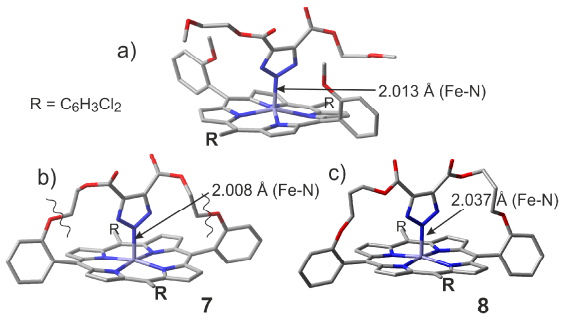

Figure 3: PBE(D3)/def2svp optimized structures of the triazolate strapped target compounds **7** and **8** (b) and c)) and a structural reference (a)) with a corresponding not covalently attached ligand. Hydrogen atoms and the *meso* 2,5-dichlorophenyl substituents are omitted for clarity. The bond lengths of the Fe-N coordination bonds indicate the accuracy of fit of the tether lengths. The reference compound exhibits the optimum Fe-N distance because the porphyrin and the ligand were optimized without further geometry constraints. The reference compound a) was constructed by cutting structure b) at the wavy lines and complementing the free valences by methyl groups.

In principle, there are three strategies to synthesize strapped porphyrins (capped[33], hindered[1] and bridged porphyrins)[34]. (a) Bridging a prefabricated porphyrin, e.g. reaction of a 5,15-bis(2-hydoxyphenyl) porphyrin with a chain-like building block with a leaving group at both ends. b) and c) Alternatively, one can use building blocks that already include the bridge to prepare the porphyrin (mixed aldehyde synthesis). There are two options for the latter strategy[1,35] b) using a bridged bisaldehyde and two equivalents of dipyrromethane [1,36,37,38] or c) using a bridged bisdipyrromethane and two equivalents of an aldehyde (see Figure 4).[39]

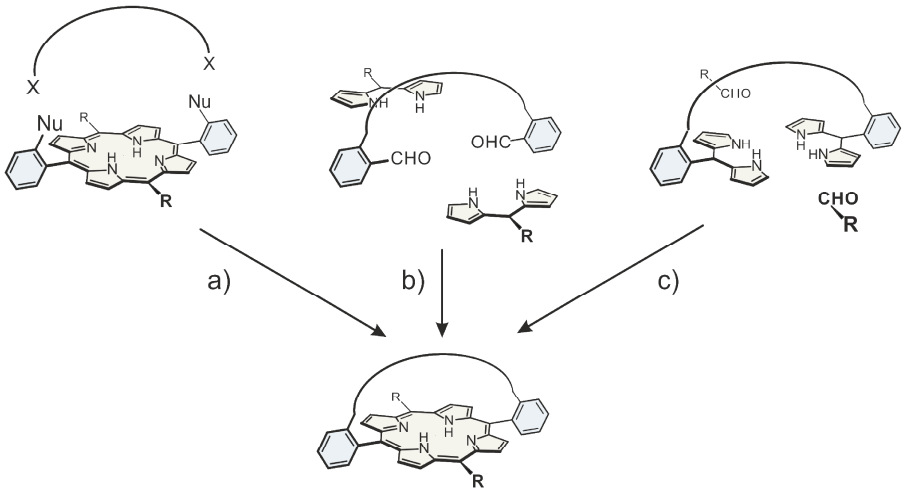

Figure 4: Three strategies to synthesize strapped porphyrins.

Synthetic pathway (a) was not successful. Therefore, we pursued strategy (b). Salicylaldehyde (**9**) and chloroethanol (**10a**) were reacted to 2-(2-hydroxyethoxy)benzaldehyde (**11a**).[40] Acetylene dicarboxylic acid (**12**) with **11a** yields dialdehyde **13a** (85%). **13a** was used in Lindsay type cyclization reactions with different 5-substituted dipyrromethanes[41] to afford strapped porphyrins (see scheme 2) with yields up to 35%.

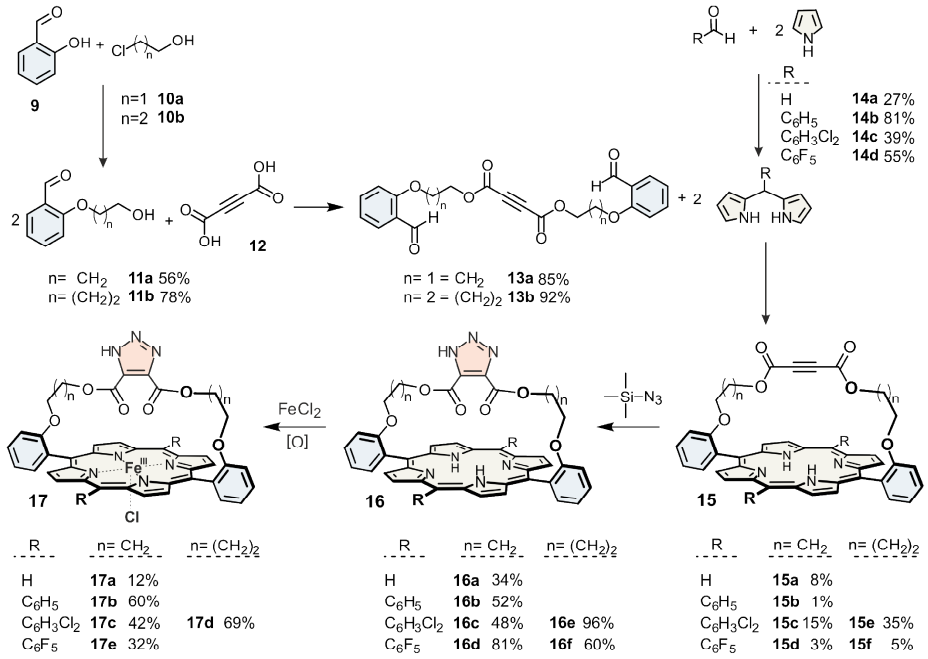

Scheme 1: Stepwise synthesis of the strapped porphyrins (pathway b).

The yield of **15b** is low (1%) because of severe scrambling.[42] The main product is tetraphenyl porphyrin (TPP). **15c** is formed in 15% yield. A crystal structure analysis reveals a strained structure with an approximate C_2 symmetry. The acetylene unit is not exactly linear and the porphyrin ring distorts towards a ruffled type geometry (see Figure 5).

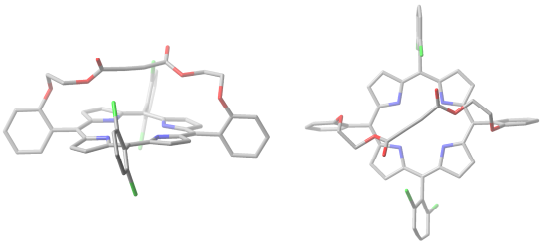

9

Figure 5: Crystal structure of **15c (Christian Näther)**.

We also prepared an analogously strapped porphyrin **15e** with longer -O-CH_2-CH_2-CH_2-bridges (extended by an additional CH_2 group). With 35% the yield is more than double compared to **9c**, obviously because the longer bridge imposes less strain. A similar trend albeit with lower yields is observed with the bis(pentafluoro) substituted strapped porphyrins **15d** (3%) and **15f** (5%). Scrambling was not detected in any strapped porphyrin except **15b**.

Electron deficient acetylenes are known to undergo 1,3-dipolar cycloaddition with azide.[43] Reaction of the strapped porphyrins **15a-f**, with trimethylsilyl azide afforded the corresponding triazoles **16a-f** in 34-96% yield. A crystal structure analysis of **16e** confirms the structural assignment. The porphyrin ring is planar which is in agreement with our assumption that the bridge does not impose strain (see Figure 6).

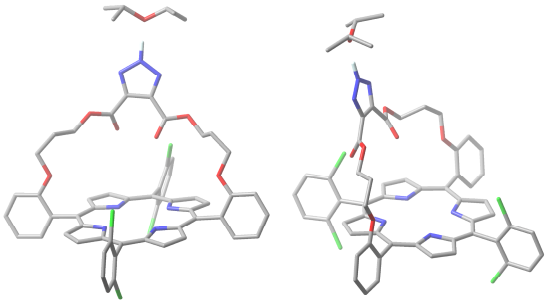

Figure 6: Crystal structure of **16e (Kari Rissanen)**.

Upon heating a solution of the free base porphyrins with $FeCl_2$ in acetonitrile to 80°C under nitrogen and subsequent oxidation upon exposure to air Fe(III)porphyrins were obtained in 12–

69% yield.[44] NMR analysis reveals that all iron(III) porphyrins are high-spin ($S=^5/_2$). The pyrrole protons resonate at 70-80 ppm which is characteristic for high-spin Fe(III)porphyrins.[45]

No signals were observed at -10 to -20 ppm which would indicate the formation of low-spin ($S=^1/_2$) complexes.[46] Obviously, the strapped, protonated triazole units do not coordinate to the Fe^{3+} ion in agreement with the corresponding free protonated triazoles (DMTDH, Figure 2). To double check the non-coordinating behavior of the triazole unit, trifluoroacetic acid was added. If coordinated, the triazole should decoordinate upon protonation. No change in the UV-vis spectrum was observed.

Since the free triazole ligand DMTDH upon deprotonation coordinates to FeTPPCl (Figure 2), a similar intramolecular coordination was expected after deprotonation of the strapped DMTDH ligand in **17c**. Upon addition of K_2CO_3 to the chloride complex **17c** the four high-spin signals of the pyrrole protons at 85.7, 83.0, 80.2 and 78.4 ppm form two broad signals at 78.9 and 84.9 ppm (see SI (V.2)). No signals are visible in the low-spin range and the magnetic moment was determined to 5.62 B.M. (see SI (IV)) confirm a high-spin $S=^5/_2$ state for a solution of 0.77 mM **17c** with K_2CO_3 in acetone-d_6. Characteristic changes are also observed in the UV-vis spectrum. A strong Q band at 576 nm appears, which is typical for five-coordinate nitrogen Fe(III)TPP complexes (see Figure 7).[47] Protonation of the 5-coordinate strapped triazolate complex **18** with HCl leads back to the chloride complex **17c**.

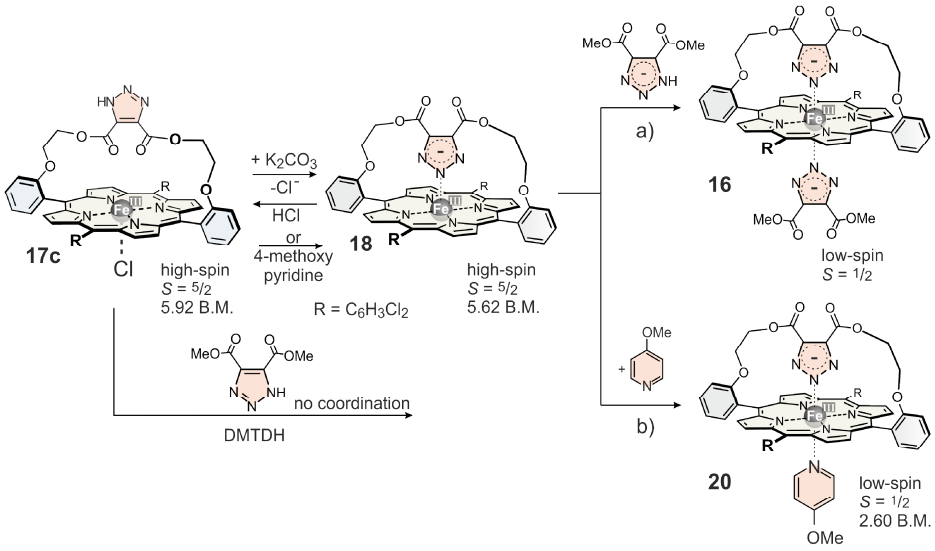

Figure 7: Switching the spin state of triazole strapped porphyrins. Deprotonation of the triazole leads to coordination of the triazolate, the spin state remaining high-spin ($S=^5/_2$). Additional coordination of an external ligand a) triazolate ($DMTD^-$), b) *p*-methoxypyridine, switches the spin state to low-spin ($S=^1/_2$). The change in coordination number, charge and spin state leads to a change in the UV spectrum (a) **16** similar to **5** (see Figure 2, SI (V.1 and V.3)).

p-Methoxypyridine acts both as a base and a ligand. Upon addition of 100 eq. *p*-methoxypyridine, triazole is deprotonated and replaces the chloride. The pyrrole proton chemical shifts (-0.61, -26.08 ppm) clearly indicate that the complex **20** is low-spin ($S=^1/_2$) (see Figure 7, SI (V.4)) in agreement with the magnetic moment of 2.56 B.M. (see SI (IV)). Hence, the overall neutral 5-coordinate, strapped triazolate complex **18** performs spin switching upon coordination of an additional axial anionic (Figure 7a) as well as a neutral nitrogen ligand (Figure 7b).

Similar to the addition of methoxypyridine to **17c** (Figure 7) the addition of the photodissociable ligand (PDL) *trans*-4-chloro-3-(3,5-ditert-butylphenyl)azopyridine leads to the formation of a

low-spin complex with the typical ^{1}H NMR signals at 26.6 ppm and a magnetic moment of YY B.M.. Irradiation with UV light (365 nm) switches the trans azopyridine to the *cis* configuration, which in turn gives rise to a decrease of the low-spin signals and an increase of the magnet moment to YY B.M.. Irradiation with light of 430 nm restores the original magnetic moment and the low spin signals in ^{1}H NMR. We attribute the change in magnetic moment to the dissociation of the ligand in the *cis* configuration and re-coordination of the *trans* isomer. The spin state switching is reversible over a large number of cycles.

Conclusion

In summary we report on the design, synthesis and investigation of a Fe(III) based molecular ($S=^5/_2 \rightleftarrows S=^1/_2$) spin switch. The two-component system, includes a Fe(III)porphyrin with a covalently attached triazolate unit and a separate pyridine ligand. The triazole is strapped to the porphyrin in such a way that the nitrogen lone pair in 2-position of the corresponding triazolate is placed in an optimal geometry to coordinate to the Fe(III) ion. Upon deprotonation of the triazole, the triazolate coordinates and serves as both the counter ion and axial ligand. The acidity of the ester substituted triazole is sufficient for facile deprotonation, and ligand field strength of the resulting triazolate is strong enough to coordinate. But it is still in a range preserving the high-spin state and weak enough to allow coordination of pyridines to the remaining axial site, which in turn leads to a spin switch to the low-spin state. Upon addition of a photoswitchable ligand, the spin state of the complex can be reversibly switched with light. Our 5-coordinate high-spin complexes **18** could serve as model compounds for a number of natural iron(III)porphyrins, such as cytochrome P450 and catalase. Further potential applications include responsive contrast agents and spintronics.

ASSOCIATED CONTENT

The Supporting Information is available free of charge on the ACS Publications website at DOI:

AUTHOR INFORMATION

Corresponding Author

Email: Rainer Herges*-rherges@oc.uni-kiel.de

ACKNOWLEDGMENT

The authors gratefully acknowledge funding from the collaborative research center SFB 677 Function by Switching.

REFERENCES

[1] Momenteau, M.; Mispelter, J.; Loock, B.; Bisagni E. Both-faces hindered porphyrins. Part 1. Synthesis and characterization of basket-handle porphyrins and their iron complexes. *J. Chem. Soc., Perkin Trans.* **1983**, *1*, 189-196.

[2] Andrioletti, B.; Ricard, D.; Boitrel, B. Cyclam-strapped porphyrins and their iron (III)–copper (II) complexes as models for the resting state of cytochrome c oxidase. *New J. Chem.* **1999**, *23*, 1143-1150.

[3] Kozuch, S.; Leifels, T.; Meyer, D.; Sbaragli, L.; Shaik, S.; Woggon, W. D. New synthetic models of cytochrome P450: How different are they from the natural species? *Synlett* **2005**, 4, 675–684.

[4] Konishi, K.; Oda, K.; Nishida, K.; Takuzo, A.; Shohei, I. Asymmetric Epoxidationof Olefins Catalyzed by Manganese Complexesof Chiral "Strapped" Porphyrins with Diastereotopic Faces. A Novel Strategy for Stereochemical Modeling of the Active Site of Cytochrome P-450. *J. Am. Chem. Soc.* **1992**, *114*, 1313-1317.

[5] Collman, J. P.; Lee, V. J.; Kellen-Yuen, C. J.; Zhang, X.; Ibers, J. A.; Brauman, J. I. Threitol-strapped manganese porphyrins as enantioselective epoxidation catalysts of unfunctionalized olefins. *J. Am. Chem. Soc.* **1995**, *117*, 692-703.

[6] Gunter, M. J.; Hockless, D. C. R.; Johnston, M. R.; Skelton, B. W. Self-assembling porphyrin [2]-catenanes. *J. Am. Chem. Soc.* **1994**, *116*, 4810-4823.

[7] Morgan, B.; Dolphin, D. Synthesis and structure of biomimetic porphyrins Synthesis and structure of biomimetic porphyrins. *Structure and Bonding* **1987**, *64*, 115-203.

[8] Meunier, B.; de Visser, S. P.; Shaik, S. Mechanism of oxidation reactions catalyzed by cytochrome P450 enzymes. *Chem. Rev.* **2004**, *104*, 3947–3980.

[9] Baik, M.-H., Newcomb, M., Friesner, R. A. & Lippard, S. J. Mechanistic studies on the hydroxylation of methane by methane monooxygenase. *Chem. Rev.* **2003**, *103*, 2385–2419.
[10] Nagababu, P.; Yu, S. S.-F.; Maji, S.; Ramu, R.; Chan, S. I., *Catalysis Science & Technology* **2014**, *4*, 930-935.
[11] Ferrando-Soria, J. et al. Molecular magnetism, quo vadis? A historical perspective from a coordination chemist viewpoint. *Coord. Chem. Rev.* **2017**, *339*, 17–103.
[12] Dommaschk, M.; Peters, M.; Gutzeit, F.; Schuett, C.; Naether, C.; Soennichsen, F. D.; Tiwari, S.; Riedel, C.; Boretius, S.; Herges, R., Photoswitchable Magnetic Resonance Imaging Contrast by Improved Light-Driven Coordination-Induced Spin State Switch, *J. Am. Chem. Soc.* **2015**, *137*, 7552-7555.
[13] Heitmann, G.; Schuett, C.; Groebner, J.; Huber, L.; Herges, R., Azoimidazole functionalized Ni-porphyrins for molecular spin switching and light responsive MRI contrast agents, *Dalton Trans.* **2016**, *45*, 11407-11412.
[14] Herges, R.; Jansen, O.; Tuczek, F.; Venkatamarani, S., Transition metal complexes with photosensitive tethered ligands as visible light-induced spin-crossover magnetic molecular switches, PCT Int. Appl. (2012), WO 2012022299 A1 20120223.
[15] Shankar, S.; Peters, M.; Steinborn, K.; Krahwinkel, B.; Sönnichsen, F. D.; Grote, D., Sander, W.; Lohmiller, T; Rüdiger, O.; Herges, R. Light-controlled switching of the spin state of iron(III). *Nature Communications* **2018**, *9*, 1-12.
[16] Byers, W.; Cossham, J. A.; Edwards, J. O.; Gordon, A. T.; Jones, J. G.; Kenny, E. T. P.; Mahmood, A.; McKnight, J.; Sweigart, D. A.; Tondreau, G. A.; Wright, T. Hydrogen Bonding in Metalloporphyrins. Mechanistic Study of the Reactions of (Tetraphenylporphinato) iron (111) Azide with Imidazole and N-Methylimidazole. *Inorg. Chem.* **1986**, *25*, 4767-4774.
[17] Bond, A. M.; Sweigart, D. A. - Low temperature electrochemistry of metalloporphyrins in dichloromethane: characterization of transient species. *Inorgan. Chim. Acta* **1986**, *123,* 167-173.
[18] Adams, K. M.; Rasmussen, P. G.; Scheidt, W. R.; Hatano, K. Structure and properties of an unsymmetrically substituted six-coordinate iron (III) porphyrin. *Inorg. Chem.* **1979**, *18*, 1892-1899.
[19] Zhang, Y.; Hallows, W. A.; Ryan, W. J.; Jones, J. G.; Carpenter, G. B.; Sweigart D. A. Models for Steric Interactions in Heme Proteins. Structures of the Five-Coordinate Complex Iron(III) Tetraphenylporphyrin Azide and Its Six-Coordinate 1:1 Adducts with 1-Methylimidazole and 1,2-Dimethylimidazole. *Inorg. Chem.* **1994**, *33*, 3306-3312.
[20] Meyer, D.; Leifels, T.; Sbaragl, L.; Woggon, W.-D.; Reactivity of a new class of P450 enzyme models. *Biochemical and Biophysical Research Communications* **2005**, *338*, 372–377.
[21] Higuchi, T.; Hirobe, M. Four recent studies in cytochrome P450 modelings: A stable iron porphyrin coordinated by a thiolate ligand; a robust ruthenium porphyrin-pyridine N-oxide derivatives system; polypeptide-bound iron porphyrin; application to drug metabolism studies. *Journal of Molecular Catalysis A: Chemical* **1996**, *113*, 403-422.
[22] Staubli, B.; Fretz, H.; Piantini, U.; Woggon, W.-D. Synthetic Models of the Active Site of Cytochrome P-450. 1st Communication. The Synthesis of a Doubly-Bridged Iron(II)-Porphyrin Carrying a Tightly Bound Thiolate Ligand. Helvetica *Chimica Acta* **1987**, *70*, 1173-1193.
[23] Narula, C. K.; Janik, J. Fr.; Duesler, E., N.; Paine, R. T.; Schaeffer, R. Convenient Synthesis,Separation,and-rayCrystalStructureDeterminationsof 1(e),3(e),5(e)-

Trimethylcycloborazaneand1(e),3(e),5(a)-TrimethylcycIoborazane. *Inorganic Chemistry* **1986**, *25*, 3346-3349.
[24] Hawker, C. J.; Fréchet, J. M. J. Preparation of Polymers with Controlled Molecular Architecture. A New Convergent Approach to Dendritic Macromolecules. *J. Am. Chem. Soc.* **1990**, *112,* 7638-7647.
[25] Geiger, D. K.; Chunplang, V.; Scheidt, W. R., Control of Spin State in (Porphinato)iron(III) Complexes. A New Crystalline Phase of (Isothiocyanato) (pyridine) (meso - tetraphenylporphine)iron(III) with Two Magnetically Distinct Sites. *Inorg. Chem.* **1985**, *24*, 4736-4741
[26] M. S. A. Hamza, J. M. Pratt, Hemes and hemoproteins. Part 10. Co-ordination of imidazole and other azoles by the iron (III) porphyrin microperoxidase-8. *J. Chem. Soc. Dalton Trans.* **1994**, 1367-1371.
[27] Smith, R. M.; Martell, A. E., Critical Stability Constants, Vol . 2, Amines, Plenum Press, New York, **1975**.
[28] Wichems, D. N.; Nag, S.; Mills, J.; Fishbein, J. C. Evidence for intermediates and a change in rate-limiting step in the aminolysis of the carcinogen N-methyl-N'-nitro-N-nitrosoguanidine by cyclic amines. *J. Am. Chem. Soc.* **1992**, 114, 8846-8851.
[29] Walker, F. A.; Lo, M.-W.; Ree, M. T. Electronic Effects in Transition Metal Porphyrins. The Reactions of Imidazoles and Pyridines with a Series of Para-Substituted Tetraphenylporphyrin Complexes of Chloroiron(III). *J. Am. Chem. Soc.* **1976**, 98, 5552-5560.
[30] Doeff, M. M.; Sweigart, D. A. Hydrogen bonding in metalloporphyrin reactions. Reaction of (tetraphenylporphinato) iron (III) chloride and N-methylimidazole. *Inorg. Chem.* **1982**, 21, 3699-3705.
[31] Tondreau, G. A.; Sweigart, D. A. Hydrogen bonding in metalloporphyrin reactions. Reaction of (tetraphenylporphinato) iron (III) chloride and imidazole. *Inorg. Chem.* **1984**, 23, 1060-1065.
[32] Adams, K. M.; Rasmussen, P. G.; Scheidt, R.; Hatano, K. Structure and properties of an unsymmetrically substituted six-coordinate iron(III) porphyrin. *Inorg. Chem.* **1979**, *18*, 1892-1999.
[33] Ganesh, K. N.; Sanders, J. K. M. Quinone-capped metalloporphyrins: synthesis and co-ordination chemistry. *J. Chem. Soc., Chem. Commun.* **1980**, 1129-1131.
[34] Battersby, A. R.; Hamilton, A. D. Synthesis of a doubly-bridged oxygen-carrier which shows reduced affinity for carbon monoxide. *J. Chem. Soc., Chem. Commun.* **1980**, 117-119.
[35] Nagata, T. Synthesis and characterization of doubly-strapped porphyrins. *Bull. Chem. Soc.Jpn.* **1992**, *65*, 385-391.
[36] Meyer, D.; Woggon, W.-D. Synthesis and characterization of a new family of iron porphyrins. *Chimia* **2005**, *59*, 85–87.
[37] Almog, J.; Baldwin, J. E.; Crossley, M. J.; Debernardis, J. F.; Dyer, R. L.; Huff, J. R.; Peters, M. K. Synthesis of “capped porphyrins”. *Tetrahedron*, **1981**, 37, 3589-3601.
[38] Shao, X.-B.; Jiang, X.-K.; Wang, X.-Z.; Li, Z.-T.; Zhu, S.-Z. A novel strapped porphyrin receptor for molecular recognition. *Tetrahedron* **2003**, *59*, 4881–4889.
[39] Gonçalves, D. P. N.; Sanders, J. K. M. Synthesis of new strapped porphyrins via a bisdipyrromethane condensation. *Synlett* **2007**, *4*, 591–594.

[40] He, J.; Zheng, J.; Liu, J. She, X.; Pan, X. N-heterocyclic carbene catalyzed nucleophilic substitution reaction for construction of benzopyrones and benzofuranones. *Org. Lett.* **2006**, *8* , 4637–4640.
[41] Littler, B. J.; Miller, M. A.;Hung, C.-H.;Wagner, R. W.; O'Shea, D. F.; Boyle, P. D.; Lindsey, J. S. Refined synthesis of 5-substituted dipyrromethanes. *J. Org. Chem.* **1999**, *64,* 1391-1396.
[42] Geier, G. R.; Littler, B. J.; Lindsey, J. S. Investigation of porphyrin-forming reactions. Part 3.1 The origin of scrambling in dipyrromethane + aldehyde condensations yielding trans-A2B2-tetraarylporphyrins. *J. Chem. Soc., Perkin Trans.* **2001**, 2, 701–711.
[43] Taherpour, A. A.; Kheradmand, K. One-pot microwave-assisted solvent free synthesis of simple alkyl 1, 2, 3-triazole-4-carboxylates by using trimethylsilyl azide. *J. Heterocyclic Chem.*, **2009**, *46*, 131-133.
[44] Evans, S.; Smith, J. R. L. The oxidation of ethylbenzene and other alkylaromatics by dioxygen catalysed by iron (III) tetrakis (pentafluorophenyl) porphyrin and related iron porphyrins. *J. Chem. Soc., Perkin Trans.* **2000**, *2*, 1541–1551.
[45] Reed, C. A.; Guiset, F. A "Magnetochemical" Series. Ligand Field Strengths of Weakly Binding Anions Deduced from S = 3/2, 5/2 Spin State Mixing in Iron(III) Porphyrins. *J. Am. Chem. Soc.* **1996**, 118, 3281-3282.
[46] Nakamura, M., Dissociation rates of axially coordinated imidazoles and formation constants of low spin ferric complexes derived from tetraphenylporphyrin and tetramesitylporphyrin. *Inorg. Chim. Acta* **1989**, 161, 73-80.
[47] Quinn, R.; Nappa, M.; Valentine, J. S. New five-and six-coordinate imidazole and imidazolate complexes of ferric tetraphenylporphyrin. *J. Am. Chem. Soc.* **1982**, 104, 2588-2595.

3.3 Synthese eines neuen photoschaltbaren Liganden

Nicht nur die Entwicklung neuer Metallkomplexe ist für die Optimierung von intelligenten Kontrastmitteln in der MRT von großer Bedeutung, sondern auch die Synthese von neuen photoschaltbaren Liganden.

Mit ihren zahlreichen Anwendungsmöglichkeiten gehören photoschaltbare Azobenzole zu den am häufigsten verwendeten photochromen Verbindungen.[91] Darüber hinaus sind Azobenzole leicht zugänglich und überzeugen durch ihre photochromen Eigenschaften.

Das *trans*-Isomer ist üblicherweise thermodynamisch stabil und kann bei Bestrahlung mit UV-Licht in das *cis*-Isomer überführt werden. Diese *cis*-Konformation kehrt bei Bestrahlung mit sichtbarem Licht oder thermochemisch wieder zum *trans*-Isomer zurück.[92] Eine sehr wichtige Klasse der Azobenzole sind die Azopyridine, da diese durch ihr Pyridin in der Lage sind, an verschiedene Metalle wie z.B. Nickel zu koordinieren[53] und somit eine Spin-Änderung hervorzurufen.

Diese Eigenschaft spielt bei den LD-CISSS-Systemen und neu designten Plattenspielern eine große Rolle, weswegen die Synthese neuer Azopyridine unumgänglich ist.

Crystal structure of 2-[2-(pyridin-3-yl)diazen-1-yl]aniline

Morten K. Peters, Christian Näther and Rainer Herges

Acta Crystallographica **2018***, E74,* 1013-1016.
doi: 10.1107/S2056989018008605

Eigenanteil: Die Synthesen wurden von Morten Peters durchgeführt. Die Eiskristallstrukturanalyse wurde von Prof. Dr. Christian Näther gelöst. Das Manuskript wurde von Morten Peters, Christian Näther und Prof. Dr. Rainer Herges verfasst.

Zusammenfassung

In dieser Veröffentlichung konnte durch Röntgen-Strukturanalyse das 2-[2-(pyridin-3-yl)diazen-1-yl]anilin charakterisiert werden.

Aus dem (2-Acetanilid)azo-pyridin konnte durch Entschützung unter basischen Bedingungen das 2-[2-(pyridin-3-yl)diazen-1-yl]anilin erhalten werden. Durch eine anschließende Umkristallisation aus Aceton konnten Einkristalle isoliert werden. Diese ergaben ein monoklines Kristallsystem mit der Raumgruppe P2/n. Zusätzlich war erkennbar, dass die Azo-Verbindung ausschließlich in der *trans*-Konfiguration vorliegt (Abbildung 17), was auf die Wasserstoffbrückenbindung zwischen dem Stickstoff der Azo-Gruppe und dem Amin zurückzuführen ist.

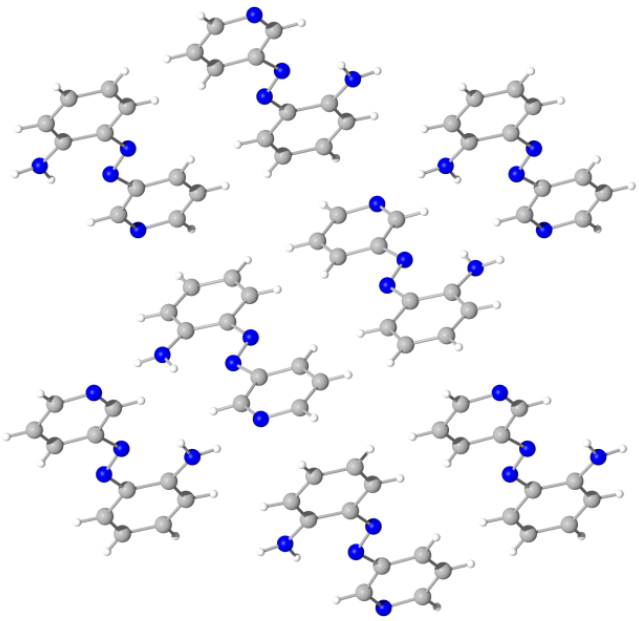

Abbildung 17: Darstellung der Einkristallstruktur aus der B-Achse.

research communications

Acta Cryst E CRYSTALLOGRAPHIC COMMUNICATIONS

ISSN 2056-9890

Crystal structure of 2-[2-(pyridin-3-yl)diazen-1-yl]aniline

Morten K. Peters,[a] Christian Näther[b] and Rainer Herges[a]*

[a]Otto-Diels-Institut für Anorganische Chemie, Christian-Albrechts-Universität Kiel, Otto-Hahn-Platz 4, D-24098 Kiel, Germany, and [b]Institut für Anorganische Chemie, Christian-Albrechts-Universität Kiel, Max-Eyth Str. 2, D-24118 Kiel, Germany. *Correspondence e-mail: rherges@oc.uni-kiel.de

Received 8 June 2018
Accepted 12 June 2018

Edited by M. Weil, Vienna University of Technology, Austria

Keywords: crystal structure; hydrogen bonding; azopyridine.

CCDC reference: 1848833

Supporting information: this article has supporting information at journals.iucr.org/e

The crystal structure of the title compound, $C_{11}H_{10}N_4$, comprises molecules in a *trans* conformation for which all the atoms are located in general positions. The six-membered rings are coplanar and this arrangement might be stabilized by intramolecular N—H···N hydrogen bonding. In the crystal, the molecules are linked into helical chains parallel to the *b* axis *via* N—H···N hydrogen bonding. The molecular packing shows a herringbone-like pattern along the *a* axis. Comparison of the X-ray powder diffraction with that calculated from single crystal data proves that a pure crystalline phase was obtained and UV–Vis measurements reveal that only the *trans* isomer is present.

1. Chemical context

Azobenzenes are among the most frequently used photochromic compounds with numerous applications in different fields being reported (Szymański *et al.*, 2013; Merino & Ribagorda, 2012; Kay *et al.*, 2007). Moreover, azobenzenes are easily accessible, and their photochromic functions are quite reliable. The stretched *trans* isomer is usually the thermodynamically stable conformation. Upon irradiation with UV light, the bent *cis* isomer is formed. This *cis* conformation switches back to the *trans* isomer either upon irradiation with visible light or thermochemically (Hartley, 1937). A highly important variation of azobenzenes are azopyridines, as pyridines coordinate to various metals, *e.g.* nickel (Thies *et al.*, 2010; Dommaschk *et al.*, 2015*c*). Thus, azopyridines can be used as switchable ligands. In this context, we have reported an approach to switch the spin state of azopyridine-functionalized Ni-porphyrins (Thies *et al.*, 2011, 2012; Venkataramani *et al.*, 2011; Dommaschk *et al.*, 2015*a*,*b*). Aiming at further functionalization of azopyridines and in view of applications as molecular spin switches, we have synthesized 2-[2-(pyridin-3-yl)diazen-1-yl]aniline and report here its molecular and crystal structure.

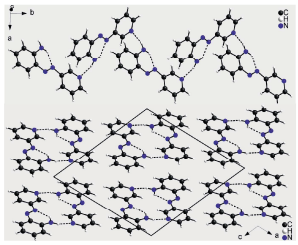

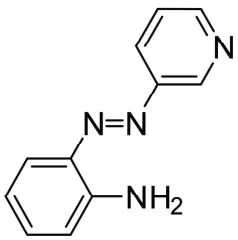

OPEN ACCESS

Table 1
Hydrogen-bond geometry (Å, °).

D—H···A	D—H	H···A	D···A	D—H···A
N4—H1*N*4···N2	0.881 (16)	2.066 (15)	2.6922 (14)	127.3 (12)
N4—H2*N*4···N1^{i}	0.904 (16)	2.163 (16)	3.0274 (14)	159.7 (14)

Symmetry code: (i) $-x+\frac{1}{2}, y-1, -z+\frac{3}{2}$.

2. Structural commentary

The crystal structure of the title compound comprises 2-[2-(pyridin-3-yl)diazen-1-yl]aniline molecules, located on general positions, adopting a *trans*-conformation with a C1—N2—N3—C6 torsion angle of −179.80 (8)°, which corresponds to the energetically favored arrangement (Fig. 1). The two six-membered rings are coplanar [the maximum deviation from the least-squares plane for all non-H atoms is 0.0569 (9) Å for N4] and the dihedral angle between the ring planes is 0.11 (8)°. The amino H atoms are also in the plane of the adjacent benzene ring. There is an intramolecular N—H···N hydrogen bond between one of the amino H atoms and one nitrogen atom of the azo group with an N···H distance of 2.066 (15) Å and an N—H···N angle of 127.30 (12)° (Table 1). Even if this corresponds to a weak interaction, it might stabilize the planar arrangement.

3. Supramolecular features

In the crystal structure of the title compound, the molecules are linked into chains along the *b*-axis direction *via* N—H···N hydrogen bonds between the amino hydrogen atom that is not involved in intramolecular hydrogen bonding and one of the nitrogen atoms of the azo group (Fig. 2, top). The N···H distance amounts to 2.163 (16) Å and the N—H···N angle of 159.7.14 (12)° is slightly bent, indicating that this is a relatively strong interaction (Table 1). The dihedral angle between the pyridine ring that carries the acceptor N atom and the aminophenyl moiety of a neighbouring molecule that carries the donor group is 66.12 (8)°. Therefore, the molecules exhibit a helical arrangement along the chain (Fig. 2, top). The chains are closely packed in such a way that each chain is surrounded by eight neighboring chains (Fig. 2, bottom). The molecules

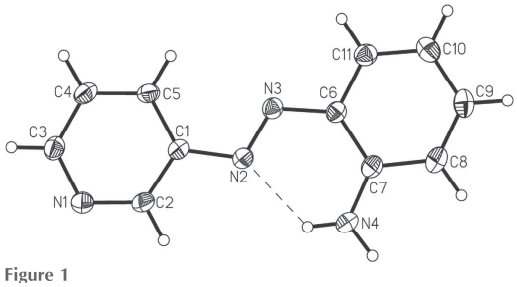

Figure 1
Molecular structure of the title compound with labeling and displacement ellipsoids drawn at the 50% probability level. The intramolecular N—H···N hydrogen bond is shown with dashed lines.

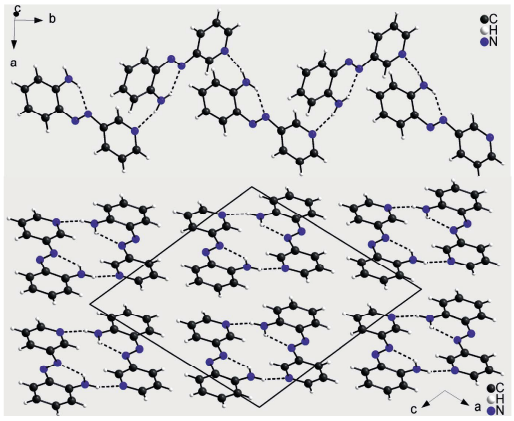

Figure 2
Crystal structure of the title compound showing a chain (top) and a view along the *b* axis (bottom). Intra- and intermolecular hydrogen bonds are indicated by dashed lines.

exhibit a herringbone-like pattern along the *a* axis (Fig. 3) in which the pyridine and benzene rings of adjacent molecules are perfectly coplanar. The distance between the ring planes is 3.462 Å and the centroid–centroid distance is 3.8040 (7) Å, indicating π–π interactions between the chains.

4. Database survey

According to a search of the Cambridge Structural Database (CSD; Groom *et al.*, 2016), 3-azopyridine molecules substi-

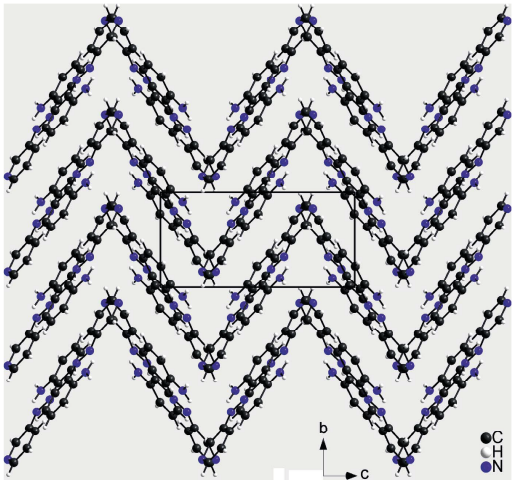

Figure 3
Crystal structure of the title compound in a view along the *a* axis.

tuted with an amino group in the *ortho*-position are unknown. However, one *ortho*-substituted phenyl-azopyridine was reported, *viz*. 2,6-diamino-3-[(2-carboxymethyl)phenyl-azo]pyridine (Tan *et al.*, 2010). 4-Aminophenyl-azopyridines such as *N*,*N*-diethyl-4-[(*E*)-(pyridine-3-yl)diazenyl]aniline (Draguta *et al.*, 2015) and *N*,*N*-dimethyl-4-(pyridine-3-yldiazenyl)aniline (Draguta *et al.*, 2013) are also known. Furthermore, structure reports on 2-azopyridine molecules that are substituted in the *ortho*-position, such as 5-[(5-bromo-2-pyridyl)azo]-2,4-toluenediamine (Jinzi *et al.*, 1984) and 5-[(3,5-dibromo-2-pyridyl)azo]-2,4-diaminotoluene (Kailiang *et al.*, 1985), have been published. Other azo compounds, substituted similarly to the title molecule, are highly important for coordination chemistry, which is shown in their crystal structures (Maiti *et al.*, 2001, 2003; Pratihar *et al.*, 2005, 2007).

5. Synthesis and crystallization

The synthesis of the title compound can be performed in two steps.

(i) Synthesis of 3-(2-acetanilide)azopyridine: 2-nitroacetanilide (4.00 g, 29.0 mmol) was dissolved in ethanol (150 ml). An aqueous solution of ammonium chloride (2.01 g, 37.7 mmol in 15 ml) was added. The mixture was warmed up to 313 K until the dispersion changed into a clear solution. After cooling to room temperature, zinc dust (4.93 g, 75.3 mmol) was added and the mixture was stirred for 1 h at 333 K. After filtration, the filtrate was poured into an aqueous ice-cooled iron(III) chloride solution (hexaaqua complex, 5.40 g, 20.3 mmol in 150 ml) whereby a green solid precipitated. After 15 min of stirring, the solid was filtered off and washed with water. The crude product was a mixture of 2-nitrosoacetanilide and starting material, which was used for azo condensation without further purification. 3-Aminopyridine (800 mg, 8.51 mmol) was dissolved in a mixture of pyridine (25 ml) and aqueous sodium hydroxide (5 ml, 25%). The crude product of 2-nitrosoacetanilide dissolved in pyridine (30 ml) was added to the solution containing the 3-aminopyridine. The reaction mixture was stirred for 1 h at 353 K and overnight at room temperature. After addition of dichloromethane (200 ml) the phases were separated. The organic layer was washed with water twice and dried over sodium sulfate. The solvent was removed under reduced pressure. The crude product was purified by column chromatography (ethyl ester/*n*-hexane, R_f = 0.16). The product was obtained as an orange solid. Yield: 200 mg (0.83 mmol, 10%).

^{1}H NMR (500 MHz, 300 K, CDCl3): δ = 9.88 (*s*, br, 1H, N-H), 9.11 (*d*, ^4J = 2.4 Hz, 1H), 8.71 (*dd*, ^3J = 4.7 Hz, ^4J = 1.5 Hz), 8.66 (*d*, *br*, ^3J = 8.3 Hz, 1H), 8.07 (*ddd*, ^3J = 8.2 Hz, ^4J = 2.4 Hz, ^4J = 1.5 Hz, 1H), 7.83 (*dd*, ^3J = 8.1 Hz, ^4J = 1.4 Hz 1H), 7.51–7.44 (*m*, 2H), 7.16 (*td*, ^3J = 8.1 Hz, ^4J = 1.3 Hz 1H), 2.26 (*s*, 3H) ppm. ^{13}C NMR (150 MHz, 300 K, CDCl3): δ = 168.3, 151.9, 147.7, 146.3, 138.9, 136.4, 133.8, 127.3, 124.1, 123.4, 120.6, 120.4, 25.2 ppm. HRMS (EI): *m*/*z* $[M]^+$ calculated for $C_{13}H_{12}N_4O$: 240.10111, found: 240.10136.

Table 2
Experimental details.

Crystal data	
Chemical formula	$C_{11}H_{10}N_4$
M_r	198.23
Crystal system, space group	Monoclinic, *P*2/*n*
Temperature (K)	200
a, *b*, *c* (Å)	13.2798 (8), 5.9792 (3), 13.4130 (9)
β (°)	113.046 (7)
V (Å^3)	980.03 (11)
Z	4
Radiation type	Mo $K\alpha$
μ (mm^{-1})	0.09
Crystal size (mm)	0.20 × 0.15 × 0.15
Data collection	
Diffractometer	Stoe IPDS1
No. of measured, independent and observed [$I > 2\sigma(I)$] reflections	8233, 2137, 1731
R_{int}	0.073
(sin $\theta/\lambda)_{max}$ (Å^{-1})	0.639
Refinement	
$R[F^2 > 2\sigma(F^2)]$, $wR(F^2)$, *S*	0.039, 0.113, 1.04
No. of reflections	2137
No. of parameters	145
H-atom treatment	H atoms treated by a mixture of independent and constrained refinement
$\Delta\rho_{max}$, $\Delta\rho_{min}$ (e Å^{-3})	0.21, −0.18

Computer programs: *X-AREA* (Stoe, 2008), *SHELXS97* and *XP* (Sheldrick, 2008), *SHELXL2014* (Sheldrick, 2015), *DIAMOND* (Brandenburg, 2014) and *publCIF* (Westrip, 2010).

(ii) Synthesis of 2-[2-(pyridin-3-yl)diazen-1-yl]aniline: 3-(2-acetanilide)azopyridine (640 mg, 2.66 mmol) was dissolved in methanol (50 ml). A sodium hydroxide solution (5 ml, 30%) was added and stirred for 6 h at 343 K. 2-[2-(Pyridin-3-yl)diazen-1-yl]aniline precipitated and was filtered off. The solid was washed with water. Recrystallization from acetone gave orange single crystals. Yield: 520 mg (2.63 mmol, 99%).

^{1}H NMR (500 MHz, 300 K, $CDCl_3$): δ = 9.08 (*dd*, ^4J = 2.4 Hz, ^5J = 0.8Hz, 1H), 8.63 (*dd*, ^3J = 4.7 Hz, ^4J = 1.6 Hz, 1H), 8.08 (*ddd*, ^3J = 8.2 Hz, ^4J = 2.4 Hz, ^4J = 1.6 Hz, 1H), 7.84 (*dd*, ^3J = 8.1 Hz, ^4J =1.4 Hz, 1H), 7.41 (*ddd*, ^3J =8.2 Hz, ^3J = 4.7 Hz, ^5J = 0.8 Hz, 1H),7.24 (*ddd*, ^3J = 8.3 Hz, ^3J = 7.1 Hz, ^4J = 1.4 Hz, 1H), 6.83 (*ddd*, ^3J = 8.1 Hz, ^3J = 7.1 Hz, ^4J = 1.3 Hz, 1H), 6.77 (*dd*, ^3J = 8.3 Hz, ^4J = 1.3 Hz, 1H), 6.01 (*s*, *br*, 2H, N—H) ppm. ^{13}C NMR (150 MHz, 300 K, $CDCl_3$): δ = 150.6, 148.3, 146.51, 143.0, 137.1, 133.1, 128.5, 126.4, 123.9, 117.5, 117.1 ppm. MS (EI, TOF): *m*/*z* (%) = 199 $[M]^+$, 198 $[M]$, 120 $[M - C_5H_4N]^+$, 92 $[M - C_6H_6N_2]^+$.

Comparison of the experimental X-ray powder diffraction pattern with that calculated from single crystal data proves that the title compound was obtained as a pure phase (see Fig. S1 in the supporting information). The UV–Vis spectrum shows the strong $\pi \rightarrow \pi^*$ band of the *trans* conformation (Fig. S2 in the supporting information). If the sample is exposed to light of 365 nm, no isomerization into the cis conformer is observed, and the sample starts to decompose. However, conversion of the amino to an amide group will probably restore the photochromic properties.

6. Refinement

Crystal data, data collection and structure refinement details are summarized in Table 2. The C—H hydrogen atoms were located in a difference map but were positioned with idealized geometry and refined with $U_{iso}(H) = 1.2U_{eq}(C,N)$ using a riding model with $C_{aromatic}—H = 0.95$ Å. The N—H hydrogen atoms were located in a difference map and were freely refined.

Acknowledgements

We thank Professor Dr Wolfgang Bensch for access to his experimental facilities.

Funding information

The authors gratefully acknowledge financial support from the Deutsche Forschungsgesellschaft within the Sonderforschungsbereich 677.

References

Brandenburg, K. (2014). *DIAMOND*. Crystal Impact GbR, Bonn, Germany.
Dommaschk, M., Näther, C. & Herges, R. (2015*a*). *J. Org. Chem.* **80**, 8496–8500.
Dommaschk, M., Peters, M., Gutzeit, F., Schütt, C., Näther, C., Sönnichsen, F. D., Tiwari, S., Riedel, C., Boretius, S. & Herges, R. (2015*b*). *J. Am. Chem. Soc.* **137**, 7552–7555.
Dommaschk, M., Thoms, V., Schütt, C., Näther, C., Puttreddy, R., Rissanen, K. & Herges, R. (2015*c*). *Inorg. Chem.* **54**, 9390–9392.
Draguta, S., Fonari, M. S., Leonova, E. & Timofeeva, T. (2015). *J. Mol. Struct.* **1098**, 206–215.
Draguta, S., Leonova, E., Fokina, M., Denisyuk, I. & Timofeeva, T. V. (2013). *Acta Cryst.* E**69**, o1280.
Groom, C. R., Bruno, I. J., Lightfoot, M. P. & Ward, S. C. (2016). *Acta Cryst.* B**72**, 171–179.
Hartley, G. S. (1937). *Nature*, **140**, 281–281.
Jinzi, Q., Jiaxing, Y., Haifu, F., Kailiang, S. & Shenghua, H. (1984). *Acta Scient. Nat. Univ. Sunyatseni*, **17**, 2.
Kailiang, S., Shenghua, H., Jinzi, Q., Jiaxing, Y. & Haifu, F. (1985). *Chem. J. Chin. Univ.* **6**, 573.
Kay, E. R., Leigh, D. A. & Zerbetto, F. (2007). *Angew. Chem. Int. Ed.* **46**, 72–191.
Maiti, N., Dirghangi, B. K. & Chattopadhyay, S. (2003). *Polyhedron*, **22**, 3109–3113.
Maiti, N., Pal, S. & Chattopadhyay, S. (2001). *Inorg. Chem.* **40**, 2204–2205.
Merino, E. & Ribagorda, M. (2012). *Beilstein J. Org. Chem.* **8**, 1071–1090.
Pratihar, J. L., Maiti, N. & Chattopadhyay, S. (2005). *Inorg. Chem.* **44**, 6111–6114.
Pratihar, J. L., Shee, B., Pattanayak, P., Patra, D., Bhattacharyya, A., Puranik, V. G., Hung, C. H. & Chattopadhyay, S. (2007). *Eur. J. Inorg. Chem.* pp. 4272–4281.
Sheldrick, G. M. (2008). *Acta Cryst.* A**64**, 112–122.
Sheldrick, G. M. (2015). *Acta Cryst.* A**71**, 3–8.
Stoe (2008). *X-AREA*. Stoe & Cie, Darmstadt, Germany.
Szymański, W., Beierle, J. M., Kistemaker, H. A. V., Velema, W. A. & Feringa, B. L. (2013). *Chem. Rev.* **113**, 6114–6178.
Tan, X., Xie, X., Chen, J. & Zhan, S. (2010). *Inorg. Chem. Commun.* **13**, 1455–1458.
Thies, S., Bornholdt, C., Köhler, F., Sönnichsen, F. D., Näther, C., Tuczek, F. & Herges, R. (2010). *Chem. Eur. J.* **16**, 10074–10083.
Thies, S., Sell, H., Bornholdt, C., Schütt, C., Köhler, F., Tuczek, F. & Herges, R. (2012). *Chem. Eur. J.* **18**, 16358–16368.
Thies, S., Sell, H., Schütt, C., Bornholdt, C., Näther, C., Tuczek, F. & Herges, R. (2011). *J. Am. Chem. Soc.* **133**, 16243–16250.
Venkataramani, S., Jana, U., Dommaschk, M., Sönnichsen, F. D., Tuczek, F. & Herges, R. (2011). *Science*, **331**, 445–448.
Westrip, S. P. (2010). *J. Appl. Cryst.* **43**, 920–925.

3.4 Insertion von Nickel(0) in Porphyrine bei Raumtemperatur

In der Natur sowie in bestimmten Technologien spielen Nickelporphyrine und Nickel-Hydroporphyrine eine wichtige Rolle, da sie als starke Katalysatoren fungieren und somit an Reduktionsprozessen beteiligt sind. Ein Beispiel hierfür ist das Nickelporphyrin F430, welches ein Coenzym ist und im letzten Schritt der Methanfreisetzung in Archaeen als eine Schlüsselkomponente im globalen Kohlenstoffkreislauf dient.[93] Des Weiteren werden reduzierte Ni-Porphyrine als Schlüsselintermediate bei der Reduktion von Alkylhalogeniden verwendet.[94] Ein für die Wirtschaft besonders interessantes Anwendungsgebiet ist die Wasserstoffentwicklungsreaktion. Hierbei werden die sogenannten Ni-Hydroporphyrine als Katalysatoren verwendet. Bei detaillierten Untersuchungen dieser Prozesse konnten mehrere reduzierte Ni-Spezies identifiziert werden.[6-9]

Um solche Nickelporphyrine herzustellen, gibt es jedoch der Literatur zufolge nur wenige unterschiedliche Ansätze. Eine Möglichkeit ist die Reaktion eines Porphyrins mit einem Metallsalz in einem sauren Medium, wie zum Beispiel Essigsäure,[95,96] oder unter basischen Bedingungen, z. B. Pyridin.[96,97] Eine weitere Variante ist die Umsetzung eines Porphyrins mit einem Metallsalz oder Metallkomplex in hochsiedenden, polaren organischen Lösungsmitteln, beispielsweise Dimethylformamid.[98] Die letzte Möglichkeit ist der Ansatz der mikrowellenunterstützten Insertion von Metallsalzen.[99]

Neben dem Problem der Löslichkeit, das sich daraus ergibt, dass die hydrophoben Porphyrine und die wasserlöslichen Metallsalze gleichzeitig in Lösung gebracht werden müssen, kommt es bei der Einlagerung zusätzlich zu kinetischen Schwierigkeiten. Die Insertion von Nickelionen in Porphyrine leidet unter der Tatsache, dass Ni(II) zu klein ist, um perfekt in den von den vier Pyrrolen gebildeten quadratisch planaren Hohlraum zu passen. Dadurch ist das Porphyrin in seiner Geometrie verzerrt und erlaubt keine günstigen Ni-N-Abstände.[100] Beim Vergleich der Eisen-Einlagerung in Porphyrine mit der von Nickel zeigt sich, dass das Eisen zunächst als Fe(II) eingelagert wird und erst durch anschließende Oxidation der Fe(III)-Komplex erhalten wird.[101] Daraus ergibt sich eine interessante Variante für die Insertion von Nickel.

Insertion of Ni(0) in Porphyrins at Room Temperature: Preparation of Ni(II)porphyrins, and Ni(II)chlorins and Observation Hydroporphyrin Intermediates

Morten K. Peters and Rainer Herges

Inorganic Chemistry **2018***, 57,* 3177–3182.
doi:10.1021/acs.inorgchem.7b03164

Eigenanteil: Die Synthesen und Messungen wurden von Morten Peters durchgeführt. Das Manuskript wurde von Morten Peters und Prof. Dr. Rainer Herges verfasst.

Zusammenfassung

Diese Arbeit beschreibt eine sehr milde und effiziente Methode, um Nickel unter Verwendung von $Ni(COD)_2$ in Porphyrine einzulagern. Die Reaktion wurde bei 20 °C durchgeführt. Dieses neue Verfahren liefert Ausbeuten zwischen 90 % und 100 % mit elektronenreichen sowie elektronenarmen Porphyrinen. Je nach elektronischer Natur des Porphyrins entstehen zunehmende Mengen der entsprechenden Ni(II)-Chlorine, die quantitativ zu den entsprechenden Porphyrinen oxidiert werden können. Das elektronenarme *meso*-Tetrakis(pentafluorphenyl)porphyrin **8a** ergibt das Ni(II)-Chlorin mit einer Ausbeute von 66 % (Abbildung 18). Dieses Molekül war bisher durch keine herkömmliche Methode zugänglich. Die extrem schwierige Trennung von Porphyrin und Chlorin konnte unter Ausnutzung der starken Koordination von Ni(II)-Chlorinen an die Aminoliganden von aminofunktionalisiertem Kieselgel realisiert werden.

Besonders interessant ist die Einlagerung von Nickel unter Gegenwart von Basen, da dieses in Lösung zu stabilen Ni(II)-Hydroporphyrinen führt. Die reduzierten Ni(II)-Porphyrine sind Schlüsselintermediate in verschiedenen technologisch interessanten Prozessen und Enzymreaktionen. Ihre Reaktivität kann nun im großen Maßstab untersucht werden.

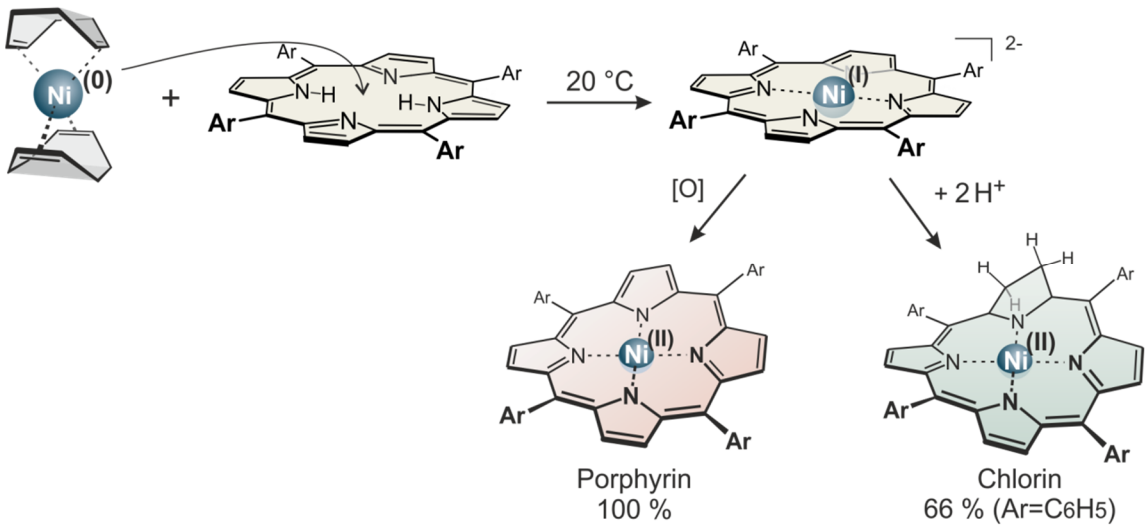

Abbildung 18: Darstellung der Einlagerung von Nickel mit $Ni(COD)_2$.

Inorganic Chemistry
Article
Cite This: Inorg. Chem. 2018, 57, 3177−3182
pubs.acs.org/IC

Insertion of Ni(I) into Porphyrins at Room Temperature: Preparation of Ni(II)porphyrins, and Ni(II)chlorins and Observation of Hydroporphyrin Intermediates

Morten K. Peters[†] and Rainer Herges*[,†]

[†]Otto Diels-Institute of Organic Chemistry, Christian-Albrechts-University Kiel, Otto-Hahn-Platz 4, 24118 Kiel, Germany

Supporting Information

ABSTRACT: Reduced Nickel porphyrins play an important role as enzymatic cofactors in the global carbon cycle (cofactor F430), and as powerful catalysts in solar-to-fuel-processes such as the hydrogen evolution reaction, and the reduction of CO and CO_2. The preparation of Ni(II)porphyrins requires harsh conditions, and characterization of the reduced species is intricate. We present a very mild, convenient, and high yielding method of inserting Ni into electron rich, and electron deficient porphyrins which at the same time gives access to to Ni(II) phlorins and Ni(II)chlorins and Ni(II)porphyrins.

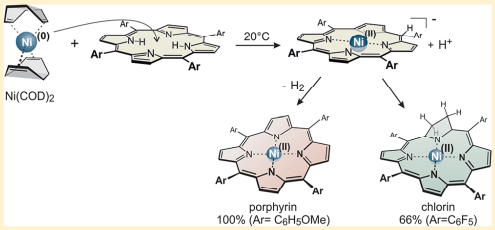

INTRODUCTION

Nickel-hydroporphyrins are powerful catalysts in reduction processes in nature, and in technologically important reactions. F430, a nickel containing corphine acts as the coenzyme in the final step of methane release in archaea by methyl-CoM reductase, and thus is a key component in the global carbon cycle.[1] Ni-chlorins have been found in marine tunicates, however, their biochemical role is yet unknown.[2] Reduced Ni-porphyrins are also key intermediates in the reduction of alkyl halides[3,4] and, intriguingly, in the electrochemical reduction of CO producing H_2 and ethylene.[5] The hydrogen evolution reaction (reduction of protons) is another important direct solar-to-fuel process which has been catalyzed by Ni-hydroporphyrins. This process has been studied in detail, and several reduced Ni species were identified.[6−9] While the above processes start from stable Ni(II)porphyrins, and generate the reduced species electrochemically, we introduce Ni(0) (using $Ni(COD)_2$) into the free base porphyrins generating Ni-hydroporphyrins which can be oxidized to Ni(II)porphyrins in very good yields. This approach is not only a very mild and convenient synthesis of Ni(II)porphyrins, it also provides direct, chemical access to reduced Ni-porphyrins, such as the corresponding phlorin (Ni^{2+}porph-H^{3-}, **7c**) and chlorins Ni^{2+}porph-H_2^{2-}, **3b**,**c**). Ni(II)porphyrins have been used as responsive contrast agents in functional magnetic resonance imaging (*f*MRI).[10,11]

The conventional synthesis of nickel porphyrins requires harsh conditions. Various methods have been published for the synthesis of transition metal porphyrins, which can be classified into several general reaction types:[12] (1) reaction of a porphyrin with a metal salt in an acidic medium (e.g., HOAc),[13−16] or (2) under basic conditions (e.g., pyridine),[16,17] (3) reaction of a porphyrin with a metal salt, or metal complex in high boiling, polar organic solvents (e.g., DMF)[12,18−21] and (4) the microwave-promoted insertion of metal salts.[22] A typical procedure for the preparation of Ni-porphyrins involves heating of the porphyrin with a large excess of nickel acetate in DMF (151 °C) to reflux for several hours.[23] Metal insertions usually have to overcome high activation barriers.

Besides the kinetic problem and the problem of bringing the hydrophobic porphyrins and the water-soluble metal salts simultaneously in solution, insertion of nickel ions into porphyrins suffers from the fact that Ni^{2+} is too small to perfectly fit into the square planar cavity formed by the four pyrrole nitrogen atoms. The porphyrin must distort to a strained, ruffled geometry to adopt favorable Ni−N distances.[24,25]

Following an analogous strategy which is used to prepare Fe(III)porphyrins by introducing Fe(II), and subsequent oxidation to the Fe(III) complex,[26] we explored the possibility to introduce the larger Ni(0) and oxidize the low valent intermediates to the Ni(II)porphyrin.

RESULTS AND DISCUSSION

We chose $Ni(COD)_2$ as a readily available Ni(0) complex, and three electronically different porphyrins to investigate the scope of the approach: 5,10,15,20-tetrakis(4-methoxyphenyl)-porphyrin (TPPOMe) **1a**, as an example for an electron rich porphyrin, the parent 5,15,10,20-tetraphenylporphyrin (TPP) **1b**, and 5,10,15,20-tetrakis(pentafluorophenyl)porphyrin ($TPPF_{20}$) **1c**, which is a typical example of an electron deficient porphyrin. Transition metal carbonyl complexes have been used before to insert metals into porphyrins,[27,28] however, in our hands $Ni(CO)_4$ did not react with **1c**. Upon simple mixing

Received: December 22, 2017
Published: March 2, 2018

DOI: 10.1021/acs.inorgchem.7b03164
Inorg. Chem. 2018, 57, 3177−3182

of the free base porphyrin with a two- to 4-fold excess of $Ni(COD)_2$ in toluene at room temperature under a nitrogen atmosphere, the color immediately changes from red to green and after stirring for 1−2 h the corresponding Ni-porphyrins and the Ni-chlorins are isolated (^{1}H NMR and UV−vis spectra see Figure 1).

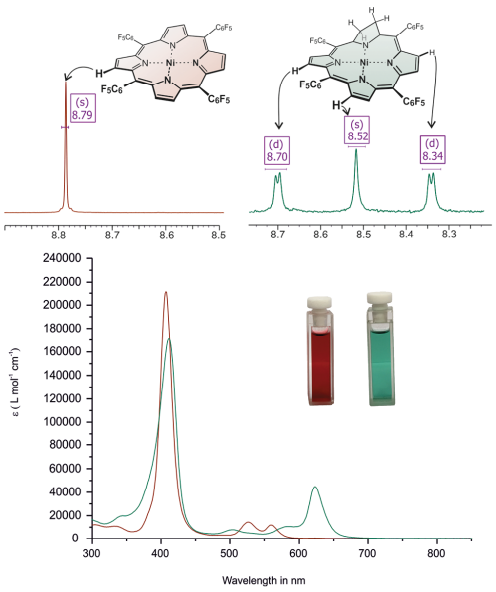

Figure 1. ^{1}H NMR of $NiTPPF_{20}$ **2c** in $CDCl_3$, at 300 K (left, red) and the $NiTPPF_{20}$-chlorin **3c** in acetone-d_6, at 300 K (right, green) and the UV−vis spectra at 24 °C in benzene (porphyrin concentration 13.3 μM).

The ratio of the latter two compounds depends on the electronic nature of the porphyrin. Electron rich TPPOMe **1a** forms exclusively the Ni-porphyrin (100% yield), TPP **1b** gives 10% Ni-chlorin and 90% porphyrin, and in case of the electron poor $TPPF_{20}$, Ni-porphyrin and Ni-chlorin are formed in approximately equal amounts (51:49%). A larger excess of $Ni(COD)_2$ favors the formation of the chlorin, however, no change is observed if more than four equivalents are used. Chlorins are quite susceptible to oxidation, and can be quantitatively converted to the corresponding porphyrins using DDQ (see Table 1).

So, nickel can be inserted into electron-rich as well as electron-deficient free base porphyrins in a two-step, one-pot procedure at room temperature in quantitative yields. The isolated yields in case of the parent tetraphenyl porphyrin **1b** with 91% are somewhat lower because of solubility problems of Ni-TPP during workup. The formation of Ni-chlorins from the corresponding free base porphyrins is of synthetic interest as well. Particularly, electron-deficient chlorins are difficult to prepare, because catalytic hydrogenation as well as reduction with in situ generated diimide fail.[29] Our method provides a convenient access to the strongly electron-poor Ni-tetrakis-(pentafluorophenyl)chlorin **3c**, which cannot be prepared by hydrogenation of the corresponding porphyrin ($TPPF_{20}$, **1c**; see Scheme 1). Purification of the chlorin **3c** by chromatography initially turned out to be very difficult, because porphyrin **2c** and chlorin **3c** exhibit very similar retention times on standard stationary phases. Separation was achieved on an amino-functionalized silica gel (see Experimental Section), taking advantage of the fact that Ni-chlorins exhibit a much stronger coordination to axial nitrogen ligands as the corresponding Ni-porphyrins.[30]

Information about the possible mechanism of our Ni(0) insertion reaction is provided by studies on the electrochemical reduction of Ni(II)porphyrins, which should pass through the same intermediates, albeit in a reverse sequence. Previous spectroelectrochemical and electron spin resonance (ESR)

Table 1. Conditions and Product Distributions for the Insertion of Nickel into Free Base Porphyrins[a,b,c]

				yield (%)			
entry	free base porphyrin	equiv of $Ni(COD)_2$	equiv of KHMDS	starting material	Ni-porphyrin	Ni-chlorin	Ni-porphyrin after DDQ
1	**1a**	2	0	60 **1a**	40 **2a**		
2	**1a**	4	0		99 **2a**		
3	**1a**	8	0		99 **2a**		
4	**1b**	2	0	13 **1b**	87 **2b**		
5	**1b**	4	0		90 **2b**	10 **3b**	91 **2b**[d]
6	**1b**	8	0		89 **2b**	11 **3b**	90 **2b**[d]
7	**1c**	0.5	0	48 **1c**	42 **2c**	10 **3c**	52 **2c**
8	**1c**	1.2	0	7 **1c**	66 **2c**	27 **3c**	93 **2c**
9	**1c**	2	0		51 **2c**	49 **3c**	100 **2c**
10	**1c**	4	0		51 **2c**	49 **3c**	100 **2c**
11	**1c**	8	0		50 **2c**	50 **3c**	100 **2c**
12	**1c**	2	1	100 **4c**			
13	**1a**	4	2	28 **1a**	72 **2a**		
14	**1b**	4	2	71 **1b**	27 **2b**	1 **2c**	
15	**1c**	2	2		34 **2c**	66 **3c**	
16	**1a**	2	7	100 **4a**			
17	**1b**	2	7	100 **4b**			
18	**1c**	2	7	100 **4c**			

[a]Anhydrous toluene was used as a solvent. [b]At room temperature. [c]In all experiments 50 mg of porphyrin was used. [d]Part of the product was lost through the purification.

DOI: 10.1021/acs.inorgchem.7b03164
Inorg. Chem. 2018, 57, 3177−3182

Scheme 1. Metallation of Porphyrins with $Ni(COD)_2$[a]

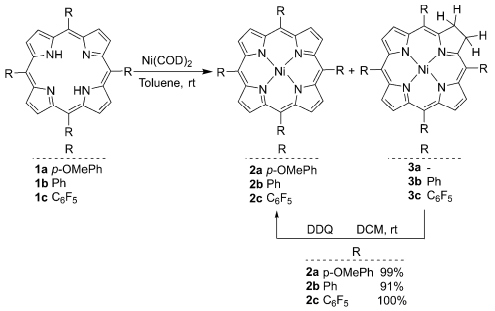

[a]The yields are isolated yields of **2a–c** after DDQ oxidation. The yields depend on the reaction conditions; see Table 1.

studies[31−33] and, more recently, experiments combined with high-level DFT calculations[6,23] provide evidence that the one-electron reduction of Ni(II)TPP **2b** and $Ni(II)TPPF_{20}$ **2c** produces a Ni(I) species rather than a Ni(II) anion radical.

The second electron goes to the porphyrin, forming a Ni(I)-anion radical with one unpaired electron at the Ni^+ and one in the π system of the porphyrin ligand (triplet state). DFT calculations predict a planar structure for this complex. Electron transfer is accompanied by proton transfer. Subsequent protonation could either occur at the Ni ion forming a hydride, at the pyrrole double bond (β position), or at a meso position. According to Solis et al.[6] protonation at the meso carbon atom interrupting aromatic conjugation, and forming a Ni(II)phlorin **7**, is most favorable.

We therefore propose the following tentative mechanism (Scheme 2). $Ni(COD)_2$ coordinates in a stepwise fashion to the porphyrin. Two of the pyrrole nitrogen atoms replace one of the COD ligands forming a Ni(0) chelate, and subsequent intramolecular electron transfer and proton shift forms a Ni(II)phlorin (Ni^{2+}porph-H^{3-} **7**).

The phlorin **7** probably is a key intermediate. It would either eliminate H_2 (according to the known hydrogen evolution reaction) and form the stable Ni(II)porphyrin **2**, or it is protonated forming the stable chlorin **3**. The electronic nature of the porphyrin, obviously, determines whether the hydrogen evolution reaction, and thus porphyrin **2** formation, or the protonation, and chlorine **3** formation, is dominant.

If this mechanism is correct, addition of a base before metalation should prevent proton transfer and thus the hydrogen evolution reaction. With 1 equiv of base, the reaction should stop at the phlorin **7** stage (monoprotonation). After addition of 1 equiv of potassium hexamethyldisilazane (KHMDS) to the free base tetrakis(pentafluorophenyl)-porphyrin (**1c**) and subsequent addition of 2 equiv of $Ni(COD)_2$, a very broad band at ~740 nm in the UV–vis spectrum is observed, which is typical for phlorins (**7c**). A similar spectrum has been observed by Solis et al. upon

Scheme 2. Proposed Mechanism of the Metalation of Free Base Porphyrins 1a–c with $Ni(COD)_2$ and Formation of Ni(II)-porphyrin 2a–c, and Ni(II)chlorin 3b–c

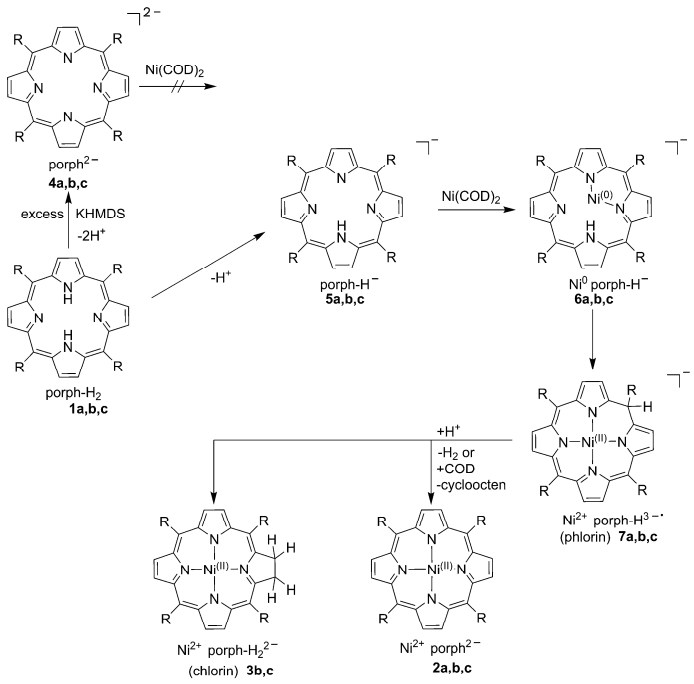

DOI: 10.1021/acs.inorgchem.7b03164
Inorg. Chem. 2018, 57, 3177–3182

electrochemical reduction of $NiTPPF_{20}$ ($Ni^{2+}porph^{2-}$, **2c**).[6,34] The UV−vis spectrum of our solution exhibits additional absorption bands. The absorptions at 526 and 572 nm are due to $NiTPPF_{20}$ ($Ni^{2+}porph^{2-}$, **2c**; see Figure 2).

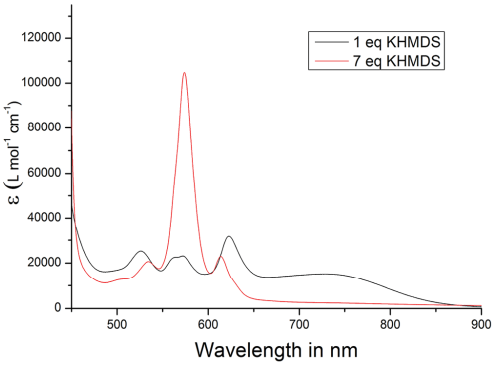

Figure 2. UV−vis absorption spectra of reduced and deprotonated porphyrin species recorded in benzene-d_6 at 25 °C (100 μM). Spectrum in black: free base porphyrin **1c** treated with 1 equiv of KHMDS and subsequent addition of 2 equiv of $Ni(COD)_2$. The spectrum exhibits the broad signature of phlorin **7c** (>700 nm) and the typical Q bands of **2c** (526 and 572 nm). Spectrum in red: Free base porphyrin **1c** treated with 7 equiv of KHMDS and 2 equiv $Ni(COD)_2$. The spectrum is identical to the doubly deprotonated free base porphyrin **4c**.

Unfortunately, NMR cannot be applied to further characterize the radical anions because of severe paramagnetic line broadening. Upon addition of 2 equiv of base the phlorin band **7c** almost disappeared, and no signature of parent $Ni^{2+}porph^{2-}$ **2c** is visible. Quenching of the solution with water yields 66% chlorin **3c** and 34% porphyrin **2c**. The results support our mechanism proposed in Scheme 2. A solution of free base porphyrin **1c** containing 7 equiv of base does not react with $Ni(COD)_2$. Only the deprotonated free base porphyrin is present (574 nm) in solution (see Supporting Information).[35]

■ CONCLUSION

In conclusion, we describe a very mild (20 °C) and very efficient method to insert nickel into free base porphyrins using $Ni(COD)_2$. This method provides isolated yields between 90% and 100% with electron-rich as well as electron-deficient porphyrins. Depending on the electronic nature of the porphyrin increasing amounts of the corresponding Ni-chlorins are formed, which can be quantitatively oxidized to the corresponding porphyrins. Electron-deficient $TPPF_{20}$ **2c** yields 66% Ni-chlorin, which is not accessible by any conventional method. The notoriously difficult separation of porphyrin and chlorin was achieved on an amino-functionalized silica gel, taking advantage of the very strong coordination of Ni-chlorins to amino ligands. Particularly interesting is the insertion of nickel in the presence of base, giving rise to stable solutions of Ni-hydroporphyrins. Reduced Ni-porphyrins are key intermediates in several technologically interesting processes and enzyme reactions. Their reactivity can now be investigated in bulk.

■ EXPERIMENTAL SECTION

General Comments. Procedures were performed in a nitrogen-filled MBraun glovebox or using standard Schlenk techniques unless otherwise specified. Toluene was dried over calcium hydride and stored over molecular sieves in the glovebox. NMR spectra were measured in deuterated solvents (Deutero). Analytic measurements were performed by the following instruments: Bruker CABAV 500neo (^{1}H NMR: 500 MHz, ^{13}C NMR: 125 MHz) and Bruker AV 600 (^{1}H NMR: 600 MHz, ^{13}C NMR: 150 MHz). The high-resolution (HR) mass spectra were measured with an APEX 3 FT-ICR with a 7.05 T magnet by co. Bruker Daltonics. Electron impact (EI) and matrix-assisted laser desorption/ionization (MALDI) mass spectra were measured with a Biflex III by co. Bruker. As matrix was used Cl-CCA. Infrared spectra were measured on a PerkinElmer 1600 Series FT-IR spectrometer with an A531-G Golden-Gate-Diamond-ATR-unit. Signals were abbreviated with w, m, and s for weak, medium, and strong intensities. Broad signals were additionally labeled with br. UV−Vis spectra were measured on a Lambda 650 or a Lambda 14 spectrometer (PerkinElmer), at 25 °C, in quartz cuvettes of 1 or 10 mm path length. For column chromatography purifications silica gel (Merck, particle size 0.040−0.063 mm) was used. R_f values were determined by thin layer chromatography onPolygram Sil G/UV254 (Macherey-Nagel, 0.2 mm particle size). For column chromatography purifications amino-functionalized silica gel (Sigma-Aldrich, particle size 75−200 μm) was used. R_f values were determined by TLC-KPNH-0510-Fl (Biotage).

Synthetic Procedures. 5,10,15,20-Tetra(4-methoxyphenyl) porphyrin (TPPOMe) **1a**, tetraphenylporphyrin (TPP) **1b**, and *meso*-tetrakis(pentafluorophenyl)porphyrin ($TPPF_{20}$) **1c** were synthesized as reported.[36−38]

Nickel-tetraphenylporphyrin (NiTPP) ***2b.*** Tetraphenylporphyrin (50.0 mg, 78.0 μmol) and 4 equiv of bis(cycloocta-1,5-diene)nickel (85.8 mg, 312 μmol) were dissolved in 50 mL of toluene under nitrogen (glovebox). After stirring for 1 h at room temperature, the solvent was removed under reduced pressure, and the crude product was filtered on a short column with dichloromethane. A mixture of the Ni-chlorin and Ni-porphyrin was obtained. This mixture was dissolved in dichloromethane (100 mL), and 2,3-dichlor-5,6-dicyano-1,4-benzoquinone (100 mg, 440 μmol) was added. After it was stirred for 2 h at room temperature, the solvent was removed under reduced pressure, and the crude product was purified by column chromatography on silica gel (dichloromethane, R_f = 0.82). Violet crystals were obtained. Yield: 47.8 mg (71.0 μmol, 91%). ^{1}H NMR (500 MHz, 300 K, $CDCl_3$): δ = 8.74 (s, 8H), 8.01 (dd, ^3J = 7.8 Hz, ^4J = 1.6 Hz, 8H), 8.72−8.65 (m, 12H) ppm. MS (MALDI): m/z (%) = 670 $[M]^+$. HRMS (EI): m/z $[M]^+$ calcd. for $C_{44}H_{28}N_4Ni$: 670.166 74; found: 670.16510.

Nickel-5,10,15,20-tetra(4-methoxyphenyl) porphyrin (NiTPPOMe) ***2a.*** 5,10,15,20-(4-Methoxy)tetraphenylporphyrin (50.0 mg, 68.1 μmol) and 4 equiv of bis(cycloocta-1,5-diene)nickel (74.8 mg, 272 μmol) were dissolved in 150 mL of toluene under nitrogen (glovebox). After it was stirred for 1 h at room temperature, the solvent was removed under reduced pressure, and the crude product was purified by column chromatography on silica gel (dichloromethane, R_f = 0.76). Violet crystals were obtained. Yield: 53.1 mg (67.2 μmol, 99%). ^{1}H NMR (500 MHz, 300 K, $CDCl_3$): δ = 8.76 (s, 8H), 7.92 (d, ^3J = 8.7 Hz, 8H), 7.21 (d, ^3J = 8.7 Hz, 8H), 4.05 (s, 12H) ppm. MS (MALDI): m/z (%) = 791 $[M]^+$. HRMS (EI): m/z $[M]^+$ calcd. for $C_{48}H_{36}N_4NiO_4$: 790.209 00; found: 790.207 43.

Nickel-tetrakis(pentafluorophenyl)porphyrin ($NiTPPF_{20}$) ***2c.*** Method 1 (glovebox): Free base 5,10,15,20-tetrakis(pentafluorophenyl)-porphyrin **1c** (50.0 mg, 51.3 μmol) and 2 equiv of bis(cycloocta-1,5-diene)nickel ($Ni(COD)_2$), (28.2 mg, 102 μmol) were dissolved in 50 mL of toluene under nitrogen (glovebox). After it was stirred for 30 min at room temperature, the solvent was removed under reduced pressure, and the crude product was filtered over a short column with dichloromethane to obtain a mixture of Ni-chlorin and Ni-porphyrin. This mixture was dissolved in dichloromethane (100 mL), and 2,3-dichloro-5,6-dicyano-1,4-benzoquinone (100 mg, 440 μmol) was

DOI: 10.1021/acs.inorgchem.7b03164
Inorg. Chem. 2018, 57, 3177−3182

added. After it was stirred for 2 h at room temperature, the solvent was removed under reduced pressure, and the crude product was purified by column chromatography on silica gel (dichloromethane, R_f = 0.89). Violet crystals were obtained.

Method 2 (Schlenk line): 5,10,15,20-Tetrakis(pentafluorophenyl)-porphyrin **1c** (50.0 mg, 51.3 μmol) was dissolved in 50 mL of dry toluene under nitrogen. Then 2 equiv of bis(cycloocta-1,5-diene)nickel ($Ni(COD)_2$) (28.2 mg, 102 μmol) was added in counter current flow of nitrogen. After it was stirred for 30 min at room temperature, the solvent was removed under reduced pressure, and the crude product was filtered over a short column with dichloromethane to obtain a mixture of Ni-chlorin and Ni-porphyrin. This mixture was dissolved in dichloromethane (100 mL), and 2,3-dichlor-5,6-dicyano-1,4-benzoquinone (100 mg, 440 μmol) was added. After it was stirred for 2 h at room temperature, the solvent was removed under reduced pressure, and the crude product was purified by column chromatography on silica gel (dichloromethane, R_f = 0.89). Violet crystals were obtained. Yield: (52.8 mg, 51.2 μmol, quant). ^{1}H NMR (500 MHz, 300 K, $CDCl_3$): δ = 8.79 (s, 8H) ppm. ^{19}F NMR (470 MHz, 300 K, $CDCl_3$, $CFCl_3$): δ = −136.64 (dd, ^3J = 22.8 Hz, ^5J = 7.5 Hz, 8F, *o*-F), −151.31 (t, ^3J = 20.9 Hz, 4F, *p*-F), −161.20 (td, ^3J = 22.6 Hz, ^5J = 7.5 Hz, 8F, *m*-F) ppm. MS (MALDI): *m*/*z* (%) = 1030 $[M]^+$. HRMS (EI): *m*/*z* $[M]^+$ calcd. for $C_{44}H_8F_{20}N_4Ni$: 1029.978 31; found: 1029.977 14.

Nickel-tetrakis(pentafluorophenyl)chlorin (NiTPCF$_{20}$ chlorin) ***3c.*** Method 1 (without KHMDS): Free base porphyrin **1c** and $Ni(COD)_2$ were reacted as described in the first part of the synthesis of ($NiTPPF_{20}$) **2c** (vide supra). The mixture of Ni-chlorin and Ni-porphyrin was purified by column chromatography on amino-functionalized silica gel (59791 Supelco) (dichloromethanen/*n*-pentane − 1:3, R_f − 0.63). Yield: 25.9 mg (25.1 μmol, 49%).

Method 2 (with KHMDS): 5,10,15,20-Tetrakis-(pentafluorophenyl)porphyrin **1c** (50.0 mg, 51.3 μmol) and 2 equiv potassium bis(trimethylsilyl)amide (KHMDS) (20.5 mg, 102 μmol) were dissolved in 4 mL of benzene-d_6 under nitrogen. After 1 min of stirring at room temperature, 2 equiv bis(cycloocta-1,5-diene)nickel (28.2 mg, 102 μmol) was added. After 30 min of stirring at room temperature the mixture of Ni-chlorin and Ni-porphyrin was separated by column chromatography on an 3-aminopropyl-functionalized silica gel (59791 Supelco), (dichloromethane/*n*-pentane = 1:3, R_f = 0.63). Yield: 34.9 mg (33.9 μmol, 66%).^{1}H NMR (500 MHz, 300 K, acetone-d_6): δ = 8.70 (d, ^3J = 5.0 Hz, 2H), 8.52 (s, 2H), 8.34 (d, ^3J = 5.0 Hz, 2H), 4.16 (s, 4H) ppm. ^{19}F NMR (470 MHz, 300 K, $CDCl_3$, acetone-d_6): δ = −139.23 (dd, ^3J = 23.0 Hz, ^5J = 7.7 Hz, 4F, *o*-F), −139.68 (dd, ^3J = 23.0 Hz, ^5J = 7.7 Hz, 4F, *o*-F), −154.90 (t, ^3J = 20.5 Hz, 2F, *p*-F), −155.15 (t, ^3J = 20.5 Hz, 2F, *p*-F), −162.79 (td, ^3J = 22.5 Hz, ^5J = 7.7 Hz, 4F, *m*-F), −163.36 (td, ^3J = 22.5 Hz, ^5J = 7.7 Hz, 4F, *m*-F) ppm. MS (MALDI): *m*/*z* (%) = 1032 $[M]^+$. HRMS (EI): *m*/*z* $[M]^+$ calcd. for $C_{44}H_{10}F_{20}N_4Ni$: 1031.993 96; found: 1031.989 96. IR: $\tilde{\nu}$ = 2921 (m), 2852 (m), 1741 (m), 1632 (w), 1517 (w), 1494 (m), 1466 (w), 1356 (w), 1261 (m), 1074 (w), 1017 (m), 990 (m), 939 (m), 690 (w), 631 (s), 536 (s), 498 (s), 419 (s), 409 (s) cm^{-1}.

■ ASSOCIATED CONTENT

Supporting Information

The Supporting Information is available free of charge on the ACS Publications website at DOI: 10.1021/acs.inorgchem.7b03164.

Analytical equipment and methods, spectra (PDF)

■ AUTHOR INFORMATION

Corresponding Author

*E-mail: rherges@oc.uni-kiel.de.

ORCID

Rainer Herges: 0000-0002-6396-6991

Notes

The authors declare no competing financial interest.

■ ACKNOWLEDGMENTS

The authors gratefully acknowledge financial support by the Deutsche Forschungsgesellschaft within the Sonderforschungsbereich 677, "Function by Switching".

■ REFERENCES

(1) Li, Y.; Zamble, D. B. Nickel Homeostasis and Nickel Regulation: An Overview. *Chem. Rev.* **2009**, *109*, 4617−4643.

(2) Sings, H. L.; Bible, K. C.; Rinehart, K. L. Acyl tunichlorins: a new class of nickel chlorins isolated from the Caribbean tunicate Tridemnum solidum. *Proc. Natl. Acad. Sci. U. S. A.* **1996**, *93*, 10560−10565.

(3) Gosden, C.; Healy, K. P.; Pletcher, D. Reaction of electrogenerated square-planar nickel(I) complexes with alkyl halides. *J. Chem. Soc., Dalton Trans.* **1978**, 972−976.

(4) Bakac, A.; Espenson, J. H. Mechanistic Investigation of Carbon-Carbon Bond Formation in the Reduction of Alkyl Halides by Organonickel Complexes in Aqueous Solution. *J. Am. Chem. Soc.* **1986**, *108*, 719−723.

(5) Gong, M.; Cao, Z.; Liu, W.; Nichols, E. M.; Smith, P. T.; Derrick, J. S.; Liu, Y.-S.; Liu, J.; Wen, X.; Chang, C. J. Supramolecular Porphyrin Cages Assembled at Molecular−Materials Interfaces for Electrocatalytic CO Reduction. *ACS Cent. Sci.* **2017**, *3*, 1032−1040.

(6) Solis, B. H.; Maher, A. G.; Dogutan, D. K.; Nocera, D. G.; Hammes-Schiffer, S. Nickel phlorin intermediate formed by proton-coupled electron transfer in hydrogen evolution mechanism. *Proc. Natl. Acad. Sci. U. S. A.* **2016**, *113*, 485−492.

(7) Whitlock, H. W.; Hanauer, J. R.; Oester, M. Y.; Bower, B. K. Diimide reduction of porphyrins. *J. Am. Chem. Soc.* **1969**, *91*, 7485−7489.

(8) Stolzenberg, A. M.; Simerly, S. W.; Steffey, B. D.; Haymond, G. S. The Synthesis, Properties, and Reactivities of Free-Base- and Zn(II)-*N*-Methyl Hydroporphyrin Compounds. The Unexpected Selectivity of the Direct Methylation of Free-Base Hydroporphyrin Compounds. *J. Am. Chem. Soc.* **1997**, *119*, 11843−11854.

(9) Nascimento, B. F.; Rocha Gonsalves, A. M.; Pineiro, M. MnO_2 instead of quinones as selective oxidant of tetrapyrrolic macrocycles. *Inorg. Chem. Commun.* **2010**, *13*, 395−398.

(10) Venkataramani, S.; Jana, U.; Dommaschk, M.; Sönnichsen, F. D.; Tuczek, F.; Herges, R. Magnetic Bistability of Molecules in Homogeneous Solution at Room Temperature. *Science* **2011**, *331*, 445−448.

(11) Dommaschk, M.; Peters, M.; Gutzeit, F.; Schütt, C.; Näther, C.; Sönnichsen, F. D.; Tiwari, S.; Riedel, C.; Boretius, S.; Herges, R. Photoswitchable magnetic resonance imaging contrast by improved light-driven coordination-induced spin state switch. *J. Am. Chem. Soc.* **2015**, *137*, 7552−7555.

(12) Adler, A. D.; Longo, F. R.; Kampas, F.; Kim, J. On the Preparation of Metalloporphyrins. *J. Inorg. Nucl. Chem.* **1970**, *32*, 2443−2445.

(13) Kingham, D. J.; Brisbin, D. A. Kinetics of metalloporphyrin formation in glacial acetic acid. *Inorg. Chem.* **1970**, *9*, 2034−2037.

(14) Brisbin, D. A.; Balahura, R. J. Kinetic studies of metalloporphyrin formation. Part I. Mn(II) with hematoporphyrin. *Can. J. Chem.* **1968**, *46*, 3431−3436.

(15) Choi, E. I.; Fleischer, E. B. Kinetics of the Reaction of Some Divalent Transition Metal Ions with α, β, γ, δ-Tetra-(4-pyridyl)-porphine. *Inorg. Chem.* **1963**, *2*, 94−97.

(16) Rothemund, P.; Menotti, A. R. Porphyrin Studies. The Metal Complex Salts of α,β,γ,δ-Tetraphenylporphine. *J. Am. Chem. Soc.* **1948**, *70*, 1808−1812.

(17) Barnes, J. W.; Dorough, G. D. Exchange and Replacement Reactions of α,β,γ,δ-Tetraphenyl-metalloporphins. *J. Am. Chem. Soc.* **1950**, *72*, 4045−4050.

(18) Pasternack, R. F.; Vogel, G. C.; Skowronek, C. A.; Harris, R. K.; Miller, J. G. Copper (II) incorporation into tetraphenylporphine in dimethyl sulfoxide. *Inorg. Chem.* **1981**, *20*, 3763−3765.

DOI: 10.1021/acs.inorgchem.7b03164
Inorg. Chem. 2018, 57, 3177−3182

(19) Bain-Ackerman, M. J.; Lavallee, D. K. Kinetics of metal-ion complexation with n-methyltetraphenylporphyrin. *Inorg. Chem.* **1979**, *18*, 3358−3364.
(20) Baum, S. J.; Plane, R. A. Kinetics of the Incorporation of Magnesium(II) into Porphyrin. *J. Am. Chem. Soc.* **1966**, *88*, 910−913.
(21) Bhyrappa, P.; Nethaji, M.; Krishnan, V. Structure of nonplanar octabromotetraphenyl porphyrin and kinetics of rapid metalation reactions. *Chem. Lett.* **1993**, *22*, 869−872.
(22) Dean, M. L.; Schmink, J. R.; Leadbeater, N. E.; Brückner, C. Microwave-promoted insertion of Group 10 metals into free base porphyrins and chlorins: scope and limitations. *Dalton Trans.* **2008**, 1341−1345.
(23) Han, Y.; Fang, H.; Jing, H.; Sun, H.; Lei, H.; Lai, W.; Cao, R. Singly versus Doubly Reduced Nickel Porphyrins for Proton Reduction: Experimental and Theoretical Evidence for a Homolytic Hydrogen-Evolution Reaction. *Angew. Chem., Int. Ed.* **2016**, *55*, 5457−5462.
(24) Fleischer, E. B. Structure of porphyrins and metalloporphyrins. *Acc. Chem. Res.* **1970**, *3*, 105−112.
(25) Alden, R. G.; Crawford, B. A.; Doolen, R.; Ondrias, M. R.; Shelnutt, J. A. Ruffling of nickel (II) octaethylporphyrin in solution. *J. Am. Chem. Soc.* **1989**, *111*, 2070−2072.
(26) Buchler, J. W. In *Porphyrins and Metalloporphyrins;* Smith, K. M., Ed.; Elsevier: Amsterdam, Netherlands, 1975; p 157.
(27) Tsutsui, M.; Velapoldi, R. A.; Suzuki, K.; Vohwinkel, F.; Ichikawa, M.; Koyano, T. Unusual metalloporphyrins. IV. Novel methods for metal insertion into porphyrins. *J. Am. Chem. Soc.* **1969**, *91*, 6262−6266.
(28) Ostfeld, D.; et al. Novel metalloporphyrins. Syntheses and implications. *Acc. Chem. Res.* **1974**, *7*, 52−58.
(29) Peters, M. K.; Thoms, V.; Herges, R. unpublished results.
(30) Dommaschk, M.; Thoms, V.; Schütt, C.; Näther, C.; Puttreddy, R.; Rissanen, K.; Herges, R. Coordination-Induced Spin-State Switching with Nickel Chlorin and Nickel Isobacteriochlorin. *Inorg. Chem.* **2015**, *54*, 9390−9392.
(31) Lexa, D.; Momenteau, M.; Mispelter, J.; Savéant, J. M. Does one-electron transfer to nickel (II) porphyrins involve the metal or the porphyrin ligand? *Inorg. Chem.* **1989**, *28*, 30−35.
(32) Kadish, K. M.; van Caemelbecke, E.; Royal, G. Electrochemistry of Metalloporphyrins in Nonaqueous Media. In *The Porphyrin Handbook;* Kadish, K. M., Smith, K. M., Guilard, R., Eds.; Academic Press: San Diego, CA, 2000; Vol. *8*, pp 1−114.
(33) Campbell, C. J.; Rusling, J. F.; Brückner, C. Nickel(II) *meso*-Tetraphenyl-Homoporphyrins, -secochlorins, and -chlorophin: Control of Redox Chemistry by Macrocycle Rigidity. *J. Am. Chem. Soc.* **2000**, *122*, 6679−6685.
(34) Fang, Y.; Gorbunova, Y. G.; Chen, P.; Jiang, X.; Manowong, M.; Sinelshchikova, A. A.; Enakieva, Y. Y.; Martynov, A. G.; Tsivadze, A. Y.; Bessmertnykh-Lemeune, A.; Stern, C.; Guilard, R.; Kadish, K. M. Electrochemical and Spectroelectrochemical Studies of Diphosphorylated Metalloporphyrins. Generation of a Phlorin Anion Product. *Inorg. Chem.* **2015**, *54*, 3501−3512.
(35) Guo, H.; Jiang, J.; Shi, Y.; Wang, Y.; Wang, Y.; Dong, S. Sequential Deprotonation of *meso*-(*p*-Hydroxyphenyl)porphyrins in DMF: From Hyperporphyrins to Sodium Porphyrin Complexes. *J. Phys. Chem. B* **2006**, *110*, 587−594.
(36) Maqueira, L.; Iribarren, A.; Valdes, A. C.; De Meloc, C. P.; Dos Santos, C. G. Preparation and characterization of SDS-stabilized hydrophobic porphyrinic nanoaggregates in water. *J. Porphyrins Phthalocyanines* **2012**, *16*, 267−272.
(37) Plater, M. J.; Aiken, S.; Bourhill, G. Metallated porphyrins containing lead (II), copper (II) or zinc (II). *Tetrahedron* **2002**, *58*, 2415−2422.
(38) Dommaschk, M.; Gutzeit, F.; Boretius, S.; Haag, R.; Herges, R. Coordination-Induced Spin-State-Switch (CISSS) in water. *Chem. Commun.* **2014**, *50*, 12476−12478.

DOI: 10.1021/acs.inorgchem.7b03164
Inorg. Chem. 2018, 57, 3177−3182

3.5 Herstellung und Isolierung von Isobenzofuran

Das Isobenzofuran (IBF) **12** stellt eines der in der Literatur bekanntesten reaktivsten Diene für Diels-Alder-Reaktionen dar.[102,103,104] Der Hauptgrund für die hohe Reaktivität beruht auf der Resonanzenergie, welche durch die Bildung eines Benzolrings in der Cycloaddition frei wird (Abbildung 19).[105]

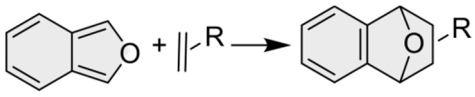

12

Abbildung 19: Darstellung einer Diels-Alder-Reaktion von Isobenzofuran und der Bildung eines Benzolrings im Cycloaddukt.

Nach der Literatur findet das IBF **12** als 4-Elektronen-Dien in Diels-Alder-Reaktionen seine Anwendung. Darüber hinaus wird es in anderen Cycloadditionen wie den [4+3], [4+4], [8+8] und [4+6] eingesetzt.[106,107] Eine der wichtigsten synthetischen Anwendungen ist wahrscheinlich die Herstellung anellierter polycyclischer aromatischer Kohlenwasserstoffe durch die Cycloaddition an Arine.[107,108] Des Weiteren sind die Derivate des IBFs **12** hochinteressant. Beispielsweise wird das 1,3-Diphenylisobenzofuran (DPBF) als Abfangreagens für Singulettsauerstoff verwendet und dient somit als Nachweis für die Erzeugung von $^1O_2$ in der photodynamischen Therapie.[102,109]

Das DPBF ist weitestgehend stabil, dadurch kommerziell erhältlich und somit eines der am häufigsten verwendeten Isobenzofuranderivate. Jedoch ist das Stammsystem **12** etwa zehnmal reaktiver, aber dadurch auch instabiler.[110] Aus diesem Grund erweisen sich die Herstellung und Isolation extrem schwierig.[104]

Preparation and isolation of isobenzofuran

Morten K. Peters and Rainer Herges

Beilstein Journal of Organic Chemistry **2017**, *13,* 2659–2662.
doi:10.3762/bjoc.13.263

Eigenanteil: Die Synthesen und Messungen wurden von Morten Peters durchgeführt. Das Manuskript wurde von Morten Peters und Prof. Dr. Rainer Herges verfasst.

Zusammenfassung

In dieser Veröffentlichung werden unterschiedliche Synthesewege des IBFs **12** diskutiert und auf ihre Durchführbarkeit überprüft. Zusätzlich wird die Isolierung und Charakterisierung des instabilen Isobenzofurans **12** vorgestellt.

Für praktische Anwendungen wurde IBF *in situ* erzeugt und umgesetzt, da es in Lösungsmitteln mittlerer Polarität wie Chloroform eine Halbwertszeit von 2 Stunden aufweist. Die kurze Lebensdauer liegt an der raschen Dimerisierung und Polymerisation. Es wurde gezeigt, dass sich die Halbwertszeiten in Lösungsmitteln mit geringer Polarität ($t_{1/2}$ = 12 h in Toluol-d_8, 150 mM, 27 °C) verlängern. Zusätzlich gelang es erstmals, die Verbindung durch Chromatographie zu reinigen und sie als farblosen Feststoff zu isolieren (Schmelzpunkt 20 ºC). In kristalliner Form ist dieser bei -15 °C über 8 Monate ohne Zersetzung stabil. Nach oxidativer Methoxylierung von kommerziell erhältlichem Phthalan **22** (85 % Ausbeute)[111] und anschließender 1,4-Eliminierung mit LDA[112] konnte durch eine Trapping-Reaktion mit Acetylendicarbonsäuredimethylester eine Ausbeute von 78 % erhalten werden. Nach Chromatographie wurde hingegen lediglich eine Ausbeute von 66 % an Isobenzofuran **12** isoliert (Abbildung 20).

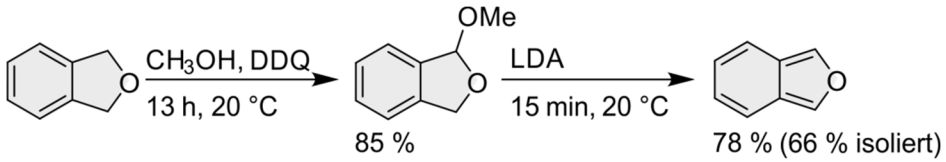

Abbildung 20: Die optimierte Synthese des Isobenzofurans **12**.

BEILSTEIN JOURNAL OF ORGANIC CHEMISTRY

Preparation and isolation of isobenzofuran

Morten K. Peters and Rainer Herges*

Letter

Open Access

Address:
Otto-Diels-Institut für Organische Chemie, Christian-Albrechts-Universität, Otto-Hahn-Platz 4, 24118 Kiel, Germany

Email:
Rainer Herges* - rherges@oc.uni-kiel.de

* Corresponding author

Keywords:
[4 + 2] cycloaddition; Diels–Alder; isobenzofuran; trapping reagent

Beilstein J. Org. Chem. **2017,** *13,* 2659–2662.
doi:10.3762/bjoc.13.263

Received: 16 October 2017
Accepted: 01 December 2017
Published: 12 December 2017

Associate Editor: B. Stoltz

Abstract

The synthesis, isolation and characterization of isobenzofuran are described in this publication. Isobenzofuran is of general interest in synthetic and physical organic chemistry because it is one of the most reactive dienes known. A number of synthetic pathways have been published which all suffer from disadvantages such as low yields and difficult purification. We present a synthetic pathway to prepare isobenzofuran in laboratory scale with high yields, from affordable, commercially available starting materials.

Introduction

Isobenzofurans have been described as the most reactive dienes for Diels–Alder reactions [1-5]. Their high reactivity is mainly due to the resonance energy gained by formation of a benzene ring in the cycloaddition product (Scheme 1) [6].

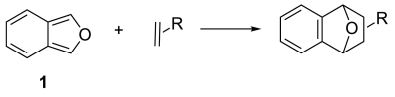

1

Scheme 1: Diels–Alder reaction of isobenzofuran and formation of a benzene ring in the cycloadduct.

Isobenzofurans have been extensively used as 4 electron (diene) components in Diels–Alder reactions, and moreover in other cycloaddition reactions such as [4 + 3], [4 + 4], [8 + 8] and [4 + 6] additions [7-10]. Highly strained alkenes and alkynes have been trapped with isobenzofurans. 1,3-Diphenylisobenzofuran is the preferred trapping reagent for singlet oxygen and is used to quantify the generation of $^1O_2$ in photodynamic therapy [4,11]. The most important synthetic application is probably the preparation of annulated polycyclic aromatic hydrocarbons by cycloaddition to arynes [8,12]. However, the high reactivity of isobenzofurans comes at the cost of low stability [13]. 1,3-Diphenylisobenzofuran is reasonably stable and commercially available and therefore the most frequently used isobenzofuran derivative. The parent system isobenzofuran (IBF, **1**) is about 10 times more reactive but generally described as a reagent that is difficult to prepare and to purify [1]. Therefore, it should be generated in situ, and used without isolation.

Beilstein J. Org. Chem. 2017, 13, 2659–2662.

Results and Discussion

We now present a reliable and convenient synthesis providing high yields of isobenzofuran. In contrast to previous reports, the compound is stable for more than 8 months in pure form as a solid at −15 °C. The half-life of IBF (**1**) in solution (150 mM, 27 °C, toluene-d_8) is about 12 h. A half-life of 2 h in $CDCl_3$ has been previously reported [14]. Isobenzofurans are light sensitive. Warrener et al. reported on [8 + 8] cycloaddition products upon irradiation. Depending on the solvent further dimers are formed [14].

Several procedures have been published for the synthesis of IBF (**1**). The key step in the majority of the reported methods is a retro Diels–Alder reaction [6,13,15-17]. Fieser and Haddadin [17] describe IBF as a transient intermediate and Warrener and Wege [13,15] isolated IBF at −80 °C on a cold finger. The disadvantages of these methods are high reaction temperatures during vacuum pyrolysis and multistep syntheses of the precursors.

The alternative way to synthesize IBF (**1**) is 1,4-elimination of 1,3-dihydro-1-methoxyisobenzofuran (**7**, DMIBF), which provides access to IBF (**1**) at ambient temperature [18]. Three methods have been published to prepare **7** (DMIBF). Reduction of phthalic acid (**2**) or phthalic acid ester **3** to 1,2-bis(hydroxymethyl)benzene (**4**) [19], acid promoted ring closure, and subsequent oxidation with hypochlorite in the presence of methanol gives **7** in a moderate yield of 65% [18].

Alternatively, phthalide **5** has been reduced to 1,3-dihydroisobenzofuran-1-ol (**6**) and methylated to DMIBF (**7**) [8]. However, yields in our hands are quite low.

It is known that benzyl ethers are prone to oxidative functionalization [20]. 2,3-Dichloro-5,6-dicyano-1,4-benzoquinone (DDQ) has been used to selectively oxidize benzyl ethers to acetals in the presence of alcohols [21]. Following a procedure of Doyle et al. we reacted commercially available phthalan (**8**) with DDQ and methanol in dry dichloromethane under a nitrogen atmosphere at room temperature, and obtained DMIBF (**7**) with a yield of 85% (Scheme 2) [22]. DMIBF (**7**) was treated with freshly prepared lithium diisopropylamide (LDA) in benzene and IBF (**1**) was obtained as a solution in benzene which was washed with aqueous NH_4Cl to remove lithium salts and amines (Scheme 2) [8,18].

To determine the yield of IBF (**1**), this solution was reacted with acetylenedicarboxylic acid dimethyl ester (DMAD, **9**) and prod-

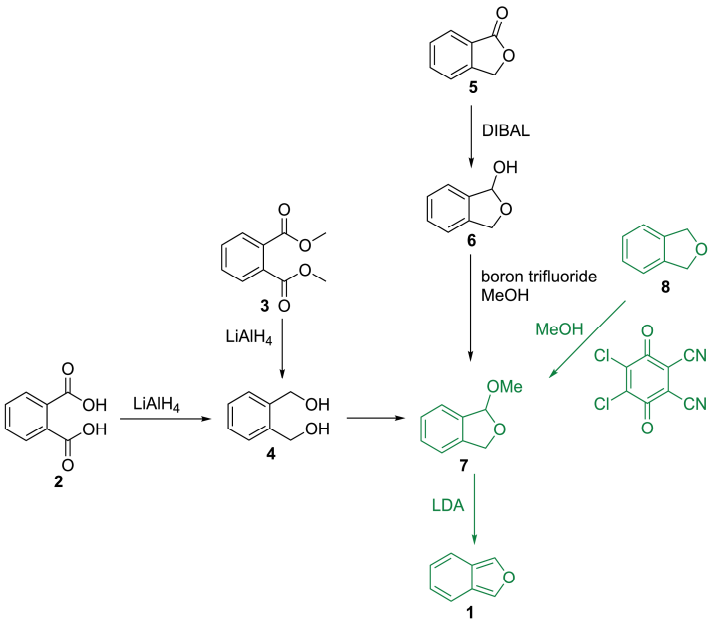

Scheme 2: Different approaches for the synthesis of IBF (**1**).

uct **10** was obtained with a yield of 78% relative to the precursor DMIBF (**7**, Scheme 3).

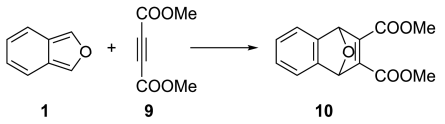

Scheme 3: Reaction of in situ prepared IBF (**1**) with DMAD (**9**).

To further purify isobenzofuran (**1**), the benzene solution was carefully evaporated and the residue was subjected to column chromatography over silica gel (cyclohexane/ethyl acetate). We were able to isolate IBF (**1**) as a colorless solid (mp 20 °C) with a yield of 66%. The solid compound can be stored for up to 8 months at −15 °C without decomposition (polymerization).

Conclusion

Isobenzofuran (**1**) is one of the most reactive dienes in Diels–Alder reactions and other cycloadditions. For practical applications it has been generated and reacted in situ, because it rapidly dimerizes or polymerizes in solvents of medium polarity such as chloroform ($t_{1/2}$ = 2 h). We observed longer half-lives in low polarity solvents ($t_{1/2}$ = 12 h in toluene-d_8, 150 mM, 27 °C). We have been able to purify the compound by chromatography and to isolate it as a colorless solid (mp 20 °C). In crystalline form, it is stable for 8 months at −15 °C without decomposition. Upon oxidative methoxylation of commercially available phthalane (85% yield) [22], and subsequent 1,4-elimination with LDA [18] we obtained isobenzofuran (**1**) in 78% yield (trapping reaction) or in 66% isolated yield after chromatography.

Experimental

NMR spectra were measured in deuterated solvents (Deutero). Analytic measurements were performed by the following instruments: Bruker CABAV 500neo (^{1}H NMR: 500 MHz, ^{13}C NMR: 125 MHz) and Bruker AV 600 (^{1}H NMR: 600 MHz, ^{13}C NMR: 150 MHz). Infrared spectra were recorded on a Perkin-Elmer 1600 Series FTIR spectrometer with an A531-G Golden-Gate-Diamond-ATR-unit. The high-resolution (HR) mass spectra were measured with an APEX 3 FT-ICR with a 7.05 T magnet by co. Bruker Daltonics. Electron impact (EI).

1,3-Dihydro-1-methoxyisobenzofuran (7) [22]: 2,3-Dichloro-5,6-dicyano-1,4-benzoquinone (DDQ, 5.00 g, 22.0 mmol), dry dichloromethane (100 mL), methanol (900 µL, 22.2 mmol) and phthalan (**8**, 2.00 g, 16.7 mmol) were dissolved under a nitrogen atmosphere. The reaction mixture was stirred for 13 h at room temperature. The reaction was quenched with aq sodium hydrogen carbonate solution and filtered over Celite. The aqueous phase was extracted three times with dichloromethane. The combined organic layers were dried over magnesium sulfate and the solvent was removed under reduced pressure. The crude product was purified by column chromatography on silica gel (cyclohexane/ethyl acetate 8:2, R_f 0.58) A colorless oil was obtained. Yield: 2.13 g (14.2 mmol, 85%); ^{1}H NMR (500 MHz, 300 K, $CDCl_3$) δ 7.41 (d, ^3J = 7.3 Hz, 1H), 7.39–7.33 (m, 2H), 7.27 (d, ^3J = 7.4 Hz, 1H), 6.19 (d, ^4J = 2.2 Hz, 1H), 5.22 (dd, ^2J = 12.7 Hz, ^4J = 2.2 Hz, 1H), 5.05 (d, ^2J = 12.7 Hz, 1H), 3.44 (s, 3H) ppm; ^{13}C NMR (150 MHz, 300 K, $CDCl_3$) δ 140.0, 137.3, 129.3, 127.9, 123.0, 121.0, 107.3, 72.2, 54.2 ppm.

Isobenzofuran (1, IBF) [18]: Diisopropylamine (1.43 g, 14.2 mmol) was dissolved in benzene (5.00 mL), and cooled to 0 °C. 2.5 M *n*-butyllithium solution in hexane (6.70 mL) was added dropwise and the mixture was stirred for 15 min. The freshly prepared LDA solution was warmed up to room temperature. Then 1-methoxy-1,3-dihydroisobenzofuran (**7**, 800 mg, 5.33 mmol), dissolved in benzene (8 mL), was added dropwise and stirred for 5 min. The mixture was washed with ammonium chloride solution and then twice with water. The combined organic layers were dried over magnesium sulfate and the solvent was removed under reduced pressure. The crude product was purified by column chromatography on silica gel (cyclohexane/ethyl acetate 8:2, R_f 0.92). The solvent was carefully evaporated at 20 °C. A colorless solid was obtained. Yield: 415 mg (3.52 mmol, 66%); mp 20 °C; IR (ATR): 3138 (w), 3044 (w), 2923 (w), 1774 (w), 1695 (m), 1462 (m), 1428 (m), 1368 (m), 1195 (w), 1043 (s), 976 (s), 950 (s), 888 (s), 871 (m), 758 (s), 672 (m), 635 (s), 601 (s), 539 (s), 496 (s) cm $^{-1}$; ^{1}H NMR (600 MHz, 300 K, DMSO-d_6) δ 8.32 (s, 2H), 7.45 (dd, ^3J = 6.8 Hz, ^4J = 2.8 Hz, 2H), 6.86 (dd, ^3J = 6.8 Hz, ^4J = 2.8 Hz, 2H) ppm; ^{13}C NMR (150 MHz, 300 K, DMSO-d_6) δ 136.1, 124.2, 123.5, 119.0 ppm; HRMS (EI) *m/z*: $[M]^+$ calcd. for C_8H_6O, 118.04173; found, 118.04186.

Dimethyl 1,4-epoxy-1,4-dihydronaphthalene-2,3-dicarboxylate (10): Dimethyl acetylenedicarboxylate (**9**, 1.00 g, 7.04 mmol) was dissolved in benzene (25 mL) under a nitrogen atmosphere. A freshly prepared solution of isobenzofuran (**1**), which was prepared from DMIBF (**7**, 1.10 mmol, 165 mg), prior to purification by chromatography (see procedure above) was added dropwise and stirred for 16 h at 50 °C. The crude product was purified by column chromatography on silica gel (cyclohexane/ethyl acetate 8:2, R_f 0.27). A colorless oil was obtained. Yield: 223 mg (858 µmol, 78%); IR (ATR): 2953 (w), 1710 (s), 1637 (m), 1435 (m), 1291 (m), 1250 (s), 1211 (s), 1109 (s), 1064 (m), 976 (m), 910 (m), 854 (s), 755 (s), 734 (m), 655 (s) cm^{-1}; ^{1}H NMR (600 MHz, 300 K, $CDCl_3$) δ 7.43 (dd, ^3J = 5.2 Hz, ^4J = 3.0 Hz, 2H), 7.07 (dd, ^3J = 5.2 Hz, ^4J =

3.0 Hz, 2H), 5.96 (s, 2H), 3.80 (s, 6H) ppm; ^{13}C NMR (150 MHz, 300 K, $CDCl_3$) δ 162.8, 151.2, 146.2, 126.1, 121.4, 84.8, 52.4 ppm; HRMS (EI) *m/z*: $[M]^+$ calcd. for $C_{12}H_{12}O_5$, 260.06847; found, 260.06800.

Supporting Information

Supporting Information File 1

Analytical equipment and methods, experimental procedures and NMR spectra.
[http://www.beilstein-journals.org/bjoc/content/supplementary/1860-5397-13-263-S1.pdf]

Acknowledgements

The authors gratefully acknowledge funding from the collaborative research center SFB 677 Function by Switching.

References

1. Tobia, D.; Rickborn, B. *J. Org. Chem.* **1987,** *52,* 2611. doi:10.1021/jo00388a055
2. Rickborn, B. In *Advances in Theoretically Interesting Molecules;* Thummel, R. P., Ed.; JAI Press: Greenwich, 1989; Vol. 1.
3. Rodrigo, R. *Tetrahedron* **1988,** *44,* 2093. doi:10.1016/S0040-4020(01)81720-8
4. Friedrichsen, W. *Adv. Heterocycl. Chem.* **1980,** *26,* 135. doi:10.1016/S0065-2725(08)60141-5
5. Haddadin, M. J. *Heterocycles* **1978,** *9,* 865. doi:10.3987/R-1978-07-0865
6. Packe-Wirth, R.; Enkelmann, V. *J. Mol. Struct.* **1998,** *448,* 1. doi:10.1016/S0022-2860(98)00324-X
7. Takeshita, H.; Wada, Y.; Mori, A.; Hatsui, T. *Chem. Lett.* **1973,** *2,* 335. doi:10.1246/cl.1973.335
8. Man, Y. M.; Mak, T. C. W.; Wong, H. N. C. *J. Org. Chem.* **1990,** *55,* 3214. doi:10.1021/jo00297a043
9. Itô, S.; Ohtani, H.; Narita, S.; Honma, H. *Tetrahedron Lett.* **1972,** *13,* 2223. doi:10.1016/S0040-4039(01)84811-5
10. Sasaki, T.; Kanematsu, K.; Hayakawa, K. *J. Chem. Soc., Perkin Trans. 1* **1972,** 1951. doi:10.1039/P19720001951
11. Rio, G.; Scholl, M.-J. *J. Chem. Soc., Chem. Commun.* **1975,** 474. doi:10.1039/c3975000047 4
12. Wong, H. N. C.; Man, Y.-M.; Mak, T. C. W. *Tetrahedron Lett.* **1987,** *28,* 6359. doi:10.1016/S0040-4039(01)91373-5
13. Warrener, R. N. *J. Am. Chem. Soc.* **1971,** *93,* 2346. doi:10.1021/ja00738a057
14. Warrener, R. N.; Pitt, I. G.; Russell, R. A. *Aust. J. Chem.* **1993,** *46,* 1515. doi:10.1071/CH9931515
15. Wege, D. *Tetrahedron Lett.* **1971,** *12,* 2337. doi:10.1016/S0040-4039(01)96856-X
16. Wiersum, U. E.; Mijs, W. J. *J. Chem. Soc., Chem. Commun.* **1972,** 347. doi:10.1039/C39720000347
17. Fieser, L. F.; Haddadin, M. J. *J. Am. Chem. Soc.* **1964,** *86,* 2081. doi:10.1021/ja01064a044
18. Naito, K.; Rickborn, B. *J. Org. Chem.* **1980,** *45,* 4061. doi:10.1021/jo01308a028
19. Nystrom, R. F.; Brown, W. G. *J. Am. Chem. Soc.* **1947,** *69,* 1197. doi:10.1021/ja01197a060
20. Goh, S. H. *J. Org. Chem.* **1972,** *37,* 3098. doi:10.1021/jo00985a013
21. Shen, Z.; Dai, J.; Xiong, J.; He, X.; Mo, W.; Hu, B.; Sun, N.; Hu, X. *Adv. Synth. Catal.* **2011,** *353,* 3031. doi:10.1002/adsc.201100429
22. Arendt, K. M.; Doyle, A. G. *Angew. Chem., Int. Ed.* **2015,** *54,* 9876. doi:10.1002/anie.201503936

License and Terms

3.6 Eine neue und effiziente Synthesemethode von Chlorinen, Iso- und Bakteriochlorinen

Porphyrine **8** und ihre reduzierten Derivate, die Chlorine **9**, Bakteriochlorine **11** und Isobakteriochlorine **10**, sind allgegenwärtig in der Natur und somit von großer Bedeutung für die Naturwissenschaften (Abbildung 21). Dies wird durch die mehr als 50000 Publikationen in der Literatur untermauert.[113]

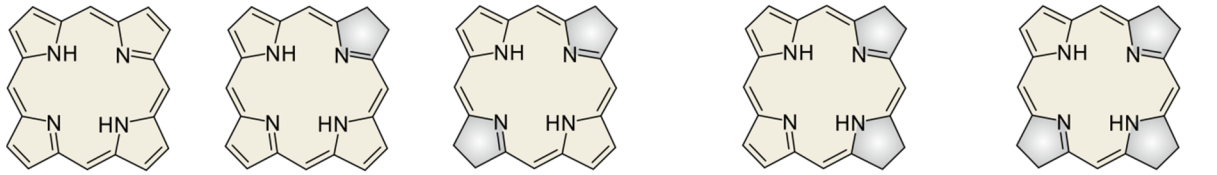

Porphyrin **8** Chlorin **9** Bacteriochlorin **11** Isobacteriochlorin **10** Pyrrocorphin **24**

Abbildung 21: Schematische Strukturen von Tetrapyrrolverbindungen (Hydrierte Pyrrolringe sind in grauer Farbe).

Zu den besonderen Eigenschaften gehören die hohe Stabilität, die katalytischen Aktivitäten sowie die photophysikalischen Eigenschaften, welche ein breites Anwendungsspektrum bieten.[114] Porphyrin- und Hydroporphyrinderivate werden unter anderem als Photosensibilisatoren für die photodynamische Therapie,[115] als Lichtsammelantennen in der Photosynthese,[116] als Chromophore in farbstoffsensibilisierten Solarzellen[117] und für das Design einer Reihe molekularer photonischer Vorrichtungen und Materialien verwendet.[118] Die Hydroporphyrine wie Chlorine und Bakteriochlorine sind die wichtigsten Pigmente in photosynthetischen Systemen von grünen Pflanzen und verschiedenen Bakterien. Die synthetischen Beispiele für Hydroporphyrine nehmen jedoch mit zunehmendem Hydrierungsgrad ab. Die meisten Bakterio- und Isobakteriochlorine sind Derivate von Naturstoffen,[119] da die Zahl der synthetischen Methoden begrenzt ist.[120] Ausgehend von Porphyrinen gibt es im Allgemeinen drei Ansätze zur Herstellung von Chlorinen und (Iso-)Bakteriochlorinen.[121] Hierbei kann die Umwandlung von Pyrrol-Doppelbindungen durch (1) direkte Reduktion, (2) Oxidation oder (3) Cycloadditionen erreicht werden.

One-Pot Approach to Chlorins, Isobacteriochlorins Bacteriochlorins and Pyrrocorphins

Morten K. Peters, Fynn Röhricht, Christian Näther and Rainer Herges

Organic Letters
angenommen: DOI: 10.1021/acs.orglett.8b03433

Eigenanteil: Die Synthesen und Messungen wurden von Morten Peters durchgeführt. Die DFT-Rechnungen wurden von Fynn Röhricht angefertigt. Das Manuskript wurde von Morten Peters und Prof. Dr. Rainer Herges verfasst.

Zusammenfassung

In dieser Veröffentlichung wird ein neuer, leicht durchzuführender, ergiebiger, regio- und stereoselektiver Syntheseweg von Chlorinen **9**, Bakteriochlorinen **11**, Isobakteriochlorinen **10** und Pyrrocorphinen **24** (Hexahydroporphyrinen) vorgestellt. Mit Nickel(II) im Tetrapyrrolkern wird erstmals die gesamte Reihe von Hydroporphyrinen hergestellt und charakterisiert (Abbildung 22).

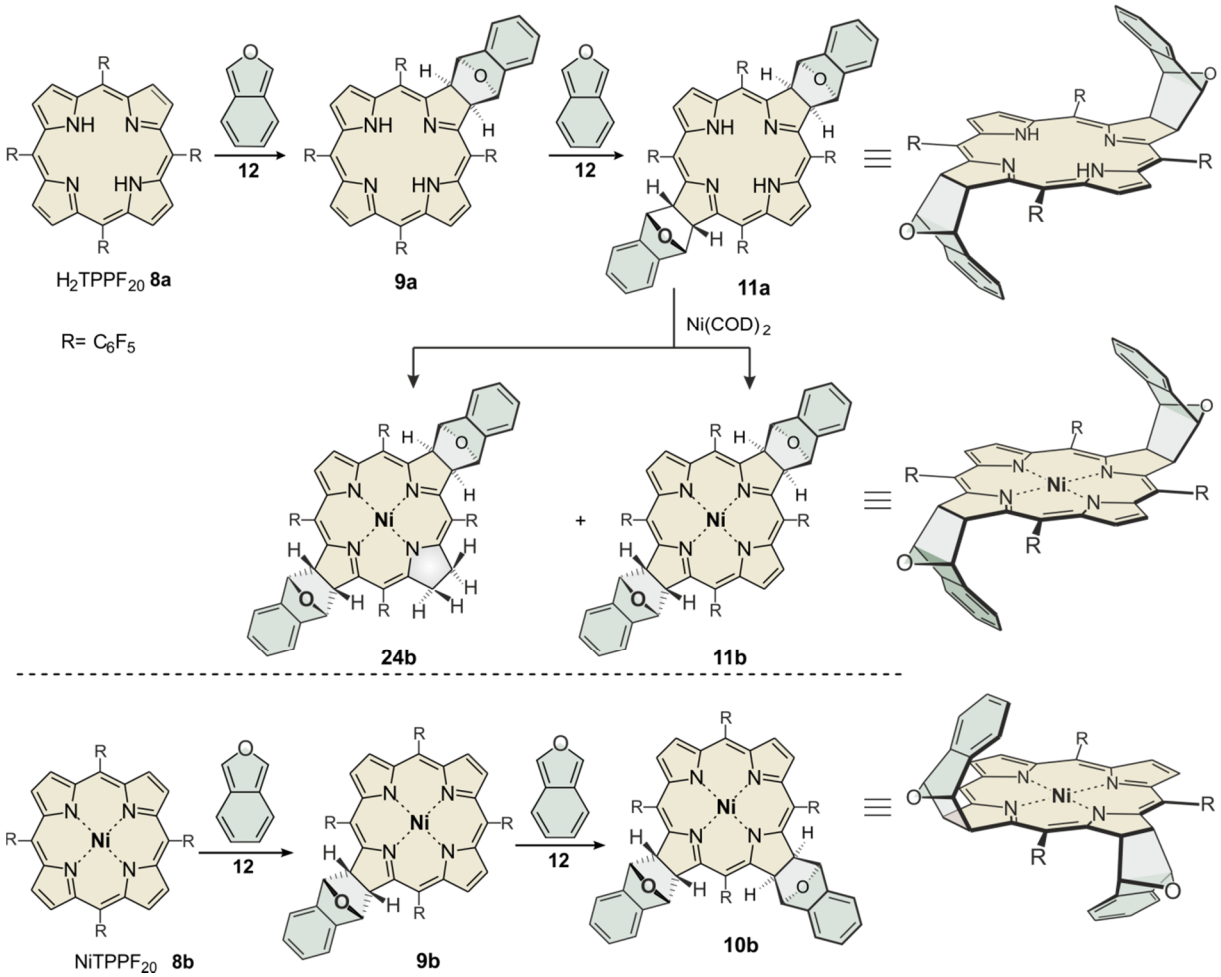

Abbildung 22: Darstellung der Synthese verschiedener Porphyrinderivate über eine [4+2] Cycloaddition.

Von besonders großem Interesse ist das Bakteriochlorin **11a**, da dieses eine starke Absorptionsbande (733 nm) im NIR-Bereich zeigt. Da menschliches Gewebe in diesem Wellenlängenbereich die höchste Transparenz aufweist, bietet **11a** optimale Voraussetzungen für die Anwendung in der PDT. Des Weiteren ist das Bakteriochlorin **11a** stark fluoreszierend, was für die Diagnostik bei der PDT von großer Bedeutung ist. Das entsprechende Ni(II)-Bakteriochlorin **11b** ist nicht-fluoreszierend und ein stabiler NIR-Farbstoff, der bei 757 nm eine intensive Absorption aufweist.

Organic LETTERS
Letter
Cite This: Org. Lett. XXXX, XXX, XXX−XXX
pubs.acs.org/OrgLett

One-Pot Approach to Chlorins, Isobacteriochlorins, Bacteriochlorins, and Pyrrocorphins

Morten K. Peters,[†] Fynn Röhricht,[†] Christian Näther,[‡] and Rainer Herges*[,†]

[†]Otto Diels-Institute of Organic Chemistry, Christian Albrechts University Kiel, Otto Hahn Platz 4, 24118 Kiel, Germany
[‡]Institut für Anorganische Chemie, Christian Albrechts University Kiel, Max-Eyth-Strasse 2, 24118 Kiel, Germany

Supporting Information

ABSTRACT: A Diels−Alder strategy is reported to synthesize the complete set of hydroporphyrins: chlorins, bacteriochlorins, isobacteriochlorins, and pyrrocorphins. Porphyrins and Ni-porphyrins react with isobenzofuran in very high yields at 70 °C to form the corresponding chlorins. Electron-deficient porphyrins react with a second equivalent of isobenzofuran yielding exclusively bacteriochlorin (82%), and Ni-porphyrin gives only isobacteriochlorin (99%). All cycloadditions are completely regio- and stereoselective. The regiochemistry is correctly predicted using the ACID method.

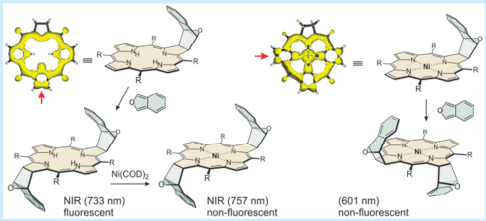

Porphyrins and their reduced derivatives (chlorins, bacteriochlorins, isobacteriochlorins, and pyrrocorphins; Scheme 1) are ubiquitous in nature, and more than 50 000 synthetic analogues have been synthesized so far.[1] Besides stability and catalytic activity, their photophysical properties,[2] found a wide range of applications. Porphyrin and hydroporphyrin derivatives have been used as photosensitizers for photodynamic therapy,[3−5] as light-harvesting antennae in artificial photosynthesis,[6,7] as chromophores in dye-sensitized solar cells,[8] for multiphoton microscopy[9] and for the design of a number of molecular photonic devices and materials.[10]

Even though hydroporphyrins such as chlorins and bacteriochlorins are the most important pigments in the photosynthetic systems of green plants and bacteria, their favorable absorption maxima in the visible and NIR range notwithstanding, examples of synthetic hydroporpyrins decrease with increasing hydrogenation state (porphyrins: 45 000, chlorins: 5100, bacteriochlorins: 576, isobacteriochlorins: 180, pyrrocorphins: 68).[1] Most of the bacterio- and isobacteriochlorins are semi-synthetic derivatives of natural products[11] because the number of fully synthetic methods is limited.[12] There are three general synthetic approaches to chlorins and (iso)bacteriochlorins starting from porphyrins.[13]

Scheme 1. Schematic Structures of Tetrapyrrolic Compounds Including 18 Electron Annulene Substructures[a]

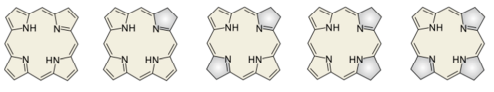

[a]Hydrogenated pyrrole rings are shown in gray.

Scheme 2. [4 + 2] Cycloaddition of Isobenzofuran 4 with Free-Base H_2TPPF_{20} (1), $NiTPPF_{20}$ (2), and TPP (11) Forming the Corresponding Chlorins

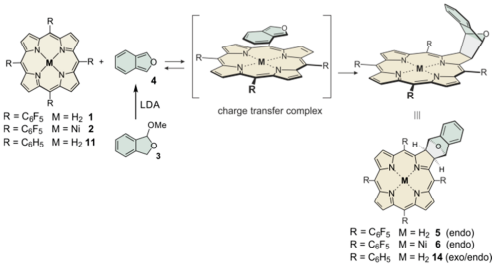

The conversion of β,β' pyrrolic double bonds can be achieved by (1) direct reduction, (2) oxidation, and (3) cycloadditions. Direct reduction (1) leads to chlorins that rapidly oxidize back to the porphyrins. Oxidation (2) is usually performed with OsO_4 and leads to the dihydroxylated chlorins, which are further derivatized. Cycloadditions (3), while providing a convenient, one-step access to chlorins, suffer from the low reactivity of the β,β' pyrrolic double bond. Only very reactive 1,3-dipoles, such as azomethine ylides,[14−16] nitrile oxides,[17] and nitronates[18] react via 1,3-dipolar cycloadditions. Diels−Alder reactions are restricted to highly reactive quinodimethanes as dienes, which have to be generated at very high temperatures *in situ*, leading to chlorins and (iso)-bacteriochlorins that are susceptible to oxidation to porphyrins under air, limiting applications in photodynamic therapy.[19,20]

Received: October 26, 2018

DOI: 10.1021/acs.orglett.8b03433
Org. Lett. XXXX, XXX, XXX−XXX

Scheme 3. Synthesis of Different Porphyrin Derivatives via [4 + 2] Cycloadditions

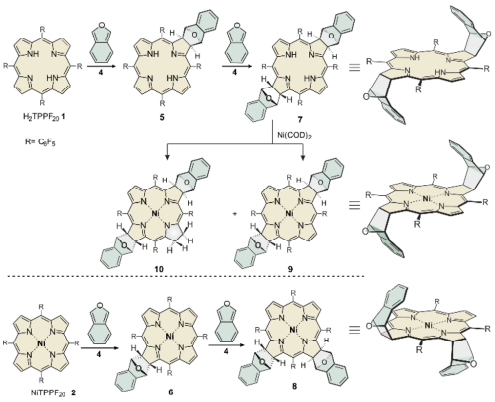

Table 1. Diels-Alder Reactions of Different Porphyrins with IBF at 70 °C[a]

			yield (%)					
tetrapyrrole		eq of IBF	remaining starting material		monoadduct		bisadduct	
H_2TPPF_{20}	**1**	5	**1**	(6)	**5**	(88)	**7**	(6)
H_2TPPF_{20}	**1**	15	**1**	(9)	**5**	(26)	**7**	(65)
H_2TPCF_{20}	**5**	10	**5**	(2)	**5**	(16)[b]	**7**	(82)
Ni-$TPPF_{20}$	**2**	5	**2**	(1)[d]	**6**	(14)	**8**	(83)
Ni-$TPPF_{20}$	**2**	10	–		–[d]		**8**	(99)
H_2P	**13**	10	not isolated				–	
H_2TPP	**11**	10	**11**	(21)[d]	**14**	(72)[c]	–	
Ni-TPP	**12**	10	not isolated				–	

[a]Reaction time was 36 h in all cases; anhydrous benzene was used as a solvent.; and in all experiments, 50 mg of porphyrin was used (except H_2P). [b]Some product was lost through retro Diels–Alder reactions [c]*exo* 53%, *endo* 19% [d]Some product was lost during column chromatography

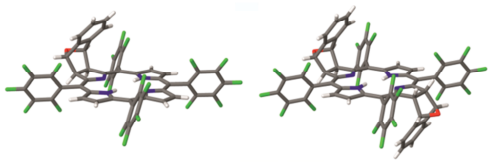

Figure 1. Crystal structure of *endo* free-base chlorin **5** and the *anti–endo* free-base bacteriochlorin **7**.

Driving force for oxidation is the rearomatization of the newly formed cyclohexene ring. In principle, re-oxidation could be prevented if stable, cyclic quinodimethanes such as the commercially available 1,3-diphenylisobenzofuran (DBPF) would be applied because a bridged cyclohexene would be formed that is not susceptible to rearomatization. Unfortunately, in our hands, DBPF does not react even with electron-poor porphyrins such as tetrakis(pentafluorophenyl)porphyrin **1**. Model calculations reveal that the phenyl substituents in DBPF impose severe sterical hindrance with the aryl groups at

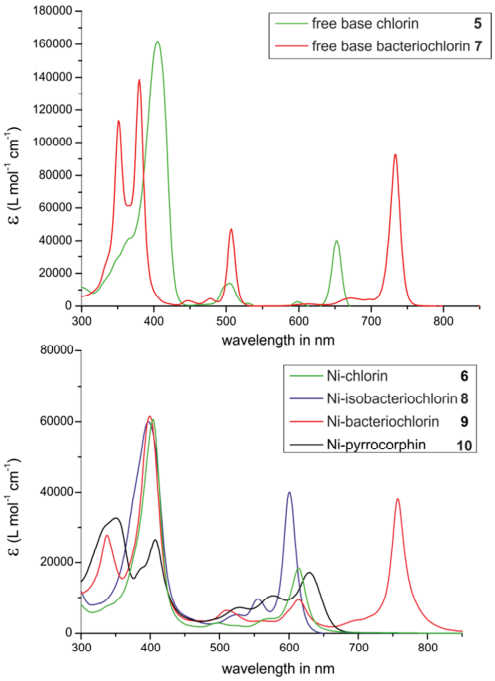

Figure 2. Electronic absorption spectra of chlorin **5** and bacteriochlorin **7** and their reduced derivatives **6**, **8**, **9**, and **10** at 25 °C in acetonitrile (tetrapyrrole concentration of 10 μM).

the *meso* position of the porphyrin. It was therefore straightforward to use the parent isobenzofuran **4** (IBF) as the diene in the Diels–Alder reaction with porphyrins. IBF **4** is considerably more reactive than DBPF and concomitantly sterically less hindered. On the downside, IBF is less stable than DBPF and has to be freshly prepared before use. We recently published a convenient synthesis of pure IBF **4**, which can be stored indefinitely as a solid at −20 °C.[21] We here report on the high reactivity and selectivity of IBF **4** in Diels–Alder reactions with free-base porphyrins and Ni-porphyrins, forming chlorins (1:1 addition products) and (iso)-bacteriochlorins (2:1 addition) with complete regio and stereoselectivity.

We selected tetrakis(pentafluorophenyl)porphyrin (H_2TPPF_{20}) **1** and Ni-tetrakis(pentafluorophenyl)porphyrin (Ni-$TPPF_{20}$) **2** as dienophiles because they are readily accessible and have been previously subjected to cycloadditions. We reacted both porphyrins with freshly prepared IBF **4** for 36 h at 70 °C in benzene. After workup, 1:1 (chlorins), and 2:1 cycloaddition adducts (bacterio- and isobacteriochlorins) were isolated (Schemes 2 and 3). The electron-rich IBF and electron-deficient porphyrins form charge-transfer complexes in a pre-equilibrium preceding the cycloaddition. The formation of porphyrin charge-transfer complexes is typically indicated by the quenching of the fluorescence of the porphyrin.[22,23] The fluorescence of H_2TPPF_{20} **1** (emissions at 643 and 702 nm) is indeed quenched upon addition of IBF **4** (see the Supporting

DOI: 10.1021/acs.orglett.8b03433
Org. Lett. XXXX, XXX, XXX−XXX

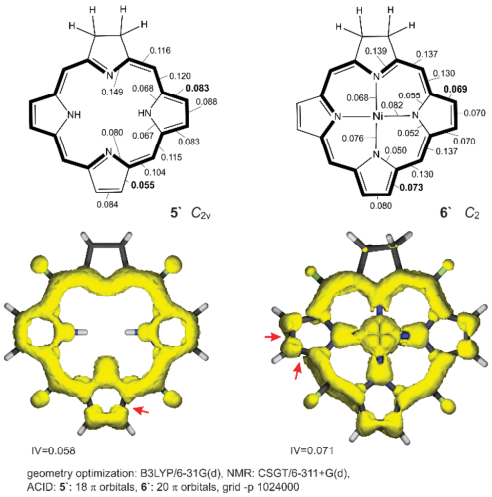

Figure 3. ACID plots predicting the regiochemistry of the Diels–Alder reaction of free base chlorin **5′** and the Ni-chlorin **6′** with isobenzofuran (IBF, **4**). Both chlorins include an aromatic ^{18}annulene subunit (highlighted with bold lines) and are represented as contiguous isosurfaces in the ACID plot, leaving one double bond isolated, i.e., olefinic in nature and, thus, more reactive toward a cycloaddition (indicated with red arrows). For the sake of simplicity and to save computer time, the pentafluorophenyl substituents are replaced by fluorine, and the 1,3-dihydroisobenzofuran unit is replaced by two hydrogen atoms. Critical isosurface values (CIV) are given for all conjugated C–C and C–N bonds. Large CIV values represent bonds with strong conjugation.

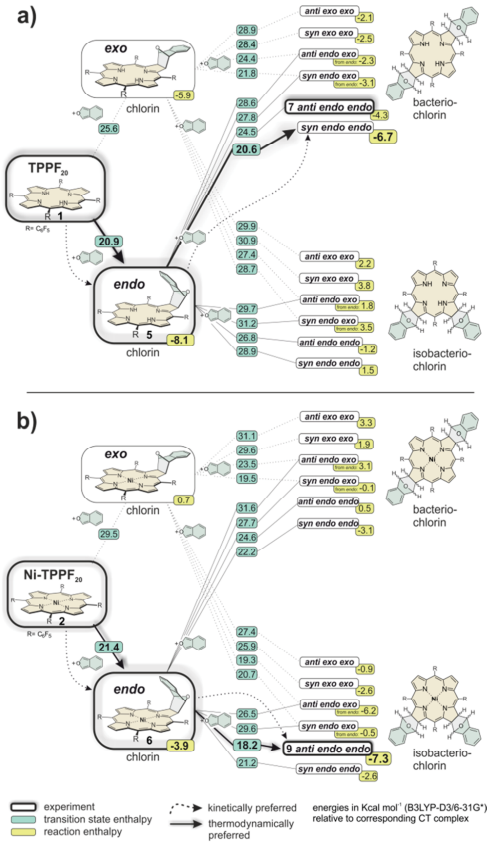

Figure 4. (a) DFT calculations of the Diels–Alder reactions of the free base porphyrin $TPPF_{20}$ **1** with isobenzofuran (IBF, **4**) yielding the corresponding chlorins **5** in *endo* and *exo* configurations and the subsequent Diels–Alder reactions with a second molecule of IBF (**4**) to form all 12 conceivable isomers of the 2:1 addition products (bacterio- and isobacteriochlorins) in *exo*, *endo*, *anti*, and *syn* configurations. (b) DFT calculations of the Diels–Alder reactions of the Ni-porphyrin Ni-$TPPF_{20}$ **2** analogous to that shown in panel a). All reaction energies and activation barriers are given relative to the corresponding charge-transfer (van der Waals) complex from which the cycloaddition starts. The experimentally observed pathways and products are highlighted. Predicted and observed products are identical with one exception. According to experiment, the cycloaddition of IBF to the free base chlorin **5** gives *anti*, *endo*, and *endo* bacteriochlorin **7**. DFT calculations favor the formation of the *syn*, *endo*, and *endo* isomers based on kinetic as well as thermodynamic data.

Information).[24] The formation of stable charge-transfer complexes is further corroborated by density functional theory calculations (see the vide infra results).

Ni-porphyrin **2** is more reactive than the corresponding free-base porphyrin **1** and forms higher amounts of 2:1 products (see Table 1). NMR spectra and a crystal structure analysis (Figure 1) reveal that only *endo* products are formed. Remaining starting material (porphyrin), 1:1 (chlorins), and 2:1 products can be easily separated by column chromatography (see the Supporting Information). We attribute the strong *endo* stereospecifity to the pre-orientation of IBF **4** in the charge-transfer complex (Scheme 2). Electron-rich H_2TPP **11** forms a much-weaker complex with IBF **4**, and therefore, both *endo* and *exo* products are formed.

With a higher excess (10–15 equiv) of IBF **4** (at 70 °C), predominantly 2:1 products are formed. Free-base porphyrin **1** exclusively forms the corresponding bacteriochlorin **7** with an 82% yield, and Ni-porphyrin **2** gives 99% Ni-isobacteriochlorin **8**. Compared to previously published cycloadditions, both yields are exceptional. Moreover, both cycloadditions are completely regio- and stereoselective. Among the 12 conceivable isomers (iso/bacteriochlorin, *endo*/*exo*, and *syn*/*anti*), only one isomer is formed. Nuclear magnetic resonance and a crystal-structure analysis (Figure 1) prove that only the *anti* and *endo*–*endo* products of the free base bacterio- and Ni-isobacteriochlorin are isolated. To gain access to the complete series of Ni-tetrapyrroles: Ni-porphyrin, Ni-chlorin, Ni-isobacteriochlorin, Ni-bacteriochlorin, and Ni-pyrrocorphin,[25,26] we inserted Ni into bacteriochlorin **7** (Scheme 3; for UV–vis spectra, see Figure 2).

Ni^{2+} insertion into **7** following conventionally procedures such as treatment with $Ni(OAc)_2$ in DMF at 150 °C were unsuccessful because cycloreversion took place at high temperatures. We therefore used a previously published method that allows Ni^{2+} insertion under mild conditions. Treatment of **7** with $Ni(COD)_2$ at 20 °C yielded the Ni-

DOI: 10.1021/acs.orglett.8b03433
Org. Lett. XXXX, XXX, XXX–XXX

bacteriochlorin **9** and Ni-pyrrocorphin **10**.[27] The Ni-pyrrocorphin **10** can be converted to the Ni-bacteriochlorin **9** using trifluoroacetic acid under air (see the Supporting Information).

To explore the scope and limitation of our new method, we subjected tetraphenylporphyrin **11** (TPP), Ni-tetraphenylporphyrin **12** (Ni-TPP), and parent porphin **13** (H_2P) to cycloadditions with IBF **4**. TPP gives chlorin **14** with *endo* and *exo* configurations that can be separated by column chromatography. However, no 2:1 products are formed. Ni-TPP and parent porphin also give chlorins that have not been further characterized because of very poor solubility (Table 1). The Diels–Alder reactions also proceed at room temperature; however, reaction times until complete conversion are several days.

A similar regioselectivity in the cycloadditions of electron-deficient free-base chlorins yielding bacteriochlorins and of the corresponding Ni-chlorins forming isobacteriochlorins has been previously observed upon reaction of $TPPF_{20}$ and Ni-$TPPF_{20}$ with two equivalents of azomethine ylides, quinodimethanes, and hydrogenation.[19,25,28] Bruhn and Brückner explain this regioselectivity based on their average ionization energy (ALIEs) procedure.[28] We here apply our ACID method that is known to reliably predict stereoelectronic effects.[29,30] The ACID scalar field is interpreted as the density of delocalized electrons, which is represented as an isosurface (just as the total electron density). The degree of conjugation between atoms or bonds can be quantified by the critical isosurface value (CIV). CIV is defined as the ACID value at points where the gradient of the ACID scalar field is zero and the Laplacian has two negative and one positive eigenvalues. High CIV values indicate strong conjugation. ACID applied to the chlorins **5′** and **6′** gives an intuitive and conclusive picture. Both chlorins include ^{18}annulene subunits (bold lines in Figure 3, top), which are aromatic with $4n + 2$ delocalized electrons. The ACID plot of free base chlorin **5′** clearly reflects this classical view. The aromatic subsystem is readily identifiable as a contiguous ACID isosurface (yellow surface in Figure 3, bottom, left). Separate and isolated from this ^{18}annulene unit is the β_{12},β_{13} double bond, opposite to the hydrogenated C–C bond (indicated with a red arrow, Figure 3). This double bond is rather olefinic (CIV: 0.055) and, hence, more reactive as a dienophile in Diels–Alder reactions or any other reaction converting this C=C double bond into a single bond. The C=C bonds participating in the aromatic system (CIV: 0.083) are less reactive, which explains the experimental finding that exclusively the bacteriochlorin is formed. The situation is more complicated in Ni-chlorin **6′**. A pair of degenerate, symmetry-equivalent valence bond substructures can be drawn to describe the aromatic ^{18}annulene subunit (one of them is shown in Figure 3 top, right). Here the β_7,β_8 and β_{17},β_{18} double bonds (indicated with red arrows, Figure 3 bottom right) are more isolated (CIV: 0.069) compared to the β_{12},β_{13} double bond (CIV: 0.073), which explains the experimentally observed formation of the isobacteriochlorins.

To further elucidate the reason for the remarkable stereo- and regioselectivity of our cycloadditions, we performed calculations at the B3LYP-D3/6-31G* level of density functional theory (DFT), including dispersion.[31] Reaction enthalpies and activation barriers were determined relative to the charge-transfer (van der Waals) complex from which the cycloaddition starts. These complexes are stable minima on the potential energy hypersurface. The results are summarized in Figure 4. Thermodynamic and kinetic data are within the expected range for Diels–Alder reactions proceeding at room temperature or slightly elevated temperatures. Our calculations correctly predict the stereo- and regiochemistry except for the experimentally observed formation of *anti*, *endo*, *endo* bacteriochlorin **7**. According to the DFT calculations, the formation of the corresponding *syn* product should be preferred (Figure 4 a). This discrepancy can be explained by the fact that our calculations do not include entropy. The formation of the *syn* isomer is entropically disfavored because the attack of IBF at the porphyrin π hemisphere, which is already shielded by the first IBF addition, is disfavored. Cycloaddition therefore takes place from the less-hindered side.

In summary, we present a convenient, high-yielding, regio- and stereoselective synthesis of chlorins, bacteriochlorins, isobacteriochlorins, and pyrrocorphins (hexahydroporphyrins). With Ni^{2+} in the tetrapyrrolic core, the whole series of hydroporphyrins has been prepared and characterized. In particular, bacteriochlorins are highly interesting chromophores because they exhibit strong absorption bands in the near-infrared. At these wavelengths, blood-supported tissue is relatively transparent. Free-base bacteriochlorin **7** is strongly fluorescent and stable toward oxidation, and with a strong absorption band at 733 nm, it is a good candidate for applications in photodynamic therapy. The corresponding Ni-bacteriochlorin **9** is non-fluorescent and a stable NIR dye with a strong absorbance at 757 nm. Both compounds are good starting points for further derivatization because the pentafluorophenyl rings are susceptible to aromatic substitution with nucleophiles, including water-solubilizing groups.[32]

■ ASSOCIATED CONTENT

Supporting Information

The Supporting Information is available free of charge on the ACS Publications website at DOI: 10.1021/acs.orglett.8b03433.

Experimental procedures and spectral data, details of computational studies, and crystallographic data (PDF)

Accession Codes

CCDC entries nos. 1851406 and 1851407 contain the supplementary crystallographic data for this paper. These data can be obtained free of charge via www.ccdc.cam.ac.uk/data_request/cif, by e-mailing data_request@ccdc.cam.ac.uk, or by contacting The Cambridge Crystallographic Data Centre, 12 Union Road, Cambridge CB2 1EZ, U.K.; fax: +44 1223 336033.

■ AUTHOR INFORMATION

Corresponding Author

*E-mail: rherges@oc.uni-kiel.de.

ORCID

Christian Näther: 0000-0001-8741-6508

Rainer Herges: 0000-0002-6396-6991

Notes

The authors declare no competing financial interest.

DOI: 10.1021/acs.orglett.8b03433
Org. Lett. XXXX, XXX, XXX–XXX

■ ACKNOWLEDGMENTS

The authors gratefully acknowledge financial support by the Deutsche Forschungsgesellschaft (DFG) within the Sonderforschungsbereich 677, "Function by Switching".

■ REFERENCES

(1) Reaxys database May 2018.
(2) *Porphyrins: Optical spectra and electronic structure of porphyrins and related rings*; Gouterman, M.; Dolphin, D., Eds.; Academic Press: Boston, 1978; Vol 3 (Part A), pp 1−165.
(3) Bonnett, R. *Chem. Soc. Rev.* **1995**, *24*, 19−33.
(4) Sternberg, E. D.; Dolphin, D.; Bruckner, C. *Tetrahedron* **1998**, *54*, 4151−4202.
(5) Mazor, O.; Brandis, I.; Plaks, V.; Neumark, E.; Rosenbach-Belkin, V.; Salomon, Y.; Scherz, A. *Photochem. Photobiol.* **2005**, *81*, 342−351.
(6) Gust, D.; Moore, T. A.; Moore, A. L. *Acc. Chem. Res.* **2009**, *42*, 1890−1898.
(7) Esswein, A. J.; Nocera, D. G. *Chem. Rev.* **2007**, *107*, 4022−4047.
(8) Li, L.-L.; Diau, E. W.-G. *Chem. Soc. Rev.* **2013**, *42*, 291−304.
(9) Konig, K. *J. Microsc.* **2000**, *200*, 83−104.
(10) Holten, D.; Bocian, D. F.; Lindsey, J. S. *Acc. Chem. Res.* **2002**, *35*, 57−69.
(11) Scheer, H. An Overview of Chlorophylls and Bacteriochlorophylls: Biochemistry, Biophysics, Functions and Applications. *Advances in Photosynthesis and Respiration* **2006**, *25*, 1−26.
(12) Pandey, R. K.; Zheng, G. *Porphyrin Handbook (Porphyrins as photosensitizers in photodynamic therapy)*, Kadish, K. M.; Smith, K. M.; Guilard, R., Eds; Academic Press: Boston; Vol 6, Chapter 43, pp 157−230.
(13) Taniguchi, M.; Lindsey, J. S. *Chem. Rev.* **2017**, *117*, 344−535.
(14) Silva, A. M. G.; Tomé, A. C.; Neves, M. G. P. M. S.; Silva, A. M. S.; Cavaleiro, J. A. S. *J. Org. Chem.* **2005**, *70*, 2306−2314.
(15) Silva, A. M. G.; Tomé, A. C.; Neves, M. G. P. M. S.; Silva, A. M. S.; Cavaleiro, J. A. S. *Chem. Commun.* **1999**, 1767−1768.
(16) Silva, A. M. G.; Tomé, A. C.; Neves, M. G. P. M. S.; Silva, A. M. S.; Cavaleiro, J. A. S. *J. Org. Chem.* **2002**, *67*, 726.
(17) Liu, X.; Li, C.; Peng, X.; Zhou, Y.; Zeng, Z.; Li, Y.; Zhang, T.; Zhang, B.; Dong, Y.; Sun, D.; Cheng, P.; Feng, Y. *Dyes Pigm.* **2013**, *98*, 181−189.
(18) Ebrahim, M. M.; Moreau, M.; Senge, M. O. *Heterocycles* **2011**, *83*, 627−630.
(19) Tomé, A. C.; Lacerda, P. S. S.; Neves, M. G. P. M. S.; Cavaleiro, J. A. S. *Chem. Commun.* **1997**, 1199−1200.
(20) Vicente, M. G. H.; Cancilla, M. T.; Lebrilla, C. B.; Smith, K. M. *Chem. Commun.* **1998**, 2355−2356.
(21) Peters, M. K.; Herges, R. *Beilstein J. Org. Chem.* **2017**, *13*, 2659−2662.
(22) Gouterman, M.; Stevenson, P. E. *J. Chem. Phys.* **1962**, *37*, 2266−2269.
(23) Aoki, T.; Sakai, H.; Ohkubo, K.; Sakanoue, T.; Takenobu, T.; Fukuzumi, S.; Hasobe, T. *Chem. Sci.* **2015**, *6*, 1498−1509.
(24) Rahman; Harmon, H. J. *Spectrochim. Acta, Part A* **2006**, *65*, 901−906.
(25) Ide, Y.; Kuwahara, T.; Takeshita, S.; Fujishiro, R.; Suzuki, M.; Mori, S.; Shinokubo, H.; Nakamura, M.; Yoshino, K.; Ikeue, T. *J. Inorg. Biochem.* **2018**, *178*, 115−124.
(26) Schwesinger, R.; Waditschatka, R.; Rigby, J.; Nordmann, R.; Schweizer, W. B.; Zass, E.; Eschenmoser, A. *Helv. Chim. Acta* **1982**, *65*, 600−610.
(27) Peters, M. K.; Herges, R. *Inorg. Chem.* **2018**, *57*, 3177−3182.
(28) Bruhn, T.; Brückner, C. *J. Org. Chem.* **2015**, *80*, 4861−4868.
(29) Geuenich, D.; Hess, K.; Köhler, F.; Herges, R. *Chem. Rev.* **2005**, *105*, 3758−3772.
(30) Herges, R.; Geuenich, D. *J. Phys. Chem. A* **2001**, *105*, 3214−3220.
(31) Grimme, S.; Antony, J.; Ehrlich, S.; Krieg, H. *J. Chem. Phys.* **2010**, *132*, 154104.
(32) Dommaschk, M.; Gutzeit, F.; Boretius, S.; Haag, R.; Herges, R. *Chem. Commun.* **2014**, *50*, 12476−12478.

DOI: 10.1021/acs.orglett.8b03433
Org. Lett. XXXX, XXX, XXX−XXX

3.7 Herstellung von Singulett-Sauerstoff durch ein wasserlösliches Bakteriochlorin

Die PDT ist eine anerkannte Methode zur gezielten Zerstörung von Tumoren, wobei eine Schädigung des umliegenden Gewebes verhindert wird.[122] Anwendung findet diese Therapie bereits bei Hautkrebs, Brustkrebs, früh erkanntem Lungenkrebs sowie Kopf-Hals-Tumoren.[57,123]

In der PDT werden Photosensibilisatoren unter Verwendung von Licht eingesetzt, um aggressiven Singulett-Sauerstoff zu generieren. Bis jetzt ist jedoch nur eine kleine Anzahl von PS auf dem Markt zugelassen. Dies liegt an den strengen Auflagen und an der begrenzen Auswahl an geeigneten NIR-Farbstoffen.[124]

Ein idealer PS sollte eine Absorption im langwelligen Bereich (700-900 nm) aufweisen, da hier die größte Eindringtiefe in Gewebe ermöglicht wird.[125] Außerdem sind auch die Singulett-Sauerstoff-Quantenausbeute und die Stabilität entscheidende Faktoren, die die Wirksamkeit eines PSs beeinflussen.[126]

Das Photofrin dient als eines der meistverwendeten PSs speziell in klinischen Studien sowie PDT-Protokollen. Hierbei handelt es sich um eines der vielen Derivate des Hämatoporphyrins. Diese Derivate haben jedoch einige Nachteile wie z.B. Photobleaching, Instabilität oder toxische Schwermetalle, die die allgemeine klinische Verwendung einschränken. Aus diesem Grund ist die Untersuchung und Weiterentwicklung der publizierten Chlorine und Bakteriochlorine für die Medizin von großer Bedeutung.

Singlet oxygen generation by water soluble bacteriochlorin

Morten K. Peters, Jens Gröbner and Rainer Herges

Manuskript für
Chemical Communications

Eigenanteil: Die Synthesen und Messungen wurden von Morten Peters durchgeführt. Das Manuskript wurde von Morten Peters und Prof. Dr. Rainer Herges verfasst.

Zusammenfassung

In dieser Veröffentlichung wird die Untersuchung des Bakteriochlorins **11a** auf die Anwendbarkeit als PS sowie die Weiterentwicklung von **11a** (hinsichtlich der guten Eigenschaften) dargestellt. Durch die Umsetzung mit Triglycerol-Dendrimer (G[2.0]-OH) und die anschließende Entschützung der acetalgeschützten Hydroxygruppen konnte das Molekül **26** synthetisiert werden, welches ein wasserlösliches Bakteriochlorin darstellt (Abbildung 23).

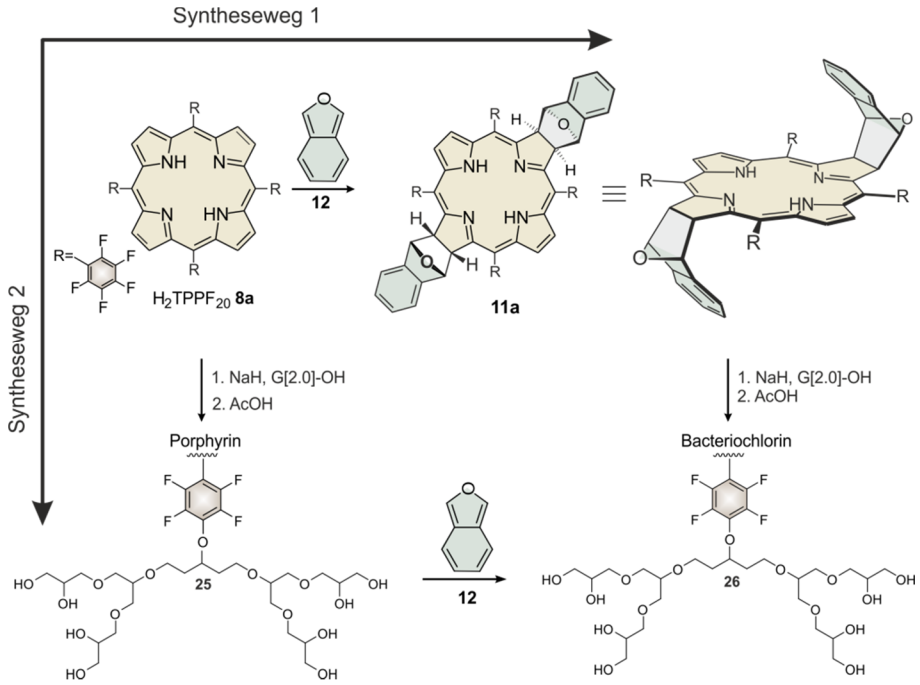

Abbildung 23: Synthese des wasserlöslichen Bakteriochlorins **26** durch eine [4+2] Cycloaddition.

Die beiden Bakteriochlorine **11a** und **26** zeigen eine Absorption im NIR-Bereich des elektromagnetischen Spektrums bei 733 nm. Dies stellt eine der wichtigsten Voraussetzungen für einen PS in der PDT dar. Aber auch das Emittieren von Licht bei 738 nm ist für die Diagnostik vorteilhaft.

Das Bakteriochlorin **26**, welches durch die Wasserlöslichkeit für *in vivo*-Anwendung interessanter ist als **11a**, zeigt bei der Untersuchung der Singulett-Sauerstoff- und Hydroxylradikal-Erzeugung, dass es 16-mal effektiver ist als das klinisch zugelassene Protoporphyrin IX. Dies macht diese Chromophore für die Bildgebung sowie die PDT hochinteressant.

Journal Name

COMMUNICATION

Singlet oxygen generation by water soluble bacteriochlorin

Morten K. Peters[a], Jens Gröbner[a] and Rainer Herges[a*]

Received 00th January 20xx,
Accepted 00th January 20xx

DOI: 10.1039/x0xx00000x

www.rsc.org/

Bacteriochlorin derivatives are promising photosensitive agents for photodynamic therapy (PDT). In this study, the photodynamic activity of a novel near-infrared water soluble bacteriochlorin derivative was investigated. The bacteriochlorin shows high singlet oxygen generation, which was detected by using 1,3-diphenylisobenzofuran (DPBF).

Porphyrins and their reduced derivatives have a wide range of applications.[1,2,3,4,5] For this reason, these syntheses of new molecules are of great importance. Chlorins and bacteriochlorins can be used as a photosensitizer (PS) for singlet oxygen generation in solution, which can be relevant for the photodynamic therapy (PDT).[6,7] The PDT has gained acceptance as a front line cancer therapy [8,9,10,11] being approved mainly concerning tumors, such as skin cancers, breast cancer, early lung cancers and tumors of the head and neck by regulatory agencies in the U.S.A and many European countries.[8, 12,13,14,15,16]
Photofrin® has been used as a PS for most approved clinical trials and PDT protocols.[17] This PS is a derivative of Hematoporphyrin. However, the Photofrin® has several disadvantages which limit its general clinical use. A few of them show a minimum absorption in the visible region of the bio-optical window, where the penetration depth into tissue is maximum. Available PS tend to lose absorbance during irradiation due to rapid photobleaching and long-term skin photosensitivity. [18]
In this study, we report on the synthesis and photophysical properties of a new near-infrared water-soluble bacteriochlorin. This PS was designed from the *meso*-Tetra(pentafluorophenyl)porphyrin (H_2-TPPF$_{20}$) **1**, and was produced via two different synthesis routes (see Scheme 1). (1) We recently published a convenient synthesis of pure Isobenzofuran (IBF) **2**,[19] which can be used as diene in the Diels-Alder reaction with H_2-TPPF$_{20}$ **1**.[20] The reaction with the porphyrins **1** and freshly prepared IBF **2** yielding the bacteriochlorin **3**, which was functionalized with the second generation glycerol (G[2.0]-OH).[21,22] Afterwards the 32 alcohol functions of the bacteriochlorin were deprotected with acetic acid. (2) H_2-TPPF$_{20}$ was functionalized with the second generation glycerol (G[2.0]-OH). Following the Diels-Alder with the IBF **2** results the bacteriochlorin, which was deprotected with acetic acid. The synthesis route 1, compared to 2, gives the better yield and was able to purify.

Scheme 1: Synthesis of bacteriochlorin derivatives via [4+2] cycloadditions.

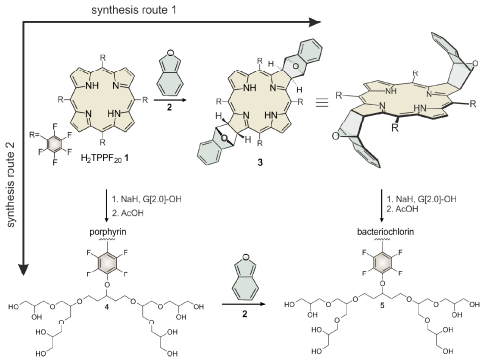

The PSs bacteriochlorin **3** and novel near-infrared water soluble bacteriochlorin **5** showed excellent optical properties in solution. The PSs display an intense green color as well as sharp absorption in the near-infrared region at 733 nm and with moderate quantum yields of fluorescence at 738 nm (see Figure 1).

[a] Otto-Diels-Institut für Organische Chemie, Christian-Albrechts-Universität, Otto-Hahn-Platz 4, 24098 Kiel, Germany. Mail: rherges@oc.uni-kiel.de

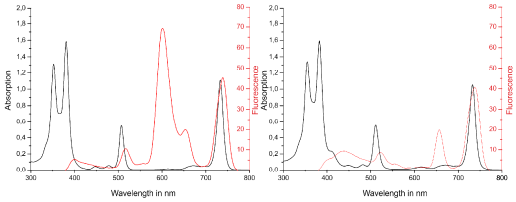

Figure 1. The absorption (black) and fluorescence emission (red) spectra of compounds **3** (right: methanol, 25 °C, concentration: 10 µM) and **5** (right: methanol, 25 °C, concentration: 10 µM).

A study of singlet oxygen generation in solutions was performed to assess the ability of **3** and **5** to generate singlet oxygen. Several samples were irradiated by light with different wavelengths at an intensity of 0.5 mW/cm^2. Singlet oxygen generation was proved experimentally in tetrahydrofuran (THF) by 1,3-diphenylisobenzofuran (DPBF) (Figure 2) and in water by betanin (Figure 3), which are known as indicators for singlet oxygen indicators.[23,24,25] (1) The experiment in THF: The decrease of the absorbance band at 410 nm was monitored. It was caused by the oxidation of DPBF with reactive oxygen species such as singlet oxygen.

The experiments were performed with starting concentrations of 5 x 10^{-6} M of PS and 90 x 10^{-6} M of DPBF (see Figure 2). As a reference PS, Protoporphyrin IX **6** was used, which is commercially available. The Protoporphyrin **6** (clinically approved PDT agent) shows high generation of singlet oxygen and its quantum yield $\Phi(^1O_2)$ = 0.56 was published in previous experiments.[26]

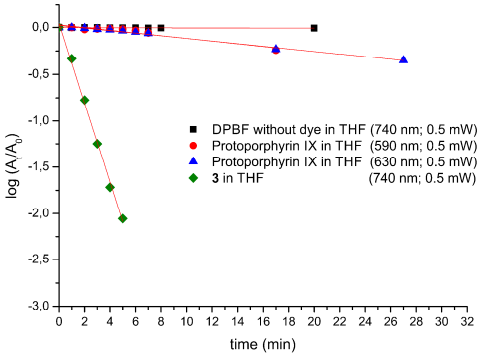

Figure 2. Time-dependent decrease of absorbance at 410 nm by oxidation of DPBF (90 X 10^{-6} M) with a dye (5 X 10^{-6} M) under light (at 0.5 mW/cm^2).

(2) The experiment in water: The decrease of the absorbance band of betanin at 540 nm was monitored. The experiments were performed with starting concentrations of 5 x 10^{-6} M of PS and 5 x 10^{-6} M of betanin (see Figure 3). As a reference PS, Methylene blue was used, which is commercially available.

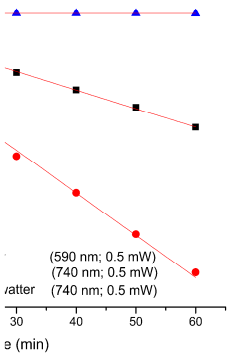

Figure 3. Time-dependent decrease of absorbance at 540 nm by oxidation of betanin (5 X 10^{-6} M) with a dye (5 X 10^{-6} M) under light (at 0.5 mW/cm^2).

The PS **3** shows high generation of singlet oxygen in the experiment (see Figure 2), being 30 times higher in tetrahydrofuran compared to the Protoporphyrin IX and the new NIR water soluble bacteriochlorin **5** is 2 times better in water than Methylene blue (see Figure3). This is highly important for second generation PSs. However, for a number of second generation PSs, in particular bacteriochlorin PSs, photobleaching is one of the major problems in PDT.[27] For this reason, the photostability of the new bacteriochlorins **3** and **6** was investigated under harsh conditions with an irradiation of light at 740 nm with an intensity of 1000 mW/cm^2 for about 60 min. The photobleaching of compounds **3** and **5**, was obtained experimentally by observing the absorption maxima at 733 nm. The PS **3** and **5** are very stabile and no decomposition or change in the UV spectrum was detected (see supporting information).

Conclusions

In conclusion, new PSs analogues were developed that absorb (733 nm) and emit (738 nm) in the NIR region of the electromagnetic spectrum. Compound **3** showed over 30 times more singlet oxygen generations in THF compared to clinically approved Protoporphyrin IX **6** and the water soluble bacteriochlorin **5** is 2 times better in water than Methylene blue. Additionally, they are highly resistant to photobleaching. Due to that they are a promising NIR photosensitizers in PDT. These chromophores could be useful for combined purposes such as imaging and PDT.

Notes and references

There are no conflicts to declare.

1 …

1 E. S. Nyman and P. H. Hynninen, *J. Photochem. Photobiol.*, 2004, **73**, 1.
2 T. Goslinski and J. Piskorz, *J. Photochem. Photobiol.*, 2011, **12**, 304.
3 A. B. Ormond and H. S. Freeman, *Materials*, 2013, **6**, 817.
4 L. B. Josefsen and R. W. Boyle, *Theranostics*, 2012, **2**, 916.
5 M. K. Peters and R. Herges, *Inorg. Chem.*, 2018, **57**, 3177.
6 M. Ethirajan, Y. Chen, P. Joshi and R. K. Pandey, Chem. *Soc. Rev.*, 2011, **40**, 340.
7 R. Bonnett, *Chem. Soc. Rev.*, 1995, **24**, 19.
8 T. J. Dougherty, C. J. Gomer, B. W. Henderson, G. Jori, D. Kessel, M. Korbelik, J. Moan and Q. Peng, *Photodynamic Therapy. J. Natl. Cancer Inst.,* 1998 , **90** , 889.
9 B. W. Henderson and T. J. Dougherty, *Photochem. Photobiol.*, 1992 , **55** , 145.
10 W. M. Sharman, C. M. Allen and J. E. van Lier, *Drug Discovery Today*, 1999, **4**, 507.
11 M. R. Detty, *Expert Opinion on Therapeutic Patents*, 2001, **11**, 1849.
12 H. Kato, *J. Photochem. Photobiol.*, 1998, **42**,96.
13 F. Guillemin, X. Feintrenie and D. Lignon, Rev. Pneumologie Clin., 1992, **48**, 111.
14 P. Puolakkainen and T. Schroder, *Dig. Dis.*, 1992, **10**, 53.
15 D. P: Noske, J. G. Wolbers and H. J. C. M. Sterenborg, *Clin. Neurol. Neurosurg.*, 1991, **93**, 293.
16 K. T. Moesta, P. Schlag, H. O. Douglass, T. S. Jr. Mang, *Lasers Surg. Med.*, 1995, **16**, 84.
17 Y. You, S. L. Gibson, R. Hilf, S. R. Davies, A. R. Oseroff, I. Roy, T. Y. Ohulchanskyy, E.J. Bergey, and M. R. Detty, *J. Med. Chem.* 2003, **46**, 3734.
18 D. A. Bellnier and T. J. Dougherty, *J. Clin. Laser Med. Surg.*, 1996, **14**, 311.
19 M. K. Peters and R. Herges, *Beilstein J. Org. Chem.,* 2017, **13**, 2659.
20 submitted *JACS* **2018**.
21 M. Dommaschk, F. Gutzeit, S. Boretius, R. Haag and R. Herges, *Chem. Commun.* 2014, **50**, 12476.
[22] M. Wyszogrodzka and R. Haag, *Chem. Eur. J.*, 2008, **14** , 9202.
23 E. A. Lissi, M. V. Encinas, E. Lemp and M. A. Rubio, *Chem. Rev.* 1993, **93**, 699.
24 S. G. Awuah, J. Polreis, V. Biradar and Y. You, *Org. Lett.*, 2011, **15**, 3884.
[25] J. A. Bonacin, F. M. Engelmann, D. Severino, H. E. Toma and M. S. Baptista, *J. Braz. Chem. Soc.,* 2009, **20**, 31.
[26] J. M. Fernandez, M. D. Bilgin, and L. I. Grossweiner, *J. Photochem. Photobiol.*, 1997, **37**, 131.
[27] R. Bonnett, D. D. Birgul, P. A Hamilton, G. Martinez, F. Wierrani, *J. Photochem. Photobiol.*, 1999, **53**, 136.

Bacteriochlorin for medical use and for generating singlet oxygen and other reactive oxygen species and production process

Europäische Patentanmeldung 18206883.3
Christian-Albrechts-Universität zu Kiel
Application number: EP18206883.3

TARUTTIS
PATENTANWALTSKANZLEI

TARUTTIS – Aegidientorplatz 2b – D-30159 Hannover

Europäisches Patentamt

80298 MÜNCHEN

Dr. rer. nat. Stefan Taruttis
Diplom-Ingenieur
Patentanwalt
European Patent Attorney
European Trademark Attorney

D-30159 Hannover, Aegidientorplatz 2b
TORHAUS AM AEGI
Tel.: ++49 511 123 32 670
Fax: ++49 511 123 32 678
www.taruttis.com info@taruttis.com

in Kooperation mit
Dr. rer. medic Dirk Vollmer
Patentanwalt, European Patent Attorney
D-74523 Schwäbisch Hall, Hilde-Domin-Str. 8

Your Ref.: Our Ref.: K1033EP 17. November 2018

New European patent application Bacteriochlorin for medical use and for generating singlet oxygen and other reactive oxygen species and production process -Christian-Albrechts-Universität zu Kiel

Bacteriochlorin for medical use and for generating singlet oxygen and other reactive oxygen species and production process

The present invention relates to a novel compound comprising the general structure of a bacteriochlorin. The compound can be for use as a medicament, e.g. for use in medical treatment, especially in a medical treatment using activation of the compound by irradiation with light, which is also referred to as photodynamic therapy. The medical treatment can be the treatment of solid tumours, of a skin disease, an infection, e.g. a bacterial, fungal or viral infection, of macular degeneration, wherein the infectious agent may be resistant to at least one antibiotic. The compound generates singlet oxygen and optionally other reactive oxygen species (ROS) from oxygen, which singlet oxygen and ROS are highly reactive and inactivate e.g. bacteria, viruses and mammalian cells, e.g. tissue.

The compound has the advantage that it is stable against oxidation, e.g. it is not quickly inactivated by the singlet oxygen that it generates under irradiation. Further, the compound is useful in a technical process for generating singlet oxygen and ROS, because irradiation with

a wavelength in the near infrared range, especially a wavelength of 740 nm, activates the compound to generate singlet oxygen from gaseous or dissolved oxygen. The compound can be derivatized by various substituents to adjust its hydrophilicity, respectively lipophilicity. Specifically, the compound can be derivatized by substituents, which render the compound non-immunogenic.

Further, the invention relates to an embodiment in which the compound contains a complexed metal ion, which is selected from alkaline earth metals and transition metals e.g. ions of Mg, Pt, Pd, Ni. In the embodiment in which the complexed metal ion is Ni^{2+}, the compound does not produce singlet oxygen under irradiation. In this embodiment, the compound forms an oxidation-stable dye.

Further, the invention relates to a technical process for producing singlet oxygen, wherein the compound is preferably immobilized on a carrier, e.g. by a covalent linkage to the carrier, contacting the compound with oxygen and irradiating the compound. The oxygen can be contained in a gas, e.g. air, or in a liquid, e.g. water.

The invention also provides a process for producing the compound. The production process has the advantage of optionally being purely synthetic, i.e. without the use of reactants of natural origin. The production process also has the advantage of requiring only moderate temperatures, e.g. below 70°C, e.g. at room temperature, and that the process does not use a metal-containing catalyst.

State of the art

Padeliporphin, which is known for use in photodynamic therapy of cancer, produces singlet oxygen from oxygen present in tissue. Padeliporphin has the disadvantage to contain the heavy metal palladium and that, under irradiation, it is degraded by the singlet oxygen it produces.

Peters and Herges, Beilstein J. Org. Chem. 2017, 13, 2659-2662 describe a synthetic method for producing isobenzofuran.

Object of the invention

The object of the invention is to provide alternative compounds, which are stable against

oxidation, especially for use as a medicament in the medical treatment e.g. of cancer or in a technical process for producing singlet oxygen and optionally ROS, and which can be produced e.g. without use of OsO_4 and at temperatures of below 100°C, e.g. at below 70°C. Preferably, the compounds generate singlet oxygen from surrounding oxygen under irradiation. More preferably, the compounds shall have an absorption in the wavelength range of 680-900 nm, which is generally known as the range for which human tissue is transmissible.

Description of the invention

The invention achieves the object by the features of the claims, especially by providing a compound comprising

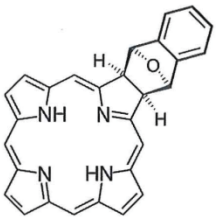

Structure 1,

and/or preferably

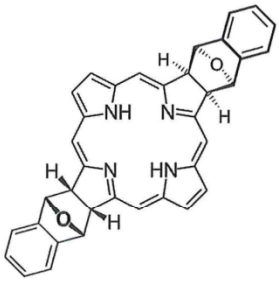

Structure 2.

In a preferred embodiment, the compound comprises

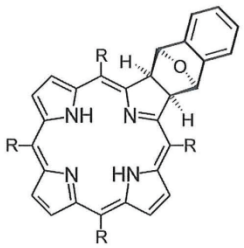

Structure 3

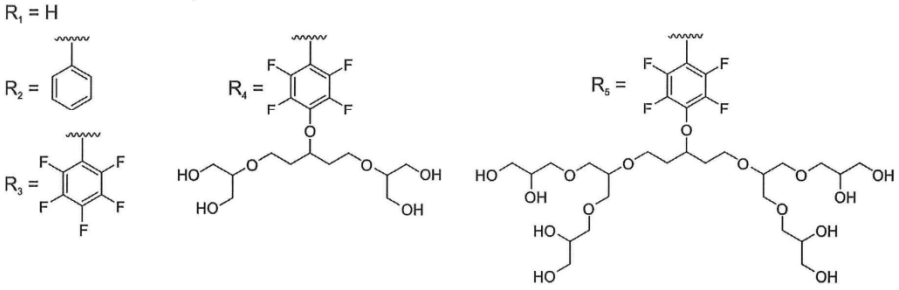

and/or, more preferred,

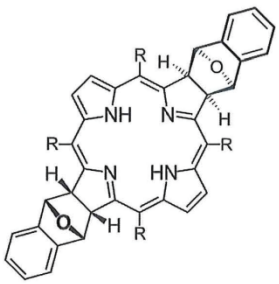

Structure 4

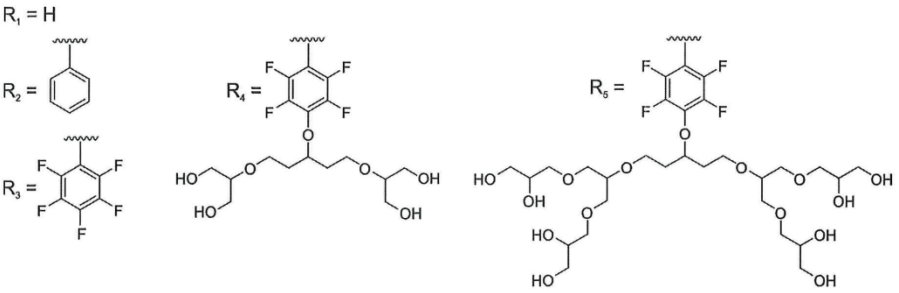

The substituents R1 to R5 shown here in the *meso* positions are examples for substituent R, which can be the same or a different substituent in each position. Generally, especially in

Structure 1 and Structure 2, atoms having valences at which no substituent is explicitly shown, e.g. in the β positions, may be substituted with H or any other substituent.

The porphyrin moiety can optionally carry substituents, e.g. in at least one or all of the *meso* positions of the porphyrin moiety and/or in at least one or in all of the 8 β positions of the porphyrin ring. In Structure 3 and Structure 4 the substituents R can be different in each position or the same substituent. The substituents R can be selected from linear, branched or circular alkyl or aryl groups, e.g. C1 to C12, optionally containing at least one hetero atom, and aliphatic or aromatic groups, e.g. containing at least one five-membered or six-membered ring, optionally containing at least one hetero atom, and R can be as shown for Structure 4. Structure 3 and Structure 4 show R1 being H, R2 being phenyl, R3 being pentafluorophenyl, and R4 and R5 being para-substituted tetrafluorophenyl with the para-substituent being dendrimers of different lengths as preferred substituents R. Preferably, in Structure 3 and Structure 4, atoms having valences at which no substituent is explicitly shown, may be substituted with any substituent, preferably with H.

Generally, the carbon atoms in the 4, 5, 6 and 7 positions of the phenyl ring of the isobenzofuran moiety can be substituted with hydrogen or with any other substituent, e.g. a substituent selected from linear, branched or circular alkyl or aryl groups, e.g. C1 to C12, optionally containing at least one hetero atom, and aliphatic or aromatic groups, e.g. containing at least one five-membered or six-membered ring, which can be annelated to the phenyl ring of the isobenzofuran moiety, each substituent optionally containing at least one hetero atom, and R can be as shown for Structure 4. Substituents of the 4, 5, 6 and 7 carbon atoms in positions of the isobenzofuran moiety can be the same as the substituents of *meso* and/or of β positions of the porphyrin moiety, or substituents of the 4, 5, 6 and 7 carbon atoms in positions of the isobenzofuran moiety can differ from the substituents of *meso* and/or of β positions of the porphyrin moiety. Further, a substituent may be annelated to a carbon atom in β position and one carbon atom in *meso* position of the porphyrin moiety (schematically shown in Fig. 9a), and/or a substituent may be annelated to two neighbouring carbon atoms in β positions of the porphyrin moiety (schematically shown in Fig. 9b).

The compounds of the invention have the advantage of not agglomerating; especially not forming agglomerates by their porphyrin moieties. Currently, it is assumed that the isobenzofuran cycloaddition product prevents stacking of the porphyrin moieties.

In a preferred embodiment, the compound is for use as a medicament, e.g. for use in a medical treatment, e.g. for use in photodynamic therapy, especially for use in the treatment of pre-cancerous tissue, of solid cancer, e.g. skin cancer, prostate cancer, of a skin disease, e.g. psoriasis, acne, skin infections, macular degeneration, in antimicrobial photodynamic chemotherapy, especially for the treatment of oral infections and/or of biofilms, e.g. attached to tissue or mucosa, including infections by antibiotic-resistant microorganisms. The medicament comprising the compound can e.g. contain the compound in an aqueous or lipophilic composition, e.g. in a formulation for injection, especially for intra-tumoral injection, for systemic injection, or in a formulation for topic application. Substituents having dendrimer portions, e.g. as shown for R4 and R5, have the advantage of having low immunogenicity or being non-immunogenic.

Optionally, the compounds of the invention can be contained in molecules which contain at least two or at least three of Structure 1 and/or Structure 2, e.g. linked together by their substituents. Such molecules may have a molecular weight in the range of 20 to 200 kDa, e.g. to provide for the EPR effect resulting in an accumulation of the molecules in tumour tissue after systemic administration. As an example, a compound having a molecular weight in this range can be obtained by reacting Structure 4 which is substituted with R5 in all *meso* positions, with additional Structure 4 IV which is substituted with R3, and subsequent dendronisation. An exemplary compound is shown in Fig. 10.

The compounds have the advantage of having an absorption maximum of 740 nm, which is in the range of wavelengths for which human and animal tissue is transmissible, e.g. to a depth of 1 to 4 cm. Accordingly, the compounds are suitable for use in photodynamic therapy, wherein the compounds are located within the tissue and the compounds are accessible by irradiation. Irradiation is by light comprising an activating wavelength, e.g. 700 to 800 nm, preferably comprising 740 nm, or consisting thereof. Irradiation of the compounds in the presence of oxygen, e.g. oxygen dissolved in living blood, mucus or tissue, or gaseous oxygen results in the production of singlet oxygen, optionally also other ROS, which are known to inactivate mammalian cells, bacteria and viruses. In the following, references to singlet oxygen comprise other ROS.

The compounds have the advantage of allowing various substituents, especially bound to the porphyrin moiety, so that the hydrophilicity, respectively lipophilicity, can be adjusted by the substituents.

Optionally, the substituents, especially substituents to the porphyrin moiety, can comprise a peptide that has affinity for cancer cells or for bacteria or viruses. In this embodiment, the peptide having affinity for cancer cells or for bacteria or for viruses promotes the arrangement of the compound in the vicinity of cancer cells, bacteria or viruses, respectively, and singlet oxygen is generated upon irradiation in this vicinity.

In a further embodiment, the compounds can be used in technical processes for producing singlet oxygen, e.g. for disinfection of air or water. The compounds can be immobilized on a carrier, e.g. adsorbed to a carrier, preferably covalently bound by a substituent to a carrier. In a process for producing singlet oxygen, the immobilized compound is contacted with oxygen and irradiated. Irradiation can generally be by light comprising an activating wavelength, e.g. sunlight, preferably light comprising 700 to 800 nm, preferably comprising 740 nm, or consisting thereof. For immobilizing the compound, the carrier can e.g. be selected from functionalized resins, e.g. weak ion exchange resins, e.g. resins having free amine groups. Preferably, the carrier is at least partially transmissible for light of the activating wavelength. Optionally, the compounds can be immobilized on a surface in order to provide production of singlet oxygen upon irradiation, e.g. for providing surfaces which upon irradiation are self-sterilizing.

In a further embodiment, the invention provides for novel compounds, e.g. for use as IR dye. In this embodiment, the compounds contain a metal ion, preferably Ni, complexed in the porphyrin moiety of Structure 1 and/or of Structure 2, e.g. complexed in the porphyrin moiety of Structure 3 and/or of Structure 4. Schematically, these compounds are

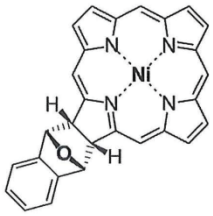

Structure 5,

and/or preferably

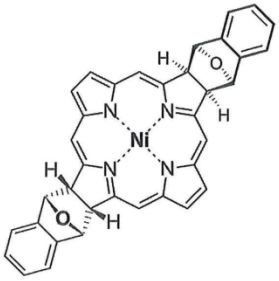

Structure 6

In a preferred embodiment, the compound comprises

Structure 7

and/or preferably

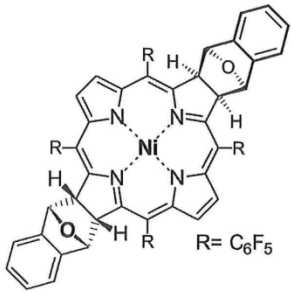

Structure 8

In this embodiment, the substituents R can alternatively be those described for Structure 3 and Structure 4.

Also the embodiment of the compounds containing a metal ion complexed within the porphyrin moiety has the advantages of being stable against oxidation and of being producible by a process for production which can be performed at temperatures below 100°C, e.g. at room temperature to 70°C, of using only fully synthetic starting compounds, i.e. no starting compounds isolated from a natural source, and of being free from metal-containing catalysts,

e.g. free from OsO_4. Embodiments containing Ni as the metal ion complexed within the porphyrin moiety do not generate singlet oxygen. In embodiments containing complexed Ni^{2+}, the compounds are not fluorescent. Embodiments containing a Pt ion or Pd ion as the complexed metal ion under irradiation show intense production of singlet oxygen.

In a further embodiment, the invention provides a process for producing compounds comprising Structure 1 and/or Structure 2, preferably Structure 3 and/or Structure 4. The process for producing the compounds comprises the step of performing a Diels-Alder-cycloaddition on a porphyrin moiety with IBF. In the process, the porphyrin moiety can optionally carry substituents, e.g. on carbon atoms which are in the β positions of the porphyrin. The process for producing the compounds has the advantage of process temperatures below 100°C, e.g. at a temperature between room temperature and 70°C, and that the process is free from metal-containing catalysts, e.g. free from OsO_4. Further, the starting compounds, i.e. the porphyrin-containing starting compound and isobenzofuran, are available as fully synthetic compounds also in a commercial scale, so that the process can be performed without isolation of natural compounds, e.g. without use of compounds isolated from natural sources. Isobenzofuran is e.g. available by the process according to Peters and Herges, Beilstein J. Org. Chem. 2017, 13, 2659-2662. Accordingly, the process preferably is performed completely synthetically, i.e. without use of a starting compound isolated from a natural source. The production processes have the advantage of having high yields.

The invention is also described with reference to the figures, which show in

- Fig. 1 a schematic representation of a synthetic process of the invention,
- Fig. 2 a schematic representation of a further synthetic process of the invention,
- Fig. 3 a schematic representation of a synthetic process of the invention,
- Fig. 4 a schematic representation of a further synthetic process of the invention,
- Fig. 5 a schematic representation of a synthetic process of the invention,
- Fig. 6 a schematic representation of a synthetic process of the invention for a metal-complex of the invention,
- Fig. 7 results for stability measurements of compounds of the invention and of comparative compounds, and the rate of singlet oxygen production measured as the decrease of the trapping reagent diphenylbenzisofuran as a function of irradiation time,
- Fig. 8 shows results of absorption and fluorescence measurements for compounds of the invention,

- Fig. 9 exemplary compounds of the invention having annelated substituents, and
- Fig. 10 an exemplary compound having a molecular weight in the range of 20 to 200 kDa.

Schematically, the synthesis of a compound of Structure 1 by the Diels-Alder cycloaddition reaction is according to Fig. 1. As the porphyrin moiety, porphyrin I is reacted with isobenzofuran II to yield the chlorin III according to structure 1.

As shown in Fig. 2, the further reaction of the chlorin III with isobenzofuran II yields bacteriochlorin IV according to Structure 2.

In Figures 3 and 4, exemplary substituents to the porphyrin moiety are shown. Other substituents, e.g. linear, branched or circular alkyl or aryl groups, e.g. C1 to C12, optionally containing at least one hetero atom, and aliphatic or aromatic groups, e.g. containing at least one five-membered or six-membered ring, optionally containing at least one hetero atom, e.g. halogens (e.g. F, Cl, Br) or functional groups such as ether, carbonyl and/or acid groups, can form substituents. Further optionally, at least one or all of the *meso* positions of the porphyrin can form a five- or six-membered ring to form a bridge with one of the neighbouring β positions. The β positions can also be substituted, either by alkyl, aryl, or heteroatom substituents, or two neighbouring β positions can be connected by a ring.

Fig. 3 shows that the process for producing a compound comprising Structure 1, e.g. to produce a chlorin IIIa, e.g. a compound of Structure 3, can also be done using a porphyrin Ia which is substituted, e.g. at those carbon atoms which are not part of the 5-membered rings of the porphyrin portion I, Ia, in a Diels-Alder cycloaddition with isobenzofuran II.

Fig. 4 shows that the process for producing a compound comprising Structure 2 can be done using a chlorin IIIa as a porphyrin moiety which is substituted, e.g. at those carbon atoms which are not part of the 5-membered rings of the prophyrin moiety, in a Diels-Alder-cycloaddition with isobenzofuran II to produce a substituted bacteriochlorin IVa, e.g. of Structure 4.

In the examples, isobenzofuran was synthesized according to Peters and Herges, Beilstein J. Org. Chem. 2017, 13, 2659.

Example 1: Production of Structure 3

For synthesis of 5,10,15,20-tetrakis-(2,3,4,5,6-pentafluorophenyl)-chlorin according to Structure 3 having pentafluorophenyl as substituents R, 5,10,15,20-Tetrakis(pentafluorphenyl)porphyrin (50.0 mg, 51.3 µmol, (obtained from Sigma-Aldrich Company) was dissolved in 15 ml of benzene under a nitrogen atmosphere. Then a freshly prepared isobenzofuran solution in benzene (257 µmol, 5 eq.) was added dropwise. After stirring for 36 h at 70°C, the solvent was removed under reduced pressure and the crude product was purified by column chromatography on silica gel (dichloromethane/pentane 7:3, Rf = 0.68). Green crystals were obtained. Yield: 49.3 mg (45.1 µmol, 88%).

The structure of the product was determined as

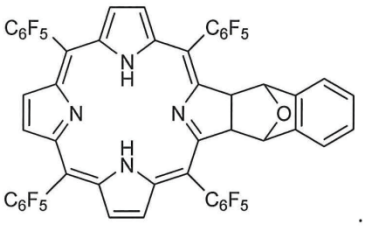

Example 2: Production of Structure 4

For synthesis of 5,10,15,20-Tetrakis-(2,3,4,5,6-pentafluorophenyl)-bacteriochlorin according to Structure 4 (substituted with R2 = pentafluorophenyl), two processes could be employed:

Process 1: 5,10,15,20-Tetrakis(pentafluorophenyl)porphyrin (50.0 mg, 51.3 µmol) was dissolved in 15 ml of benzene under a nitrogen atmosphere. Then a freshly prepared isobenzofuran solution in benzene (770 µmol, 15 eq.) was added dropwise. After stirring for 36 h at 70°C, the solvent was removed under reduced pressure and the crude product was purified by column chromatography on silica gel (dichloromethane/pentane 7:3, Rf = 0.49). A green solid was obtained. Yield: 40.3 mg (33.3 µmol, 65%).

Process 2: 5,10,15,20-Tetrakis-(2,3,4,5,6-pentafluorophenyl)-chlorin (50.0 mg, 45.8 µmol) was dissolved in 15 ml of benzene under a nitrogen atmosphere. Then a freshly prepared isobenzofuran solution in benzene (458 µmol, 10 eq.) was added dropwise. After stirring for 36 h at 70°C, the solvent was removed under reduced pressure and the crude product was

purified by column chromatography on silica gel (dichloromethane/pentane 7:3, Rf = 0.49). A green solid was obtained. Yield: 45.5 mg (37.6 µmol, 82%).

For both process 1 and process 2, the structure of the product was determined as

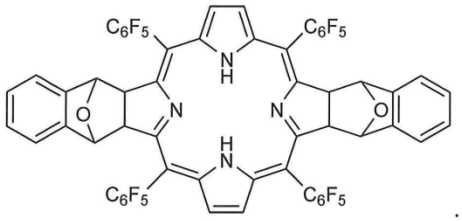

Fig. 5 schematically shows the synthetic routes of Example 1 and Example 2. Using X-ray analysis, it was found that the Diels-Alder reaction product contains the porphyrin and the substituents originating from the condensed isobenzofuran essentially completely in an anti - endo configuration as shown in Fig. 5.

Example 3: Production of Structure 5

For synthesis of 5,10,15,20-Tetrakis-(2,3,4,5,6-pentafluorophenyl)-nickel(II)chlorin according to Structure 5 having pentafluorophenyl as substituents R, 5,10,15,20-Tetrakis(pentafluorophenyl)nickel(II)-porphyrin (50.0 mg, 48.5 µmol) was dissolved in 15 ml of benzene under a nitrogen atmosphere. Then a freshly prepared isobenzofuran solution in benzene (243 µmol, 5 eq.) was added dropwise. After stirring for 36 h at 70°C, the solvent was removed under reduced pressure and the crude product was purified by column chromatography on silica gel (dichloromethane/pentane 7:3, Rf = 0.68). A turquoise solid was obtained. Yield: 9.00 mg (6.97 µmol, 14%). The structure of the product was determined as

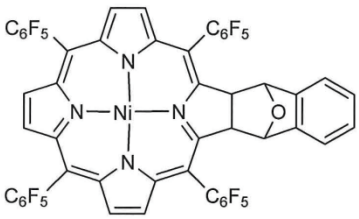

Example 4: Production of Structure 6

For synthesis of 5,10,15,20-Tetrakis-(2,3,4,5,6-pentafluorophenyl)-nickel(II)-bacteriochlorin

according to Structure 6 having pentafluorophenyl as substituents R, 5,10,15,20-Tetrakis-(2,3,4,5,6-pentafluorophenyl)-bacteriochlorin (50.0 mg, 41.3 µmol) and 18 eq. bis(cycloocta-1,5-dien)nickel ($Ni(COD)_2$) (205 mg, 744 µmol) were dissolved in 50 ml of toluene in the glove box. After 30 min of stirring at room temperature, the solvent was removed under reduced pressure and the crude product purified by column chromatography on silica gel (dichloromethane/pentane 1:1). A turquoise solid was obtained. Yield: 413.6 mg (10.7 µmol, 26%). The structure of the product was determined as

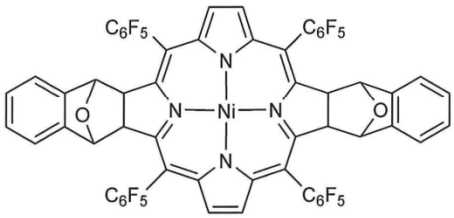

Fig. 6 schematically shows the synthetic routes of Example 3 and Example 4. Using X-ray analysis, it was found that the Diels-Alder reaction product contains the porphyrin and the substituents originating from the condensed isobenzofuran in an anti - endo configuration as shown.

Example 5: Production of Structure 4 substituted in all *meso* positions

For synthesis of acetal protected *bacteriochlorin,* sodium hydride (21.8 mg, 544 µmol) (60% dispersion in mineral oil) was suspended in 7 mL of dry tetrahydrofuran under nitrogen atmosphere. [G2.0]-OH (248 mg, 496 mol, this second generation glycerol (G[2.0]-OH) was synthesised according to a procedure of Haag et al. as described in: M. Wyszogrodzka and R. Haag, Chem. Eur. J., 2008, 14, 9202–9214) was dissolved in 6 mL of tetrahydrofuran and slowly added to the sodium hydride suspension. The suspension was stirred for 30 min. *Bacteriochlorin* (75.0 mg, 62.0 µmol) was added and the mixture was stirred for 4 d. The reaction was quenched with water and added to 100 mL of diethyl ether. The organic layer was washed with 100 mL of 0.1 M hydrochloric acid and dried over magnesium sulphate. The solvent was removed under reduced pressure. The crude product was purified by column chromatography (silica gel, dichloromethane/methanol = 97/3, *R*f = 0.49). The product was obtained as a green, viscous oil.

Yield: 128 mg (34.8 µmol, 56%). The following structure was determined:

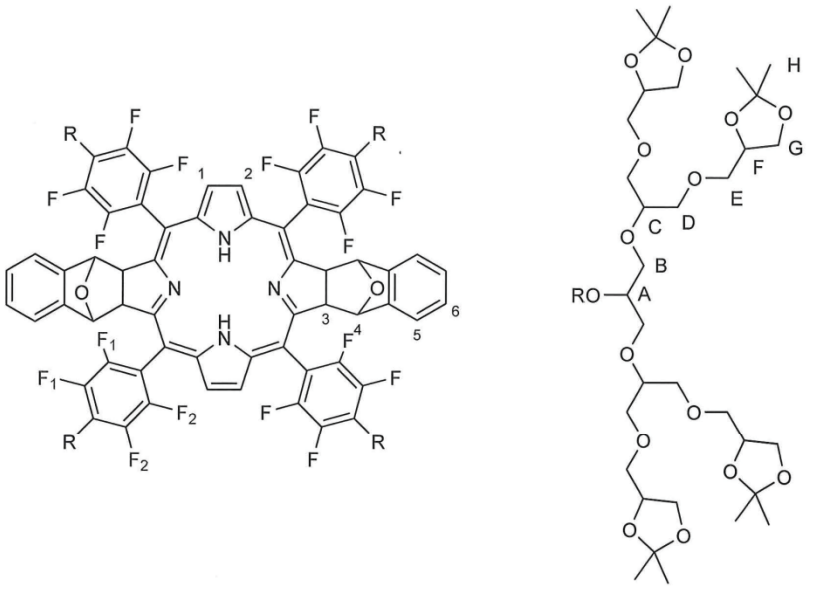

For synthesis of the deprotected *bacteriochlorin* (5),
acetal protected porphyrin (38.0 mg, 10.3 µmol) was dissolved in a mixture of 0.30 mL of acetic acid, 1 mL of methanol and 0.50 mL of water and stirred for 18 h at 40 °C. The solvent was removed under reduced pressure. The product was obtained as a green, viscous oil. Yield: 30.0 mg (9.97 µmol, 97%). The following structure was determined

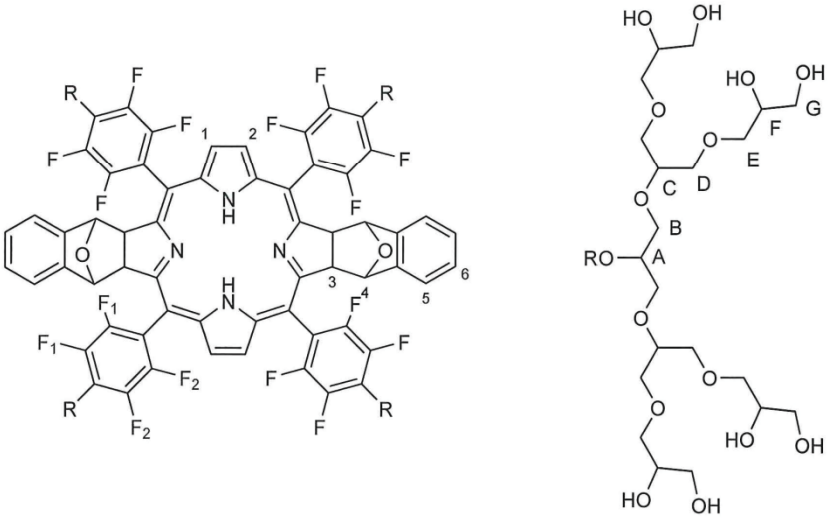

, wherein in the substituent R, the designators A, B, C, D, E, F and G indicate the carbon atoms of the dendrimer chain.

Example 6: Production of singlet oxygen under irradiation

As a representative for a compound comprising Structure 2, the 5,10,15,20-Tetrakis-(2,3,4,5,6-pentafluorophenyl)-bacteriochlorin was dissolved in a concentration of 5 µM and irradiated with light of 740 nm, 0.5 mW/cm² in the presence of 1,3-diphenylisobenzofuran (DPBF) as an indicator for presence of singlet oxygen. The decrease of the absorbance band at 410 nm was monitored as a measure for oxidation of the DPBF by the reactive singlet oxygen.

Fig. 7 shows the results of the decrease of the absorbance band of DPBF, in comparison to DPBF in tetrahydrofuran (THF) irradiated with 740 nm, of protoporphyrin IX in THF irradiated with 590 nm, of protoporphyrin IX (obtained from ABCR Germany) in THF irradiated with 630 nm, of protoporphyrin IX in methanol irradiated with 630 nm, and of 5,10,15,20-tetrakis-(2,3,4,5,6-pentafluorophenyl)-bacteriochlorin according to Structure 2 (3 in Fig. 7) in THF or in methanol, and of 5,10,15,20-tetrakis-(2,3,4,5,6-pentafluorophenyl)-bacteriochlorin according to Structure 2 substituted with R5 = tetrafluorophenyl substituted in *para* position with a dendrimer (5 in Fig. 7) in methanol, irradiated with 740 nm. Measurements of singlet oxygen production by Structure 2 substituted with R5 were also made using betanin, which is water-soluble, as an indicator. Structure 2 substituted with R5 is soluble in water and aqueous media, e.g. blood serum.

These results show that the indicator DPBF under irradiation, without a sensitizer added, is essentially stable and that the protoporphyrin IX effectively produces singlet oxygen. The compounds of the invention comprising Structure 2 show a markedly higher production of singlet oxygen, for Structure 2 substituted with pentafluorophenyl a singlet oxygen production that is 30 times higher in THF compared to protoporphyrin IX, and for Structure 2 substituted with R5 a singlet oxygen production that is 16 times higher. Further, the constant rates of singlet oxygen production show that the compounds of the invention are stable against degradation under conditions of singlet oxygen production.

Example 7: Photostability measurements

The stability of compounds of the invention against irradiation was measured by irradiating 5,10,15,20-tetrakis-(2,3,4,5,6-pentafluorophenyl)-bacteriochlorin according to Structure 2 and 5,10,15,20-tetrakis-(2,3,4,5,6-pentafluorophenyl)-bacteriochlorin according to Structure 2 substituted with R5 at 740 nm with an intensity of 1 W/cm² for 60 min. For determination of degradation (photobleaching), the absorbance maxima at 733 nm were determined. Both compounds showed high stability by showing no decomposition and no change in the UV spectrum.

Example 8: Absorption and fluorescence measurements

The optical properties of compounds of the invention were measured for the examples of 5,10,15,20-tetrakis-(2,3,4,5,6-pentafluorophenyl)-bacteriochlorin according to Structure 2 and 5,10,15,20-tetrakis-(2,3,4,5,6-pentafluorophenyl)-bacteriochlorin according to Structure 2 substituted with R5. The compounds were dissolved in methanol to 10 µM, measurements were made at 25°C. Fig. 8 shows the absorbance (solid line) and the fluorescence (dashed line), in Fig. 8 A) for 5,10,15,20-tetrakis-(2,3,4,5,6-pentafluorophenyl)-bacteriochlorin, in Fig. 8 B) for 5,10,15,20-tetrakis-(2,3,4,5,6-pentafluorophenyl)-bacteriochlorin according to Structure 2 substituted with R5. Both compounds show excellent optical properties in solution, e.g. a sharp absorption in the near infrared region at 733 nm and with moderate quantum yields of fluorescence at 738 nm.

Claims

1. Compound comprising

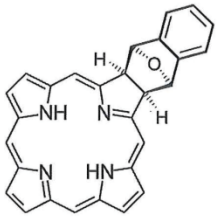

Structure 1.

2. Compound according to claim 1, comprising

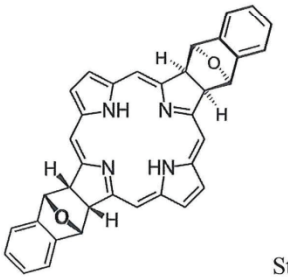

Structure 2.

3. Compound according to one of the preceding claims, wherein the structure comprises substituents according to

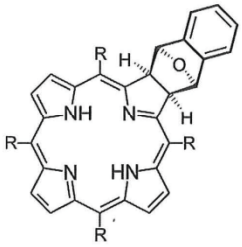

Structure 3 or

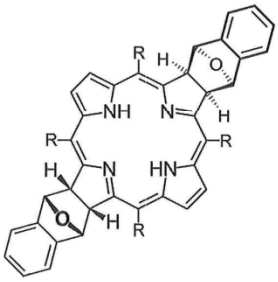

Structure 4

wherein at least one substituent R in the *meso* position of the porphyrin and/or at least one substituent in the β position of the porphyrin is independently selected from hydrogen, linear, branched or circular alkyl or aryl groups, e.g. C1 to C12, optionally containing at least one hetero atom and/or a functional group such as ether, carbonyl and/or acid groups, and

aliphatic or aromatic groups, e.g. containing at least one five-membered or six-membered ring, optionally containing at least one hetero atom, e.g. , or

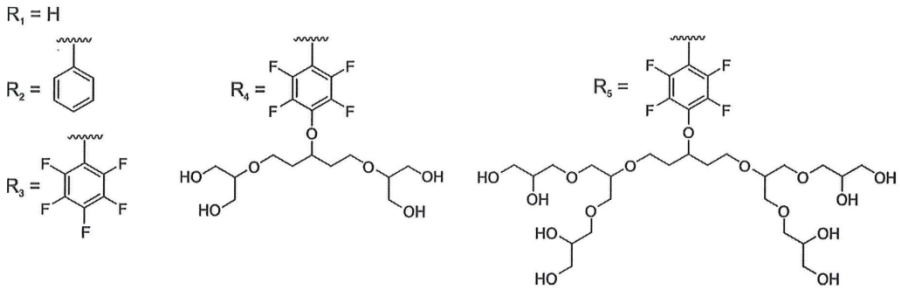

and/or two neighbouring β positions or one β position and one *meso* position are connected by a five- or six-membered ring forming an annelated substituent connecting two neighbouring β positions or one β position and one *meso* position, or one, two, three or all four *meso* positions each are connected to a neighbouring β position by an annelated substituent.

4. Compound according to one of the preceding claims, wherein the compound is immobilized on a carrier.

5. Compound according to one of the preceding claims, containing a metal ion complexed within the porphyrin moiety.

6. Compound according to one of the preceding claims, wherein at least one of the carbon atoms of the phenyl ring of the isobenzofuran moiety is substituted by a substituent which is independently selected from hydrogen, linear, branched or circular alkyl or aryl groups, e.g. C1 to C12, optionally containing at least one hetero atom and/or a functional group such as ether, carbonyl and/or acid groups, and aliphatic or aromatic groups, e.g. containing at least one five-membered or six-membered ring, optionally containing at least one hetero atom, or

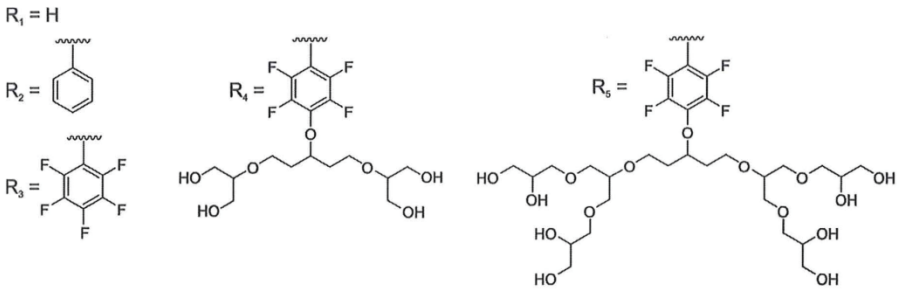

7. Compound according to one of the preceding claims for use in medical therapy.

8. Compound according to claim 7 for use in medical therapy, wherein the medical therapy is a photodynamic therapy for the treatment of solid tumours, of a skin disease, an infection, e.g. a bacterial, fungal or viral infection, of macular degeneration, wherein the infectious agent may be resistant to at least one antibiotic.

9. Compound according to one of claims 7 to 8 for use in medical therapy of solid tumours, characterized in that the compound is contained in a molecule having a size in the range of 20 to 200 kDa.

10. Process for producing a compound according to one of claims 1 to 7, characterized by comprising a Diels-Alder cycloaddition reaction condensing a porphyrin moiety with one or two isobenzofuran per porphyrin moiety.

11. Process according to claim 10, characterized in that the Diels-Alder cycloaddition reaction is carried out at a temperature below 100°C.

12. Process according to one of claims 10 to 11, characterized in that the Diels-Alder cycloaddition reaction is carried out in the absence of a metal-containing catalyst.

13. Process according to one of claims 10 to 12, characterized in that the porphyrin is not isolated from a natural source.

14. Process for producing singlet oxygen from oxygen by irradiating a compound which is in contact with oxygen, characterized in that the compound is according to one of claims 1 to 10.

15. Process according to claim 14, characterized in that the compound is immobilized on a carrier and is in contact with an aqueous or gaseous medium containing oxygen while the compound is irradiated.

Figures

Fig. 1

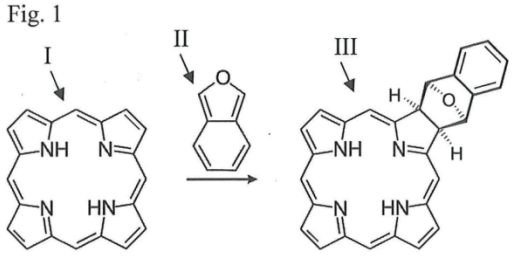

Fig. 2

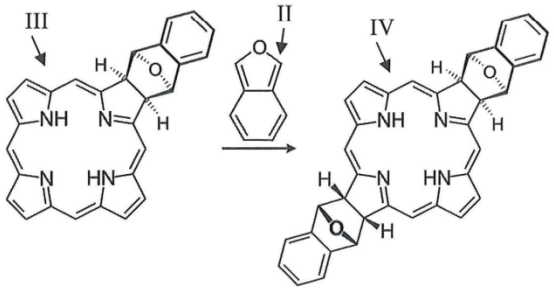

Fig. 3

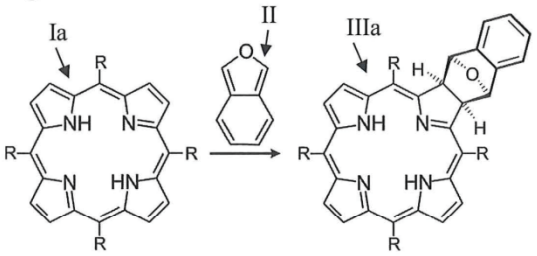

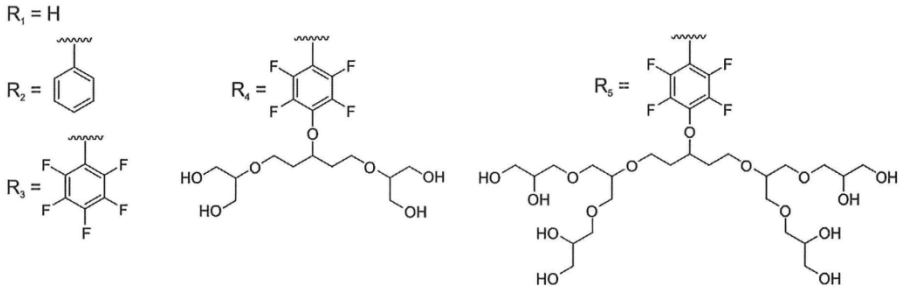

Fig. 4

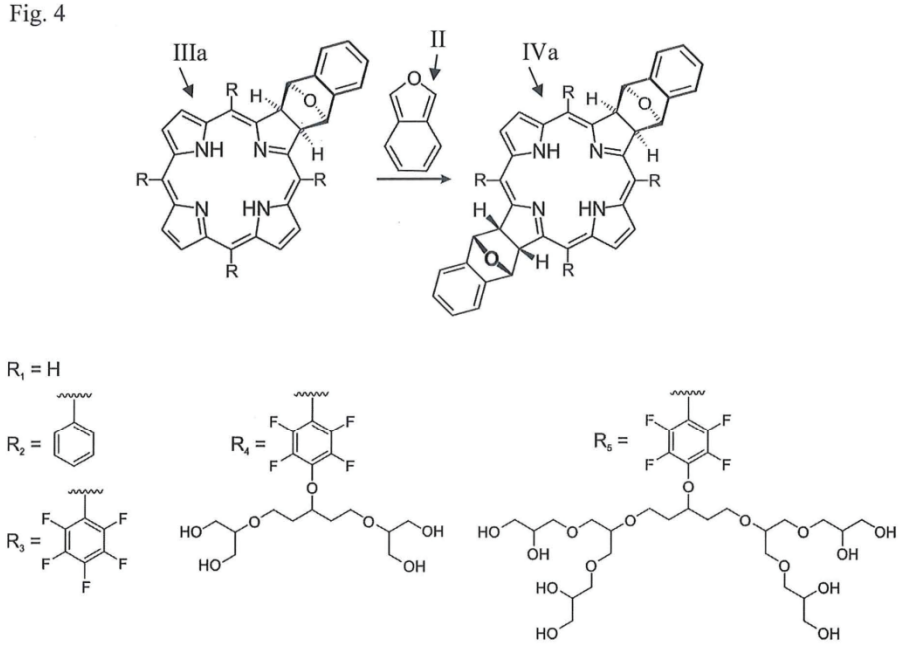

Fig. 5

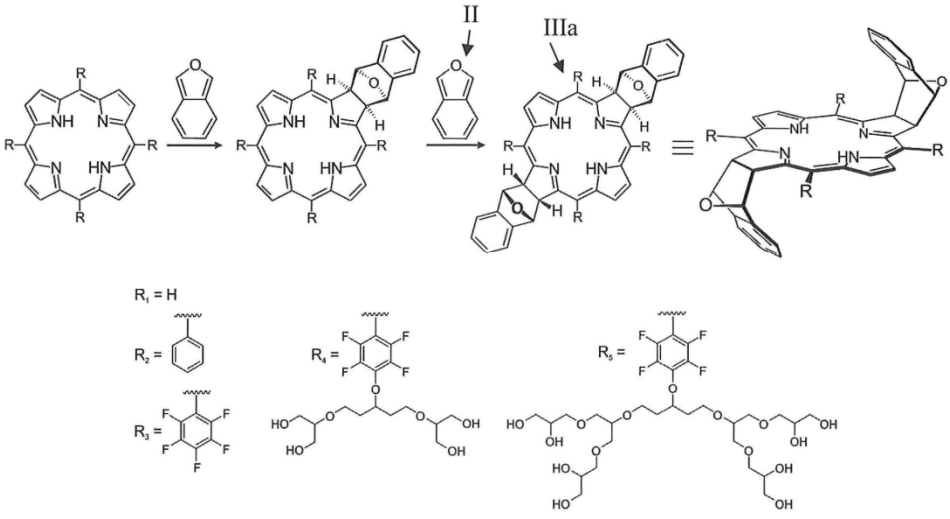

Fig. 6

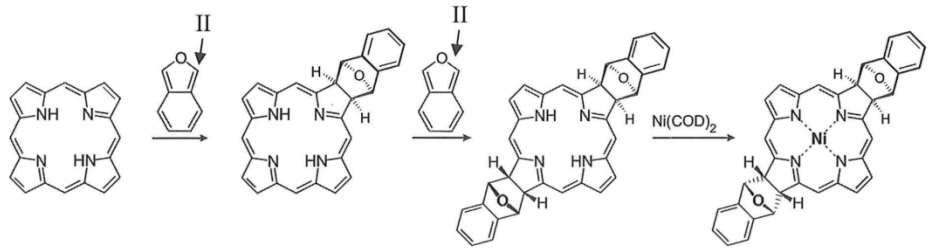
II
II
Ni(COD)2
Ni

Fig. 7

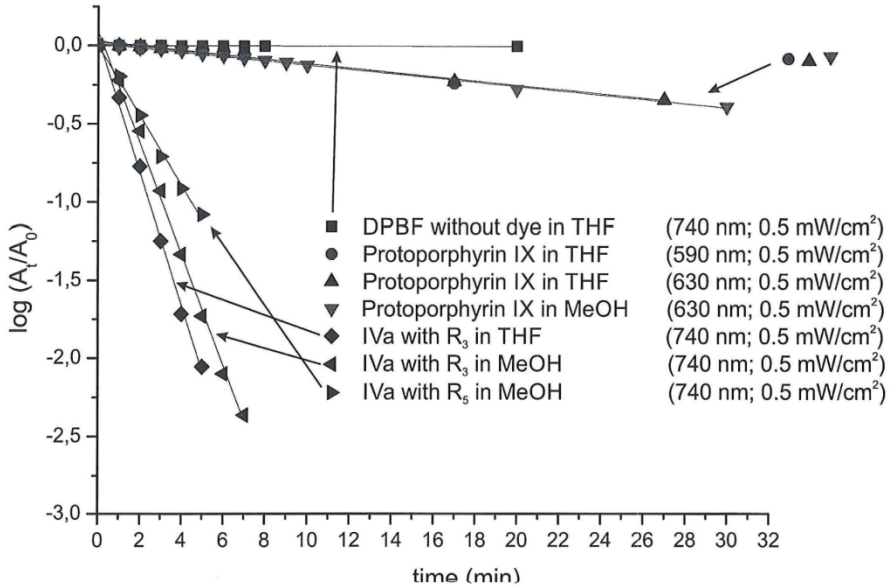
log (A_t/A_0)
time (min)
DPBF without dye in THF (740 nm; 0.5 mW/cm²)
Protoporphyrin IX in THF (590 nm; 0.5 mW/cm²)
Protoporphyrin IX in THF (630 nm; 0.5 mW/cm²)
Protoporphyrin IX in MeOH (630 nm; 0.5 mW/cm²)
IVa with R3 in THF (740 nm; 0.5 mW/cm²)
IVa with R3 in MeOH (740 nm; 0.5 mW/cm²)
IVa with R5 in MeOH (740 nm; 0.5 mW/cm²)

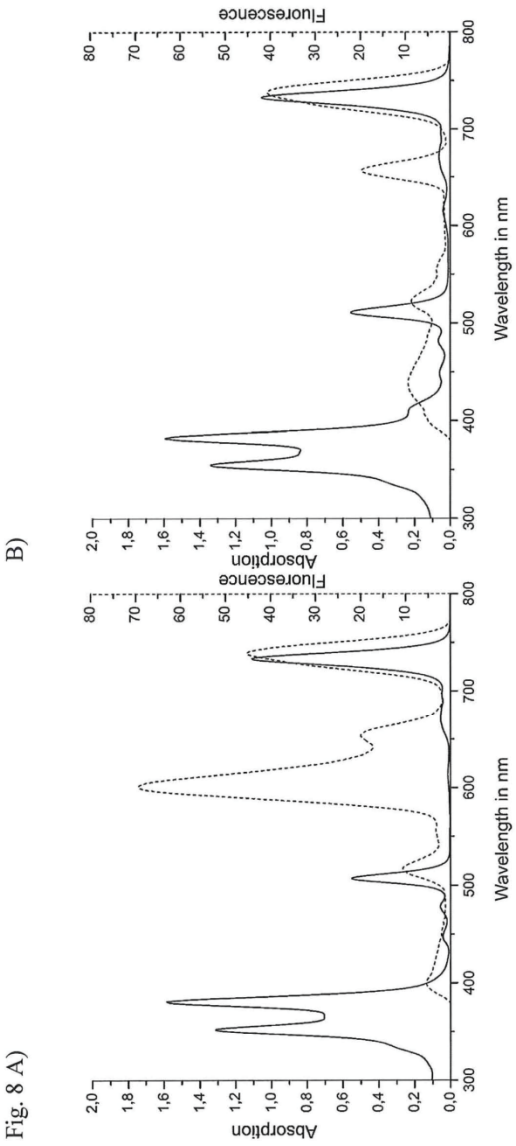

Fig. 8 A)

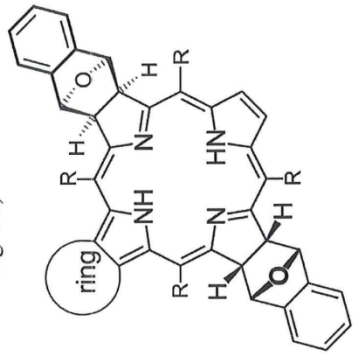

Fig. 9B)

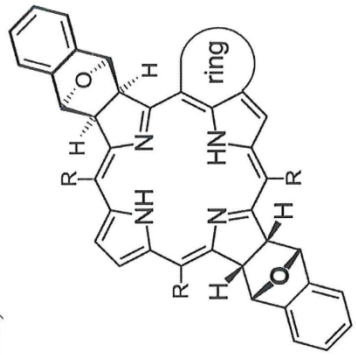

Fig. 9 A)

24

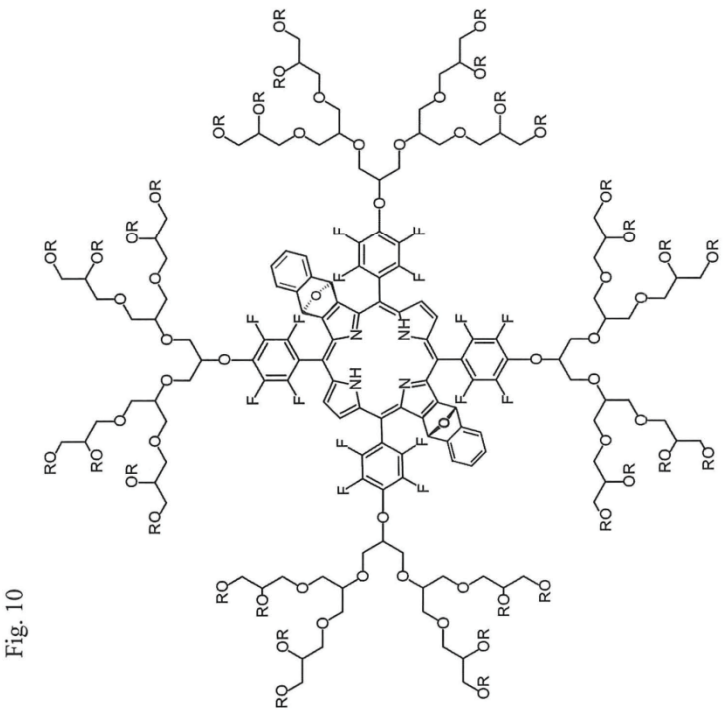

Fig. 10

25

4 Zusammenfassung und Ausblick

In dieser Arbeit wurde die lichtgesteuerte molekulare Spinschaltung von Fe(III)-Porphyrinen untersucht. Hierbei war bis vor Kurzem die magnetische Bistabilität im Wesentlichen auf Festkörper bei sehr tiefen Temperaturen beschränkt.[9] Erst im Jahr 2011 konnte im Arbeitskreis HERGES anhand von Ni(II)-Komplexen der Light-Driven Coordination-Induced Spin State Switch (LD-CISSS) entwickelt und veröffentlicht werden, welcher einen Ansatz für eine effiziente und reversible Spinschaltung von isolierten Einzelmolekülen in homogener Lösung bei Raumtemperatur bietet.[119] Basierend auf den vorherigen Arbeiten konnte in dieser Dissertation die erste reversible lichtgesteuerte molekulare Spinschaltung auf Fe(III)-Basis vorgestellt werden. Hierbei wird als Ausgangskomplex das Fe(III)Tetraphenyl-porphyrin-perchlorat verwendet, welches in einer Aceton/DMSO-Lösung als High-Spin-Komplex (S = 5/2) mit zwei axialen DMSO-Liganden vorliegt. Die Spin-Änderung wird durch einen photoschaltbaren Azopyridinliganden induziert. Dieser ist so entworfen, dass er durch eine stärkere Bindungskonstante als DMSO in seiner *trans*-Konfiguration an das Eisenporphyrin koordiniert und somit einen Low-Spin-Komplex (S = 1/2) mit zwei axialen *trans*-Azopyridin-Liganden bildet.

Werden diese *trans*-Azopyridine mit 365 nm bestrahlt, wandelt sich das *trans*-Isomer in die *cis*-Konfiguration um. Dieses *cis*-Isomer kann aus sterischen Gründen nicht mehr an das Eisenporphyrin binden, wodurch die DMSO-Liganden wieder koordinieren und der High-Spin-Zustand regeneriert wird (Abbildung 24).

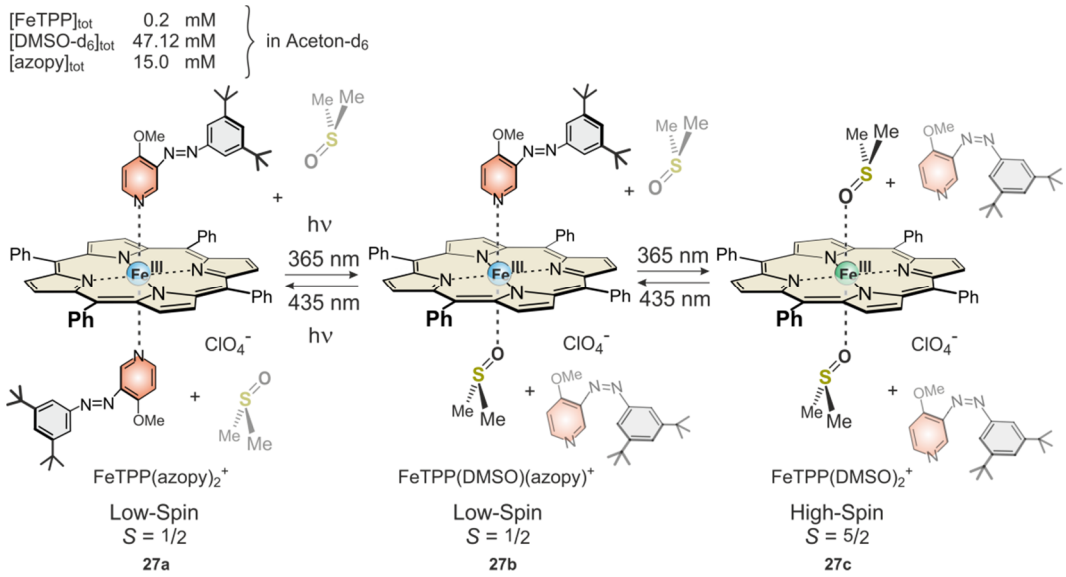

Abbildung 24: Darstellung der lichtgesteuerten molekularen Spinschaltung von Fe(III).

Dieser Ligandenaustausch ist reversibel. Mit einer Wellenlänge von 435 nm können die *cis*-Azopyridine wieder in die *trans*-Form überführt werden, welche wiederum die DMSO-Liganden verdrängen. Der Prozess ist extrem robust und zeigt nach mehr als 1000 Schaltzyklen unter Luft, Feuchtigkeit sowie Raumtemperatur keine Ermüdung, Nebenreaktionen oder Zersetzungen.

Neben der Spin-Schaltung ändert sich in diesem Modell ebenfalls das Redoxpotential analog zu enzymatischen Hämproteinen um 58 mV beim Wechsel von $S = 1/2$ zu $S = 5/2$, wodurch die Relaxationszeit reversibel um den Faktor zehn geschaltet werden kann. Somit ist der Grundstein gelegt, Eisen(III)-Porphyrine als intelligente Kontrastmittel in der MRT zu verwenden.

Für die Anwendung als Kontrastmittel und für einen verlässlichen intramolekularen LD-CISSS mit Fe(III)-Porphyrinen muss allerdings bedacht werden, dass das Eisen(III)-Zentralatom im Normalfall einen zusätzlichen anionischen Liganden in der Koordinationssphäre bevorzugt. Um einen unkontrollierten Anionenaustausch zu verhindern, soll das Porphyrindesign angepasst werden. Durch ein kovalent gebundenes Anion soll ein Neutralkomplex erhalten werden, der eine ideale Plattform für einen intramolekularen LD-CISSS darstellt.

Dafür wurde zunächst das acetylenverbrückte Pophyrin **28** synthetisiert, um festzustellen, ob ein starker Ligand allein in der Lage ist, die oben aufgeführte Spin-Änderung durchzuführen. Mittels ^{1}H-NMR-Spektroskopie und Evans-Messungen konnte gezeigt werden, dass die Änderung des Spins durch zum Beispiel 1-Methylimidazol hervorgerufen werden kann (Abbildung 25).

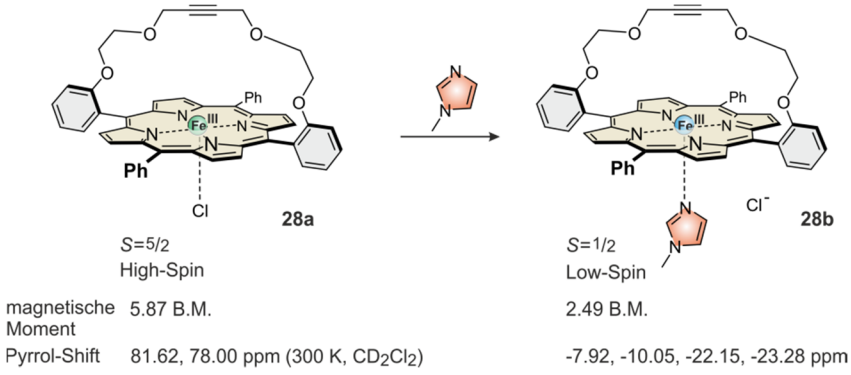

Abbildung 25: Schaltung des Spinzustandes an einem überbrückten, 5-fach koordinierten Modell-Porphyrin **28a**. Der Spinwechsel von High-Spin zu Low-Spin bei Austausch des Chlorid-Liganden durch 1-Methylimidazol beweist, dass bereits ein axialer Stickstoff-Ligand zu einem Low-Spin Komplex **28b** führt. Die Addition des zweiten Liganden wird durch die Brücke verhindert.

Um nun einen neutralen Eisen(III)-Komplex herzustellen, in dem die Koordinationsstelle intramolekular besetzt ist, wurden weitere acetylenüberbrückte Porphyrine synthetisiert, welche durch eine 1,3-dipolare Cycloaddition mit Azid in 1,2,3-Triazole umgewandelt wurden. Die anschließende Einlagerung von Eisen(III) in diese Porphyrine konnte erfolgreich durchgeführt werden. In der Abbildung 26 wird exemplarisch die Synthese des verbrückten Porphyrins, welches in der *meso*-Postion 1,6-Dichlorbenzol trägt, dargestellt.

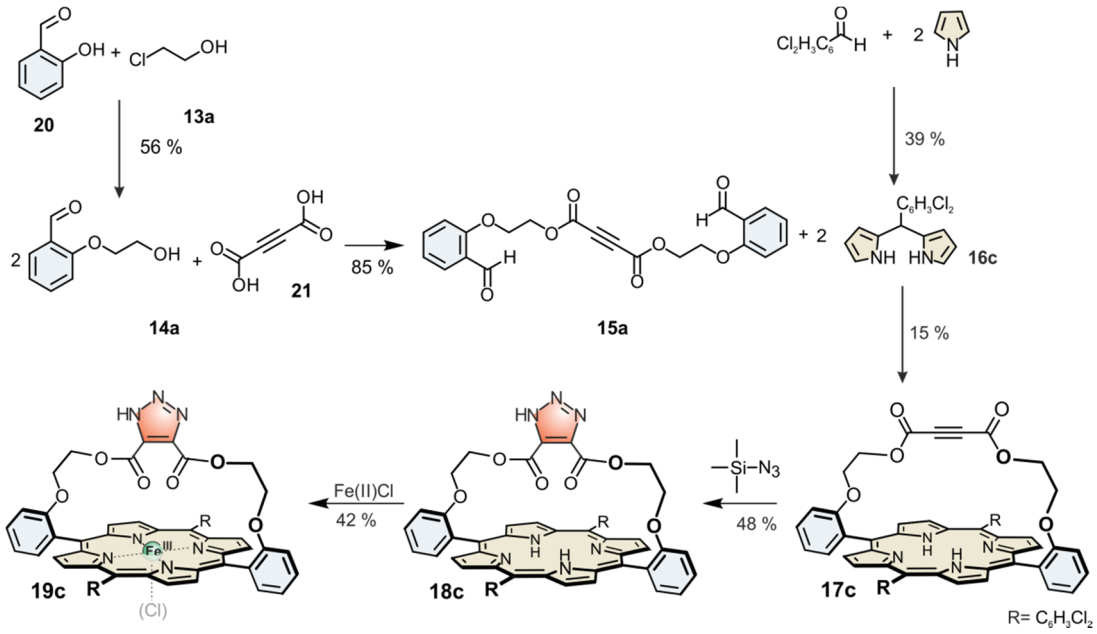

Abbildung 26: Synthese des verbrückten Fe(III)-Porphyrins **19c**.

Durch die Zugabe einer Base wie zum Beispiel Kaliumcarbonat wird das Triazol in **19c** zum stärker bindenden Triazolat deprotoniert. Im darauf folgenden Schritt kommt es zur Verdrängung des Chlorids, welches zur Bildung eines fünffach koordinierten neutralen High-Spin-Komplexes (S = 5/2) führt. Ein weiterer axialer Ligand wie zum Beispiel das *p*-Methoxypyridin führt zu einem CISSS und bildet einen Low-Spin-Komplex (S = 1/2). Auf dem Weg zu einem nur aus einem Molekül bestehenden Spin-Schalter (Plattenspieler) auf der Basis von Fe(III) muss nun noch ein photochemisch schaltbarer Ligand kovalent an das Porphyrin gebunden werden (Abbildung 27). Gegenüber den bereits bekannten, schaltbaren Ni(II)-Porphyrinen hätten die Fe(III)-Porphyrine bei der Verwendung als schaltbare Kontrastmittel den Vorteil, dass sowohl das absolute magnetische Moment (S= 5/2 statt 1) als auch der Unterschied im magnetischen Moment zwischen den beiden Schaltzuständen größer ist (ΔS= 2 statt 1).

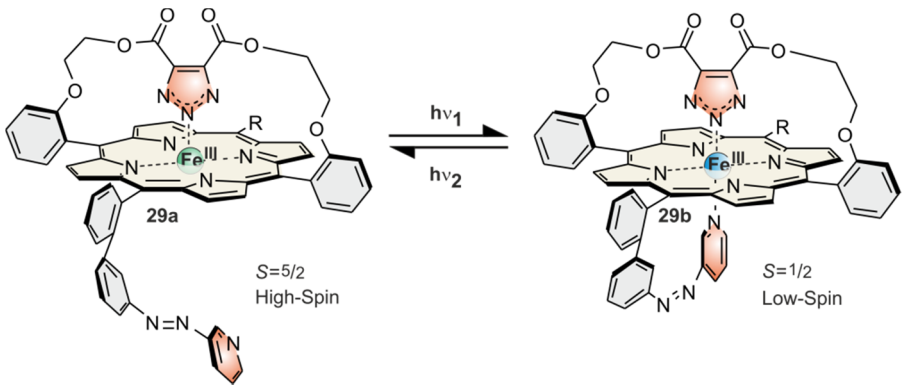

Abbildung 27: Darstellung eines theoretisch denkbaren intramolekularen LD-CISSS basierend auf dem Fe(III)-Porphyrins **29**.

In einem weiteren Teilbereich dieser Dissertation wurde die Funktionalisierung von Porphyrinen untersucht. Ziel hierbei war es, einen neuen Syntheseansatz zu entwickeln, um reduzierte Porphyrin-Derivate herzustellen, wodurch eine bathochrome Verschiebung und eine Absorption im Nahen Infrarot (NIR)-Bereich des elektromagnetischen Spektrums gewährleistet werden kann. Für medizinische Anwendungen hat dies Vorteile, denn im Bereich von 690-900 nm ist blutversorgtes Gewebe transparent (Eindringtiefe des Lichtes: 1-2 cm). Ausgehend vom Porphyrin gibt es im Allgemeinen drei Ansätze, um Chlorine, Bakterio- und Isobakteriochlorine herzustellen.[121] Hierbei kann die Umwandlung der Pyrrol-Doppelbindungen in C-C-Einfachbindungen durch (1) direkte Reduktion, (2) Oxidation oder (3) Cycloadditionen erreicht werden.

Um die gewünschten NIR-Farbstoffe zu erhalten, wurde die Variante (3) gewählt. Hierfür wurde das Isobenzofuran **12** als Dien verwendet.[104,105] Wegen seiner hohen Reaktivität und der damit verbundenen geringen Stabilität ließ sich bislang das Isobenzofuran nur sehr umständlich herstellen und isolieren. Aus diesem Grund wurde ein neuer Syntheseweg entworfen, der sich leicht und kostengünstig im Labormaßstab durchführen lässt (Abbildung 28).

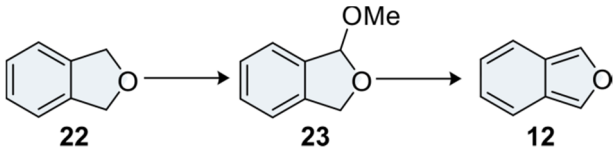

Abbildung 28: Die optimierte zweistufige Synthese des Isobenzofurans **12** mit 66 % Ausbeute.

Mit dem frisch hergestellten Isobenzofuran **12** konnte in einer Diels-Alder-Reaktion ein neuer, leicht durchzuführender, ergiebiger, regio- und stereoselektiver

Syntheseweg von Chlorinen, Bakterio- und Isobakteriochlorinen entwickelt werden (Abbildung 29).

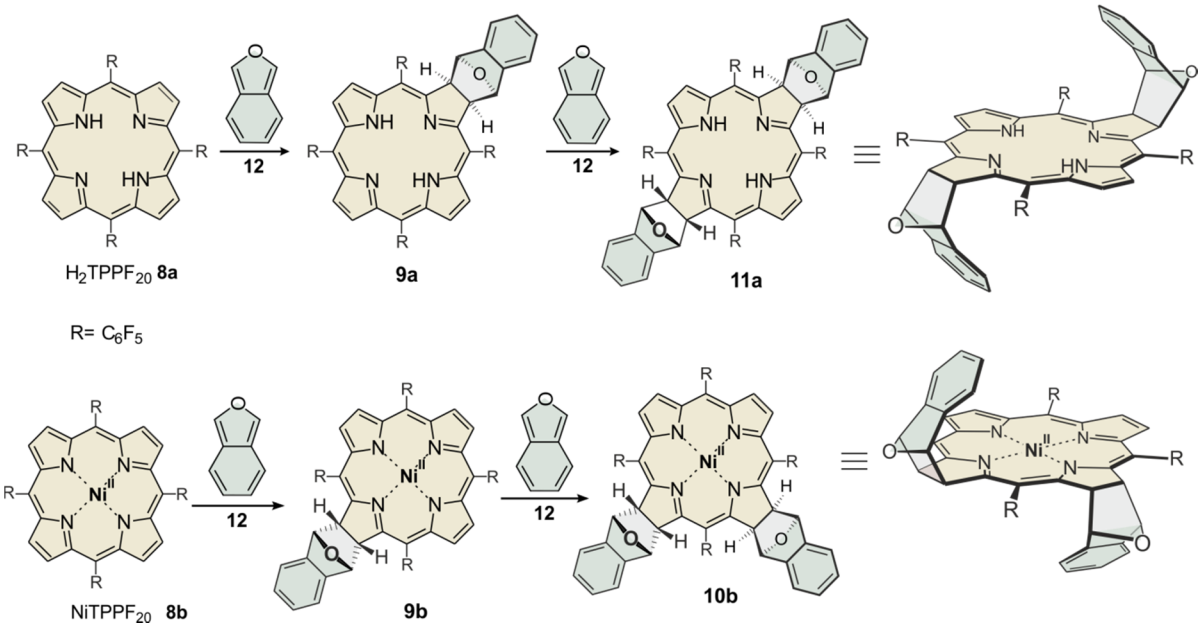

Abbildung 29: Darstellung der Synthese verschiedener Porphyrinderivate über eine [4+2] Cycloaddition.

Das in der Abbildung 29 dargestellte Bakteriochlorin **11a** ist von besonders großem Interesse, da dies eine starke Absorptionsbande (733 nm) im NIR-Bereich zeigt, bei der das Gewebe relativ transparent ist. Dies stellt eine optimale Voraussetzung für die Photodynamische Therapie (PDT) zur Behandlung von Krebs dar. Die starke Fluoreszenz spielt für die Diagnostik eine ebenso große Rolle. Aus diesem Grund wurde das Bakteriochlorin **11a** auf die Anwendbarkeit als Photosensibilisator (PS) untersucht. Hierbei stellte sich heraus, dass die Singulett-Sauerstoff- sowie Sauerstoffradikal-Generierung der Verbindung **11a** in THF 30-mal höher ist als beim klinisch zugelassenen Protoporphyrin IX. Aufgrund dieser vielversprechenden Eigenschaft wurde das Molekül **11a** weiterentwickelt. Durch die Umsetzung mit Triglycerol-Dendrimer (G[2.0]-OH) und anschließender Entschützung konnte das wasserlösliche Bakteriochlorin **26** synthetisiert werden. Dieses ist für die Anwendung in der PDT optimal geeignet. Es zeigt eine starke Absorption bei 733 nm und ist 16-mal effektiver als das klinisch zugelassene Protoporphyrin IX (Abbildung 30).

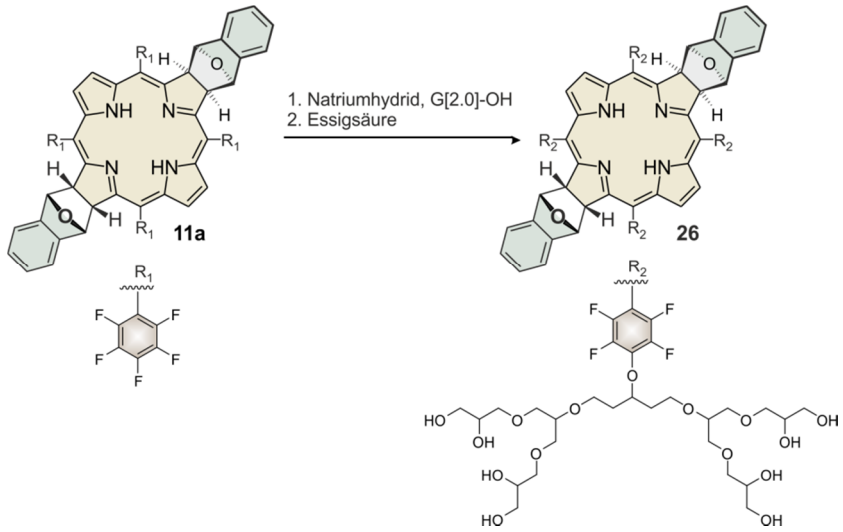

Abbildung 30: Darstellung der für die PDT untersuchten Chromophore **11a** und **26** für die PDT.

Die Bakteriochlorine sind jedoch nicht nur wegen ihrer Absorptionsbanden im NIR-Bereich für die PDT interessant, sondern bieten durch diese Eigenschaft zusätzlich einen neuen Ansatz für den nickelbasierten LD-CISSS, welcher im bio-optischen Fenster und somit *in vivo* realisiert werden könnte. Ein Problem bei der Nickelierung des Bakteriochlorins **11a** stellt die Retro-Diels-Alder-Reaktion dar, die bei Temperaturen über 80 °C auftritt. Aus diesem Grund wurde eine neue sehr milde und effiziente Methode entwickelt, um Nickel unter Verwendung von Bis(cycloocta-1,5-dien)nickel in Porphyrine einzulagern. Diese Reaktion kann bei 20 °C durchgeführt werden und liefert Ausbeuten zwischen 90 % und 100 % mit elektronenreichen sowie elektronenarmen Porphyrinen. Besonders interessant ist die Einlagerung von Nickel in Gegenwart einer Base, da dies in Lösung zu stabilen Radikalen führt. Die reduzierten Ni(II)-Porphyrine sind Schlüsselintermediate in verschiedenen technologisch interessanten Prozessen und Enzymreaktionen. Fortan können diese nun in großen Mengen synthetisiert und untersucht werden.

Wird diese neue Methode der Nickel-Einlagerung auf das Bakteriochlorin **11a** angewendet, entsteht das entsprechende Ni(II)-Bakteriochlorin **11b**, welches ein nicht-fluoreszierender und stabiler NIR-Farbstoff ist, der bei 757 nm eine starke Absorption aufweist (Abbildung 31).

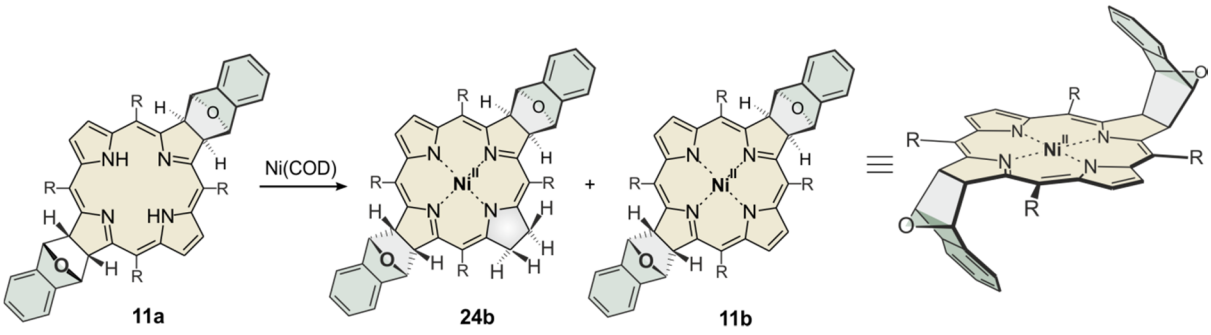

Abbildung 31: Nickel-Einlagerung mit $Ni(COD)_2$ in das Bakteriochlorin **11a**.

Zusätzlich entsteht bei dieser Reaktion das Pyrrocorphin **24b**, wodurch erstmals die gesamte Reihe von Hydroporphyrinen mit Ni(II) im Tetrapyrrolkern hergestellt und charakterisiert werden konnte. Die UV/Vis-Spektren dieser Verbindungen sind in der folgenden Grafik dargestellt.

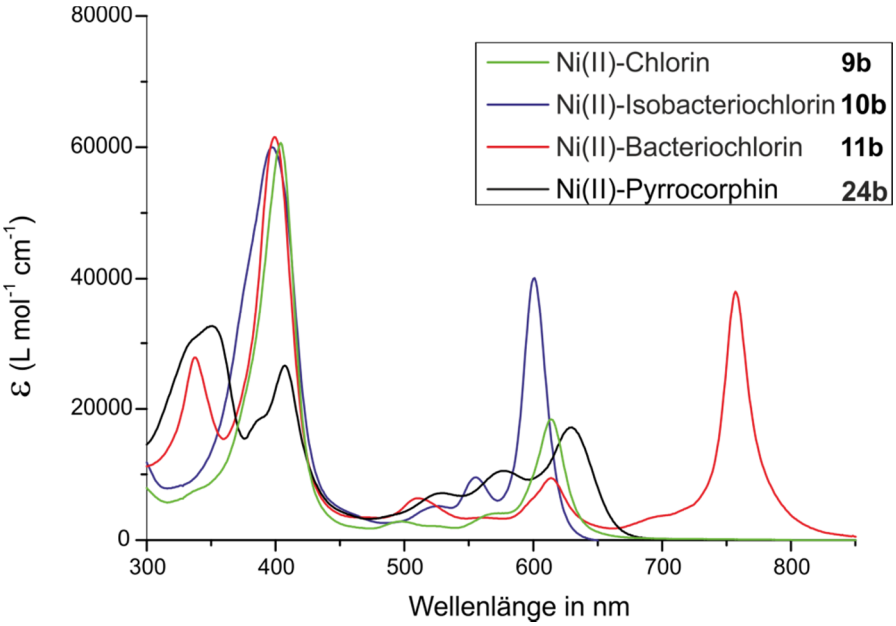

Abbildung 32: Darstellung der UV/Vis-Spektren der gesamten Reihe von Hydroporphyrinen.

Das Ni(II)-Bakteriochlorin **11b** zeigt einen CISSS bei Zugabe von koordinierenden Molekülen, welche als axiale Liganden fungieren können. Dies ist überaus bedeutsam für den LD-CISSS mit Ni(II)-Komplexen. Durch das Vereinen der neuen Synthesemethoden könnte ein nickelbasierter, intramolekularer LD-CISSS im NIR-Bereich entwickelt werden. Eine mögliche Syntheseroute ist in Abbildung 33 dargestellt.

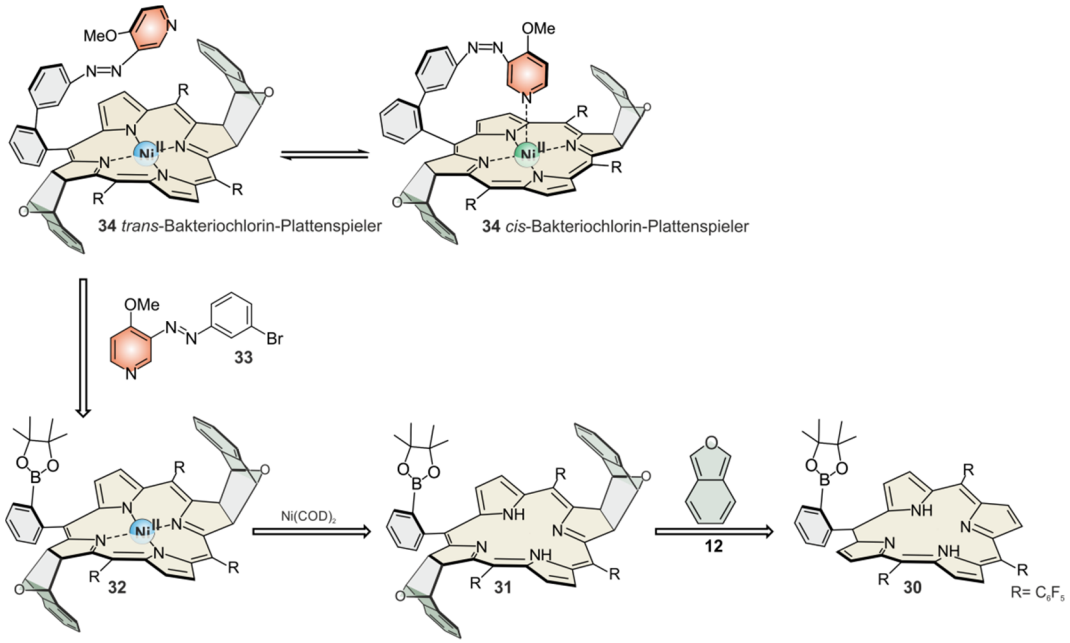

Abbildung 33: Mögliche Retrosynthese eines intramolekularen LD-CISSS im NIR-Bereich basierend auf dem NI(II)-Porphyrins **34**.

Dafür könnte der literaturbekannte Precursor **30**[127] mit dem nun leicht zugänglichen Isobenzofuran **12** zum Bakteriochlorin **31** umgesetzt werden. Die anschließende milde Nickelierung wird auf dem neuen Syntheseweg mit Bis(cycloocta-1,5-dien)nickel durchgeführt. Folgend darauf liefert die Kreuzkupplung das Produkt **34**, welches einen LD-CISSS im bio-optischen Fenster ermöglicht. Durch die anschließende Einführung der Triglycerol-Dendrimere wird zudem die Wasserlöslichkeit erreicht. Somit sind alle wichtigen Eigenschaften für das erste photoschaltbare MRT-Kontrastmittel gegeben, welches *in vivo* geschaltet werden kann.

5 Begleitmaterial (Supporting Information) zu den Publikationen

5.1 Begleitmaterial zu der Publikation: "Light Controlled Switching of the Spin State of Iron(III)"

Sreejith Shankar, Morten Peters, Kim Steinborn, Bahne Krahwinkel, Frank Sönnichsen, Dirk Grote, Wolfram Sander, Thomas Lohmiller and Rainer Herges

Nature Communications **2018**, *9*, 1-12.
doi:10.1038/s41467-018-07023-1

DVD: Kapitel 1

5.2 Begleitmaterial zu der Publikation: "Spin switching of ferrous porphyrins strapped with triazolate"

Morten K. Peters, Sebastian Hamer, Torben Jäkel, Fynn Röhrich, Carolina von Essen, Manu Lahtinen, Christian Näther, Frank Sönnichsen, Kari Rissanen and Rainer Herges

Manuskript für
Inorganic Chemistry

DVD: Kapitel 2

5.3 Begleitmaterial zu der Publikation: "Crystal structure of 2-[2-(pyridin-3-yl)diazen-1-yl]aniline"

Morten K. Peters, Christian Näther and Rainer Herges

Acta Crystallographica **2018***, E74,* 1013-1016.
doi: 10.1107/S2056989018008605

DVD: Kapitel 3

5.4 Begleitmaterial zu der Publikation: "Insertion of Ni(0) in Porphyrins at Room Temperature: Preparation of Ni(II)porphyrins, and Ni(II)chlorins and Observation Hydroporphyrin Intermediates"

Morten K. Peters and Rainer Herges

Inorganic Chemistry **2018***, 57,* 3177–3182.
doi:10.1021/acs.inorgchem.7b03164

DVD: Kapitel 4

5.5 Begleitmaterial zu der Publikation: "Preparation and isolation of isobenzofuran"

Morten K. Peters and Rainer Herges

Beilstein Journal of Organic Chemistry **2017**, *13,* 2659–2662.
doi:10.3762/bjoc.13.263

DVD: Kapitel 5

5.6 Begleitmaterial zu der Publikation: "One-Pot Approach to Chlorins, Isobacteriochlorins Bacteriochlorins and Pyrrocorphins"

Morten K. Peters, Fynn Röhricht, Christian Näther and Rainer Herges

Organic Letters
angenommen: DOI: 10.1021/acs.orglett.8b03433

DVD: Kapitel 6

5.7 Begleitmaterial zu der Publikation: "Singlet oxygen generation by water soluble bacteriochlorin"

Morten K. Peters, Jens Gröbner and Rainer Herges

Manuskript für
Chemical Communications

DVD: Kapitel 7

6 Abbildungsverzeichnis

7 Tabellenverzeichnis

8 Abkürzungsverzeichnis

CT	Computertomographie
DMSO	Dimethylsulfoxid
DPBF	1,3-Diphenylisobenzofuran
Fe	Eisen
HS	High-Spin
IBF	Isobenzofuran
LS	Low-Spin
MALDI	Matrix Assisted LASER Desorption Ionization
MRT	Magnetresonanztomographie
Ni	Nickel
$Ni(COD)_2$	Bis(cycloocta-1,5-dien)nickel
NIR	nahinfraroter Spektralbereich
nm	Nanometer
NMR	Nuclear Magnetic Resonance
UV/Vis	Ultraviolett / visible

9 Literaturverzeichnis

[1] B. Daniela, *Dissertation Universität Bremen* **2011**.

[2] K. C. Nicolaou, T. Montagnon, *Molecules that changed the World. A brief history of the art and science of synthesis and its impact on society*, Wiley-VCH, Weinheim, **2008**.

[3] A. Fleming, *British Journal of Experimental Pathology* **1929**, *10*, 226.

[4] J. C. Sheehan, K. R. Henery-Logan, *Journal of the American Chemical Society* **1957**, *79*, 1262.

[5] R. P. Baum, H. R. Kulkarni, P. Albers, *Onkologe* **2017**, *23*, 597.

[6] R. P. Baum, H. R. Kulkarni, *Theranostics* **2012**, *2*, 437.

[7] B. E. Hertz, K. E. Schuller, *Endocrine practice : official journal of the American College of Endocrinology and the American Association of Clinical Endocrinologists* **2010**, *16*, 713.

[8] P. C. Lauterbur, *Nature* **1973**, *242*, 190.

[9] G. Heitmann, *Dissertation Christian-Albrechts-Universität zu Kiel* **2016**.

[10] D.Weishaupt, V. D. Köchli, B. Marincek, *Wie funktioniert MRI? Springer-Verlag* **2014**, *7*.

[11] a) P. Mansfield, *Journal of Physics C: Solid State Physics* **1977**, *10*, L55–L58; b) A. N. Garroway, P. K. Grannell, P. Mansfield, *Journal of Physics C: Solid State Physics* **1974**, *7*, L457–L462.

[12] C. G. Fry, *Journal of Chemical Education* **2004**, *81*, 922.

[13] F. A. Gallagher, *Clinical Radiology* **2010**, *65*, 557.

[14] B. M. Dale, M. A. Brown, R. C. Semelka, *MRI basic principles and applications*, Wiley Blackwell, Chichester, West Sussex, UK, **2015**.

[15] F. A. Jolesz, *Journal of Magnetic Resonance Imaging* **1998**, *8*, 3.

[16] S. Konstandin, L. R. Schad, *Magnetic Resonance Materials in Physics, Biology and Medicine* **2014**, *27*, 1.

[17] J. Belliveau, D. Kennedy, R. McKinstry, B. Buchbinder, R. Weisskoff, M. Cohen, J. Vevea, T. Brady, B. Rosen, *Science* **1991**, *254*, 716.

[18] M. K. Peters, *Masterarbeit Christian-Albrechts-Universität zu Kiel* **2014**.

[19] L. M. Fletcher, J. B. Barsotti, J. P. Hornak, *Magnetic Resonance in Medicine* **1993**, *29*, 623.

[20] L. Kjær, C. Thomsen, F. Gjerris, B. Mosdal, O. Henriksen, *Acta Radiologica* **1991**, *32*, 498.

[21] S. Aime, M. Botta, M. Fasano, E. Terreno, *Accounts of Chemical Research* **1999**, *32*, 941.

[22] P. Caravan, J. J. Ellison, T. J. McMurry, R. B. Lauffer, *Chemical Reviews* **1999**, *99*, 2293.

[23] R. V. P. Reimer, *Der Radiologe* **2004**, *44*, 273.

[24] a) S. Kulaksız, M. Bau, *Applied Geochemistry* **2011**, *26*, 1877; b) D. Hao, T. Ai, F. Goerner, X. Hu, V. M. Runge, M. Tweedle, *Journal of Magnetic Resonance Imaging* **2012**, *36*, 1060.

[25] C. de Haen, *Topics in Magnetic Resonance Imaging* **2001**, *12*, 221.

[26] a) N. Bloembergen, E. M. Purcell, R. V. Pound, *Physical Review* **1948**, *73*, 679; b) F. Bloch, *Physical Review* **1946**, *70*, 460.

[27] R. B. Lauffer, *Chemical Reviews* **1987**, *87*, 901.

[28] J.-M. Idée, M. Port, I. Raynal, M. Schaefer, S. Le Greneur, C. Corot, *Fundamental and Clinical Pharmacology* **2006**, *20*, 563.

[29] a) M. Essig, M. S. Shiroishi, T. B. Nguyen, M. Saake, J. M. Provenzale, D. Enterline, N. Anzalone, A. Dörfler, A. Rovira, M. Wintermark et al., *American Journal of Roentgenology* **2013**, *200*, 24; b) https://www.ncbi.nlm.nih.gov/pmc/articles/PMC3593114/.

[30] a) T. Meade, *Current Opinion in Neurobiology* **2003**, *13*, 597; b) L. M. de Leon-Rodriguez, A. J. M. Lubag, C. R. Malloy, G. V. Martinez, R. J. Gillies, A. D. Sherry, *Accounts of Chemical Research* **2009**, *42*, 948; c) E. L. Que, C. J. Chang, *Chemical Society Reviews* **2010**, *39*, 51.

[31] a) S. Aime, S. G. Crich, M. Botta, G. Giovenzana, G. Palmisano, M. Sisti, *Chemical Communications* **1999**, *16*, 1577; b) J. A. Duimstra, F. J. Femia, T. J. Meade, *Journal of the American Chemical Society* **2005**, *127*, 12847; c) M. Giardiello, M. P. Lowe, M. Botta, *Chemical Communications* **2007**, *39*, 4044; d) J. Hall, R. Häner, S. Aime, M. Botta, S. Faulkner, D. Parker, A. S. de Sousa, *New Journal of Chemistry* **1998**, *22*, 627; e) K. Hanaoka, K. Kikuchi, T. Terai, T. Komatsu, T. Nagano, *Chemistry* **2008**, *14*, 987; f) J. Hasserodt, J. L. Kolanowski, F. Touti, *Angewandte Chemie* **2014**, *53*, 60; g) A. Y. Louie, M. M. Hüber, E. T. Ahrens, U. Rothbächer, R. Moats, R. E. Jacobs, S. E. Fraser, T. J. Meade, *Nature Biotechnology* **2000**, *18*, 321; h) M. P. Lowe, D. Parker, O. Reany, S.

Aime, M. Botta, G. Castellano, E. Gianolio, R. Pagliarin, *Journal of the American Chemical Society* **2001**, *123*, 7601; i) S. Mizukami, R. Takikawa, F. Sugihara, Y. Hori, H. Tochio, M. Wälchli, M. Shirakawa, K. Kikuchi, *Journal of the American Chemical Society* **2008**, *130*, 794; j) M. Querol, J. W. Chen, R. Weissleder, A. Bogdanov, *Organic Letters* **2005**, *7*, 1719; k) M. Woods, G. E. Kiefer, S. Bott, A. Castillo-Muzquiz, C. Eshelbrenner, L. Michaudet, K. McMillan, S. D. K. Mudigunda, D. Ogrin, G. Tircsó et al., *Journal of the American Chemical Society* **2004**, *126*, 9248; l) S. Zhang, K. Wu, A. D. Sherry, *Angewandte Chemie* **1999**, *111*, 3382; m) E. Tóth, R. D. Bolskar, A. Borel, G. González, L. Helm, A. E. Merbach, B. Sitharaman, L. J. Wilson, *Journal of the American Chemical Society* **2005**, *127*, 799.

[32] a) D. Delli Castelli, E. Terreno, S. Aime, *Angewandte Chemie* **2011**, *50*, 1798; b) I.-R. Jeon, J. G. Park, C. R. Haney, T. D. Harris, *Chemical Science* **2014**, *5*, 2461.

[33] C. Carrera, G. Digilio, S. Baroni, D. Burgio, S. Consol, F. Fedeli, D. Longo, A. Mortillaro, S. Aime, *Dalton Transactions* **2007**, *43*, 4980.

[34] a) S. Aime, D. Delli Castelli, F. Fedeli, E. Terreno, *Journal of the American Chemical Society* **2002**, *124*, 9364; b) R. Trokowski, S. Zhang, A. D. Sherry, *Bioconjugate Chemistry* **2004**, *15*, 1431.

[35] a) G. Angelovski, P. Fouskova, I. Mamedov, S. Canals, E. Toth, N. K. Logothetis, *A European Journal of Chemical Biology* **2008**, *9*, 1729; b) K. Dhingra, M. E. Maier, M. Beyerlein, G. Angelovski, N. K. Logothetis, *Chemical Communications* **2008**, *29*, 3444; c) K. Hanaoka, K. Kikuchi, Y. Urano, T. Nagano, *Journal of the Chemical Society, Perkin Transactions 2* **2001**, *9*, 1840; d) H. Hifumi, A. Tanimoto, D. Citterio, H. Komatsu, K. Suzuki, *The Analyst* **2007**, *132*, 1153; e) W.-h. Li, S. E. Fraser, T. J. Meade, *Journal of the American Chemical Society* **1999**, *121*, 1413; f) J. L. Major, G. Parigi, C. Luchinat, T. J. Meade, *Proceedings of the National Academy of Sciences of the United States of America* **2007**, *104*, 13881; g) E. L. Que, E. Gianolio, S. L. Baker, A. P. Wong, S. Aime, C. J. Chang, *Journal of the American Chemical Society* **2009**, *131*, 8527.

[36] a) S. Zhang, M. Merritt, D. E. Woessner, R. E. Lenkinski, A. D. Sherry, *Accounts of Chemical Research* **2003**, *36*, 783; b) R. N. Muller, L. Vander Elst, S. Laurent, *Journal of the American Chemical Society* **2003**, *125*, 8405; c) C. Shen, E. J. New, *Current Opinion in Chemical Biology* **2013**, *17*, 158.

[37] R. A. Moats, S. E. Fraser, T. J. Meade, *Angewandte Chemie* **1997**, *36*, 726.

[38] L. Cambi, L. Szegö, *Berichte der deutschen chemischen Gesellschaft* **1931**, *64*, 2591.

[39] a) A. Bousseksou, G. Molnár, L. Salmon, W. Nicolazzi, *Chemical Society Reviews* **2011**, *40*, 3313; b) C. D. Coryell, F. Stitt, L. Pauling, *Journal of the American Chemical Society* **1937**, *59*, 633; c) E. Coronado, J. R. Galán-Mascarós, M. Monrabal-Capilla, J. García-Martínez, P. Pardo-Ibáñez, *Advanced Materials* **2007**, *19*, 1359; d) K. M. E. Koenig, *Inorganic Chemistry* **1967**, *6*, 48; e) A. H. Ewald, R. L. Martin, I. G. Ross, A. H. White, *Proceedings of the Royal Society A: Mathematical, Physical and Engineering Sciences* **1964**, *280*, 235; f) P. Gütlich, *European Journal of Inorganic Chemistry* **2013**, *5*, 581; g) P. Gütlich, A. B. Gaspar, Y. Garcia, *Beilstein Journal of Organic Chemistry* **2013**, *9*, 342; h) J. Krober, E. Codjovi, O. Kahn, F. Groliere, C. Jay, *Journal of the American Chemical Society* **1993**, *115*, 9810; i) M. NIHEI, T. SHIGA, Y. MAEDA, H. OSHIO, *Coordination Chemistry Reviews* **2007**, *251*, 2606; j) P. Gütlich, H. A. Goodwin, *Spin Crossover in Transition Metal Compounds I-III, Topicsin Current Chemistry, Springer-Verlag Berlin Heidelberg New York* **2004**; k) R. C. Stoufer, D. H. Busch, W. B. Hadley, *Journal of the American Chemical Society* **1961**, *83*, 3732; l) T. Granier, B. Gallois, J. Gaultier, J. A. Real, J. Zarembowitch, *Inorganic Chemistry* **1993**, *32*, 5305.

[40] C. Roux, J. Zarembowitch, B. Gallois, T. Granier, R. Claude, *Inorganic Chemistry* **1994**, *33*, 2273.

[41] S. Decurtins, P. Gütlich, C. P. Köhler, H. Spiering, A. Hauser, *Chemical Physics Letters* **1984**, *105*, 1.

[42] F. Hund, *Zeitschrift für Physik* **1925**, *33*, 345.

[43] a) M. A. Halcrow, *Polyhedron* **2007**, *26*, 3523; b) P. Gütlich, Y. Garcia, H. A. Goodwin, *Chemical Society Reviews* **2000**, *29*, 419; c) A. H. P. Gütlich, *Angewandte Chemie* **1994**, *33*, 2024; d) J. A. Real, A. B. Gaspar, V. Niel, M.C. Muñoz, *Coordination Chemistry Reviews* **2003**, *236*, 121.

[44] P. Gütlich, A. Hauser, H. Spiering, *Angewandte Chemie* **1994**, *106*, 2109.

[45] S. Decurtins, P. Gütlich, K. M. Hasselbach, A. Hauser, H. Spiering, *Inorganic Chemistry* **1985**, 2174.

[46] J. Z. M.-L. Boillot, *A. Sour, Spin Crossover in Transition Metal Compounds II, Bd. 234 von Topics in Current Chemistry, Kap. Ligand-Driven Light-Induced Spin*

Change (LD-LISC): A Promising Photomagnetic Effect, Springer-Verlag Berlin Heidelberg **2004**, 261.

[47] M.-L. Boillot, C. Roux, J.-P. Audière, A. Dausse, J. Zarembowitch, *Inorganic Chemistry* **1996**, *35*, 3975.

[48] S. Thies, H. Sell, C. Schütt, C. Bornholdt, C. Näther, F. Tuczek, R. Herges, *Journal of the American Chemical Society* **2011**, *133*, 16243.

[49] S. Venkataramani, U. Jana, M. Dommaschk, F. D. Sönnichsen, F. Tuczek, R. Herges, *Science* **2011**, *331*, 445.

[50] C. Bornholdt, *Dissertation Christian-Albrechts-Universität zu Kiel* **2008**.

[51] M. Dommaschk, C. Näther, R. Herges, *The Journal of Organic Chemistry* **2015**, *80*, 8496.

[52] M. Dommaschk, C. Schütt, S. Venkataramani, U. Jana, C. Näther, F. D. Sönnichsen, R. Herges, *Dalton Transactions* **2014**, *43*, 17395.

[53] M. Dommaschk, M. Peters, F. Gutzeit, C. Schütt, C. Näther, F. D. Sönnichsen, S. Tiwari, C. Riedel, S. Boretius, R. Herges, *Journal of the American Chemical Society* **2015**, *137*, 7552.

[54] G. Heitmann, C. Schütt, J. Gröbner, L. Huber, R. Herges, *Dalton Transactions* **2016**, *45*, 11407.

[55] G. Klein, J. Michaelis, C. Spix, R. Wibbing, G. Eggers, J. Ritter, P. Kaatsch, *European Journal of Cancer* **2003**, *39*, 808.

[56] J. T. Dandler, *Dissertation Ludwig-Maximilians-Universität* **2008**.

[57] T. J. Dougherty, C. J. Gomer, B. W. Henderson, G. Jori, D. Kessel, M. Korbelik, J. Moan, Q. Peng, *Journal of the National Cancer Institute* **1998**, *90*, 889.

[58] T. J. Dougherty, *Journal of Clinical Laser Medicine & Surgery* **2002**, *20*, 3.

[59] a) P. Grosjean, J. F. Savary, J. Mizeret, G. Wagnieres, A. Woodtli, J. F. Theumann, C. Fontolliet, H. van den Bergh, P. Monnier, *Journal of Clinical Laser Medicine & Surgery* **1996**, *14*, 281; b) W.C. Tan, C. Fulljames, N. Stone, A.J. Dix, N. Shepherd, D.J.H. Roberts, S.B. Brown, N. Krasner, H. Barr, *Journal of Photochemistry and Photobiology B: Biology* **1999**, *53*, 75; c) H. Kato, T. Okunaka, H. Shimatani, *Journal of Clinical Laser Medicine & Surgery* **1996**, *14*, 235; d) G. Donati, A. D. Kapetanios, C. J. Pournaras, *Seminars in Ophthalmology* **2009**, *14*, 2; e) M. S. Blumenkranz, *Archives of Ophthalmology* **2002**; f) H. Barr,

N. A. Shepherd, A. Dix, D. J.H. Roberts, W. C. Tan, N. Krasner, *The Lancet* **1996**, *348*, 584.

[60] J. D. Spikes **1985**, *The historical development of ideas on applications of photosensitised reactions in health sciences. In Primary Photoprocesses in Biology and Medicine, Plenum Press, New York*, 209.

[61] J. H. Epstein, *The New England Journal of Medicine* **1990**, 1149.

[62] M. D., Daniell, J. S. Hill, *ANZ Journal of Surgery* **1991**, 340.

[63] a) R. Ackroyd, C. Kelty, N. Brown, M. Reed, *Photochemistry and Photobiology* **2001**, *74*, 656; b) R. W. Redmond, I. E. Kochevar, *Photochemistry and Photobiology* **2006**, *82*, 1178; c) J. Moan, Q. Peng, *Anticancer Research* **2003**, *23*, 3591.

[64] O. Raab, *Über die Wirkung fluoreszierender Stoffe auf Infusorien* **1900**, *39*, 524.

[65] von Tappeiner H., *Münchener medizinische Wochenschrift* **1900**, *47*, 5.

[66] a) Jesionek A., von Tappeiner H., *Deutsches Archiv für klinische Medizin* **1905**, *85*, 223; b) von Tappeiner H, Jesionek A., *Münchener medizinische Wochenschrift* **1903**, *47*, 2042.

[67] von Tappeiner H, Jodlbauer A., *Die Sensibilisierende Wirkung fluorieszierender Substanzen. Gesammelte Untersuchungen über die photodynamische Erscheinung. F. C. W. Vogel, Leipzig* **1907**.

[68] a) W. Hausmann, *Wien Klin Wochenschr. XXI* **1908**; b) W. Hausmann, *Biochemische Zeitschrift* **1911**, *30*, 276.

[69] T. J. Dougherty, G. B. Grindey, R. Fiel, K. R. Weishaupt, D. G. Boyle, *Journal of the National Cancer Institute* **1975**, *55*, 115.

[70] a) S. S. Stylli, A. H. Kaye, *Journal of Clinical Neuroscience* **2006**, *13*, 709; b) S. S. Stylli, A. H. Kaye, *Journal of Clinical Neuroscience* **2006**, *13*, 615.

[71] a) J. Moan, *Photochemistry and Photobiology* **1986**, *43*, 681; b) J. Moan, K. Berg, *Photochemistry and Photobiology* **1992**, *55*, 931.

[72] Weishaupt, K.R., Gomer, C.J. & Dougherty, T.J., *Cancer Research* **1976**, *36*, 2326.

[73] A. M. R. Fisher, A. L. Murphree, C. J. Gomer, *Lasers in Surgery and Medicine* **1995**, *17*, 2.

[74] a) A. S. Brandis, Y. Salomon, A. Scherz in *Advances in Photosynthesis and Respiration*, *Vol. 25* (Eds.: B. Grimm, R. J. Porra, W. Rüdiger, H. Scheer),

Springer, Dordrecht, **2006**, pp. 485–494; b) A. S. Brandis, Y. Salomon, A. Scherz in *Advances in Photosynthesis and Respiration*, *Vol. 25* (Eds.: B. Grimm, R. J. Porra, W. Rüdiger, H. Scheer), Springer, Dordrecht, **2006**, pp. 461–483; c) M. G. Bonnett R, *Tetrahedron* **2001**, 9513.

[75] a) O. M., *Arzneimittel-Forschung* **1997**, *47*, 1185; b) R. W. Boyle, D. Dolphin, *Photochemistry and Photobiology* **1996**, *64*, 469.

[76] R. R. Allison, G. H. Downie, R. Cuenca, X.-H. Hu, C. J. H. Childs, C. H. Sibata, *Photodiagnosis and Photodynamic Therapy* **2004**, *1*, 27.

[77] A. Singh, W.-Y. Huang, P. Scheiner, L. W. Johnson, *Spectrochimica acta. Part A, Molecular and Biomolecular Spectroscopy* **2007**, *66*, 86.

[78] R. Couronné, *Erfassung der Pulswelle am Unterarm: Springer-Verlag* **2013**.

[79] R. R. Anderson, J. A. Parrish, *Journal of Investigative Dermatology* **1981**, *77*, 13.

[80] P. Wolf, *Der Hautarzt; Zeitschrift fur Dermatologie, Venerologie, und verwandte Gebiete* **1997**, *48*, 137-48; quiz 148.

[81] I. G. Denisov, T. M. Makris, S. G. Sligar, I. Schlichting, *Chemical Reviews* **2005**, *105*, 2253.

[82] B. Meunier, S. P. de Visser, S. Shaik, *Chemical Reviews* **2004**, *104*, 3947.

[83] a) B. Rösner, M. Milek, A. Witt, B. Gobaut, P. Torelli, R. H. Fink, M. M. Khusniyarov, *Angewandte Chemie* **2015**, *54*, 12976; b) K. Takahashi, Y. Hasegawa, R. Sakamoto, M. Nishikawa, S. Kume, E. Nishibori, H. Nishihara, *Inorganic Chemistry* **2012**, *51*, 5188; c) M.-L. Boillot, S. Chantraine, J. Zarembowitch, J.-Y. Lallemand, J. Prunet, *New Journal of Chemistry* **1999**, *23*, 179.

[84] D. Gonçalves, J. Sanders, *Synlett* **2007**, *2007*, 591.

[85] J. P. Collman, V. J. Lee, C. J. Kellen-Yuen, X. Zhang, J. A. Ibers, J. I. Brauman, *Journal of the American Chemical Society* **1995**, *117*, 692.

[86] a) B. Andrioletti, D. Ricard, B. Boitrel, *New Journal of Chemistry* **1999**, *23*, 1143; b) K. Konishi, K. Oda, K. Nishida, A. Takuzo, I. Shohei, *Journal of the American Chemical Society* **1992**, *114*, 1313; c) S. Kozuch, T. Leifels, D. Meyer, L. Sbaragli, S. Shaik, W.-D. Woggon, *Synlett* **2005**, *4*, 675; d) M. Momenteau, J. Mispelter, B. Loock, Bisagni E., *Journal of the Chemical Society, Perkin Transactions* **1983**, 189.

[87] M. J. Gunter, D. C. R. Hockless, M. R. Johnston, B. W. Skelton, *Journal of the Chemical Society* **1994**, *116*, 4810.

[88] M. Koepf, A. Trabolsi, M. Elhabiri, J. A. Wytko, D. Paul, A. M. Albrecht-Gary, J. Weiss, *Organic Letters* **2005**, *7*, 1279.

[89] B. Morgan, D. Dolphin, *Structure and Bonding* **1987**, *64*, 115.

[90] a) J. S. Lindsey, H. C. Hsu, I. C. Schreimann, P. C. Kearney, A. M. Marguerettaz, *The Journal of Organic Chemistry* **1987**, *52*, 827; b) J. S. Lindsey, R. W. Wagner, *The Journal of Organic Chemistry* **1989**, *54*, 4969.

[91] a) E. R. Kay, D. A. Leigh, F. Zerbetto, *Angewandte Chemie* **2007**, *46*, 72; b) E. Merino, M. Ribagorda, *Beilstein Journal of Organic Chemistry* **2012**, *8*, 1071; c) W. Szymański, J. M. Beierle, H. A. V. Kistemaker, W. A. Velema, B. L. Feringa, *Chemical Reviews* **2013**, *113*, 6114.

[92] G. S. Hartley, *Nature* **1937**, *140*, 281.

[93] Y. Li, D. B. Zamble, *Chemical Reviews* **2009**, *109*, 4617.

[94] a) A. Bakac, J. H. M. Espenson, *Journal of the American Chemical Society* **1986**, *108*, 719; b) C. Gosden, K. P. Healy, D. Pletcher, *Journal of the Chemical Society* **1978**, *8*, 972.

[95] a) D. A. Brisbin, R. J. Balahura, *Canadian Journal of Chemistry* **1968**, *46*, 3431; b) E. I. Choi, E. B. Fleischer, *Inorganic Chemistry* **1963**, *2*, 94; c) D. J. Kingham, D. A. Brisbin, *Inorganic Chemistry* **1970**, *9*, 2034.

[96] P. Rothemund, A. R. Menotti, *Journal of the American Chemical Society* **1948**, *70*, 1808.

[97] J. W. Barnes, G. D. Dorough, *Journal of the American Chemical Society* **1950**, *72*, 4045.

[98] a) P. Bhyrappa, M. Nethaji, V. Krishnan, *Chemistry Letters* **1993**, *22*, 869; b) S. J. Baum, R. A. Plane, *Journal of the American Chemical Society* **1966**, *88*, 910; c) M. J. Bain-Ackerman, D. K. Lavallee, *Inorganic Chemistry* **1979**, *18*, 3358; d) A. D. Adler, F. R. Longo, F. Kampas, J. Kim, *Journal of Inorganic and Nuclear Chemistry* **1970**, *32*, 2443; e) R. F. Pasternack, G. C. Vogel, C. A. Skowronek, R. K. Harris, J. G. Miller, *Inorganic Chemistry* **1981**, *20*, 3763.

[99] M. L. Dean, J. R. Schmink, N. E. Leadbeater, C. Brückner, *Dalton Transactions* **2008**, *10*, 1341.

[100] a) E. B. Fleischer, *Accounts of Chemical Research* **1970**, *3*, 105; b) R. G. Alden, B. A. Crawford, R. Doolen, M. R. Ondrias, J. A. Shelnutt, *Journal of the American Chemical Society* **1989**, *111*, 2070.

[101] J. W. Buchler, K. M. Smith, *In Porphyrins and Metalloporphyrins, Elsevier: Amsterdam, Netherlands;* **1975**, 157.

[102] W. Friedrichsen in *Advances in Heterocyclic Chemistry*, *v.26* (Ed.: A. R. Katritzky), Elsevier textbooks, s.l., **1980**, pp. 135–241.

[103] a) M. J. Haddadin, *Heterocyles* **1978**, *9*, 865; b) B. Rickborn, *In Advances in Theoretically Interesting Molecules; Thummel, R. P., Ed.; JAI Press: Greenwich* **1989**, *1*; c) R. Rodrigo, *Tetrahedron* **1988**, *44*, 2093.

[104] D. Tobia, B. Rickborn, *The Journal of Organic Chemistry* **1987**, *52*, 2611.

[105] R. Packe-Wirth, V. Enkelmann, *Journal of Molecular Structure* **1998**, *448*, 1.

[106] a) S. Itô, H. Ohtani, S.-i. Narita, H. Honma, *Tetrahedron Letters* **1972**, *13*, 2223; b) T. Sasaki, K. Kanematsu, K. Hayakawa, *Journal of the Chemical Society, Perkin Transactions 1* **1972**, 1951; c) H. Takeshita, Y. Wada, A. Mori, T. Hatsui, *Chemistry Letters* **1973**, *2*, 335.

[107] Y. M. Man, T. C. W. Mak, H. N. C. Wong, *The Journal of Organic Chemistry* **1990**, *55*, 3214.

[108] H. N.C. Wong, Y.-M. Man, T. C.W. Mak, *Tetrahedron Letters* **1987**, *28*, 6359.

[109] G. Rio, M.-J. Scholl, .*Journal of the Chemical Society, Chemical Communications* **1975**, *12*, 474.

[110] R. N. Warrener, *Journal of the American Chemical Society* **1971**, *93*, 2346.

[111] K. M. Arendt, A. G. Doyle, *Angewandte Chemie* **2015**, *54*, 9876.

[112] K. Naito, B. Rickborn, *The Journal of Organic Chemistry* **1980**, *45*, 4061.

[113] database, *Reaxys* **2018**.

[114] M. Gouterman, D. Edited by Dolphin, *Porphyrins (Optical spectra and electronic structure of porphyrins and related rings)* **1978**, *3*, 1.

[115] a) R. Bonnett, *Chemical Society Reviews* **1995**, *24*, 19; b) O. Mazor, A. Brandis, V. Plaks, E. Neumark, V. Rosenbach-Belkin, Y. Salomon, A. Scherz, *Photochemistry and Photobiology* **2005**, *81*, 342; c) E. D. Sternberg, D. Dolphin, C. Brückner, *Tetrahedron* **1998**, *54*, 4151.

[116] a) D. Gust, T. A. Moore, A. L. Moore, *Accounts of Chemical Research* **2009**, *42*, 1890; b) A. J. Esswein, D. G. Nocera, *Chemical Reviews* **2007**, *107*, 4022.

[117] L.-L. Li, E. W.-G. Diau, *Chemical Society Reviews* **2013**, *42*, 291.

[118] D. Holten, D. F. Bocian, J. S. Lindsey, *Accounts of Chemical Research* **2002**, *35*, 57.

[119] B. Grimm, R. J. Porra, W. Rüdiger, H. Scheer (Eds.) *Advances in Photosynthesis and Respiration*, *Vol. 25*, Springer, Dordrecht, **2006**.

[120] R. K. Pandey, Zheng, G., Kadish, K. M., *The Porphyrin Handbook (Porphyrins as photosensitizers in photodynamic therapy)*, *43*, 157.

[121] M. Taniguchi, J. S. Lindsey, *Chemical Reviews* **2017**, *117*, 344.

[122] a) M. Triesscheijn, P. Baas, J. H. M. Schellens, F. A. Stewart, *The Oncologist* **2006**, *11*, 1034; b) S. M. Fien, A. R. Oseroff, *Journal of the National Comprehensive Cancer Network* **2007**, *5*, 531.

[123] a) B. W. Henderson, T. J. Dougherty, *Photochemistry and Photobiology* **1992**, *55*, 145; b) W. M. Sharman, C. M. Allen, J. E. van Lier, *Drug Discovery Today* **1999**, *4*, 507; c) M. R. Detty, *Expert Opinion on Therapeutic Patents* **2005**, *11*, 1849.

[124] M. R. Hamblin, J. L. Miller, I. Rizvi, B. Ortel, E. V., Maytin, T. Hasan, *Cancer Research* **2001**, *61*, 7155.

[125] a) Z. Huang, *Technology in Cancer Research & Treatment* **2005**, *4*, 283; b) Y.-J. Yan, M.-Z. Zheng, Z.-L. Chen, X.-H. Yu, X.-X. Yang, Z.-L. Ding, L. Xu, *Bioorganic & medicinal chemistry* **2010**, *18*, 6282.

[126] a) M. Ochsner, *Journal of Photochemistry and Photobiology B* **1997**, *39*, 1; b) J. F. Lovell, T. W. B. Liu, J. Chen, G. Zheng, *Chemical Reviews* **2010**, *110*, 2839; c) D. E. J. G. J. Dolmans, D. Fukumura, R. K. Jain, *Nature Reviews Cancer* **2003**, *3*, 380.

[127] G. Heitmann, M. Dommaschk, R. Löw, R. Herges, *Organic Letters* **2016**, *18*, 5228.